Graphene Oxide Based Functional Materials Embedded with Tolerant Bio-inspired Wettability

A thesis submitted by

Avijit Das

Roll No. 156122052

to

Indian Institute of Technology Guwahati

for

the award of the degree

of

Doctor of Philosophy

Department of Chemistry

Indian Institute of Technology Guwahati

Guwahati- 781039, Assam

India

2nd March 2021

Dedicated to My Mother……

Indian Institute of Technology
Guwahati
Department of Chemistry

STATEMENT

I hereby proclaim that the work presented in the thesis entitled **"Graphene Oxide Based Functional Interfaces that Embedded with Tolerant Bio-inspired Wettability"** is the result of investigations of research work accomplished by me in the Department of Chemistry, under the supervision of Dr. Uttam Manna, Associate Professor, Department of Chemistry, Indian Institute of Technology Guwahati, Assam, India.

Research works used in this thesis from any other source has been fully cited and acknowledged. This work is original and has not been submitted elsewhere for the award of any degree.

2nd March 2021
IIT Guwahati

Avijit Das

Indian Institute of Technology
Guwahati
Department of Chemistry

CERTIFICATE

This is to certify that the work introduced in this thesis entitled **"Graphene Oxide Based Functional Interfaces that Embedded with Tolerant Bio-inspired Wettability"** by **Avijit Das**, a Ph.D. student of Department of Chemistry, Indian Institute of Technology Guwahati, for the degree of Doctor of Philosophy has been carried out under my supervision and this work has not been submitted elsewhere for the award of any degree.

2nd March 2021

Dr. Uttam Manna
Associate Professor
Department of Chemistry
Indian Institute of Technology Guwahati
Guwahati–781039
Assam, India.

Acknowledgements

Sincere gratitude is hereby extended to the following who never ceased in helping throughout this journey.

First and foremost, I would like to express my earnest gratitude to my supervisor Dr. Uttam Manna for his expert supervision, encouragement, advice and prudent suggestions without which this work would not have been possible. I am fortunate enough to have worked under his guidance which has enlightened me about scientific research and life in general. I could not have imagined a better mentor and advisor for my Ph.D. I am grateful to my doctoral committee members, Prof. Gopal Das (Chairman), Prof. Chandan K. Jana and Dr. Sunanda Chatterjee for their ingenious advice, suggestions and critique which helped me in improving the thesis work. I thank Dr. Kalyan Raidongia for his assistance in collaborative work. I am grateful to all the faculty members of Department of Chemistry, IIT Guwahati for their ingenious advice and encouragement and also all the non-teaching staffs for technical help. I am also thankful to Central Instruments Facility (CIF), IIT Guwahati for the instrumental facilities. I gratefully acknowledge the Council of Scientific & Industrial Research (CSIR) for funding without which my Ph.D. work would not have been possible.

Thanks are due to all my lovable labmates and project students for creating an environment that felt like a home away from home. Their assistance helped me a lot in completing projects in time. Staffs, students and fellows at Indian Institute of Technology, Guwahati have helped a lot in many ways and also make my tenure really memorable. My heartiest thanks to all my friends and all my teachers for being extremely supportive which makes my five years of journey truly enjoyable.

I would like to take this opportunity to thank each one of my family especially my mother and my wife for their unwavering moral and emotional support whenever required.

In the past, lotus leaf-inspired superhydrophobicity and fish-scale-inspired underwater superoleophobicity were successfully extended for developing various functional materials. A number of top-down and bottom-up approaches have been introduced to fabricate artificial bio-inspired super wetting interfaces. However, reports of durable and bio-inspired wettabilities that can perform in practically relevant severe settings are rare in the literature. Designing of bio-inspired interfaces that can sustain physical deformations and abrasions are highly challenging. In the last decades, two dimensional and flexible nano-sheets (e.g. graphene and graphene oxide etc.) have been utilized to tailor/improve the mechanical property in various materials. In this synopsis report, I have introduced approaches to covalently integrated amino graphene oxide (AGO) and chemically reactive nanocomplex (CRNC) to achieve physically deformable and abrasion tolerant superhydrophobicity and underwater superoleophobicity, where a facile and catalyst-free 1,4-conjugate addition reaction between the amine and acrylate groups played an important role. The entire synopsis report entitled "Graphene Oxide-Based Functional Interfaces that Embedded with Tolerant Super-Liquids (Oil/Water)-Wettability" is divided into six chapters. ***Chapter 1***, includes a) the introduction to the fundamentals of both the lotus leaf and fish-scale inspired liquid wettabilities and b) a brief discussion on durability related challenges of conventional artificial anti wetting interfaces. The bio-inspired interfaces that sustained diverse and various practically relevant exposures are highly important for prospective and outdoor applications. In the past, some complex and tedious approaches had been introduced to heal the damaged topography and chemistry on the application of appropriate stimuli. However, the healing of compromised topography in the damaged bio-inspired interfaces—without external intervention is rare in the literature. All these important aspects are illustrated in Chapter 1. ***Chapter 2***, introduces the design of a highly flexible and compressible superhydrophobic monolith through the strategic use of two distinct nanomaterials—a) reduced amino graphene oxide (AGO) and b) chemically reactive nano-complexes that were derived from branched polyethylenimine (BPEI) and dipentaerythritol penta-acrylate (5Acl). The appropriately selected reaction mixture provided chemically reactive and compressible polymeric materials. Further, the post covalent modification of the material with decylamine through 1,4 conjugate addition reaction yielded a highly tolerant superhydrophobic interface that remained efficient to withstand various kinds of physical insults (sand drop test, adhesive tape peeling test, knife scratching test, sand paper abrasion test), prolong chemical exposure (pH 1, pH 12,

contaminated river water and artificial seawater) and various physical manipulations (bending, creasing, rolling and twisting) without compromising its super water repellence. Furthermore, this approach was extended to develop a self-healable and abrasion tolerant superhydrophobic coating on planar substrates. On application of high (188 kPa) external pressure, the polymeric coating flattened the non-adhesive superhydrophobic interface and became highly adhesive superhydrophobic. However, the physically crushed interface remained efficient to self-restore both the physical damage and water wettability without demanding any external stimuli. The content of AGO in the polymeric coating played an important role in controlling the rate of the recovery process. This self-healing ability was further successfully extended for the selective immobilization of hydrophilic molecules on the superhydrophobic interface—directly from the water medium. The same principle is used to demonstrate rewritable patterns. ***Chapter 3***, accounts for highly stretchable and durable superhydrophobic and underwater superoleophobic interfaces. The layer-by-layer deposition of AGO and CRNC provided a chemically reactive multilayer coating that loaded with residual acrylate groups. The appropriate post covalent modifications of this single multilayer coating allowed to achieve two distinct and durable bio-inspired interfaces. The synthesized bio-inspired interfaces remained efficient to tolerate large and repetitive tensile deformations—even after incurring severe physical deformation. Next, in ***Chapter 4***, the same multilayer coatings of AGO/CRNC were extended to the fibrous substrate for developing abrasion-tolerant and selective oil or water (underwater superoleophobic) filtrating membranes. The integration of superhydrophobic and underwater superoleophobic coatings onto the fibrous substrate provided a facile basis for achieving gravity-driven selective filtration of oil and water phase respectively. Furthermore, the synthesized bio-inspired membranes were successfully applied for simultaneous collection of selectively separated oil and water phases from the oil-water mixtures under various practically relevant harsh conditions. However, such membranes are inappropriate to separate oil/water emulsions. In ***Chapter 5***, I developed magnetically active and chemically reactive two dimensional (2D) nanomaterials, where the reduced amino graphene oxide sheets were decorated with both magnetic Fe_3O_4 nanoparticles and CRNC. The post covalent modification of such chemically reactive material with octadecylamine allowed to achieve a magnetically active and superhydrophobic 2D nanomaterial for separating both 'oil-in-water' and 'water-in-oil' emulsion under practically relevant challenging conditions. In ***Chapter 6***, I

have introduced a distinct and unique approach to associate different oil-wettability with superhydrophobicity. A reaction mixture of small molecules and its strategic dilution prior to deposition allowed to achieve three different superhydrophobicity that were separately associated with superoleophilicity, oleophobicity and superoleophobicity. In ***Chapter 7***, a brief overview of the thesis work has been presented and the possible future applications of graphene-based super wetting interfaces have been proposed. Further, a brief description of each chapter is highlighted in the following sections.

Chapter 1: Introduction

In the last decades, different bio-inspired extreme liquid wettabilities have emerged as an important avenue for developing functional materials that are useful for various practically relevant different applications. In this context, both lotus leaf-inspired superhydrophobicity, as well as fish-scale inspired underwater superoleophobicity, have been widely recognized for their potential for various applications such as anti-fouling, microfluidics, liquid transportation, droplet manipulation, oil-water separation and so on. In the recent past, strategically different theoretical and experimental studies independently validated that the co-optimization of essential micro/nano scale morphology (also recognized as hierarchical topography) and appropriate chemistry (low surface energy for superhydrophobicity and high surface energy for underwater superoleophobicity) are the essential criteria for achieving both of these bio-inspired (lotus leaf and fish-scale) extreme liquid wettabilities. In the last few years, various bottom-up and top-down approaches including lithography, physical/chemical vapour deposition, template-based coating, layer-by-layer assembly, sol-gel method, dip coating, spray coating were introduced to fabricate artificial superhydrophobic and underwater superoleophobic surfaces. For preparing artificial superhydrophobic interfaces, different hydrophilic building blocks have been commonly and widely used to develop the essential hierarchical topography. Further, the tuning of appropriate chemistry (i.e. low surface energy) on top of the hydrophilic hierarchical interface has remained an essential step for adopting extreme water repellence. Such post modulation of low surface energy on top of the hierarchical topography was generally achieved by adopting weak interactions and labile bonding. For example, metal-ion interactions, metal-thiol bond and silane chemistry are known to be susceptible under prolonged exposure to harsh chemical environments and UV irradiation. Furthermore, during the harsh physical abrasion processes, the low surface energy

coating on top of the hierarchical features was easily removed and thus exposing the underneath hydrophilic material. Eventually, the embedded anti-wetting property in the conventional designs of superhydrophobic interfaces was easily compromised under practically relevant physical abrasions and manipulations. On the other hand, conventional underwater superoleophobic surfaces were generally developed by associating soft and deformable polymeric hydrogels, brittle metal oxides and weak electrostatic multilayers. Such materials are less likely to tolerate the exposures of externally applied pressure, large tensile strain, various physical abrasions and continuous exposure to chemically corrosive environments. Thus, the lack of chemical and physical durability limited their prospective applications in 'real-world' scenarios. To address these durability challenges, in the recent past, few unique superhydrophobic interfaces have been developed, and those are 1) post-repairing approach (where superhydrophobicity was regained by regeneration of the essential hierarchal topography and low surface energy coating on the damaged interface) 2) self-healing approach (where the compromised topography or chemistry was restored through the application of appropriate stimuli) and 3) three-dimensional superhydrophobicity (where essential topography and chemistry co-optimized three-dimensionally). The practical utilization of both post-repairing and self-healing approaches are limited owing to their complicated synthetic procedure and inconvenience in maintaining appropriate stimuli in practically relevant situations. Whereas, three-dimensional superhydrophobicity that can sustain physical abrasion, remained inappropriate to sustain exposure to high external pressure. Thus, the design of a self-healing and abrasion tolerant superhydrophobic interface that can recover the damaged wettability—without demanding any external intervention is essential for the outdoor application of bio-inspired wettability. Recently, two-dimensional (2D) nano materials (i.e. graphene, graphene oxide, reduced graphene oxide) have been widely recognized for their excellent mechanical property and chemical stability. A number of past demonstrations revealed that the appropriate association of graphene-based nanomaterial allowed to improve the mechanical property and chemical durability of different composite materials.

In this thesis work, two distinct nanomaterials—amino-graphene oxide (AGO) and chemically reactive nano-complexes (CRNC, derived from branched polyethylenimine (BPEI) were strategically integrated through 1,4-conjugate addition reaction for developing different functional materials—that was embedded with durable bio-inspired (lotus leaf and

fish scale) wettabilities. Furthermore, these materials were exploited for different, relevant applications such as self-cleaning, anti-wettable printing and oil-water separation.

Chapter 2: Synthesis of A Durable, Flexible and Self-Healable Superhydrophobic Interfaces

Lotus leaf-inspired nonadhesive superhydrophobicity has emerged as a potential avenue to develop various functional materials for addressing issues related to energy, sensor, healthcare, environment and so on. But, a slight perturbation in the physical and chemical parameters during the course of physical manipulations, deformations & abrasions (including bending, twisting, creasing, compressing, stretching and scratching, etc.) or harsh chemical exposures can easily damage the embedded super-water repellence in conventional superhydrophobic interfaces. In this Chapter, a highly durable, flexible and self-healable superhydrophobic interface is introduced. Here, a facile 1,4-conjugate addition reaction between aliphatic acrylates of dipentaerythritol pentaacrylate and primary amines containing branched poly(ethylenimine) was used to fabricate a durable and compressible polymeric gel material, where reduced amino graphene oxide (AGO) was strategically and covalently incorporated to modulate the mechanical property.

Moreover, the addition of AGO initiated the gelation process, and the gelation rate was increased with an increasing the content of AGO. Field emission scanning electron microscopic (FESEM) images of the synthesized polymeric gel revealed the existence of random granular topography which was appropriate for adopting nonadhesive superhydrophobicity. Moreover, the Fourier Transform Infrared Spectroscopic (FTIR) analysis revealed the presence of residual acrylate groups. The appearance of characteristic IR peaks at 1409 cm^{-1} and 1735 cm^{-1} corresponding to the C−H bond for the β carbon of the vinyl group and ester carbonyl stretching respectively indicated that the synthesized polymeric coating contained reactive residual acrylate groups. These residual acrylate groups were further post-modified with long-chain alkyl amine (decylamine) to achieve non-adhesive superhydrophobicity with advancing contact angle above 150° and contact angle hysteresis less than 5°. This polymeric gel material was embedded with three-dimensional superhydrophobicity, where the interior of the synthesized material displayed super water repellence. Moreover, the compressive modulus of the synthesized superhydrophobic

polymeric material was tailored (from 1237.56 kPa to 15.57 kPa) by increasing the content of AGO. This simple design was further extended to develop a self-healable nonadhesive and abrasion tolerant superhydrophobic coating. At first, a turbid and milky solution was deposited on a glass slide using the doctor blade method. An adequate amount of AGO provided a uniform and stable chemically reactive polymeric coating without any peeling and cracking. Further, post covalent modification of this chemically reactive coating with decylamine amine yielded a non-adhesive superhydrophobic interface, where the water droplet beaded with an advancing contact angle of 161° and contact angle hysteresis of 3°. Furthermore, this coating displayed a unique self-healing property. On exposure to very high external pressure (~188 KPa), the polymeric coating was physically crushed and the embedded lotus leaf-inspired nonadhesive superhydrophobicity (Cassie-Baxter state) was compromised. The physically crushed interface provided a highly adhesive (Cassie-Wenzel transition state) superhydrophobicity with contact angle hysteresis above 50°. Nevertheless, the physically damaged interface recovered its dimensions and non-adhesive superhydrophobicity within a few minutes without any external intervention. This self-healing process was found to be faster in increasing the content of AGO in the synthesized polymeric coating. Further, the synthesized polymeric coating can repetitively (37 times) self-heal the external pressure induced physical damages. This coating was also capable of sustaining severe physical abrasions including sand paper abrasion test, adhesive tape peeling test, and sand drop test without altering its water repellent property. This durable coating, with very unique self-healing property, was further exploited in (i) developing self-cleanable rewritable patterns and (ii) selective immobilization of water-soluble agents on the extremely water-repellent surface. Such a unique multifunctional material could be utilized for various smart applications such as sustained drug delivery, chemical catalysis, water harvesting, self-assembly of colloids, lab-on-chip, chemical sensing, cell culture systems, diagnostics tools and so on.

Chapter 3: Single Multilayer Coating for Achieving Stretchable and Abrasion Tolerant Superhydrophobic and Underwater Superoleophobic Interfaces

Design of stretchable superhydrophobic and under-water superoleophobic interfaces have immense potential for developing various smart applications related to stretchable electronics, gas sensors, flexible microfluidics, functional textiles, wearable devices, oil transportation and so on. However, reports of highly stretchable and abrasion tolerant

superhydrophobic and underwater superoleophobic interfaces that have the ability to perform at practically relevant challenging conditions are extremely rare. In Chapter 2, a doctor blade technique was adopted to prepare a thick coating (1 mm) on a planar substrate. The deposition process was inappropriate to coat geometrically complex objects and such coatings also failed to sustain tensile deformation. Thus, in this chapter (Chapter 3), the layer-by-layer (LbL) deposition technique was strategically adopted to fabricate highly stretchable and abrasion tolerant both superhydrophobic and underwater superoleophobic coatings. Further LbL deposition process allowed to coat a wide range of substrates, irrespective of their geometry. Here, the sequential deposition of AGO and CRNC on a smooth and stretchable PDMS film provided a stretchable and chemically reactive coating. The post-modifications of the chemically reactive and physically deformable multilayered coating with decylamine and glucamine provided superhydrophobic and underwater superoleophobic interfaces, respectively as shown in. Both the synthesized bioinspired coating remained efficient in sustained large tensile deformation—without compromising the embedded super liquid repellency. Even, the physically abraded bio-inspired coatings also remained tolerant to large tensile deformation. Further, FESEM analysis revealed the formation of multiple cracks on the application of large (100%) tensile strain on the physically abraded coating. Even more, these bio-inspired coatings could sustain successive (500 times) large (100 %) tensile deformations without perturbing the embedded bio-inspired wettabilities. Additionally, both of the interfaces were capable of withstanding various harsh chemicals (acidic water, basic water, sea water, river water and UV radiation) exposures. Such stretchable and durable interfaces could be very useful for practically relevant outdoor applications.

Chapter 4: Simultaneous Collection of Both Selectively Separated Oil and Water Phases from Oil/Water Mixture.

In the past, frequent oil spillage accidents and a large amount of industrial oily waste water discharge imposed a great threat for both marine ecology and environments around the globe. Therefore, the development of an energy-efficient and environmental friendly oil-water separation process is an important research topic. In the past, various oil-water separation techniques, including centrifugation, burning, air flotation, oil skimmers and marine microorganisms' treatment were introduced to remove the oil spillages. However, low oil-water separation efficiency and high operation costs limit the applications of these techniques

in a practical setting. Recently, lotus leaf-inspired superhydrophobicity and fish-scale inspired underwater superoleophobicity have been integrated with fibrous substrates and metal meshes to achieve selectively an oil-filtrating membrane and water-filtrating membrane, respectively. The use of such a bio-inspired membrane allowed the selective separation of either oil or water through the gravity-driven filtration process. In the past, mostly, single bioinspired wettability (either superhydrophobicity or underwater superoleophobicity) was applied to filtrate either the oil/oily phase or aqueous phase from the respective oil/water mixtures. The other liquid phase remained accumulated on top of the selected bio-inspired membrane. Further, most of the super wetting membranes remained inappropriate for separating the oil-water mixtures at practically relevant diverse and complex scenarios. In this chapter, lotus-leaf inspired superhydrophobic and fish-scale inspired underwater superoleophobic membranes were developed by adopting a multilayer coating introduced in Chapter 3. The multilayer coatings of CRNC and AGO was developed on a fibrous substrate. The appropriate post covalent modifications (octadecylamine for superhydrophobic property and glucamine for the underwater superoleophobic property) of the chemically reactive multilayered coating on the selected fibrous substrate provided both superhydrophobic membrane and underwater superoleophobic membrane. As expected, the synthesized bio-inspired membranes remained highly efficient to tolerate large (150%) tensile deformation (for 1000 times), creasing, bending, twisting, sandpaper abrasion, sand drop test, adhesive tape test and prolong harsh chemical exposures (extreme of acidic and basic media, artificial seawater, river water and UV irradiation (at λ_{max} = 254 and 365 nm) for 25 days. These bio-mimicked membranes were further extended for simultaneous collection of separated oil/oily phase and aqueous phase from oil-water mixtures using our lab made prototype. Two opposite open ends of a polypropylene tube were covered with the superhydrophobic membrane (left side of the tube) and underwater superoleophobic membrane (right side of the tube). A surface hole at the middle of the tube allowed to pour different oil/water mixtures. Both oil and water phase can be easily simultaneously separated easily through the gravity-driven filtration process, where the separation efficiency (above 99%) remained very high. Furthermore, oil/water separation efficiency remained unperturbed even under practically relevant various and severe physical/chemical conditions including tensile deformation, extremes of pH, sea water and contaminated river water etc.

Chapter 5: Magnetically Active Confined Superhydrophobicity for Emulsions Separation at Challenging Conditions.

In the recent past, superhydrophobic membranes and sponges were successfully applied for separating various floating and sedimented oil phases from the contaminated aqueous phase with a high separation efficiency. However, such materials remained inappropriate for separation of oil-in-water emulsion as the tiny oil droplets that dispersed in the continuous aqueous phase, have limited access to such large and bulky superhydrophobic materials (i.e. membranes and sponges). Recently, superhydrophobic microparticles were introduced to separate oil droplets from an oil-in-water emulsion, but a separation of surfactant stabilized oil-in-water emulsion remained a highly challenging task. Moreover, the separation of water-in-oil emulsion (where emulsified tiny water droplets) would be useful for cleaning the jet-engine fuel. In this chapter, amino graphene oxide (AGO) sheets were uniformly decorated with Fe_3O_4 nanoparticles and CRNC. The post covalent modification of chemically reactive and magnetically active GO nanosheets allowed to associate confined superhydrophobicity. This magnetically active confined superhydrophobicity was observed to be an efficient approach for removing both floating oils and emulsion solutions, irrespective of the viscosities and densities of the oil/oily phase. The magnetically active superhydrophobic GO (MASHGO) can easily reach out to every tiny oil droplet that is dispersed in the aqueous phase (in the case of oil-in-water emulsion). On application of an external magnetic field, an oil-free aqueous phase was achieved. Even, a surfactant stabilized tiny crude oil droplet was successfully separated from the crude oil-in-water emulsion solution following the same approach. On the other hand, the magnetically active and confined superhydrophobicity provided a facile basis for capturing the tiny water droplets that were dispersed in the oil phase by forming 'Pickering type' aqueous droplets. Further, the application of an external magnetic field allowed achieving water-free oil phase. Moreover, the synthesized material was repetitively (more than 50 times) used for oil/water separations with high separation efficiency. The oil/water emulsion separation performance remained unaltered irrespective of the size distributions of emulsified droplets in the respective emulsion solutions. The emulsion separation performance remained intact in various practically relevant and complex conditions (pH 1, pH 12, seawater, river water and surfactant contaminated). Thus, this current approach has immense potential to tackle issues related to oil spill accidents, oil purification in the petroleum industry and wastewater management. In addition, such 2D

nanomaterials embedded with confined superhydrophobicity could be very useful for other various applications such as catalysis, sensing, healthcare and energy.

Chapter 6: Common Avenue for Different Superhydrophobic Interfaces That Embedded with Tailored and Stable Oil Wettability in Air

The nature-inspired superhydrophobic interface inherently displayed an extreme affinity for oil/oily phases in air. On the other side, the superamphiphobic interface repels both the aqueous phase and oil/oily phase extremely with a contact angle above 150°. The fundamental criteria for optimizing such distinct super liquid wettabilities are different. Hence, distinct synthetic approaches were generally adopted to optimize essential physical and chemical parameters that confer two different types of liquid-repellent interfaces. In the previous chapters, sol-gel and layer-by-layer deposition techniques have been extended to develop both the fish scale and lotus leaf-inspired interfaces, where chemically reactive polymeric nanocomplex and amino graphene oxide were covalently integrated through 1,4-conjugate addition reaction, but those interfaces remained inappropriate to display in air super-oil repellence. In this Chapter 6, a rapid and scalable spray deposition of a reaction mixture of a strategically selected two small molecules (i.e. (3-aminopropyl)trimethoxysilane (APTMS) and 3,3,4,4,5,5,6,6,7,7,8,8,9,9,10,10,11,11,12,12,12- heneicosafluorododecyl acrylate (HFDDA)) allowed to tailoring different oil-wettability in air, without perturbing superhydrophobicity. The dilution of the small molecules based reaction mixture provided a facile basis for optimizing essential parameters to customize different oil wettability—starting from superoleophilicity to superoleophobicity, keeping intact the super water repellence. The synthesized superhydrophobic and superamphiphobic interfaces remained efficient for sustaining exposures of various practically relevant physical manipulations (including creasing, twisting, finger wiping and tissue paper wiping tests) & abrasions i.e. sand paper abrasion, adhesive tape test, knife test etc.) and chemically complex aqueous phases for 10 days. Furthermore, both the superhydrophobic and superamphiphobic interface was successfully extended for comparing oil/water separation, anti-fouling and self-cleaning performances. Such a simple and common synthetic approach for preparing extremely water repellent interfaces having differences in oil-wettability in the air would be useful for practically relevant outdoor applications.

Chapter 7: Conclusion and Future Direction

In conclusion, I have developed a self-healable, physical abrasion & deformation tolerant bioinspired (lotus leaf-inspired superhydrophobic and fish-scale inspired underwater superoleophobic) interfaces. A common and facile synthetic approach was adopted, where amino graphene oxide (AGO) and chemically reactive nano-complexes (CRNC) were strategically integrated following the 1,4-conjugate addition reaction at ambient conditions. The controlled association of AGO 1) allowed to tailor the mechanical property of the superhydrophobic material and 2) provide a facile basis for self-healing the damage interface and its embedded water wettability. The impact of AGO integration on the physical durability and chemical stability of the bio-inspired interfaces were examined in details. The multilayered coating of CRNC and AGO allowed to 3) achieve highly stretchable and abrasion tolerant superhydrophobic and underwater superoleophobic interfaces. Further, such a durable multilayer was extended for coating on the selected fibrous substrate to 4) achieve both superhydrophobic membrane and underwater superoleophobic membrane. Thereafter, a lab-made prototype was developed for 5) simultaneous collection of the separated oil and aqueous phases from oil/water mixture. Furthermore, a magnetically active and confined superhydrophobic material was developed by the strategic decoration of AGO with CRNC and iron oxide nanoparticles for 6) separation of both water-in-oil and oil-in-water emulsion separation at practically relevant challenging conditions.

The reduced graphene oxide is well recognized for its catalytic, electrical, thermal and other important properties. In this thesis work, reduced graphene oxide was rationally associated to develop stretchable and self-healable bio-inspired interfaces. Such interfaces can be further extended to develop various water repellent stretchable motion sensors, supercapacitors, underwater vibration sensors, piezoelectric pressure sensors and other flexible electronics. Additionally, owing to the high surface area and presence of different functional groups in graphene oxide, the current approach can be rationally associated with drugs, proteins, enzymes and other biomolecules for developing functional materials. Superhydrophobic environment could also be very useful to enhance the efficiency of various heterogeneous catalysts. Moreover, the durable underwater superoleophobic interface can be further useful for anti-platelet adhesion, oil droplets transportation and so on. Thus, the AGO-based current approach for developing durable bio-inspired anti-wetting interfaces has immense potential in developing different functional smart materials in the near future.

Table of Content

Introduction

1.1 Bio-inspired anti-wetting interface

Nature gives a boundless source of inspiration for the design and construction of various functional surfaces. Bioinspired designs of anti-wetting material such as superhydrophobic and underwater superoleophobic have been a fascinating and important research area in the recent year for their prospective and diverse applications related to energy, health and environment.[1-12] The most well known natural example of the superhydrophobic interface is the lotus leaf which not only stays dry but also shows a self-cleaning property. On the other hand, fish-scale inspired underwater superoleophobic allowed to protect from oil/oily contamination in the aqueous media. Extensive investigation on naturally occurring interfaces revealed that two essential criteria play a major role in achieving anti-wetting property and those are a) essential surface topography and b) appropriate surface chemistry.[1-7,11,13] In the last two decades, several top-down and bottom-up approaches have been introduced to construct an artificial interface that resembles bio-inspired superhydrophobic and underwater superoleophobic interfaces.[13-14] In the following sections, the evolution of the bio-inspired anti-wettability, design principles, durability challenges and prospective various applications are discussed in details. Moreover, current limitations faced by artificial bioinspired designs of anti-wetting materials are pointed out and the possible solutions are examined in the following sections.

1.2. Liquid wettability on the solid surface

Generally, the various bio-inspired super liquid wettability appears from the balance of two forces of attraction that are cohesive force (attraction force between the like molecules) and adhesive force (attraction force among unlike molecules). The high cohesive force of the liquid and low adhesive force between liquid and solid surface are the main causes of anti-wetting phenomena. When a liquid droplet is placed onto a solid surface, the three-phase contact line is formed. Then the droplet is started to spread and finally stops at the moment when cohesive and adhesive forces come into equilibrium. The liquid wettability of a solid surface is usually measured by the static contact angle (CA), which can be calculated as the tangential angle of contact made by the liquid droplet on the solid interface at the three-phase boundary (Figure 1.1A). Dynamic contact angles are also a very important characterization tool to examine the adhesive interaction between beaded liquid droplet and solid surface. There are two types of dynamic contact angles-i) advancing contact angle (θ_{Adv}) and ii)

receding contact angle (θ_{Rec}) as shown in Figure 1.1C, D.[15-17] The advancing contact angle is made when a growing liquid droplet touches the solid surface and the volume of droplet continues to increase further.[17] In contrast, the receding contact angle is measured in the opposite way, where the liquid droplet is withdrawn to the dispensing needle. At first, the droplet volume is decreased, then the contact line will also begin to decrease, the contact angle measure just before the detachment of the receding droplet is defined as the receding contact angle.

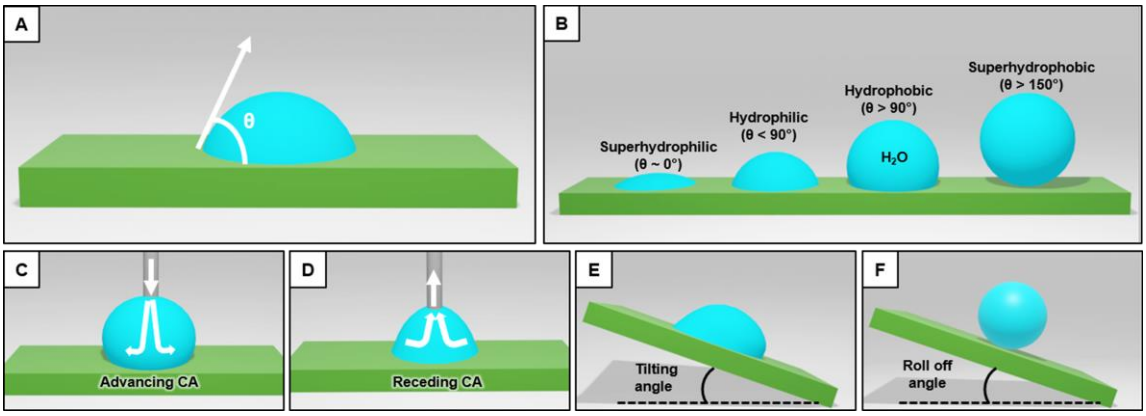

Figure 1.1: A) Schematics for contact angle (θ) which defines as the tangential angle between the liquid and the solid phases at three phases contact point. B) Representation of various wettabilities of beaded water droplet on solid surfaces based on the contact angles and those are superhydrophilic, hydrophilic, hydrophobic and superhydrophobic. C-D) Schematic representation of advancing (C), receding (D) contact angles. E-F) Schematic representation of tilting angle (E) and roll off angle (F) of beaded water droplet on solid surfaces.

The difference between advancing and receding contact angle is called contact angle hysteresis (CAH).[16] On the other side, the tilting angle is referred as the critical angle of the substrate with the horizontal line at which the water droplet starts to move by the gravitational force (Figure 1.1E, F). Both the contact angle hysteresis and tilting angle provide the qualitative estimation of adhesive interaction between a beaded liquid droplet and solid surface. Now, based on the static and dynamic contact angles of the beaded aqueous phase, the solid surfaces can be classified as hydrophilic and hydrophobic as shown in Figure 1.1B. The surfaces having a water contact angle less than 90° are considered as hydrophilic. Whereas, for the hydrophobic surface, the water contact angle should be above 90°.[18] Recently, Volger *et al,* pointed out that a water contact angle of 65° exactly divides solid materials into hydrophilic and hydrophobic instead of 90°.[19] Specifically, long-range attractive forces could appear when two planes exhibited a water contact angle greater than 65°. On the other hand, repulsive forces could be observed between surfaces with contact angle below 65°. Their results indicated that the new division of hydrophilicity and

hydrophobicity should be 65° instead of 90°.[19-20] Generally, the interfaces with static water angle > 150° are defined as superhydrophobic. Besides, superhydrophobic interfaces are also categorized as an adhesive (CAH>10°) and nonadhesive (CAH<10°) superhydrophobicity.[20] In the case of an underwater superoleophobic surface, the oil contact angle should be above 150°.[14,21]

1.3. Evolution of wettability

Nature developed various anti-wetting properties through a million years of biological evolution. Probably, in the Carboniferous period (approximately 300 million years ago), the largest dragonfly Meganeura had superhydrophobic ultrathin wings.[22] Moreover, In the Jurassic period, the Ginkgo trees had a hierarchically structured superhydrophobic surface which was constructed by the long-chain fatty alcohols. Generally, birds and terrestrial mammals including ducks, shrews and geese, which temporarily live on water are usually superhydrophobic.[22] In 1944, Baxter *et al,* discovered the extreme water-repellent property of the duck feather's which contain structural features on its feathers (Figure 1.2A).[23] In 1997, two German Botanists, Neinhuis and Barthlott revealed the morphology of the lotus-leaf (Nelumbo Nucifera) by using a scanning electron microscope (SEM) and reported the presence of randomly distributed microscale papillae (bumps; 5–10 μm) covered by hairy nanoscale wax crystalloids (diameter of 100–200 nm) resulting in two-tier micro/nano topography (Figure 1.4A-C).[24] This surface displays non-adhesive superhydrophobicity with water contact angle 161°±2.7° and roll-off angle below ~5º. As a consequence, the rolling water droplet on a lotus leaf is able to pick up the deposited dust and dirt particles, leading to self-cleaning (Figure 1.2B).[25] In 2001, Parker *et al,* discovered the mechanism of fog harvesting by the back of Namibian Desert Beetles (Stenocara gracilipes) which is made up of micro-sized hydrophilic bumps and superhydrophobic wax-coated valleys (Figure 1.2C).[26] At first, tiny water droplets condense and grow rapidly in the hydrophilic region, then those bigger size droplets are detached from the hydrophilic region and roll off towards the mouth of the beetle. In 2002, Autumn *et al,* first reported the dry adhesive superhydrophobic property of the gecko's foot with a water contact angle above 160°. A Gecko's foot consists of well-aligned millions of hydrophobic keratinous setae (approximately 5 μm in diameter and 110 μm in length), which are further split into hundreds of smaller nanoscale ends called spatula (1—200 nm diameter). These tips generated huge Van der Waals force which helps the gecko to climb or ceilings to even molecularly smooth surfaces (Figure 1.2E).[27-28] In

2002, the anisotropic super-water-wettability property of the rice leaf was reported, where the micro papillae are arranged parallel follows a quasi-one-dimensional order to the rice leaf edge and randomly distributed in other directions such that the water droplets can able to roll off along the particular direction parallel to the leaf edge (Figure 1.2D).[29] In 2007, Zheng *et al,* reported the anisotropic superhydrophobicity of the butterfly wings similar to rice leaves where water droplet can roll off along only the radial outward direction but pinning the droplet movement in the opposite direction (Figure 1.2H).[30]

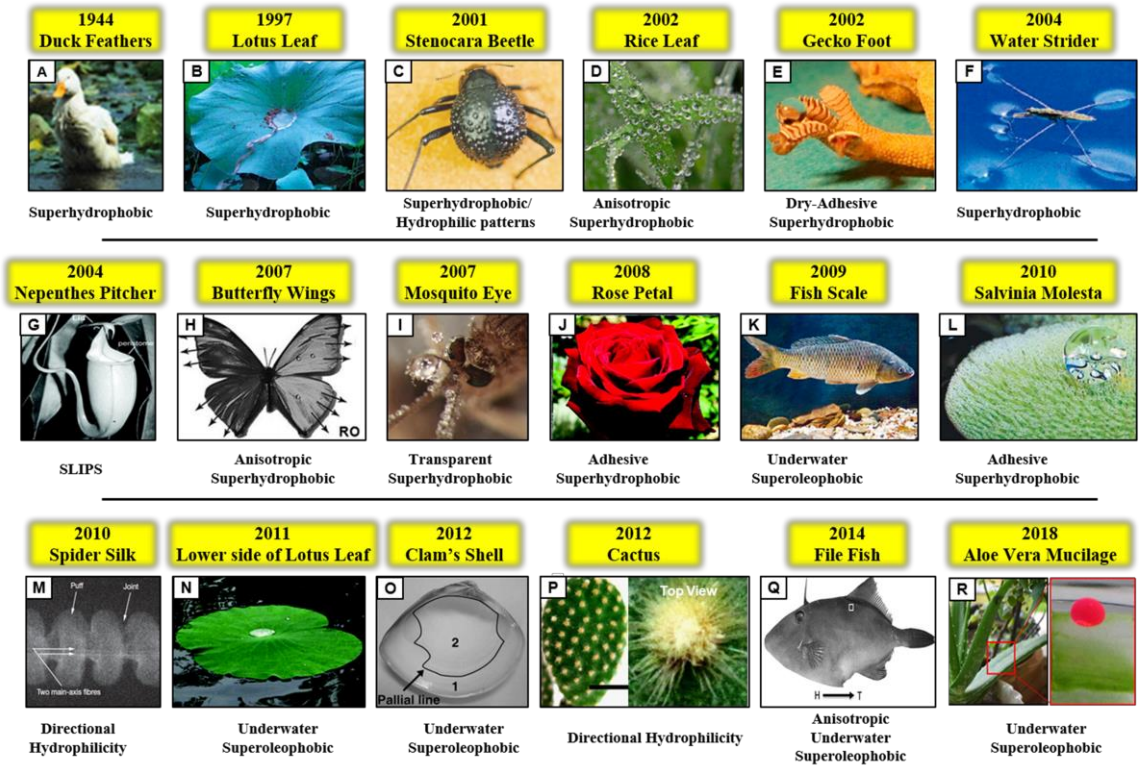

Figure 1.2. A-R) Digital images of various naturally existing superwetting interfaces including superhydrophobic duck feathers (A), superhydrophobic lotus leaf (B), stenocara beetle with superhydrophobic/hydrophilic patterns on the back (C), rice leaf with directional superhydrophobicity (D), highly adhesive superhydrophobic foot of gecko (E), superhydrophobic legs of the water strider which helps it stay afloat on water (F), slippery liquid infused peristome of nepenthes pitcher plant (G), anisotropic superhydrophobicity displayed by the wings of the butterfly wings (H), transparent superhydrophobic eye of the mosquito (I), rose petals displaying highly adhesive superhydrophobicity (J), underwater superoleophobic characteristics of the fish scales (K), the highly adhesive superhydrophobic nature of the egg-beater shaped leaf of Salvinia Molesta (L), spider silk displaying directional hydrophilicity (M), the lower side of the lotus leaf displays underwater superoleophobicity (N), underwater superoleophobic property displayed by clam's shell (O), desert cactus displaying directional hydrophilicity actus (P), file fish displays characteristic anisotropic underwater superoleophobicity (Q), aloe vera mucilage displaying underwater superoleophobicity (R). Reprinted with permission from *J. Mater. Chem. A,* 2021, **9**, 824. Royal Society of Chemistry.

Scanning electron microscope (SEM) analysis reveals periodical hierarchal scales along the radial outward direction which are composed of well-oriented nanostripes. Interestingly,

these nanostripes are stacked stepwise by tilted periodic lamellae along the radial outward direction and the nanoscale tips on the top of stripes tilted slightly upward which allowing the water droplet to roll away along with it.[30] In 2008, highly adhesive superhydrophobic 'rose petal effect' was discovered where it was found that water contact angle on the red rose petal is 152.4° but the water droplet cannot able to move even on turning the rose petal upside down (Figure 1.2J).[31]

On the other hand, in 2009, Jiang and co-workers first explored the underwater extreme oil-repelling property of fish scales (Figure 1.2K).[32] Fish scales are constructed by hydrophilic hierarchical building blocks of calcium phosphate skeleton and protein which are further coated with a relatively thin mucus layer to help the trapping a large amount of water in its rough microstructures. Microscopic images revealed the random distribution of micro papillae with a length of 100–300 mm and a width of 30–40 mm width on the surface of the fish scales. The micro-nano roughness and high surface energy coating that presence in fish scales contributed to display of underwater superoleophobicity with oil contact angle 156.4°.[32] Moreover, It was found that the lower side of the lotus leaf is also exhibiting underwater extreme oil-repellency behaviour which has the nano-grooves structured tabular and slightly convex papillae without any waxy covering (Figure 1.2N).[33] In 2014, Jiang and co-worker reported the unique anisotropic underwater oleophobic property of filefish (Navodon septentrionalis) skin which contains one direction array of hook-like spines with high surface energy organic coating (Figure 1.2Q).[34] Therefore, oil droplets on its skin surface can roll away from the head to tail direction but it was stick in the opposite direction and it can avoid the oil accumulation on the head to survive in the oil spilled aqueous environment. Later, Cai *et al,* investigated durable salt-tolerant underwater superoleophobicity of seaweed (Saccharina japonica) which is mainly because of the high content of salt-insensitive polysaccharides such as alginate, carrageenan, and agar.[35] In 2018, Shome *et al,* found that the Aloe Vera Mucilage displayed durable underwater superoleophobicity (Figure 1.2R).[36] Inspired by the aforementioned creatures, various artificial bio mimicked liquid-repellent interfaces have been developed through different approaches. But for a thorough understanding of such extreme oil/water wettability, basic theoretical models need to be discussed.

1.3.1. Basic theoretical models

1.3.1.1 Young model

In 1805, Thomas Young was the first to mathematically explained the water contact angle on an ideal smooth surface and proposed a model which is widely recognized as the Young wettability model (Figure 1.3A).[37] He considered that the liquid contact angle is arisen due to the balancing force among the interfacial energy among the solid–vapour (Υ_{SV}), liquid-vapour (Υ_{LV}) and solid-liquid (Υ_{SL}) interfaces as given below,

$$\cos\theta_Y = (\Upsilon_{SV} - \Upsilon_{SL})/\Upsilon_{LV} \quad \ldots\ldots\ldots\ldots\ldots\ldots\ldots\ldots\ldots\ldots (1)$$

where θ_Y refers to Young's contact angle.

This equation is suitable only for a completely smooth surface, however, the contact angle of beaded liquid droplet on the rough surface can not be explained. Even more, the low surface energy coated smooth material (i.e, C_9 perfluorocarbon), the water contact angle can only reach 105°–118°.[38]

1.3.1.2 Wenzel model

In 1936, Wenzel proposed a new model to explain the water wettability in the rough surface by introducing the surface roughness factor (r) into the Young model as shown in equation 2 and Figure 1.3B.[39]

$$\cos\theta_W = r\cos\theta_Y \quad \ldots\ldots\ldots\ldots\ldots\ldots\ldots\ldots\ldots\ldots\ldots\ldots\ldots\ldots\ldots\ldots (2)$$

where θ_Y refers to Wenzel's contact angle. The roughness factor is defined as the ratio of the actual surface area to the projected surface area. As the surface roughness factor is always more than one, therefore, the contact angle on the hydrophobic surface always increased and the hydrophilic surface becomes more hydrophilic with increasing the surface roughness. However, this homogenous Wenzel model on the rough surface is not capable of explaining the superhydrophobicity and underwater superoleophobicity.

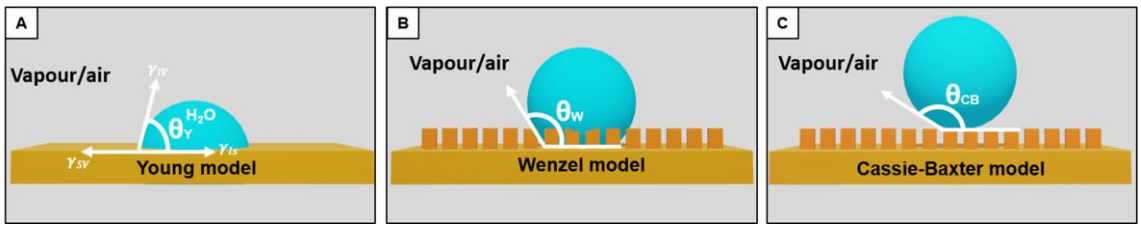

Figure 1.3. A-C) Schematic interpretation of Young's model (A), Wenzel's model (B) for homogeneous wetting and Cassie-Baxter's model (C) for heterogeneous wetting.

1.3.1.3 Cassie Baxter model

In 1944, Cassie and Baxter introduced a heterogeneous wetting model where the water droplet beaded on the rough solid interfaces with discontinuous contact—due to the presence of entrapment of air phase in between the structured grooves on the solid surface (Figure 1.3C).[40] In this model, the apparent Cassie-Baxter contact angle (θ_{CB}) is the sum of the total contributions from all the different phases as follows:

$$\cos\theta_{CB} = f_1\cos\theta_1 + f_2\cos\theta_2$$

Where, f_1 and f_2, are the geometrical fractional contact area for solid/liquid and liquid/air interfaces respectively (where $f_1 + f_2 = 1$), and θ_1, θ_2 are the contact angles of the liquid droplet on solid and air phases, respectively.

The water contact angle in the air is 180° and if the solid fraction is f, the air fraction would be 1-f. Then the modified Cassie- Baxter equation can be expressed as:

$$\cos\theta_{CB} = f\cos\theta_1 + (1-f)\cos180^o \quad \ldots\ldots\ldots\ldots\ldots\ldots\ldots\ldots (4)$$

$$\cos\theta_{CB} = f\cos\theta_1 + f - 1 \quad \ldots\ldots\ldots\ldots\ldots\ldots\ldots\ldots\ldots\ldots (5)$$

This Cassie-Baxter model can able to explain the higher contact angle above 150°. The entrapped air layer prevents the liquid phase to penetrate the micro-nano grooves of the surface which helps to get superhydrophobicity.

The Cassie-Baxter model can also be successfully extended to understand underwater superoleophobicity where the water layer is remain trapped in the high surface energy coated micro-nano grooves.[14,41] Thus oil droplet can not penetrate into the grooves and are extremely repealed by the surface under water. The apparent oil contact angle ($\theta_{CB}^{(oil)}$) for such surfaces are given by the underwater Cassie-Baxter state as shown in equation 6.

$$\cos\theta_{CB}^{(oil)} = f_w\cos\theta_{OW} + f_w - 1 \ldots\ldots\ldots\ldots\ldots\ldots\ldots\ldots\ldots\ldots (6)$$

where f_w is the fraction of solid interface in contact with the beaded underwater oil droplet and θ_{OW} is the underwater Young's oil contact angle.

1.3.2 Essential criteria for designing artificial super liquid wettability

In the last two decades, lotus leaf-inspired nonadhesive superhydrophobicity and fish-scale inspired underwater superoleophobicity have been studied thoroughly to understand the

essential criteria of super anti-wettability. In 1997, Barthlott *et al,* assumed that the superhydrophobicity was mainly caused by the micro-meter sized papillae and an epicuticular waxy layer which provided a single-tier model.

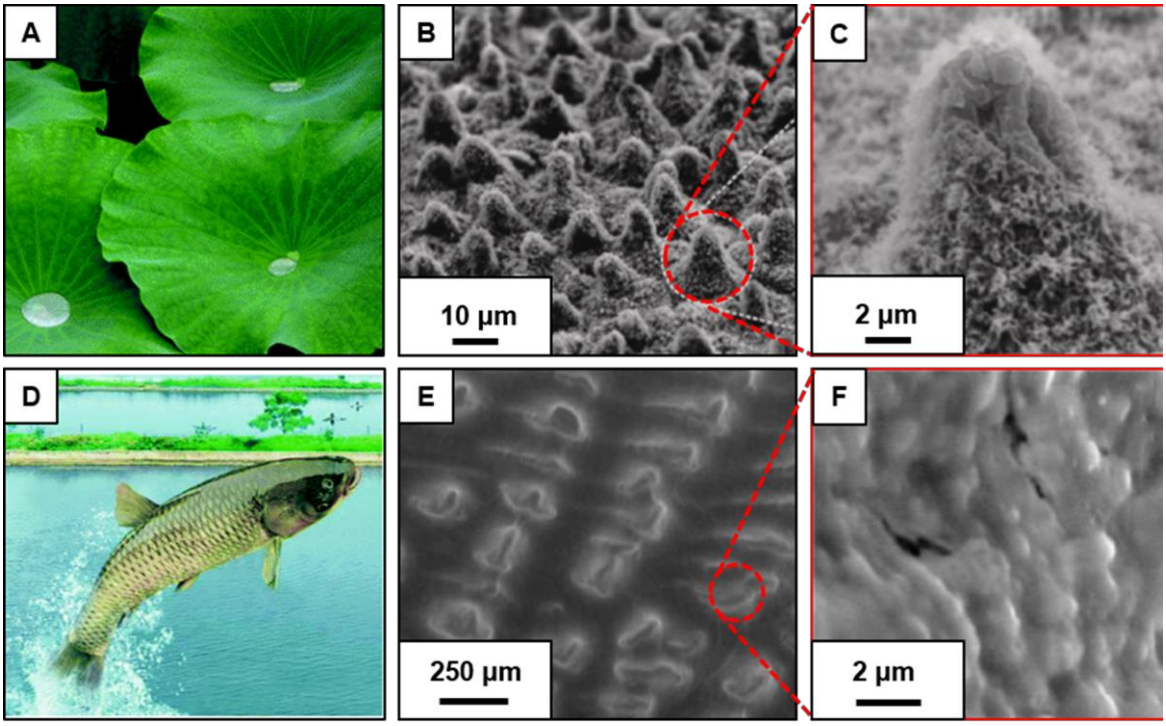

Figure 1.4. A-F) Digital photographs (A, D) and scanning electron microscope (SEM) images (B, C, E, F) of superhydrophobic lotus-leaf (A-C) and underwater superoleophobic fish-scales (D-F) in low (B, E) and high magnification (C, F). Reproduced with permission from *Chem. Soc. Rev.,* 2017, **46**, 4168. Copyright 2017, Royal Society of Chemistry.

But, It was found that only microstructure based superhydrophobic interfaces remained adhesive in nature.[24] In 2002, Jiang *et al,* pointed out that micro/nanoscale two-tier roughness of lotus leaves are essential for nonadhesive superhydrophobicity.[42] Later, Koch *et al,* confirmed the important role of micro-nano hierarchical topography for constructing lotus leaf mimicked nonadhesive artificial superhydrophobicity.[25] Therefore, detail experimental analysis revealed that two essential criteria are required to developing nonadhesive artificial superhydrophobicity, i) micro/nano hierarchical features and ii) low surface energy coating.[20] In 2009, Liu *et al,* investigated the underwater superoleophobicity of the fish scale.[32] SEM images have confirmed the presence of a random distribution of the hierarchical feathered micropapillae with 100–300 µm in length and 30–40 µm in width on the fish scales surface (Figure 1.4D-F). These hierarchical structures are made out of hydrophilic components and an additional mucus layer is present on the top. The hydrophilic mucus layer on the fish scale surface provided high water affinity and the externally trapped aqueous phase in

hierarchically structured micro-nano topography contributed to the under water oil-repellent property. Thus, micro-nano hierarchical features and high surface energy coating are the essential criteria for achieving underwater superoleophobicity.[32]

1.4. Applications

In the past, these two distinct bio-inspired super liquid repellence properties (i.e. superhydrophobicity and underwater superoleophobicity) extended for diverse and relevant applications (as shown in Figure 1.5). The superhydrophobicity was successfully demonstrated for self-cleaning, anti-fogging, antireflection, anti-corrosion, drag reduction, water harvesting, drug delivery and other biological applications (Figure 1.5).[43-44] For example, in 2015, Lu *et al,* developed a water repellent paint that consisted of TiO_2 nanoparticles and perfluorooctyltriethoxysilane and remained capable of displaying self-cleaning performance in the air as well as under oil.[45] Superhydrophobic coating was also used to address the corrosion-related challenges. Corrosion of the metal surface is a major economic problem for various industries.[45] In 2008, Zhang *et al,* demonstrated the anti-corrosion property of superhydrophobic coating where a porous anodic alumina/aluminum substrate was coated with water repellent laurate-intercalated films of ZnAl layered double hydroxide (ZnAl-LDH–laurate).[46] The superhydrophobic property of the film gave prolonged corrosion protection of the metal substrate from the aggressive chemical environment. The superhydrophobic coating can also able to show anti-icing property which is very important for radar, space flight, aviation. Tourkine *et al,* reported that freezing of water droplets could be significantly delayed on micro-nano structured superhydrophobic surfaces as compared with a flat surface.[47] It was found that the entrapped air within the micro-nano grooves of the superhydrophobic surface provides the essential thermal insulation to delay the water freezing process. Moreover, in 2012, Yohe *et al,* prepared three-dimensional superhydrophobic material adopting an electrospinning method and such coating was able to provide sustained release of the pre-loaded drug molecule in the aqueous phase. The metastable trapped air in the three-dimensional superhydrophobic material acted as a removable barrier against the aqueous phase which helps to slow down the release of the embedded water-soluble molecule.[48] Furthermore, recently, the superhydrophobic interface has been extended for developing an efficient solid acid catalyst, protein crystallization, microfluidics and miniature chemical reaction systems.[43-44] On the other hand, the underwater superoleophobic interfaces have been utilized in many applications such as oil transportation, microfluidics, underwater robotic device, anti-platelet adhesion and so on (Figure 1.5). For

example, Wang *et al,* demonstrated that underwater superoleophobic interface prevents fouling of various oil including viscous crude oil in the marine environment.[49] Furthermore, the underwater superoleophobic interface can help to prevent blood coagulation and thrombosis which is very important for implantation and many other medical uses.

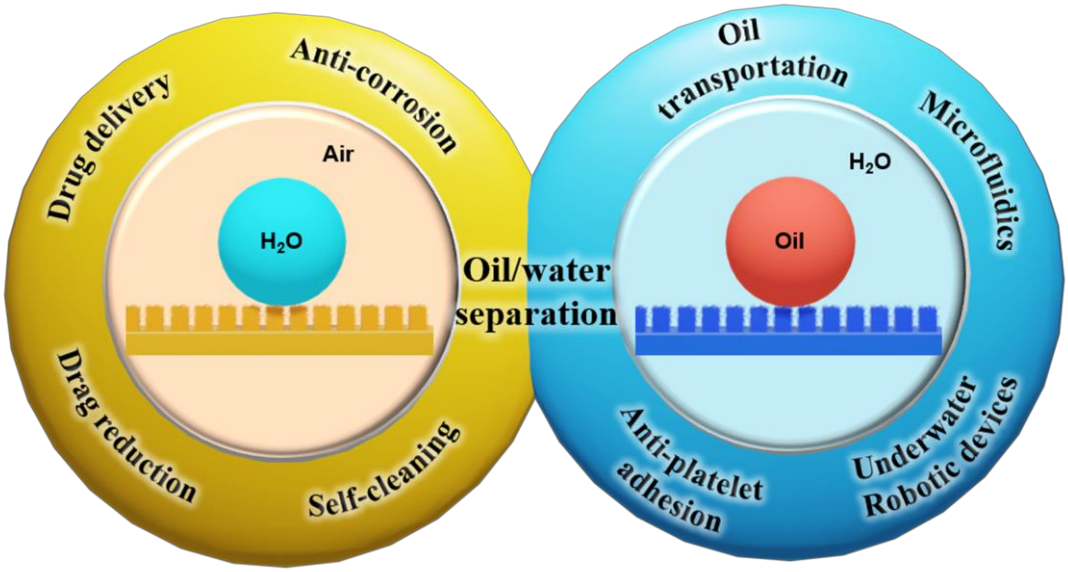

Figure 1.5. Schematic representation of various applications of superhydrophobic and underwater superoleophobic interfaces.

In 2009, Chen *et al,* fabricated nanoscale topography on poly(N-isopropylacrylamide) (PNIPAAm) surface by introducing Si nanowire arrays which showed significant anti-platelets adhesion property as compare with bare Si surface. It was found that high water content and micro-nano morphology of the underwater superoleophobic interface played a crucial role in reducing the platelets adhesion and prevent blood clotting.[50] In 2011, Su *et al,* fabricated an underwater superoleophobic device that was successfully used for oil or organic solvent droplet transportation in the miniature underwater chemical reaction. Besides, both superhydrophobic and underwater superoleophobic interfaces can be used for oil-water separation.[51] In the recent past, frequent oil-spill accidents and industrial oily-waste water discharge imposed severe worldwide challenges (Figure 1.6).[52-57] For instance, in the Gulf war, around 240 million gallons of oil were discharged into the Persian Gulf which killed hundreds of fish and marine mammals.[57] Next, the Deepwater Horizon oil spill in the Gulf of Mexico in 2010 released 200 million gallons of crude oil into the sea and caused severe damage to the marine eco-system.[58] Besides, oily-wastewater discharge from various industries such as mining, biopharmaceuticals, petrochemicals, textiles and foods poses a great threat to the environment.[59-60] Therefore, oil/water separation is an important emerging

topic in both academic and industrial research. Generally, various conventional approaches have been adopted to solve this problem such as chemical dispersants, skimming, in situ burning, etc.[61-62]

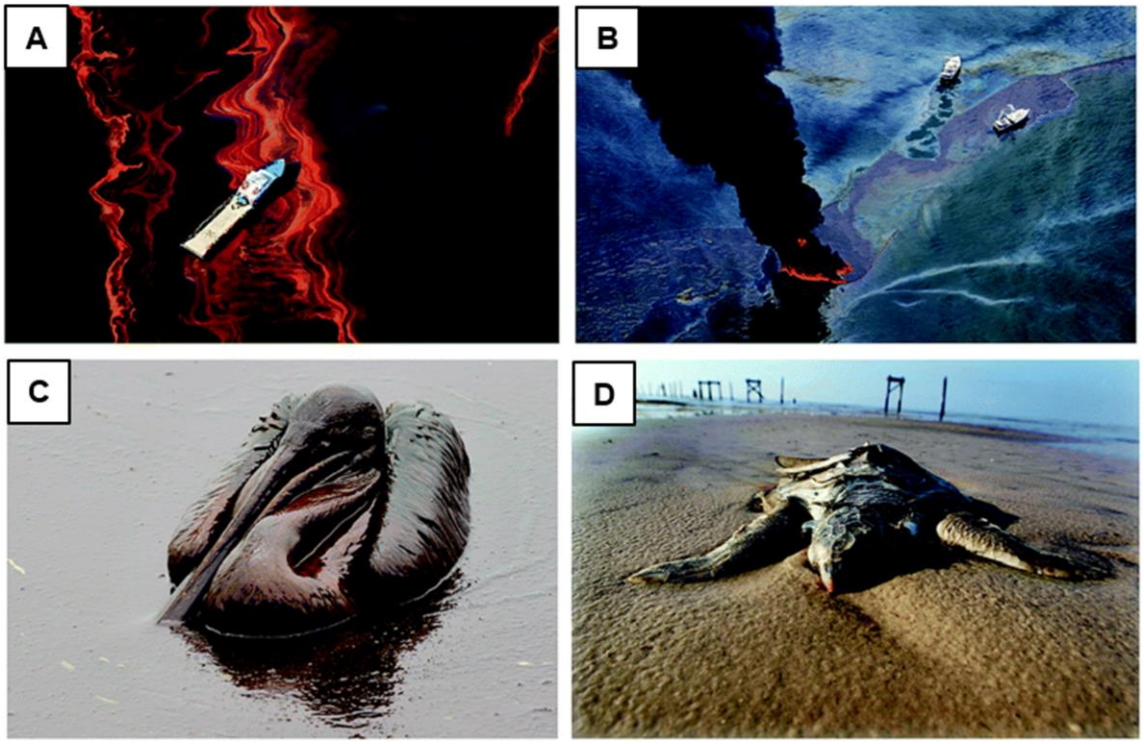

Figure 1.6. A-D) Images of the crude oil spillages on the ocean surface after oil spill accident in the Gulf of Mexico which destroyed the aqua-eco system of ocean and coastal area. Reprinted with permission from *Phys. Chem. Chem. Phys.,* 2018, **20**, 25140. Copyright 2018, Royal Society of Chemistry.

However, such traditional approaches are associated with high energy consumption, low efficiency and secondary pollutions. Therefore, the development of highly efficient, cost-effective and eco-friendly oil/water separation techniques is very essential in the current context.

Recently, the superhydrophobic and underwater superoleophobic surfaces have been used for oil-water separation with high efficiency (Figure 1.7). In 2004, Feng *et al,* first time used lotus leaf-inspired superhydrophobic material for the gravity-driven selective separation of oil/water mixture.[63] They fabricated superhydrophobic stainless steel mesh and they found that only the oil phase in the oil-water mixture was able to pass through the superhydrophobic mesh. This property was successfully utilized for gravity-driven filtration based separation of oil contaminates from oil/water mixture. Later, this bio-mimicked superhydrophobic property was further extended for selective absorption of the oil phase from the oil/water mixture.[64-65] Moreover, fish-scale inspired underwater superoleophobic material was also exploited for oil-

water separation where this material was able to separate water from various oil/water mixtures.

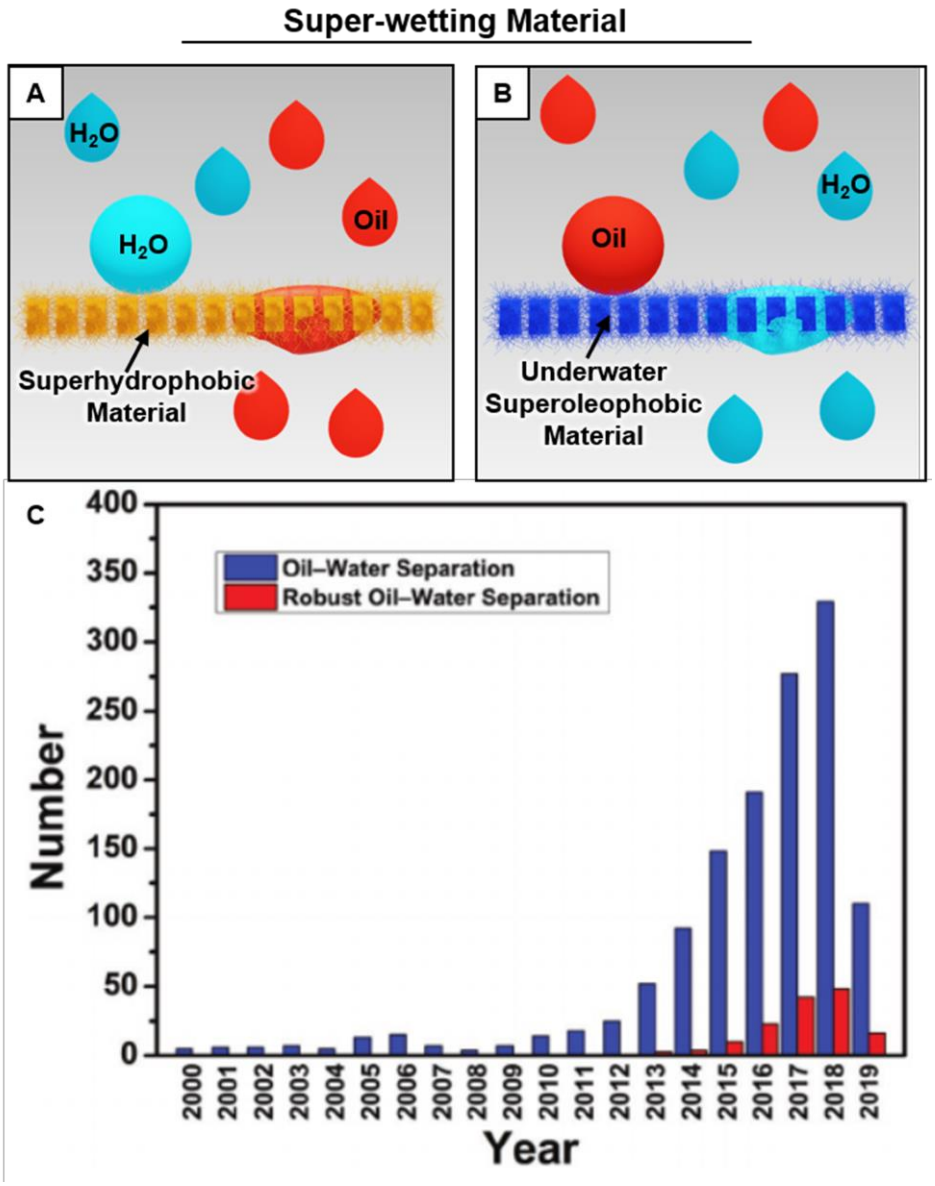

Figure 1.7. A-B) Schematic representation of the oil-water separation through superhydrophobic and underwater superoleophobic material where superhydrophobic material repel the water phase, but oil phase can easily penetrated through it. Whereas underwater superoleophobic material repel the oil phase and water phase can easily pass through it. C) Plot displaying the number of papers published on oil-water separation. Reprinted with permission from *Adv. Mater. Interfaces,* 2019, **6**, 1900126. Copyright 2019, John Wiley & Sons, Inc.

For instance, Xue *et al,* a fabricated hydrogel-coated underwater superoleophobic porous metal substrate which was able to gravity-driven selective separation of water from the oil/water mixtures with high separation efficiency (>99%) without any external intervention.[66] After that, various superhydrophobic and underwater superoleophobic material was developed to use for efficient oil/water separation.[67-70]

These two special wetting properties have great potential in energy-efficient, eco-friendly oil-water separation compared to traditional separation technology. But, the demonstration of oil/water separation in the practically relevant severe conditions is rare in the literature because of the poor physical and chemical durability of the artificial bio-mimicked interfaces under challenging scenarios.

1.5. Limitations of conventional methods

Even though both the lotus leaf-inspired superhydrophobic and fish-scale inspired underwater superoleophobic interface has immense prospective for the practically relevant application, the poor mechanical durability and chemical stability limit their relevant outdoor applications. As described before, the appropriate micro-nano morphology and surface chemistry are the essential criteria for these two bio-mimicked interfaces. In the last two decades, various top-down (lithography, plasma etching, temptation) and bottom-up (sol-gel method, layer by layer deposition, chemical and physical vapour depositions, electrospinning) approaches have been adopted to develop appropriate hierarchical topography for artificial lotus leaf and fish-scale inspired interfaces—that are mostly and commonly derived from hydrophilic constituents (Figure 1.8A).[13-14,20,21] Generally, in the case of conventional superhydrophobic interfaces, the top surface of this hydrophilic hierarchical topography was further coated with a thin layer of inert low surface energy molecules by using weak and labile interactions/bonding including metal-ion interactions, metal-thiol and silane chemistry etc., which are known to be susceptible under severe complex chemical conditions and prolonged UV radiation (Figure 1.8E).[71-81] Furthermore, the top inert coating can easily erode during harsh physical abrasions which expose the hydrophilic material underneath, thus, sacrificing the embedded superhydrophobic property (Figure 1.8B).[82-83] Besides, the conventional superhydrophobic interfaces also can not sustain the large tensile and compressive strains (Figure 1.8C-D).[82-83] On the other hand, artificial underwater superoleophobic coatings were mostly fabricated by using fragile metal oxides, delicate polymeric hydrogels, and labile electrostatic multilayers which are prone to damage under various physical abrasions, mechanical stress and prolonged exposure to aggressively corrosive aqueous environments (Figure 1.8F-H).[3,7,14,84] Recently, various approaches have been adopted to endure harsh physical and chemical insults such as i) post-repairing approach, ii) self-healing approach and iii) three-dimensional bulk anti-wetting approach (Figure 1.9) for achieving prolong the performance of artificial superhydrophobicity.[85-88] In

the post-repairing approach, the appropriate hierarchical structures and essential surface chemistry were regenerated on the damaged areas by adopting dip and spray coating methods, and thus, the anti-wetting property was restored (Figure 1.9A).

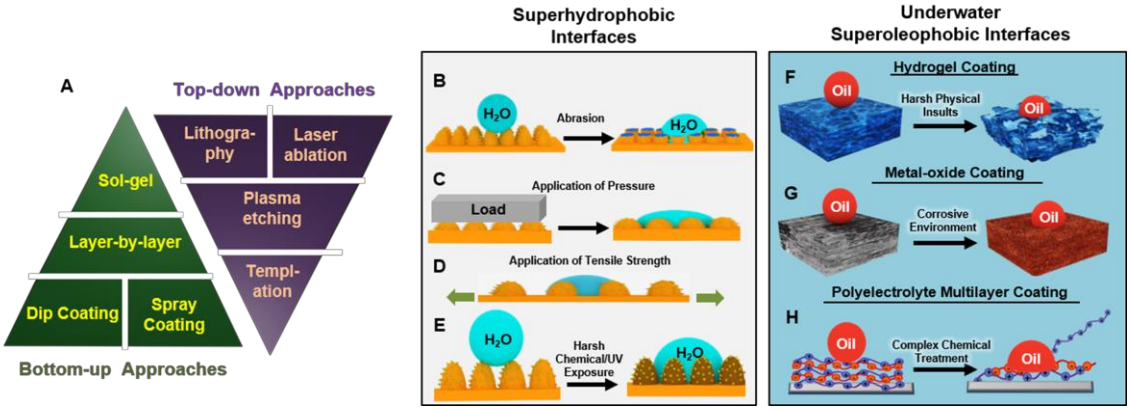

Figure 1.8. A) Schematic representation of various top-down and bottom up approach to fabricate superhydrophobic and underwater superoleophobic interfaces. B-E) Schematic illustration of the conventional designs of superhydrophobic interfaces and its limitations under practically relevant challenges—including physical abrasion (B), external pressure (C), tensile strain (D), harsh chemical and UV exposure (E). F-H) Schematic diagram of conventional hydrogel (F), metal-oxide (G) and polyelectrolyte multilayer-based (H) underwater superoleophobic interfaces which are supceptable to damage under harsh chemical and physical insults.

For instance, Zhu *et al,* introduced a mechanically durable superhydrophobic surface with post-repairing ability via Ag deposition and surface fluorination on the polymer/metal composite. After a harsh abrasion process, the surface of the material was seriously damaged and the anti-wetting property was compromised. However, after repeating the Ag deposition with the surface fluorination process, the material regained the anti-wetting property.[85] Li *et al,* reported a repairable transparent superhydrophobic coating through spray coating of SiO_2 and diethoxydimethylsilane mixture.[89] The damaged interface restored its compromised anti-wetting property after spray deposition of essential ingredients. However, the regeneration of essential topography and chemistry would be inconvenient and laborious in diverse and outdoor settings.[85] Later, the self-healing approach was introduced to improve the durability through the release of low surface-energy agents or regenerating the surface topography by application of external stimuli (i.e. temperature, UV radiation, pH, humidity) as shown in Figure 1.9B. But, the performance of such approaches is limited to certain healing/repairing cycles. Moreover, the maintenance of proper external stimuli and repeated regeneration process would not be desirable at practically relevant scenarios. For example, Li *et al,* reported a robust self-healable superhydrophobic surface via layer-by-layer (LBL) deposition of a polyelectrolyte complex of poly(allylamine hydrochloride) (PAH), sulfonated poly(ether

ketone) (SPEEK) and polyacrylic acid (PAA) on the substrate followed by chemical vapour deposition (CVD) of 1H, 1H, 2H, 2H-perfluorooctyltriethoxysilane (POTS) at 120°C for 3 hours.

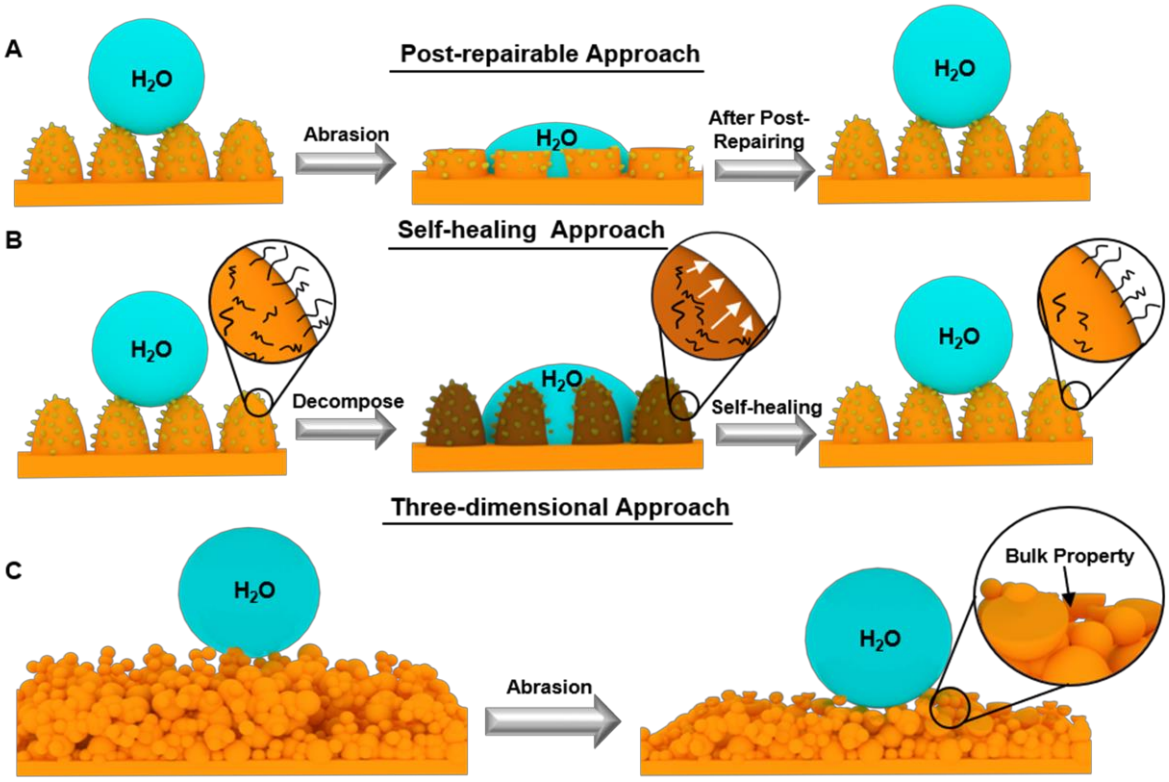

Figure 1.9. Diferent approaches to achieve durable superhydrophobicity. A) Schematic representation of regeneration of damaged superhydrophobicity following the post repairing approach. B) Schematic illustrating the working principle of the self-healing process, where an excess of physically deposited low surface energy molecules is preserved in the bulk of the material that can migrate to the damaged surface in the presence of an external stimulus, thus restoring the bio-inspired liquid wettability. C) Schematic representation of three-dimensional, abrasion tolerant bulk superhydrophobicity. Reprinted with permission from *J. Mater. Chem. A,* 2021, **9**, 824. Royal Society of Chemistry.

The porous polymeric PAH–SPEEK/PAA multilayers provided the hierarchical topography and acted as a reservoir to accommodate an excess amount of low surface energy molecule—that is POTS. After O_2 plasma-etching treatment, the multilayers became hydrophilic, but it restored the superhydrophobicity in a humid environment where the preserved POTS migrated from the bulk of the coating to the top of the multilayer coating. This etching-healing cycle was successfully carried out for six times.[87] However, these types of material can be healed only for a few cycles after which the anti-wetting property is permanently compromised due to depletion of the amount of loaded healing agents, thus, limiting its practical utility. Besides, shape memory polymers were also used to develop stimulus assisted healable-superhydrophobic coatings where crushed microstructures were able to restore the anti-wetting property by application of suitable external stimuli.[90-92] But the maintenance of

these appropriate external stimuli is inconvenient in practical application. Thus, it is very evident that the practical utilization of both the bio-mimicked properties is highly challenging due to the poor physical and chemical durability. Recently, a new kind of three-dimensional superhydrophobic coating has been developed by a few research groups. In such a design, the liquid-repellent property is not just limited to the top surface of the material but also exists in the bulk of the material (Figure 1.9C).[48,93-96]

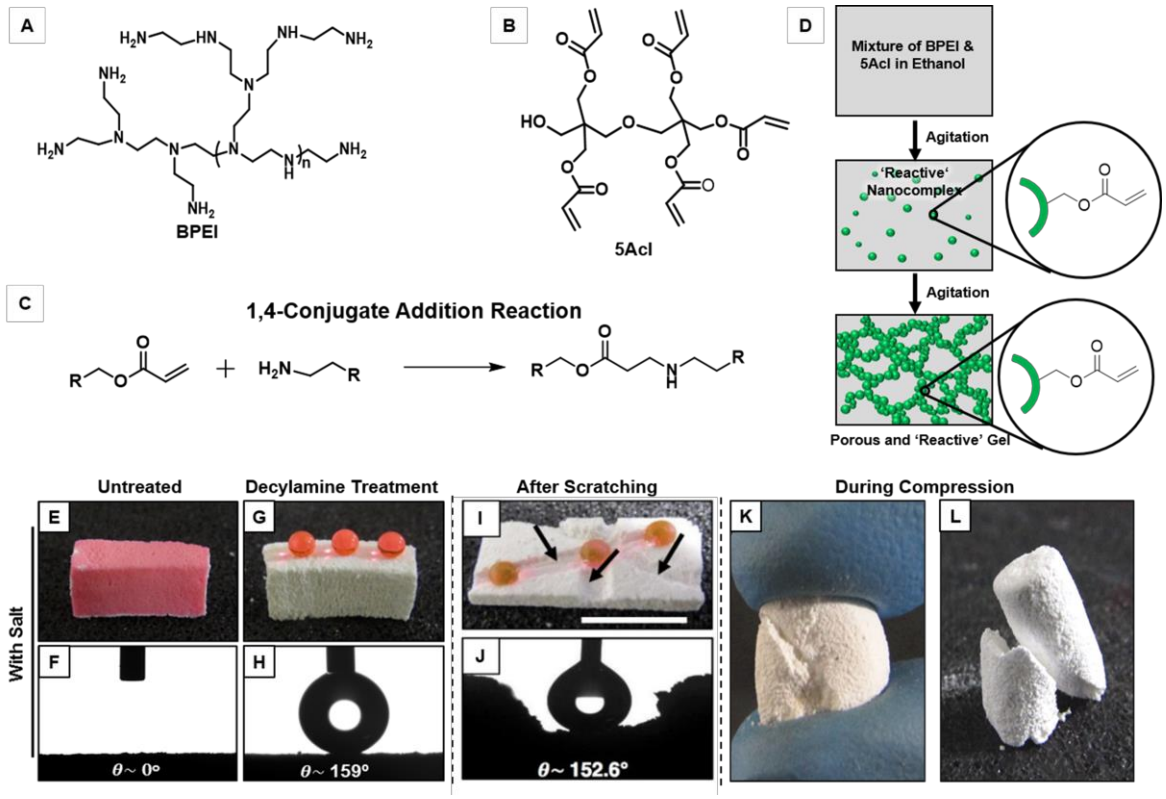

Figure 1.10. A-B) Chemical structures of branched poly(ethyleneimine) (BPEI, A) and dipentaerythritol pentaacrylate (5Acl, B) molecules. C) Depiction of the 1,4-conjugate addition reaction between primary amine of BPEI and acrylate groups of 5Acl. D) Schematic illustrating the formation of reactive polymeric gel from BPEI/5Acl mixture via the formation of reactive nanocomplex intermediate. E-H) Digital images (E, G) and advancing water contact angle (F, H) of the untreated (E, F) and decylamine treated polymeric material (G, H). I-J) Digital and advancing water contact angle image of knife scretched superhydrophobic interface where superhydrophobic property remain intact after removal of top surface of the material. K-L) Digital image demonstrated that superhydrophobic gel material was brittle in nature which can be easily broken under external pressure. Reproduce with permission from *Chem. Mater.,* 2016, **28**, 8689. Copyright 2016, American Chemical Society.

However, most of these reported materials are either fabricated through tedious/complex processes or associated with harmful and expensive chemicals that are inappropriate for industrial scale-up. Thus, this area of research requires further improvement for developing durable materials that can sustain under various and severe outdoor settings.

In 2016, Rather *et al,* exploited salt-assisted 1,4-conjugate addition reaction between amine-containing branched poly(ethyleneimine) (BPEI) and multiple acrylate group-containing dipentaerythritol pentaacrylate (5Acl) to develop chemically reactive polymeric gel via formation of chemically reactive nano-complex (CRNC) as shown in Figure 1.10.[97] This 'reactive' polymeric gel was successfully utilized to the developed durable bulk superhydrophobic monolith where anti wetting property present throughout the material and it remained intact even after removing its top surface (Figure 1.10I-J). Owing to the covalent cross-linking of the polymeric matrix, this monolith sustained its water repellent property under severe physical abrasions and prolong exposure of chemically harsh environments. But, this material was brittle in nature and it was easily broken down into pieces under the application of large and repetitive compressive or tensile strain (Figure 1.10K-L). In my thesis work, I intend for developing the chemically reactive and highly deformable monolith and coating that would be capable of providing highly durable and bio-inspired extreme anti-wettability (superhydrophobic and underwater superoleophobic). The prepared interface would be appropriate to can sustain severe physical abrasions, large tensile/compressive strain and harsh chemical environment.

1.6. Effect of graphene or graphene oxide in mechanical reinforcement of the material

In the last two decades, graphene-related materials have been explored extensively to improve the mechanical strength of the material.[98,106,108,186,187,188] Graphene is the single-layer carbon allotrope where sp^2 hybridised carbon atoms are linked through strong σ bonds in the hexagonal honeycomb lattices (Figure 1.11A).[99-102,189] Theoretical and experimental studies revealed that the mechanical strength of graphene is remarkable and it is the strongest two-dimensional material ever developed.[102-105] In 2008, Hone and coworkers first calculated the mechanical strength of graphene monolayer by applying nanoindentation technology (Figure 1.11E). The intrinsic strength of the graphene monolayer is 130 GPa and Young's modulus close to 1.0 ± 0.1 TPa (assuming an effective thickness of 0.335 nm).[102] These extraordinary mechanical properties of graphene remained an important basis for tailoring in mechanical property in the various functional materials.[98,107-108] Generally, the Halpin-Tsai model widely used to understand the mechanical reinforcement of the different material after the incorporation of graphene sheets where Young's modulus of the composite material can be measured through the following equation (i).

$$E_{Cr} = \frac{3}{8}E_{C//} + \frac{5}{8}E_{C\perp}$$

$$= [\frac{3}{8}(1+\xi\eta_L V_f)/(1-\eta_L V_f) + \frac{5}{8}(1+2\eta_T V_f)/(1-\eta_T V_f)]\, E_m \quad \ldots\ldots (i)$$

where E_{Cr}, $E_{C//}$ and $E_{C\perp}$ represent Young´s modulus of a composite material with fillers (graphene sheets) oriented random, parallel and perpendicular with the direction of the applied load respectively. E_f is Young´s modulus of fillers and E_m is the young modulus of the material matrix, respectively. V_f is the volume fraction of fillers. η_L and η_T are given by equations (ii) and (iii). ξ is depended on the structure and morphology of the fillers which is given by the equation (iv).

$$\eta_L = (\frac{Ef}{Em} - 1)/(\frac{Ef}{Em} + \xi) \quad \ldots\ldots\ldots\ldots (ii)$$

$$\eta_T = (\frac{Ef}{Em} - 1)/(\frac{Ef}{Em} + 2) \quad \ldots\ldots\ldots (iii)$$

$$\xi = \frac{2}{3}C = \frac{2}{3}\frac{l}{t} = \frac{2}{3}\alpha_f \quad \ldots\ldots\ldots\ldots\ldots (iv)$$

where α_f is the aspect ratio of the fillers where *l* and *t* are the length (or area) and thickness of the fillers. The above Halpin-Tsai model (Eqn. i) certainly shows that the aspect ratio of the fillers is one of the important factors for mechanic1al reinforcement of the composites material and the higher the aspect ratio of filler, increase Young's modulus of the composites. Graphene sheets have a very high aspect ratio and thus it enhanced the mechanical property of the composite significantly.[147]

In the last two decades, many articles have been published where graphene sheets were used for the remarkable improvement in the mechanical properties of a different kind of polymer material such as poly(vinyl alcohol), nylon-6, epoxy resin, polyurethane, polypropylene, polyethene, polytetrafluoroethylene and polymethyl methacrylate etc.[111-119] The various methods including melt mixing, solution blending, in situ polymerization, layer by layer (LbL) have been used for the preparation of graphene/polymer nanocomposites.[112,118,120-122] Nevertheless, maximum mechanical improvement can only be obtained when the graphene sheets are dispersed homogeneously in the composite materials. But the homogeneous incorporation of graphene sheets in the polymeric matrices is a very challenging task. Generally, the graphene sheets can be easily agglomerated in the polymeric matrices due to

strong van der waals interactions between the graphene monolayers.[111,123-126] Therefore, in the last decade, overcoming these van der waals interactions of the graphene sheets was a very important research topic and many groups have developed different techniques to make homogeneous dispersion of pristine graphene by using different solvents, surfactants and surface functionalizations.[125-129]

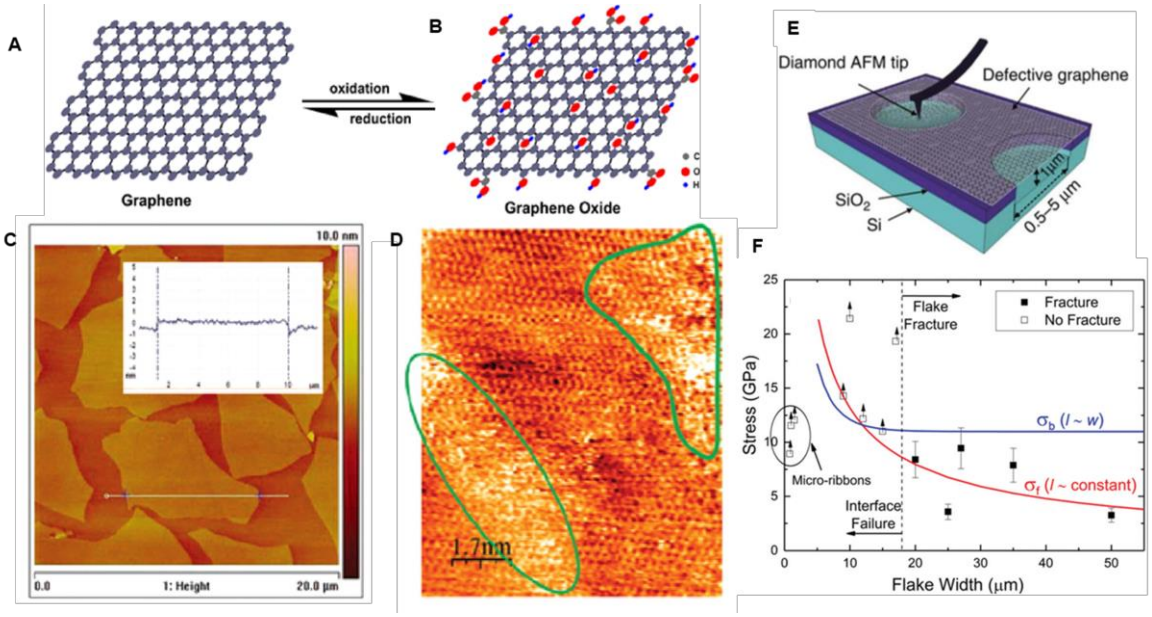

Figure 1.11. A) Scheme of structural model of graphene (A) and graphene oxide (GO, B), showing that graphene consists of only trigonally bonded sp^2 carbon atoms while GO consists of a partially sp^2 carbon network with phenol, hydroxyl, and epoxide groups on the basal plane and carboxylic acid groups at the edges. C) Atomic force microscopy (AFM) image of a GO sheet. The apparent thickness of a single sheet is around 1 nm. Reproduce with permission from *Nano Lett*. 2007, **7**, 3499. Copyright 2007 American Chemical Society. D) Scanning tunneling microscope (STM) image of a GO monolayer. Oxidized regions are marked by green contours. Reproduce with permission from *Nano Lett.* 2007, **7**, 3499. Copyright 2007 American Chemical Society. E) AFM nanoindentation on suspended graphene sheets with defects. F) Graph of the graphene failure strength versus the flake width for various monolayer graphene flakes . Reproduce with permission from *Nanoscale*, 2020, **12**, 2228. Copyright 2020 Royal Society of Chemistry.

In contrast, graphene oxide (GO) sheets that are synthesized by the oxidation of graphene can address this problem.[130-131] Graphene oxide sheets contain different functional groups, such as carbonyl, epoxy, hydroxyl, and carboxyl groups on their basal planes and edges, which significant reduce the van der waals interactions and promote the homogeneous dispersion of GO in the polymeric matrix (Figure 1.11B-D).[132-134] In the last two decades, various synthetic methods of graphene oxide have been developed such as chemical methods (Brodie, Staudenmaier, Hofmann, Hummers' and Tour's method), electrochemical methods, microbial methods.[135-140] The important advantages of graphene oxide are the easy processing and ease

of chemical post-functionalization process in comprising to the pristine graphene sheets. Eventually, the GO has emerged as an important component in the interdisciplinary fields of research. In 2007, Dikin *et al,* measured the average young's modulus of graphene oxide sheet which was ~30 GPa on average.[141]

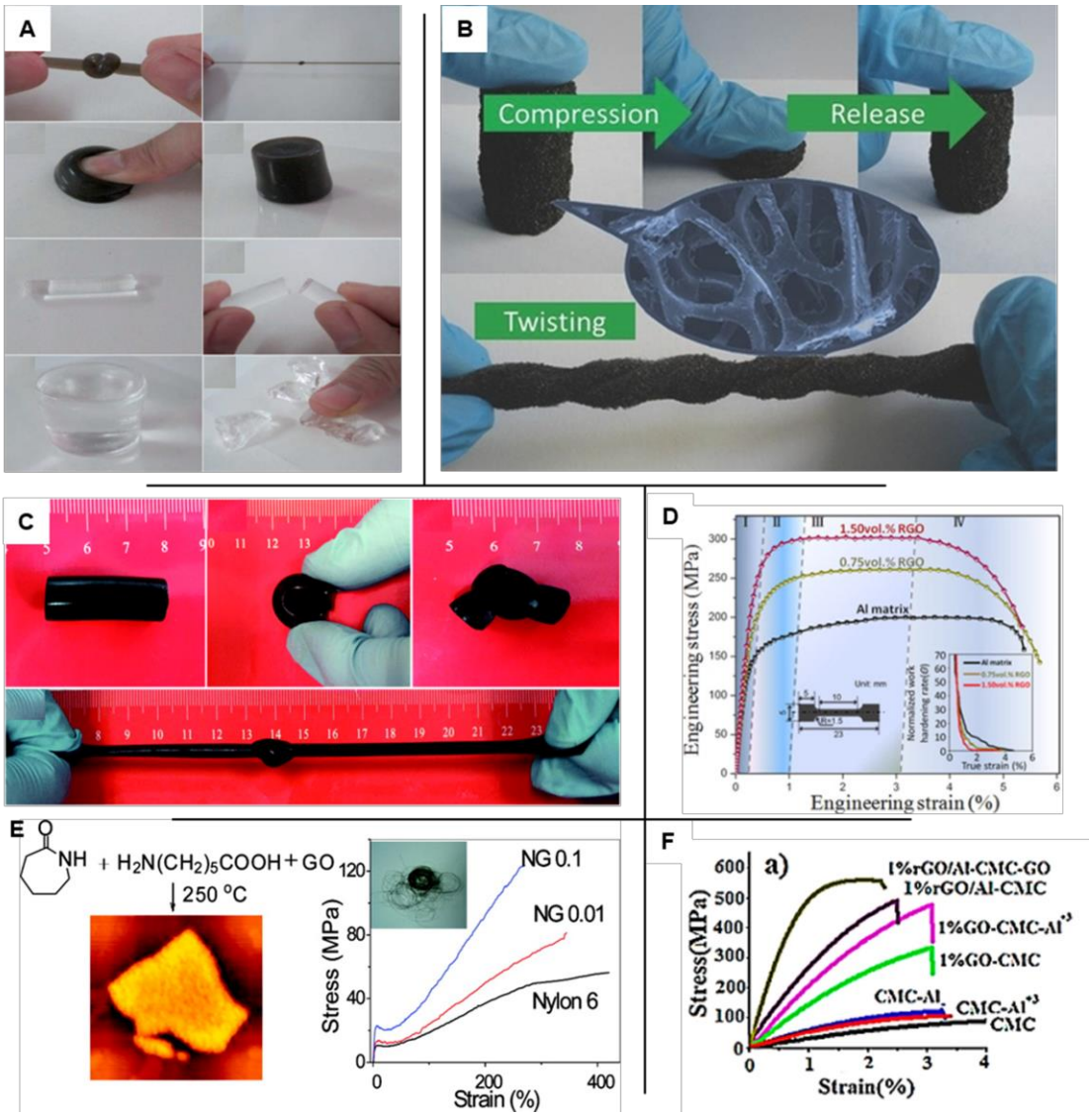

Figure 1.12. A-F) Digital images and strain-stress curve represented the mechanical reinforcement of various polymeric material and metal composites including polyacrylamide, nylon polymer, Al matrix composites after incorporation of graphene oxide into the material matrix. Reprinted with permission from *J. Mater. Chem*., 2012, **22**, 14160. Royal Society of Chemistry (A). Reprinted with permission from *Adv. Mater*., 2013, **25**, 5658. Copyright 2013 Wiley-VCH (B). Reproduce with permission from *J. Mater. Chem. A,* 2015, **3**, 17445. Copyright 2016, Royal Society of Chemistry (C). with permission from *Nano Lett.,* 2015, **12**, 8077. Copyright 2015, American Chemical Society (D). Reproduce with permission from *Macromolecules,* 2010, **16**, 6716. Copyright 2010, American Chemical Society (E). Reproduce with permission from *ACS Nano,* 2017, **11**, 5717. Copyright 2017, American Chemical Society (F).

Moreover, it was found that a single-layer GO has a larger young's modulus than the thick GO sheet. Gomez-Navarro *et al*, revealed that single-layer GO has an average young's

modulus value of ~250 GPa.[142] Zheng *et al,* have indicated that young's modulus of the graphene oxide significantly deteriorate with increasing the degree of functionalization and molecular structure of functional groups are also profound factor in the mechanical performance of GO.[143] It was also found the different functional sides and large aspect ratio of graphene oxide sheets significantly enhanced interfacial bonding between the graphene oxide sheets and the matrix which lead to improving the mechanical performance of the overall material. Furthermore, GO can be re-converted into the graphene-like structure by removing oxygen-containing groups by associating the reduction process. The reduced graphene oxide (RGO) has comparable mechanical, conductive and thermal properties to pristine graphene.[144,145] Therefore, GO and RGO have been used extensively to improve the mechanical property of different functional materials. Even a very little doping of GO and RGO can able to dramatically improve the mechanical strength of different composite materials such as polymer, cement composites, metal and metal oxide nanocomposites (Figure 1.12).[98,145-146]

In 2009, Chen and co-workers incorporated GO into the PVA (Polyvinyl alcohol) hydrogel which reinforce its mechanical durability where graphene oxide form strong H-bonding interactions through its carboxyl, hydroxyl and epoxide groups with the hydroxyl groups of Polyvinyl alcohol. A 62% increase in Young's modulus and 76% improvement in tensile strength were obtained after introducing a very low amount of graphene oxide (0.7 wt%) into a PVA matrix.[147] Xu *et al,* also revalidated that adequate doping of graphene oxide (0.1 wt%) enhanced both the tensile strength and Young's modulus more than two folds of the nylon-6 fibres.[148] In 2013, Tian *et al,* fabricated covalent crosslinked ultra-strong paper (178.9 MPa of tensile strength and 84.8 GPa of Young's modulus) of polydopamine coated graphene oxide and Polyethylenimine composite.[149] Graphene oxide has the ability of mechanical reinforcement not only for polymer material but also to metal or metal oxides where functional sites of graphene oxide form chemical bonds with metal oxides or metal ions which lead to the homogeneous dispersion of graphene oxides in the metal matrix. Hwang *et al,* reported that the elastic modulus and the yield strength of the Cu matrix were increased by 30% and 80% respectively after the incorporation of 2.5 vol% of RGO through the molecular-level doping process.[150] Concrete is the most important material in the construction industry and in 2018, Sriwong *et al,* revealed that mechanical reinforcement of concrete composites was also be obtained after the incorporation of RGO. It was found that compressive strength (146%) and flexural strength (79.5%) of RGO-concrete composite were

increased significantly compared to the pure one which makes this concrete composite more relevant for practical application.[151] GO was also extensively used to developed bio-inspired artificial nacre nanocomposite with extraordinary mechanical strength.[152] For instance, Woo *et al,* reported nacre-mimetic chemically cross-linked GO and p-diaminophenyl composite where GO act as a brick and cross-linking agent p-diaminophenyl act as a mortar. Because of the excellent tensile strength (142.9 MPa), tensile modulus (4.7 GPa) and hardness (917.4 MPa), this material was very useful in different practical applications.[153] Graphene oxide was also used in artificial bone regeneration and tissue engineering because of its good biocompatibility and excellent mechanical strength. Xue *et al,* developed multilayered graphene oxide and chitosan-based biomaterials with excellent strength and toughness by adopting a "brick and mortar" layered structure.[154] Recently, graphene oxide is widely used to develop different kinds of advance stretchable and robust electronics. For example, Cao and coworkers developed stretchable supercapacitor electrode material by using reduced graphene oxide (RGO) and titanium carbide MXene based composite. Generally, pure titanium carbide MXene electrode is brittle in nature and it can be broken and creaked during bending or application of tensile strength which decrease its electrochemical performance. But, MXene/RGO composite electrode can able to retain its electrical conductivity even after 300% of uniaxially and 200% × 200% of biaxially tensile strains for several times.[155]

Therefore, undoubtedly, graphene or graphene oxide sheets can be used to improve the mechanical durability of various kinds of material and it will pave the way for the development of different smart materials in near future.

1.7. Strategic use of graphene oxide in various applications

Graphene or graphene oxide is not only utilized for mechanical reinforcement of the material but it also has the ability to provide various kinds of different properties in material such as electronic, electrochemical, thermal and catalytic properties which give an opportunity to developed different advanced materials.[130,156] From the last decads, metal-organic frameworks (MOF) are used for its excellent gas absorption capacity because of its high porosity and large surface area. It was found that GO can able to further enhance the gas absorption ability of MOF.[157] For instance, Kumar *et al,* reported that CO_2 uptake capacity of ZIF-8 MOF can be increased significantly after the strategic association of GO where the surface area and porosity of ZIF-8/GO composite are increased significantly on changing the GO concentration. GO also provide different active binding sites with the absorbed gas molecule

which also increase the gas storage capacity of the composite material.[158] GO also acts as a good carrier of different bioactive molecules or drugs for potential biomedical applications because of its large surface area (the theoretical specific surface area of graphene is 2600 g/m^2), different functional groups and bio-compatibility.[159,162] In addition, RGO can also adsorb small polymers, proteins and nanoparticle in its surface through strong van der Waal interaction which make it potential drug delivery system.[160] Wang *et al,* developed doxorubicin-loaded gold nanoclusters anchored RGO nanocomposite which was used to inhibited HepG2 cells. Gold nanoclusters–RGO nanocomposite was also capable to carry proteins and DNA to the cancer cell.[161] Graphene oxide can be easily functionalized where the different active catalytic groups on the graphene sheets allowed to development of a metal-free heterogeneous catalyst for selective chemical reactions.[162] Graphene sheets also possess high electron mobility of 2.5 × 105 $cm^2V^{-1}s^{-1}$, which provided the basis for developing active nanoelectrocatalysts.[163] Li *et al,* prepared the Pt nano clusters-graphene nanocomposites for fuel cell application.[164] Ajayan and coworkers developed platinum nanoparticles anchored reduced graphene oxide for electro-oxidation of methanol.[165] For high conductivity, mechanical flexibility and chemical durability, graphene or reduce graphene oxide has a huge potential in energy storage application. Recently, Zhang *et al,* introduced highly redox-active sodium anthraquinone-2-sulfonate and graphene composite to be used as an anode in high-performance supercapacitors. It achieved a high volumetric specific capacitance of 650 Fcm^{-3} which was much better than pure sodium anthraquinone-2-sulfonate electrode.[166] Huang *et al,* developed graphene oxide/polyvinyl alcohol composite gel-based solid-state electrolytic system for flexible double layer supercapacitor. Graphene oxide provides good mechanical properties, thermal stability and flexibility of the electrolyte nanocomposite.[167] In 2018, Li *et al,* developed graphene aerogel with high electrical conductivity which was utilized for pressure and strain sensors. This graphene aerogel showed high elasticity, good fatigue-resistant performance and it was able to detect a very small amount of pressure (sensitivity of 0.18 kPa^{-1}) and various human body movements such as wrist pulse pressure, wrist and finger bending.[168] Besides, Rodrigues *et al,* fabricated piezoelectric material based on single-layer graphene, the piezoelectric effect was observed to be much higher (1.4 nmV^{-1}) than the conventional piezoelectric material.[169] Among its all fascinating property, the high thermal conductivity of graphene-based material grabbed the attention of many research groups. The thermal conductivity of the graphene is between 1500 and 5000 $Wm^{-1}K^{-1}$ at room temperature which can be further increased in presence of

strain.[170-171] Recently, graphene-based materials have been used to fabricate a low-cost and energy-efficient water distillation application. Monolayer graphene can absorb only 2.3 % of incident visible light, but three-dimensional graphene material appeared as an efficient light absorbent.[190] Li *et al,* developed 3D-printed porous material by using graphene oxide and graphene nanotube which was capable of broadband solar absorption (>97%) and achieved excellent efficiency for the conversion of solar energy into steam.[172] Taking one step further, Lou *et al,* fabricate TiO_2 and reduce graphene oxide composite material which can produce clean water from polluted water under sunlight irradiation. Reduce graphene oxide absorbed the solar energy and convert it to heat for water evaporation whereas TiO_2 photo-catalytically degraded the organic contamination of the water medium.[173] Furthermore, graphene-based materials have been used for crude oil-water separation. For instance, Liu *et al,* demonstrated the de-emulsification of the heavy crude oil-in-water emulsion by using graphene oxide sheets. Graphene oxide nanosheet has a large surface area and it can form both n-π and π-π interactions with asphaltenes and resins which are present in crude oil and this interaction help to phase separate crude oil from the crude oil-in-water emulsion.[174] In 2017, Ge *et al,* fabricated an oleophilic reduce graphene oxide wrapped porous substate to separate highly viscous crude oil (10^3 to 10^5 mPa s at room temperature) from the water medium by adopting the Joule-heating process. After the application of electric voltage to the material, current flows which heat up the material. The hot RGO wrapped porous material reduces the viscosity of the circumambient crude oil and increase its oil absorption speed significantly.[175] Moreover, various other advanced materials based on graphene have been developed in the last decades such as actuators, biological sensors, microbial fuel cells, solar cells and different energy storage materials.[176]

1.8. Graphene-based bio-inspired super wetting material

1.8.1. Wettability of graphene

In the conventional artificial superhydrophobic and underwater superoleophobic interfaces are mostly liable to the destruction in harsh physical insults and prolong chemical exposure. Graphene-based material can be used to address the durability issue because of its excellent mechanical property and chemical stability. Besides, the incorporation of graphene-based material into the anti-wetting interface can also be useful in diverse potential applications including catalysis, electronics and various relevant biological application.

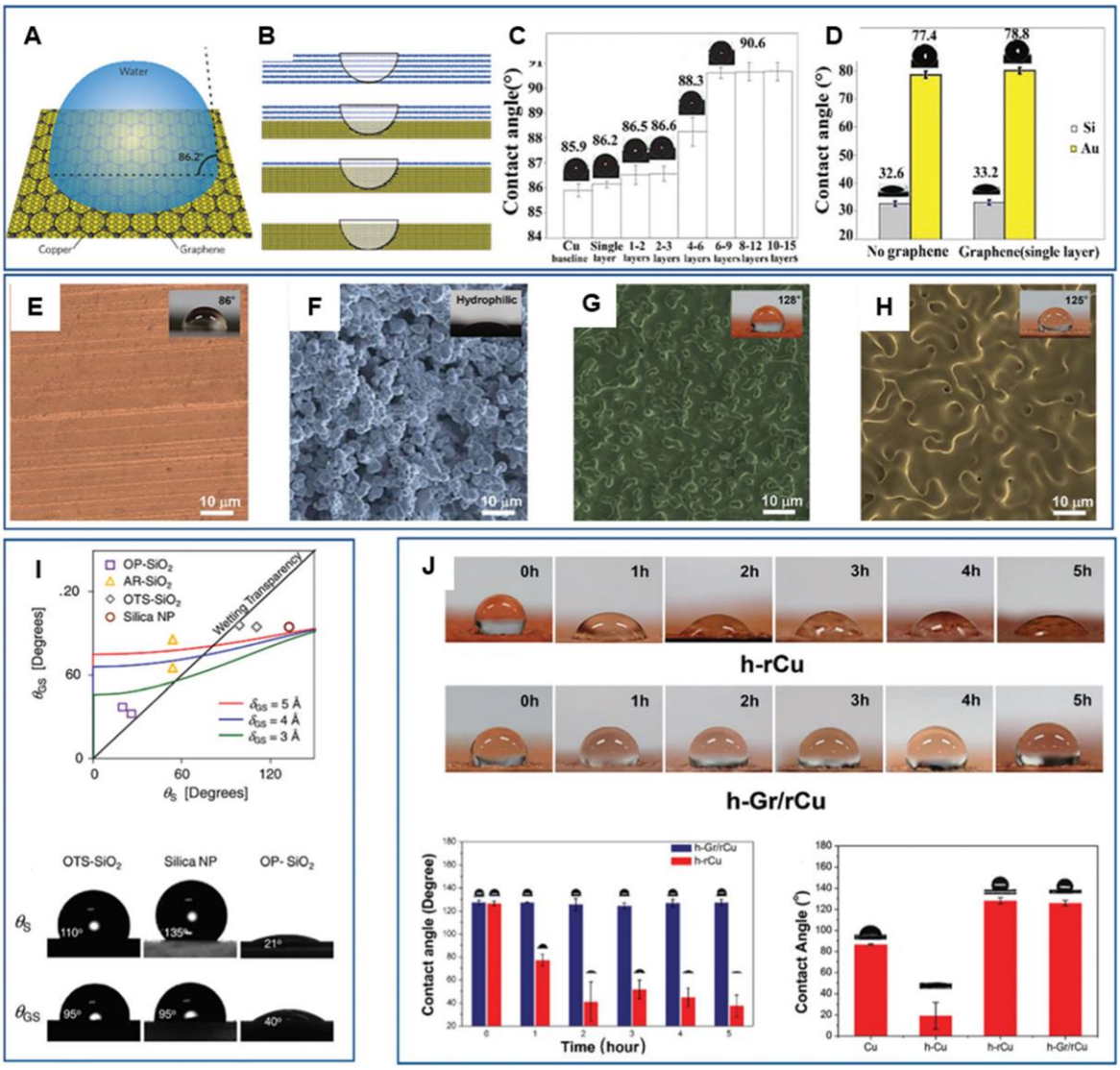

Figure 1.13. A) A water droplet on a copper substrate coated with a single layer of graphene giving rise to a contact angle of 86.2°. B) Depicting the Increasing number of graphene layers on the copper substrate. C) After gradually covering a series of graphene layers on a copper substrate, the contact angle values of water droplets on the graphene layer were measured in order. D) Contact angle measurements for Si substrate and Au substrate with and without a single layer graphene, where the contact angle values for the Si substrate and Au substrate were in good agreement with that for the graphene-coated Si and Au substrate. E-H) Scanning electron microscopy (SEM) images of: (E) pure copper substrate (Cu), (F) electroplated copper substrate (h-Cu), (G) electroplated and thermal annealed copper substrate (h-rCu), (H) electroplated and thermal annealed copper substrate coated with a monolayer graphene coating (h-Gr/rCu) by an in situ growth method. The illustrations show the contact angle value of water on each substrate. (I) The contact angle of a substrate coated with a single layer of graphene as a function of contact angle of the bare substrate. These substrates include OP-SiO_2, AR-SiO_2, OTS-SiO_2, silica NP. (J) When both h-rCu and h-Gr/rCu were immersed in the brine solution, the contact angle of h-Gr/rCu remained almost unchanged, which indicated that graphene could serve as a corrosion-resistant coating for the protective substrate. Reprinted with permission from *Nanoscale Horiz.,* 2019, **4,** 339. Copyright 2019, Royal Society of Chemistry.

In 2013, Taherian *et al,* calculated the water contact angle on the graphene sheets by using classical molecular dynamics simulations and revealed the hydrophobic property of monolayer graphene with a contact angle of 90−100° (Figure 1.13A-D).[177] On the other hand,

graphene oxide is hydrophilic in nature and its wettability is mainly dependent on the various levels of oxidization. However, the water contact angle of graphene depends on various factors such as morphology, defects, doping and external electric field etc (Figure 1.13E-J).[178] Nevertheless, the monolayer graphene sheet can not change the wetting behaviour of different substrates including gold, copper, silicon and rather showing wetting transparency.[179] But this wetting transparency of the graphene sheet disappears with increasing the thickness of graphene layer coating. In 2010, Rafiee *et al,* reported that a thick microstructured coating of graphene sheets could be able to significantly change the wetting property of the selected substrates. The wetting behaviour of their graphene-based coating was able to tune from superhydrophilic to superhydrophobic through appropriate solvent treatment.[180] Recently, Ding *et al,* developed superhydrophobic open-cell microsphere structured graphene film via pickering emulsion followed by vapour ejection. This superhydrophobic material was capable of ultrafast switching of its wettability to superhydrophilicity within a second through introducing an oxygen-containing group by plasma treatment. It was also capable of restoring its superhydrophobicity after the application of Joule heating to remove all the functional groups and this reversible transition cycle could be repeated at least ten times.[181] Huang *et al,* explored the reversible switching of graphene film from superhydrophobicity to superhydrophilicity under alternative UV irradiation and dark environment. It was found that the adsorbed oxygen molecules in the defect of graphene sheets are excited from triplet ground spin state to energized singlet spin state under UV illumination which leads to adherence of hydroxyl groups and water molecules to the graphene sheets and during dark environment, graphene film returns to its previous superhydrophobic state.[182] Surface functionalization is also an effective way to fabricate superwettable graphene-based material. Xue *et al,* fabricated superhydrophobic POSS (polyhedral oligomeric silsesquioxane) functionalized graphene oxide powder for liquid marble application.[183] Similarly, Lin *et al,* also changed the hydrophilic graphene oxide into superhydrophobic interface through covalent functionalization of low surface energy molecule i.e., octadecylamine.[184] Besides, the chemically exfoliated hydrophilic graphene oxide was widely used to fabricate fish-scale inspired underwater superoleophobic interface. For example, Liu *et al,* developed microstructured graphene oxide film coated metal mesh which was showing underwater superoleophobicity with vegetable oil contact angle above 150°.[185]

1.8.2. Graphene-based super wetting material for different applications

The incorporation of graphene (or graphene oxide) would not only help to pave the pathway for mechanical durable, chemical and thermally stable superhydrophobic or underwater superoleophobic material but also open up the possibilities of designing new smart materials for other novel applications.[176]

In the last two decades, graphene and its derivatives have been utilized in smart conducting materials for different applications such as energy harvesting, energy storage and motion sensor etc. Despite notable progress, the practical application of these materials was limited for their lack of stability in wet environments such as underwater, human sweat, rain and soapy water. The introduction of superhydrophobic properties into these materials would help in eliminating the influence of water. For example, Das *et al,* fabricated water repellent inkjet printed flexible graphene-based electronic which showed superhydrophobic property with water contact angle ~157.2° and sheet resistance of 1.1 kΩ □$^{-1}$.[193] Direct-pulsed laser writing technique was strategically used to change the surface wettability of graphene film from hydrophilic (water contact angle of 47.7°) to superhydrophobic through removing the oxygen-containing groups and generating micro-nano scale roughness on the graphene surface. Further, this strategy inspired to development of self-cleanable, wearable and washable conductive materials for various applications.[193] Ding *et al,* fabricated superhydrophobic PDMS/open-cell graphene composite material to design an underwater motion sensor (Figure 1.14B). Superhydrophobicity prevented water penetration into the material. Moreover, the Graphene layer along with the trapped air could be easily compressed by a very little amount of water pressure which decrease its resistance. Thus, various kinds of motion such as depth of the water, horizontal movement and movement speed underwater could be monitored very precisely.[194] Next, Zu *et al,* developed a superhydrophobic multifunctional sensor that could sense strain, temperature, pressure with high sensitivity (Figure 1.14C). They prepared highly durable and compressible triple-network nanostructured reduce graphene aerogel by covalent crosslinking with three different organosilanes. This material was able to sense a wide range of temperatures from 20°C to 100°C. The electrical conductance (G) was increasing with increasing the temperature (T) which can be explained by the following equation:

$$G = G_h \cdot \exp(-H/T^{1/3}) + G_t$$

Where H, G_t and G_h represent the hopping parameter, the contribution of the quantum tunnelling and temperature-independent prefactor respectively.

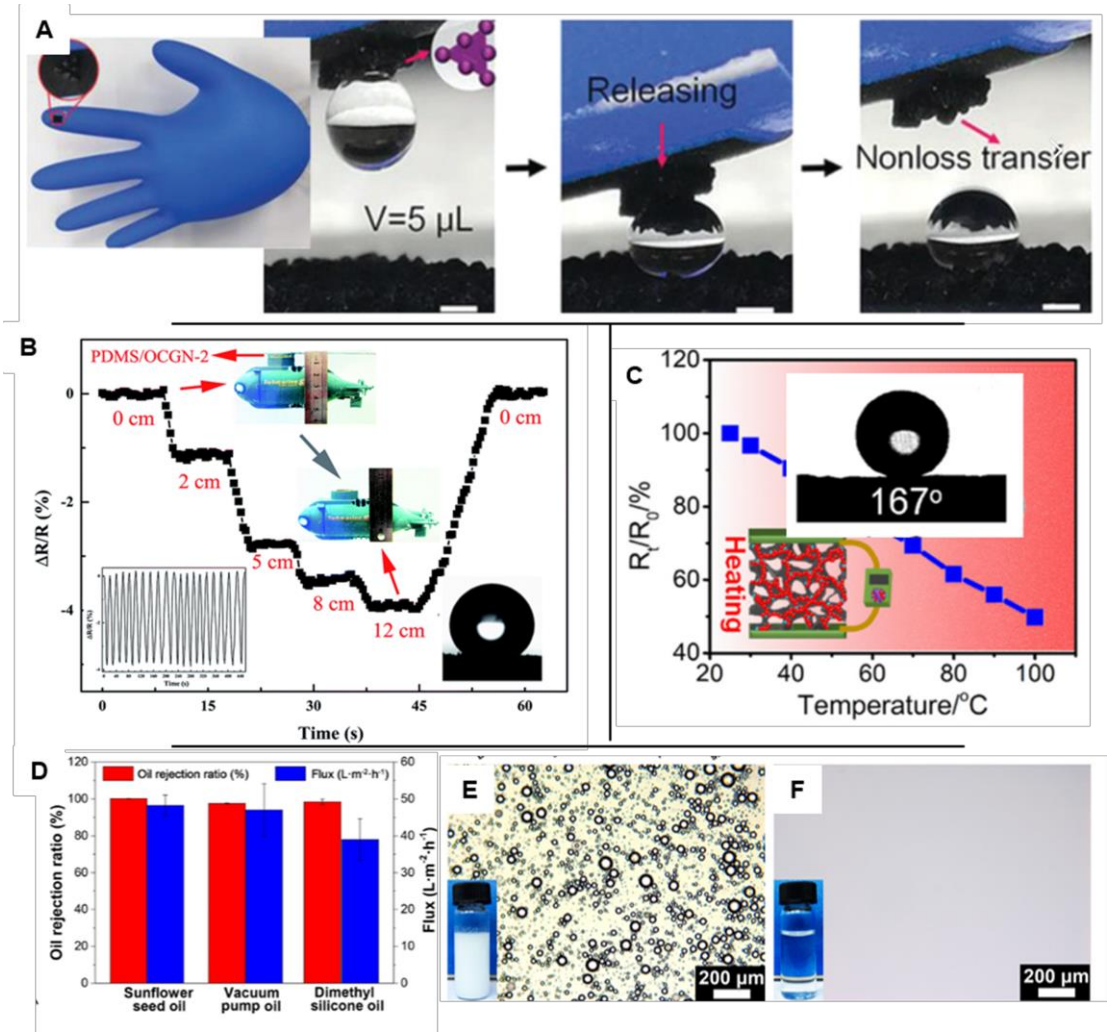

Figure 1.14. A) Application of rose petal-inspired adhesive superhydrophobic interface made from graphene oxide papillae arrays for aquous droplet manipulation (scale bar 1 mm). B) The change in ΔR/R of graphene based superhydrophobic interface during the diving and floating processes. C) Graphene based tempareture sensor where resistance of the material was changed with increasing the tempareture. D-F) Graphene based underwater superoleophobic membrane for water-in-oil emulsion separation and dye separation. Reprinted with permission from *Adv. Funct. Mater.* 2019, **29**, 1900266. Copyright 2019, Wiley-VCH (A). Reprinted with permission from *J. Mater. Chem. A*, 2019,**7**, 17766. Copyright 2019, Royal Society of Chemistry (B). Reprinted with permission from *Chem. Mater.* 2019, **31**, 16, 6276. Copyright 2019, American Chemical Society (C). Reprinted with permission from *ACS Sustainable Chem. Eng.* 2019, **7**, 15, 13379. Copyright 2016, American Chemical Society (D-F).

This material was also capable of 80% compression and it came back to its original shape after removal of pressure without any physical fracture and it remained superhydrophobic. Electrical resistance was decreased remarkably with increasing compressive strain and it could measure a wide range of pressure precisely (0-110 kPa). Superhydrophobicity provided good durability in a high humid environment (20-90%).[195] Yang *et al,* fabricated superhydrophobic wearable reduce graphene oxide graphene-based supercapacitor. It showed

high capacitive performance even after 1000 cycle charge-discharge cycle underwater and standard waterproof spraying test.[196] Recently, Thekkekara *et al*, also reported a stretchable superhydrophobic laser printed graphene-based supercapacitor. The areal capacitance of the supercapacitor remains unaltered after immersed in hot water at 90°C. Even more, it was retained its 80 % capacitance after 50 cycles of washing test.[197] Thus, these reports motivated to development of next-generation water-proof electronic devices. In 2014, Jiang reported a graphene-based superhydrophobic interface with highly ordered nano-scale roughness which can produce structural color similar to that of butterfly wings and it will be useful in various optoelectronic applications.[198] Tan *et al,* reported rose petal inspired adhesive superhydrophobic interface by using modified and wrinkled graphene oxide structures to create a hierarchical morphology and this interface was used for lossless water droplet manipulation (Figure 1.14.A).[199] Furthermore, graphene or graphene oxide has been used to produce reed leaf-like grooved structures or spider silk-like spindle knots, with the liquid-repellent property which could be useful in water harvesting and cloud seeding application.[200-203] Moreover, the hydrophilic nature of graphene oxide was further exploited to fabricate fish-scale inspired underwater superoleophobic interface. Ou *et al,* fabricated underwater superoleophobic membrane by using chitin nanocrystals modified by dopamine/graphene oxide composite. This membrane was efficient for oil-water separation and dye absorption (both cationic and anionic) from the water phase (Figure 1.14D-F).[204] Therefore, owing to various intrinsic properties of graphene or graphene oxide, graphene-based anti-wetting materials were able to induce interesting applications in the different research fields. But, in the previous reported graphene-based anti wetting material, graphene sheets were physically incorporated into most of the material and the physical and chemical durability remained as a major challenge before in outdoor application.[191,192]

1.9. Objectives and motivation

The optimization of both essential hierarchical topography and surface chemistry remained a fundamental basis for designing both the lotus leaf-inspired and the fish scale-mimicked interface. In the last two decades, graphene and graphene oxide have been explored widely to enhance the physical durability and chemical stability of various kinds of material. In addition, graphene-based materials are well known for various diverse properties such as catalytic, electrical and thermal properties. Thus, graphene oxide-based durable super wetting

interfaces will be able to open new scopes of developing advanced material for different potential applications.

In the past, various approaches have been associated to incorporate GO, where the lack of covalent integration of GO remained a major concern for the survival of embedded super-wettability in harsh settings. In this thesis work, a common and facile synthetic approach was adopted, where amine-functionalized graphene oxide (AGO) and chemically reactive polymeric nano-complexes (CRPNC) have been strategically integrated following the 1,4-conjugate addition reaction at ambient conditions. The appropriate covalent integration of CRPNC and AGO would be allowed to achieve a single platform for tailoring different and durable bio-inspired wettability. The embedded superwettability would be capable of self-healing of physical damage. Such extremely durable anti-wetting interfaces are very useful in energy-efficient oil-water separation in practical harsh conditions. Moreover, the graphene-based anti-wetting interface can be extended to develop various other advanced materials.

1.10 Reference

1. X. Feng and L. Jiang, *Adv. Mater.,* 2006, **18**, 3063.
2. Y. Y. Yan, N. Gao and W. Barthlott, *Adv. Colloid. Interface Sci.,* 2011, **169**, 80.
3. S. Wang, K. Liu, X. Yao and L. Jiang, *Chem. Rev.,* 2015, **115**, 8230.
4. M. Liu, S. Wang and L. Jiang, *Nat. Rev. Mater.*, 2017, **2**, 17036.
5. Y. Si, Z. Dong and L. Jiang, *ACS Cent. Sci*., 2018, **4**, 1102.
6. R. J. Archer, B. Becher-Nienhaus, G. J. Dunderdale and A. Hozumi, *Adv. Funct. Mater.,* 2020*,* **30**, 1907772
7. Y. Sunab and Z. Guo, *Nanoscale Horiz.,* 2019, **4**, 52.
8. M. Villegas, Y. Zhang, N. A. Jarad, L. Soleymani and T. F. Didar, *ACS Nano*, 2019, **13**, 8517.
9. X. Chen, G. Wen and Z. Guo, *Mater. Horiz.,* 2020, **7**, 1697.
10. S. Peppou-Chapman, J. K. Hong, A. Waterhouse and C. Neto, *Chem. Soc. Rev.*, 2020, **49**, 3688.
11. L. Wen, Y. Tian and L. Jiang, *Angew. Chem. Int. Ed.,* 2015, **9**, 3387.
12. C. Howell, A. Grinthal, S. Sunny, M. Aizenberg and J. Aizenberg, *Adv. Mater.,* 2018*,* **30***,* 1802724.
13. X. -M. Li, D. Reinhoudt and M. Crego-Calama, *Chem. Soc. Rev*., 2007, **36**, 1350.
14. J. Yong, F. Chen, Q. Yang J. Huo and X. Hou, *Chem. Soc. Rev*., 2017, **46**, 4168.

15. Y. Wei, H. Qi, X. Gong, and S. Zhao, *Adv. Mater. Interfaces,* 2018, **5**, 1800576.
16. S. Li, J. Huang, Z. Chen, G. Chen and Y. Lai, *J. Mater. Chem. A*, 2017, **5**, 31.
17. J. T. Korhonen, T. Huhtamäki, O. Ikkala, and R. H. A. Ras, *Langmuir,* 2013, **29**, 3858.
18. N. Nuraje, W. S. Khan, Y. Lei, M. Ceylan and R. Asmatulu, *J. Mater. Chem. A,* 2013, **1**, 1929.
19. E. A. Vogler, Adv. *Colloid Interface Sci.,* 1998, **74**, 69.
20. B. Su, Y. Tian and L. Jiang, *J. Am. Chem. Soc.,* 2016, **138**, 1727.
21. T. Darmanin and F. Guittard, *Mat. Today,* 2015, **18**, 273.
22. W. Barthlott, M. Mail and C. Neinhuis, *Phil. Trans. R. Soc.A,* 2016, **374**, 20160191.
23. A. B. D. Cassie and S. Baxter, *Trans. Faraday Soc.,* 1944, **40**, 546.
24. W. Barthlott and C. Neinhuis, *Planta,* 1997, **202**, 1.
25. (a) K. Koch, B. Bhushan, Y. C. Jung and W. Barthlott, *Soft Matter,* 2009, **5**, 1386; (b) L. Gao and T. J. McCarthy, *Langmuir*, 2006, **22,** 2966.
26. A. R. Parker and C. R. Lawrence, *Nature*, 2001, **414**, 33.
27. K. Autumn, Y. A. Liang, S. T. Hsieh, W. Zesch, W. P. Chan, T. W. Kenny, R. Fearing and R. J. Full, *Nature*, 2000, **405**, 681.
28. K. Autumn, M. Sitti, Y. A. Liang, A. M. Peattie, W. R. Hansen, S. Sponberg, T. W. Kenny, R. Fearing, J. N. Israelachvili and R. J. Full, P*roc. Natl. Acad. Sci. U. S. A.*, 2002, **99**, 12252.
29. L. Feng, S. Li, Y. Li, H. Li, L. Zhang, J. Zhai, Y. Song, B. Liu, L. Jiang and D. Zhu, *Adv. Mater*., 2002, **14**, 1857.
30. Y. Zheng, X. Gao and L. Jiang, *Soft Matter*, 2007, **3**, 178.
31. L. Feng, Y. A. Zhang, J. M. Xi, Y. Zhu, N. Wang, F. Xia and L. Jiang, *Langmuir*, 2008, **24**, 4114.
32. M. Liu, S. Wang, Z. Wei, Y. Song and L. Jiang, *Adv. Mater*., 2009, **21**, 665.
33. Q. Cheng, M. Li, Y. Zheng, B. Su, S. Wang and L. Jiang, *Soft Matter*, 2011, **7**, 5948.
34. Y. Cai, L. Lin , Z. Xue , M. Liu , S. Wang and L. Jiang, *Adv. Funct. Mater.,* 2014, **24**, 809.
35. Y. Cai, Q. Lu, X. Guo, S. Wang, J. Qiao and L. Jiang, *Adv. Mater*., 2015, **27**, 4162.

36. A. Shome, A. M. Rather and U. Manna, *J. Mater. Chem. A*, 2018, **6**, 22465.
37. T. Young, *Philos. Trans. R. Soc. London*, 1805, **95**, 65.
38. W. A. Zisman, *Ind. Eng. Chem*., 1963, **55**, 18.
39. R. N. Wenzel, *Ind. Eng. Chem*., 1936, **28**, 988.
40. A. B. D. Cassie and S. Baxter, *Trans. Faraday Soc*., 1944, **40**, 546.
41. S. Zarghami, T. Mohammadi, M. Sadrzadeh and B. van der Bruggen, *Prog. Polym. Sci*., 2019, **98**, 101166.
42. L. Feng, S. H. Li, Y. S. Li, H. J. Li, L. J. Zhang, J. Zhai, Y. L. Song, B. Q. Liu, L. Jiang and D. B. Zhu, *Adv. Mater*., 2002, **14**, 1857.
43. L. Wen, Y. Tian and L. Jiang, *Angew. Chem. Int. Ed*., 2015, **54**, 3387.
44. T. Darmanin and F. Guittard, *J. Mater. Chem. A*, 2014, **2**, 16319.
45. Y. Lu, S. Sathasivam, J. Song, C. R. Crick, C. J. Carmalt and I. P. Parkin, *Science*, 2015, **347**, 1132.
46. F. Zhang, L. Zhao, H. Chen, S. Xu, D. G. Evans and X. Duan, *Angew. Chem. Int. Ed.*, 2008, **47**, 2466.
47. P. Tourkine,M. Le Merrer and D. Qur, *Langmuir,* 2009, **25**, 7214.
48. S. T. Yohe, Y. L. Colson and M. W. Grinstaff, *J. Am. Chem. Soc.,* 2012, **134**, 2016.
49. D. Wang, H. Liu, J. Yang and S. Zhou, *ACS Appl. Mater. Interfaces,* 2019, **11**, 1353.
50. L. Chen, M. Liu, H. Bai, P. Chen, F. Xia, Dong Han and Lei Jiang, *J. Am. Chem. Soc.,* 2009, **131**, 10467.
51. B. Su, S. Wang, Y. Song and L. Jiang, *Soft Matter*, 2011, **7**, 5144.
52. Z. Xue, Y.Cao, N.Liu, L.Feng and L. Jiang, *J. Mater. Chem. A,* 2014, **2**, 2445.
53. B. Wang, W. Liang, Z. Guo and W. Liu, *Chem. Soc. Rev.,* 2015, **44**, 336.
54. Z. Chu, Y. Feng and S. Seeger, *Angew. Chem. Int. Ed.,* 2015, **54**, 2328.
55. R. K. Gupta, G. J. Dunderdale, M. W. England and A. Hozumi, *J. Mater. Chem. A*, 2017, **5**, 16025.
56. E. Stokstad, *Science,* 2010, **328**, 1618.
57. J. L. Schnoor, *Environ. Sci. Technol.,* 2010, **44**, 4833.
58. T. J. Crone and M. Tolstoy, *Science,* 2010, **330**, 634.

59. C. P. D. Brussaard, L. Peperzak, S. Beggah, L. Y. Wick, B. Wuerz, J. Weber, J. S. Arey, B. Burg, A. Jonas, J. Huisman and J. R. Meer, *Nat. Commun.,* 2016, **7**, 11206.
60. R. K. Gupta, G. J. Dunderdale, M. W. England and A. Hozumi, *J. Mater. Chem. A*, 2017, **5**, 16025.
61. S. Kleindienst, J. H. Paul and S. B. Joye, *Nat. Rev. Micro*., 2015, **13**, 388.
62. J. F. Rasmussen, S.Wegeberg and K. Gustavson, *Water Air Soil Pollut.,* 2015, **226**, 329.
63. L. Feng, Z. Y. Zhang, Z. H. Mai, Y. M. Ma, B. Q. Liu, L. Jiang and D. B. Zhu, *Angew. Chem. Int. Ed.,* 2004, **43**, 2012.
64. X. Gui, J. Wei, K. Wang, A. Cao, H. Zhu, Y. Jia, Q. Shu and D. Wu, *Adv. Mater*., 2010, **22**, 617.
65. B. Li, L. Li, L. Wu, J. Zhang and A. Wang, *Chem. Plus Chem*., 2014, **79**, 850.
66. Z. Xue, S. Wang, L. Lin, L. Chen, M. Liu, L. Feng and L. Jiang, *Adv. Mater*., 2011, **23**, 4270.
67. Z. Chu, Y. Feng and S. Seeger, *Angew. Chem. Int. Ed*., 2015, **54**, 2328.
68. Z. Shi, W. Zhang, F. Zhang, X. Liu, D. Wang, J. Jin and L. Jiang, *Adv. Mater.,* 2013, **25**, 2422.
69. D. Li, A. Wu, G. Xu, H. Lai, Z. Cheng and Y. Liu, *Langmuir*, 2016, **32**, 13493.
70. Z. Wang, X. Jiang, X. Cheng, C. H. Lau and L. Shao, *ACS Appl. Mater.* Interfaces, 2015, **7**, 9534.
71. C. R. Crick, J. A. Gibbons and I. P. Parkin, *J. Mater. Chem. A,* 2013, **1**, 5943.
72. X. Y. Zhou, Z. Z. Zhang, X. H. Xu, F. Guo, X. T. Zhu, X. H. Men and B. Ge, *ACS Appl. Mater. Interfaces*, 2013, **5**, 7208.
73. Z. Wang, Y. Wang and G. Liu, *Angew. Chem., Int. Ed*., 2016, **55**, 1291.
74. B. Wang and Z. G. Guo, *Chem. Commun*., 2013, **49**, 9416.
75. J. Osicka, M. Ilcikovaˇ, A. Popelka, J. Filip, T. Bertok, J. Tkac and P. Kasak, *Langmuir,* 2016, **32**, 5491.
76. Z. Han, B. Li, Z. Mu, S. Niu, J. Zhang and L. Ren, *Small*, 2017, **13**, 1701121.
77. C. Zhou, Z. Chen, H. Yang, K. Hou, X. Zeng, Y. Zheng and J. Cheng, ACS Appl. *Mater. Interfaces,* 2017, **9**, 9184.
78. G. Kwak, M. Lee and K. Yong, *Langmuir,* 2010, **26**, 9964.

79. K. Uosaki, M. E. Quayum, S. Nihonyanagi and T. Kondo, *Langmuir*, 2004, ***20***, 1207.
80. H. Sugimura, K. Ushiyama, A. Hozumi and O. Takai, *Langmuir*, 2000, **16**, 885.
81. G. Kwak, M. Lee and K. Yong, *Langmuir*, 2010, **26**, 9964.
82. T. Verho, C. Bower, P. Andrew, S. Franssila, O. Ikkala and R. H. A. Ras, *Adv. Mater*., 2011, **23**, 673.
83. C. H. Xue and J.-Z. Ma, *J. Mater. Chem. A*, 2013, **1**, 4146.
84. S. Zarghami, T. Mohammadi, M. Sadrzadeh and B. van der Bruggen, *Prog. Polym. Sci.,* 2019, **98**, 101166.
85. X. Zhu, Z. Zhang, X. Men, J. Yang, K. Wang, X. Xu, X. Zhou and Q. Xue, *J. Mater. Chem*., 2011, **21**, 15793.
86. J. Yang, Z. Z. Zhang, X. H. Men, X. H. Xu and X. T. Zhu, *Colloids Surf., A,* 2010, **367**, 60.
87. Y. Li, L. Li and J. Sun, *Angew. Chem., Int. Ed.,* 2010, **49**, 6129.
88. (a) L. Lonov and A. Synytska, Phys. *Chem. Chem. Phys.,* 2012, **14**, 10497; (b) H. X. Wang, Y. H. Xue, J. Ding, L. F. Feng, X. G. Wang and T. Lin, *Angew. Chem., Int. Ed.,* 2011, **50,** 11433.
89. Y. Li, Z. Zhang, M. Wang, X. Men and Q. Xuea, *J. Mater. Chem. A,* 2017, **5**, 20277.
90. T. Lv, Z. Cheng, E. Zhang, H. Kang, Y. Liu and L. Jiang, *Small*, 2017, **13**, 1503402.
91. W. Wang, J. Salazar, H. Vahabi, A. Joshi-Imre, W. E. Voit and A. K. Kota, *Adv. Mater*., 2017, **29**, 1700295.
92. T. Lv, Z. Cheng, D. Zhang, E. Zhang, Q. Zhao, Y. Liu and L. Jiang, *ACS Nano*, 2016, **10**, 9379.
93. P. A. Levkin, F. Svec and J. M. J. Fr´echet, *Adv. Funct. Mater*., 2009, **19**, 1993.
94. X. Deng, L. Mammen, H.-J. Butt and D. Vollmer, *Science*, 2012, **335**, 67.
95. U. Manna, A. H. Broderick and D. M. Lynn, *Adv. Mater*., 2012**, 24**, 4291.
96. A. H. Broderick, U. Manna and D. M. Lynn, *Chem. Mater*., 2012, **24**, 1786.
97. A. M. Rather and U. Manna, *Chem. Mater*., 2016, **28,** 8689.
98. D. G. Papageorgiou, Z. Li, M. Liu, I. A. Kinloch and R. J. Young, *Nanoscale,* 2020, **12,** 2228.
99. A. K. Geim and K. S. Novoselov, *Nat. Mater*., 2007, **6**, 187.

100. K. S. Novoselov, A. K. Geim, S. Morozov, D. Jiang, Y. Zhang, S. A. Dubonos, I. Grigorieva and A. Firsov, *Science*, 2004, **306**, 666.
101. M. J. Allen, V. C. Tung and R. B. Kaner, *Chem. Rev*., 2010, **110**, 132.
102. C. Lee, X. Wei, J. W. Kysar and J. Hone*, Science*, 2008, **321**, 385.
103. K. Geim, *Science*, 2009, **324**, 1530.
104. K. Cao, S. Feng, Y. Han, L. Gao, T. H. Ly, Z. Xu and Y. Lu, *Nat. Commun*., 2020, **11**, 284.
105. G. L-. Polín, C. G-. Navarro, V. Parente, F. Guinea, M. I. Katsnelson, F. P-. Murano and J. G-. Herrero, *Nat. Phys.,* 2014, **11**, 26.
106. M. Wang, X. Duan, Y. Xu and X. Duan, *ACS Nano,* 2016, **10**, 7231.
107. T. Ramanathan, A. A. Abdala, S. Stankovich, D. A. Dikin, M. H-. Alonso, R. D. Piner, D. H. Adamson, H. C. Schniepp, X. Chen, R. S. Ruoff, S. T. Nguyen, I. A. Aksay, R. K. Prud'homme and L. C. Brinson, *Nat. Nanotechnol.,* 2008, **3**, 327.
108. D. G. Papageorgiou, I. A. Kinloch and R. J. Young, *Prog. Mater. Sci*., 2017, **90**, 75.
109. Z. J. Li, Z. G. Cheng, R. Wang, Q. Li and Y. Fang, *Nano Lett.,* 2009, **9**, 3599.
110. Q. Su, S. P. Pang, V. Alijani, C. Li, X. L. Feng and K. Mullen, *Adv. Mater*., 2009, **21,** 3191.
111. C. Bao, Y. Guo, L. Songa and Y. Hu, *J. Mater. Chem.,* 2011, **21**, 13942.
112. Z. Xu and C. Gao, *Macromolecules,* 2010, **43**, 6716.
113. M. A. Rafiee, J. Rafiee, Z. Wang, H. Song, Z. –Z. Yu and N. Koratkar, *ACS Nano*, 2009, **3**, 3884.
114. Z. Chen and H. Lu, *J Mater. Chem.,* 2012, **22**, 12479.
115. I. Inuwa, A. Hassan, S. Samsudin, M. Haafiz, M. Jawaid and K. Majeed, *J Appl. Polym. Sci*., 2014, **15**, 131.
116. B. M. Cromer, S. Scheel, G. A. Luinstra, E. B. Coughlin and A. J. Lesser, *Polymer,* 2015, **80**, 275.
117. C. Vallés, A. M. Abdelkader, R. J. Young and I. A. Kinloch, *Compos. Sci. Technol.*, 2015, **111**, 17.
118. S. Park, S. He, J. Wang, A. Stein and C. W. Macosko, *Polymer,* 2016, **104**, 1.
119. J. Suh and D. Bae, *Compos. Part B Eng*., 2016, **95**, 317.

120. X. Wang, Y. Hu, L. Song, H. Yang, W. Xing and H. Lu, *J. Mater. Chem*., 2011, **21**, 4222.
121. M. Liebscher, M.-O. Blais, P. Pötschke and G. Heinrich, *Polymer,* 2013, **54**, 5875.
122. F.-X. Xiao, M. Pagliaro, Y.-J. Xu and B. Liu, *Chem. Soc. Rev.,* 2016, **45**, 3088.
123. M. Naebe, J. Wang, A. Amini, H. Khayyam, N. Hameed, L. H. Li and Y. Chen, *Sci. Rep.,* 2014, **4,** 4375.
124. Y. Yang, W. Rigdon, X. Huang and X. Li, *Sci. Rep.,* 2013, **3**, 2086.
125. O. –K. Park, J. –Y. Hwang, M. Goh, J. H. Lee, B.-C. Ku and N.-H. You, *Macromolecules,* 2013, **46**, 3505.
126. R. M. Santos, C. Vilaverde, E. Cunha, M. C. Paiva and J. A. Covas, *Soft Matter,* 2016, **12**, 77.
127. A. B. Bourlinos, V. Georgakilas, R. Zboril, T. A. Steriotis and A. K. Stubos, *Small,* 2009, **5,** 1841.
128. Y. Hernandez, V. Nicolosi, M. Lotya, F. M. Blighe, Z. Y. Sun, S. De, I. T. McGovern, B. Holland, M. Byrne, Y. K. Gun'ko, J. J. Boland, P. Niraj, G. Duesberg, S. Krishnamurthy, R. Goodhue, J. Hutchison, V. Scardaci, A. C. Ferrari and J. N. Coleman, *Nat. Nanotechnol.,* 2008, **3**, 563.
129. M. Lotya, P. J. King, U. Khan, S. De and J. N. Coleman, *ACS Nano,* 2010, 4, **6**, 3155.
130. D. Chen, H. Feng and J. Li, *Chem. Rev.,* 2012, **112**, 6027.
131. D. R. Dreyer, S. Park, C. W. Bielawski and R. S. Ruoff, *Chem. Soc. Rev.,* 2010, **39**, 228.
132. C. K. Chua and M. Pumera, *Chem. Soc. Rev.,* 2014, **43**, 291
133. D. R. Dreyer, A. D. Todd and C. W. Bielawski, *Chem. Soc. Rev.,* 2014, **43**, 5288.
134. F. Mouhat, F. –X. Coudert and M. –L. Bocquet, *Nat. Commun.,* 2020, **11**, 1566.
135. P. P. Briseboisa and M. Siaj, *J. Mater. Chem. C,* 2020, **8**, 1517.
136. B. C. Brodie, *Philos. Trans. R. Soc. London,* 1859, **149**, 249.
137. L. Staudenmaier, *Ber. Dtsch. Chem. Ges.,* 1898, **31**, 1481.
138. V. L. Hofmann, E. Konig and Z. Anorg. *Allg. Chem.,* 1937, **31**, 311.
139. W. S. Hummers and R. E. Offeman, *J. Am. Chem. Soc.,* 1958, **80**, 1339.
140. A. M. Dimiev and J. M. Tour, *ACS Nano,* 2014, **8,** 3060.

141. D. A. Dikin, S. Stankovich, E. J. Zimney, R. D. Piner, G. H. B. Dommett, G. Evmenenko, S. T. Nguyen and R. S. Ruoff, *Nature,* 2007, **448**, 457.
142. C. Gomez-Navarro, M. Burghard and K. Kern, *Nano Lett.,* 2008, **8**, 2045.
143. Q. Zheng, Y. Geng, S. Wang, Z. Li and J.-K. Kim, *Carbon,* 2010, **48**, 4315.
144. C. K. Chua and M. Pumera, *Chem. Soc. Rev*., 2014, **43**, 291.
145. R. Tarcan, O. T-. Boer, I. Petrovai, C. Leordean, S. Astilean and I. Botiz, J. *Mater. Chem. C,* 2020, **8**, 1198.
146. M. Khan, M. N. Tahir, S. F. Adil, H. U. Khan, M. Rafiq, H. Siddiqui, A. A. A-warthan and W. Tremel, *J. Mater. Chem. A,* 2015, **3**, 18753.
147. J. Liang, Y. Huang, L. Zhang, Y. Wang, Y. Ma,T. Guo and Y. Chen, *Adv. Funct. Mater.,* 2009,**19**,2297.
148. Z. Xu and C. Gao, *Macromolecules,* 2010, **43**, 6716.
149. Y. Tian, Y. Cao, Y. Wang, W. Yang and J. Feng. *Adv. Mater.,* 2013, **25**, 2980.
150. J. Hwang, T. Yoon, S. H. Jin, J. Lee, T. –S. Kim, S. H. Hong and S. Jeon, *Adv. Mater.,* 2013, **25**, 6724.
151. D. Dimov, I. Amit, O. Gorrie, M. D. Barnes, N. J. Townsend, A. I. S. Neves, F. Withers, S. Russo and M. F. Craciun. *Adv. Funct. Mater.,* 2018, **28**, 1705183.
152. Y. Zhang, S. Gong, Q. Zhang, P. Ming, S. Wan, J. Peng, L. Jiang and Q. Cheng, *Chem. Soc. Rev.,* 2016, **45**, 2378.
153. J. Y. Woo, J. H. Oh, S. Jo and C. –S. Han, *ACS Nano,* 2019, **13,** 4522.
154. J. Xue, C. Feng, L. Xia, D. Zhai, B. Ma, X. Wang, B. Fang, J. Chang and C. Wu, *Chem. Mater.,* 2018, **30**, 4646.
155. Y. Zhou, K. Maleski, B. Anasori, J. O. Thostenson, Y. Pang, Y. Feng, K. Zeng, C. B. Parker, S. Zauscher, Y. Gogotsi, J. T. Glass and C. Cao, *ACS Nano,* 2020, **14**, 3576.
156. W. Kong, H. Kum, S. –H. Bae, J. Shim, H. Kim, L. Kong, Y. Meng, K. Wang, C. Kim and J. Kim, *Nat. Nanotechnol.,* 2019, **14**, 927.
157. Y. Zheng, S. Zheng, H. Xue and H. Pang, Adv. Funct. Mater., 2018, **28**, 1804950.
158. R. Kumar, K. Jayaramulu, T. K. Maji and C. N. R. Rao, *Chem. Commun.,* 2013, **49**, 4947.
159. T. R. Nayak, H. Andersen, V. S. Makam, C. B. S. Khaw, X. F. Xu, P. L. R. Ee, J. H. Ahn, B. H. Hong, G. Pastorin and B. Ozyilmaz, *ACS Nano,* 2011, **5**, 4670.

160. Y. Xu, H. Bai, G. Lu, C. Li and G. Shi, *J. Am. Chem. Soc.,* 2008, **130**, 5856.
161. C. Wang, J. Li, C. Amatore, Y. Chen, H. Jiang and X. –M. Wang, *Angew. Chem. Int. Ed.,* 2011, **50**, 11644.
162. S. Navalo´n, J. Herance, M. A´lvaroa and H. Garcı, *Mater. Horiz.,* 2018, **5**, 363.
163. M. Liu, R. Zhang and W. Chen. *Chem. Rev.,* 2014, **114,** 5117.
164. Y. M. Li, L. H. Tang and J. H. Li, *Electrochem. Commun.,* 2009, **11**, 846.
165. Y. J. Li, W. Gao, L. J. Ci, C. M. Wang and P. M. Ajayan, *Carbon,* 2010, **48,** 1124.
166. L. Zhang, D. Han, Y. Tao, C. Cui, Y. Deng, X. Dong, W. Lv, Z. Lin, S. Wu, Z. Weng and Q. –H. Yang, *J. Mater. Chem. A,* 2020, **8,** 461.
167. Y. –F. Huang, P. –F. Wu, M. –Q. Zhang, W. –H. Ruan and E. P. Giannelis, *Electrochimica Acta,* 2014**, 132**, 103.
168. C. Li, D. Jiang, H. Liang, B. Huo, C. Liu, W. Yang and J. Liu, *Adv. Funct. Mater.,* 2018, **28,** 1704674.
169. G. d. C. Rodrigues, P. Zelenovskiy, K. Romanyuk, S. Luchkin, Y. Kopelevich and A. Kholkin, *Nat. Commun.,* 2015, **6**, 7572.
170. S. Ghosh, W. Bao, D. L. Nika, S. Subrina, E. P. Pokatilov, C. N. Lau and A. A. Balandin, *Nat. Mater.,* 2010, **9**, 555.
171. N. Bonini, J. Garg and N. Marzari, *Nano Lett.,* 2012, **12**, 2673.
172. Y. Li, T. Gao, Z. Yang, C. Chen, W. Luo, J. Song, E. Hitz, C. Jia, Y. Zhou, B. Liu, B. Yang and L. Hu, *Adv. Mater.,* 2017, **29,** 1700981.
173. J. Lou,Y. Liu, Z. Wang, D. Zhao, C. Song, J. Wu, N. Dasgupta, W. Zhang, D. Zhang, P. Tao, W. Shang and T. Deng, *ACS Appl. Mater. Interfaces,* 2016, **8**, 14628.
174. J. Liu, X. Li, W. Jia, Z. Li, Y. Zhao and S. Ren, *Energy Fuels,* 2015, **29**, 4644.
175. J. Ge, L. –A. Shi, Y. –C. Wang, H. –Y. Zhao, H. –B. Yao, Y. –B. Zhu, Y. Zhang, H. –W. Zhu, H.-A. Wu and S. –H. Yu, *Nat. Nanotechnol.,* 2017, **12**, 434.
176. M. Christian, R. Mazzaro and V. Morandi, *Adv. Funct. Mater.,* 2020, **30**, 2007458.
177. F. Taherian, V. Marcon, N. F. A. V. D. Vegt and F. Leroy, *Langmuir,* 2013, **29**, 1457.
178. J. Fengab and Z. Guo, *Nanoscale Horiz.,* 2019, **4**, 339.

179. J. Rafiee, X. Mi, H. Gullapalli, A. V. Thomas, F. Yavari, Y. Shi, P. M. Ajayan and N. A. Koratkar, *Nat. Mater.,* 2012, **11**, 217.
180. J. Rafiee, M. A. Rafiee, Z. -Z. Yu and N. Koratkar, *Adv. Mater.,* 2010, **22**, 2151.
181. G. Ding, W. Jiao, R. Wang, Y. Niu, L. Chen and L. Hao, *Adv. Funct. Mater.,* 2018, **28,** 1706686.
182. Y. Huang, X. Chen and M. Q. Zhang, *J. Mater. Sci.,* 2014, **49**, 3025.
183. Y. Xue, Y. Liu, F. Lu, J. Qu, H. Chen and L. Dai, *J. Phys. Chem. Lett.,* 2012, **3**, 1607.
184. Z. Lin, Y. Liu and C.-P. Wong, *Langmuir,* 2010, **26**, 16110.
185. Y. –Q. Liu, Y. –L. Zhang, X. –Y. Fu and H. –B. Sun, *ACS Appl. Mater. Interfaces,* 2015, **7**, 20930.
186. M. J. McAllister, J. L. Li, D. H. Adamson, H. C. Schniepp, A. A. Abdala, J. Liu, M. Herrera-Alonso, D. L. Milius, R. Car, R. K. Prud'homme and I. A. Aksay, *Chem. Mater.,* 2007, **19**, 4396.
187. X. Huang, X. Qi, F. Boey and H. Zhang, *Chem. Soc. Rev.,* 2012, **41**, 666.
188. D. Wu, F. Zhang, H. Liang and X. Feng, *Chem. Soc. Rev.,* 2012, **41**, 6160.
189. X. Sun, H. Sun, H. Li and H. Peng, *Adv. Mater.,* 2013, **25**, 5153.
190. J. C. Halpin and J. L. Kardos, *Polym. Eng. Sci.,* 1976, **16**, 344.
191. R. R. Nair, P. Blake, A. N. Grigorenko, K. S. Novoselov, T. J. Booth, T. Stauber, N. M. R. Peres and A. K. Geim, *Science*, 2008, **320**, 1308.
192. J. –N. Wang, Y. –L. Zhang, Y. Liu, W. Zheng, L. P. Lee and H. –B. Sun, *Nanoscale*, 2015, **7**, 7101.
193. S. R. Das, S. Srinivasan, L. R. Stromberg, Q. He, N. Garland, W. E. Straszheim, P. M. Ajayan, G. Balasubramanianf and J. C. Claussen, *Nanoscale*, 2017, **9**, 19058.
194. G. Ding, W. Jiao, R. Wang, M. Yan, Z. Chu and X. He, *J. Mater. Chem. A,* 2019, **7**, 17766.
195. G. Zu, K. Kanamori, K. Nakanishi and J. Huang, *Chem. Mater.* 2019, **31**, 6276.
196. Y. Yang, Q. Huang, L. Niu, D. Wang, C. Yan, Y. She and Z. Zheng, *Adv. Mater.,* 2017, **29**, 1606679.
197. L. V. Thekkekara and M. Gu, *Sci. Rep.,* 2019, **9**, 11822.

198. H. B. Jiang, Y. L. Zhang, D. D. Han, H. Xia, J. Feng, Q. D. Chen, Z. R. Hong and H. B. Sun, *Adv. Funct. Mater.,* 2014, **24**, 4595.
199. Y. Tan, B. Hu, Z. Chu and W. Wu, *Adv. Funct. Mater.,* 2019, **29**, 1900266.
200. H. B. Jiang, Y. Q. Y. Liu, Y. L. Zhang, Y. Q. Y. Liu, X. Y. Fu, D. D. Han, Y. Y. Song, L. Ren and H. B. Sun, *ACS Appl. Mater. Interface,* 2018, **10**, 18416.
201. Y. Y. Song, Y. Liu, H. B. Jiang, S. Y. Li, C. Kaya, T. Stegmaier, Z. W. Han and L. Q. Ren, *Sci. Rep.,* 2017, **7**, 12056.
202. Y. Y. Song, Y. Liu, H. B. Jiang, S. Y. Li, C. Kaya, T. Stegmaier, Z. W. Han and L. Q. Ren, *Nanoscale,* 2018, **10**, 16127.
203. H. Liang, M. T. Abshaev, A. M. Abshaev, B. M. Huchunaev, S. Griffiths and L. Zou, *Chem. Phys. Lett*., 2019, **728**, 167.
204. X. Ou, X. Yang, J. Zheng and M. Liu, *ACS Sustainable Chem. Eng.,* 2019, **7**, 13379.
205. A. Das, A. Shome and U. Manna, *J. Mater. Chem. A,* 2021, **9**, 824.
206. J. Yong, J. Huo, F. Chen, Q. Yang and X. Hou, *Phys. Chem. Chem. Phys.,* 2018, **20**, 25140.

Title: Synthesis of Durable, Flexible and Self-Healable Superhydrophobic Interfaces *

Here, a facile, catalyst-free, and robust 1,4-conjugate addition reaction has been strategically exploited for appropriate covalent integration of modified graphene oxide to develop polymeric materials with (1) tunable mechanical properties and (2) durable antifouling properties, which are capable of performing both in air and under oil. Furthermore, this approach provided a facile basis for (3) engineering a superhydrophobic monolith into arbitrary free-standing shapes and (4) decorating various flexible (metal, synthetic plastic, etc.) and rigid (glass, wood, etc.) substrates with thick and self-healable three-dimensional superhydrophobic coatings. The synthesized polymeric coating exhibited a remarkable ability to protect the antifouling property from various harsh physical insults, including sand paper abrasion, adhesive tape test, sand drop test etc. However, after the application of pressure on the same polymeric coating, the bioinspired, nonadhesive (contact angle hysteresis <5°) superhydrophobicity was compromised, and the physically damaged polymeric coating became highly adhesive (contact angle hysteresis ~50°) superhydrophobic. But, after releasing the pressure, the native nonadhesive (contact angle hysteresis <5°) extreme wettability was self-restored in the polymeric coating through the recovery of the essential hierarchical topography—without requiring any external stimulus. This unique material, having impeccable durability and absolute self-healing capability, was further explored in spatially selective impregnation of water-soluble agents on the surface of polymeric coating—without any permanent change in the extreme water repellency property. This spatially selective association of hydrophilic molecules was performed directly from an aqueous medium, which is extremely hard to achieve using conventional superhydrophobic materials.

* **A. Das,** J. Deka, A. M. Rather, B. K. Bhunia, P. Pratim Saikia, B. B. Mandal, K. Raidongia and U. Manna. *ACS Appl. Mater. Interfaces,* 2017, **9**, 42354.

A. Das, J. Deka, K. Raidongia and U. Manna. *Chem. Mater.*, 2017, **29**, 8720.

2.1. Introduction

Special and extreme wettability of a liquid on a solid surface, which is primarily discovered in living objects (e.g., lotus leaf, rose petal, fish scale, etc.) in nature, is composed of essential chemistry and topography, and such bioinspired artificial interfaces are being recognized as a general avenue for developing functional materials in the context of various environments, energy and healthcare-related applications.[1-6] In this regard, extremely water-repellent superhydrophobic materials (having advancing contact angles, θ_{Adv}, ≥150°, and contact angle hysteresis, θ_{Hys}, ≤10°)[1,2] are particularly well-characterized and are highly suitable for a wide variety of applications, including protein crystallization, guided water transfer, harvesting of liquid water from the mist, controlled small molecule release, synthesis of anti-biofouling coating, etc.[7−13] However, the conventional thin superhydrophobic interfaces are generally fabricated by adopting a thin layer of inert low surface energy coating on an appropriately customized hierarchical topography (either hydrophilic and/or hydrophobic).[14-15] In general, the appropriate coexistence of low surface energy and hierarchical features provided the essential metastable trapped air for the extreme heterogeneous wettability of a liquid on a solid surface. However, slight perturbations in any of these physical and/or chemical parameters during the practically relevant physical manipulations (including bending, creasing, compressing, scratching, etc.,) and severe chemical exposures are known to damage such interfacial special wettability.[16,17]

In the recent past, few elegant designs were introduced to achieve durable superhydrophobic coatings,[5,18−25] and some of them are proficient in restoring the property by re-optimization of the essential chemistry (i.e., chemically inert coating) on top of the hierarchical features through either (1) post-repairing process (redeposition of low surface energy coating) or (2) self-healing process (rehabilitation of inert coating by application of appropriate stimuli).[21−25] The coexistence of both the essential surface chemistry and the appropriate hierarchical topography primarily conferred the bioinspired superhydrophobicity. However, the hierarchical topography that is most often developed using brittle inorganic oxides or soft polymers/polymeric components is susceptible to any damage after the application of external pressure, and the physical damage becomes permanent. The antiwetting property is likely to get compromised in such practically relevant scenarios. Thus, the synthesis of material having the ability to self-heal the damaged topography is extremely challenging and highly desirable for widespread applications of this bioinspired property in diverse and severe practical circumstances. In the very recent past, shape memory polymers were successfully

exploited in restoring the native antifouling property in the physically damaged interfaces, but through the application of appropriate external stimuli.[26–29] This approach of self-healing through external intervention is likely to impose a potential complexity in the restoration process as the maintenance of an appropriate stimulus is expected to be a difficult task in diverse practical settings. To address these limitations, recently three-dimensional superhydrophobicity has been introduced where the anti-wetting property is not just restricted to the top surface of the material but also exists throughout the material. Thus, the anti-wetting property of the material remained intact even after the removal of the top interface during harsh physical abrasions. In the recent past, the 1,4-conjugate addition reaction between aliphatic acrylates of dipentaerythritol pentaacrylate and primary amines containing branched poly(ethylenimine) was used in the synthesis of a "chemically reactive" polymeric nanocomplex (CRPNC), which was further exploited to developed various three-dimensional bio-inspired interfaces (superhydrophobic and underwater superoleophobic). Here, we have extended this facile and catalyst-free chemical approach to synthesizing both (1) highly flexible and shapeable free-standing three-dimensional superhydrophobic monoliths and (2) durable and self-healable superhydrophobic coatings. The reduced amino graphene oxide (AGO) was strategically and covalently associated with CRPNC. The synthesized polymeric coating, having the remarkable ability to restore the native antifouling property through the recovery of physical deformation—without requiring any external intervention. Further, the synthesized material was also capable of printing water-soluble molecules directly from the aqueous medium during the recovery of the native hierarchical topography in the damaged interface. However, after the printing of hydrophilic molecules on the polymeric coating, any permanent change in the embedded antifouling property was not observed. The impregnation of water-soluble agents onto the superhydrophobic surface without compromising the native antifouling property is extremely difficult to achieve.[18,30] Here, the synthesized material provided a facile avenue to develop a self-healable and self-cleaning superhydrophobic print—which was made out of water-soluble agents. This facile and scalable synthetic approach is not only capable of providing bioinspired superhydrophobicity with impeccable durability—but it is also appropriate for developing unique and interesting interfaces that are extremely difficult to synthesize following the conventional fabrication process.

2.2. Experimental Section

2.2.1. Materials

Branched poly(ethyleneimine) (BPEI, MW ~ 25000 Da), dipentaerythritol penta-/hexaacrylate (5 Acl, MW ~ 524.21 g/mol) were purchased from Sigma-Aldrich, Bangalore, India. Rhodamine 6G was purchased from Labo Chemie, Mumbai, India. Conc. hydrochloric acid and potassium permanganate were obtained from Fischer Scientific, Mumbai, India. Graphite powder was purchased from Asbury Carbon. Sodium hydroxide, methanol, conc. sulfuric acid, hydrogen peroxide, nitric acid, hydrazine hydrate, and ammonium hydroxide were purchased from Merck Specialties Private Limited, India. Tetrahydrofuran (THF) was obtained from RANKEM, Maharashtra, India. Sandpaper (grit no. 400) was purchased from Million International, India. Glass slides (Boroleb, India), aluminium foil (Parekh Aluminex Ltd. India) and adhesive tape (Jonson tape Ltd. India) were acquired from different sources. Sand particles were collected from a construction site at IIT-Guwahati, Assam. This sand was used in experimental demonstrations after thorough washing with water.

2.2.2. General considerations

Dynamic light scattering (DLS) measurements were taken with a Zetasizer Nano ZS90 (model no ZEN3690) instrument. Fourier-transform infrared spectroscopy (FTIR) data were collected using a PerkinElmer instrument, where samples were first embedded in a KBr pellet following the standard protocol. Liquid water contact angles on the materials were estimated using a KRUSS Drop Shape Analyzer- DSA25 instrument at ambient temperature and deionized (DI) water droplets were used for dynamic contact angle measurements. Field-emission scanning electron microscope (FESEM) images were obtained using a Carl Zeiss field emission scanning electron microscope. All non-conductive polymeric samples were gold-sputtered under vacuum to achieve a thin layer of conductive gold coating on the polymeric samples. Raman spectra were acquired using a Laser Micro Raman System (Horiba Jobin Vyon, Model LabRam HR). All digital pictures were taken with a canon power shot SX420 IS digital camera.

2.2.3. Synthesis of graphene oxide (GO)

GO sheets were prepared by following the modified Hummers' method. First, graphite (1 g) powder was added to 50 mL of concentrated sulphuric acid and the whole system was chilled at 0°C using an ice bath. Then, $KMnO_4$ (6 g) was slowly added to the solution keeping the temperature of the reaction mixture below 10°C. The reaction mixture was then transferred to a water bath, where the temperature was maintained at 35°C for 2 h, and then the reaction mixture was diluted with 100 mL of DI water. The sudden rise in the temperature during the dilution process was controlled by submerging the reaction vessel in an ice bath. Then, 8 mL

of 30% hydrogen peroxide solution was added to the dilute solution to reduce unreacted $KMnO_4$. The prepared GO sample was thoroughly washed by adopting a two-step washing method, where HCl and acetone solvent were consecutively used.

2.2.4. Synthesis and characterization of amino-graphene oxide (AGO)

AGO sheets were synthesized from the freshly prepared GO sheets by adopting two conjugative reactions: (1) nitration followed by (2) reduction. For the nitration reaction on GO sheets, the dried GO powder (50 mg) was mixed with 100 mL of 50% nitric acid and the reaction mixture was kept for 12 h at room temperature with continuous agitation. Nitro graphene oxide obtained as such was then washed with acetone and dried under vacuum before redispersing in a 50:50 ethanol−water mixture (0.1 mg/mL) for the reduction reaction. The reduction was carried out by heating the dispersion at 70°C after the addition of 150 µL of ammonium hydroxide and 50 µL of hydrazine hydrate under continuous magnetic stirring. These AGO sheets synthesized in ethanol were directly used in the fabrication of superhydrophobic polymeric materials (details are accounted in the following section).

2.2.5. Preparation of superhydrophobic polymeric gel material

First, solutions of 5 Acl (1.325 g) and BPEI (0.5 g) in methanol were prepared in separate glass vials by dissolving each of them in 10 mL of methanol. The solutions (1 mL) of 5 Acl and BPEI (0.125 mL) in methanol were mixed together in glass vials. Then, the mixtures were doped with different amounts of amino-graphene oxide (4.25 µg/mL, 8.16 µg/mL, 15.09 µg/mL and 30.77 µg/mL; denoted SHM_1, SHM_2, SHM_3, and SHM_4, respectively) in separate glass vials and kept under agitation for 1 h. Depending on the amount of AGO sheets added in the mixture, colorless solutions appeared as turbid liquids after a certain time, and eventually, after 1 h, the reaction solution transformed into a gel material. Then, this semisolid gel was taken out and manipulated into different shapes, such as dolphin, leaf, and array of wells with the help of appropriate negative replica (doh cutter with an appropriate shape was used for giving the shape of dolphin and array of wells to the gel material, and the PDMS mold having a negative replica of guava leaf was used for preparing the polymeric material with a similar shape and structure as that of a guava leaf).

2.2.6. Post-chemical modifications

To adopt the desired superhydrophobicity, the gel materials were washed with THF for 30 min, followed by treatment with n-decylamine (37.47 mg/mL) in THF for 6 h. After this treatment, the polymeric material was washed again with THF thoroughly and dried in the

open air. After drying, these materials (SHM_1, SHM_2, SHM_3, and SHM_4) were characterized by FTIR, FESEM, Raman spectroscopy and contact angle measurements.

2.2.7. Coating on the substrate

The colorless solution of 5Acl (132.5 mg/mL in methanol, 1mL) was first mixed with BPEI (50 mg/mL in methanol, 125 µL) in presence of dispersion of amino graphene oxide (AGO), and depending on the amount of AGO in the BPEI/5Acl mixture, the polymeric coatings are denoted as SHC_1 (2.17 µg/mL), SHC_2 (4.25 µg/mL), SHC_3 (8.16 µg/mL), SHC_4 (15.09 µg/mL) and SHC_5 (30.77µg/mL), respectively. The colorless mixture of BPEI/5Acl transformed to a turbid and milky solution in the presence desired amount of AGO and this solution was spread uniformly over desired substrates (Al foil, plastic, glass, wood) with the help of a microscopic glass slide. After 30 minutes, a dry and stable coating was obtained on the glass substrate. Then, the coated glass slide was treated with decylamine solution (37.47 mg/ml) in THF for overnight. After that, the coated slide was thoroughly washed with fresh THF solvent for multiple (five) times. Then, the air-dried coating was further used in various demonstrations.

2.2.8. Self-healing of the polymeric coating

A pressure of 188 kPa was applied on the surface polymeric coating over an area of 0.5 cm^2 for 10 sec, and the polymeric coating (SHC_5, thickness = 1 mm) was crushed with a depth of 600 µm. The beaded water droplet on the crushed surface was found to be highly adhesive with contact angle hysteresis above 50°. Both the physical integrity and embedded antifouling property (non-adhesive superhydrophobicity) were self-healed within 30 minutes, without any external intervention. Further, the same process was repeated to examine the self-healing ability of other polymer coatings (SHC_3 and SHC_4) that were with a lesser amount of AGO.

2.2.9. Selective collection of the aqueous phase

Similarly, the polymeric coating was further crushed by the application of pressure (188 kPa) with three circular objects. Then, the polymer coating with three physically damaged spots was immersed in the aqueous solution of rhodamine 6G dye for a few seconds followed by drying it in air. Red-colored aqueous solution was selectively immobilized on those three locations. After air-drying, both the physical deformation and antifouling properties were self-healed in the polymeric coating. The blue-colored water droplets were placed on the self-healed surface to examining the anti-fouling property after the self-healing process.

2.2.10. Paper-based contact printing of water-soluble agents

A dolphin-shaped filter paper was soaked with an aqueous solution of rhodamine 6G, and then it was brought in contact with a flattened and crushed surface for a few seconds. Selective immobilization of the aqueous phase was noticed on the polymeric coating after removal of the dolphin-shaped paper. The polymeric coating recovered its physical damage and the blue-colored aqueous droplets were again used to examine the antifouling property on some specific locations (on the coating)—where the water-soluble rhodamine dye molecules were printed. For the proof of concept demonstration of printing multiple water-soluble agents, a triangle-shaped filter paper was first soaked with an aqueous solution of methylene blue (blue-colored) dye, and immediately that paper was placed on the crushed polymeric coating (SHC_5) and then it was allowed to air-dry. Next, the same polymeric coating was crushed again at the same location through the application of pressure, and another triangle-shaped filter paper—that soaked with an aqueous solution of rhodamine was placed on it, to immobilize the aqueous solution that was with another water-soluble molecule (rhodamine), finally, the material was allowed to dry. Thus, the complex superhydrophobic print—composed of two water-soluble agents was developed.

2.2.11. In-situ printing of hydrophilic molecules

Here, the aqueous solution of rhodamine was attached selectively on the polymeric coating during the spatially selective incurring of physical damage on the polymeric coating. A crude and lab-made wooden stamp with the shape of 'IIT' was first inked with an aqueous solution of rhodamine. Then this inked-stamp was brought in contact with the polymeric coating, and manual pressure was applied on the coating for 10 sec and at the end, the aqueous ink was transferred to the polymeric coating. Then the 'IIT' printed nonadhesive superhydrophobic surface was used in the demonstration of self-cleaning, where deposited dust and dirt on the tilted surface was self-cleaned during rolling of beaded water droplets on the surface.

2.3. Results and Discussions

2.3.1. Synthesis and characterization of AGO-doped superhydrophobic polymeric gel material

Here, in the current design, two-dimensional flexible graphene oxide (GO) sheets, which are well-recognized for their exceptional mechanical properties, were strategically functionalized and incorporated in the porous and reactive polymeric material through the facile and scalable 1,4-conjugate addition reaction, as shown in Figure 2.1. This direct covalent incorporation of such flexible GO sheets was anticipated to have the ability to modulate the

mechanical properties of the synthesized polymeric materials.

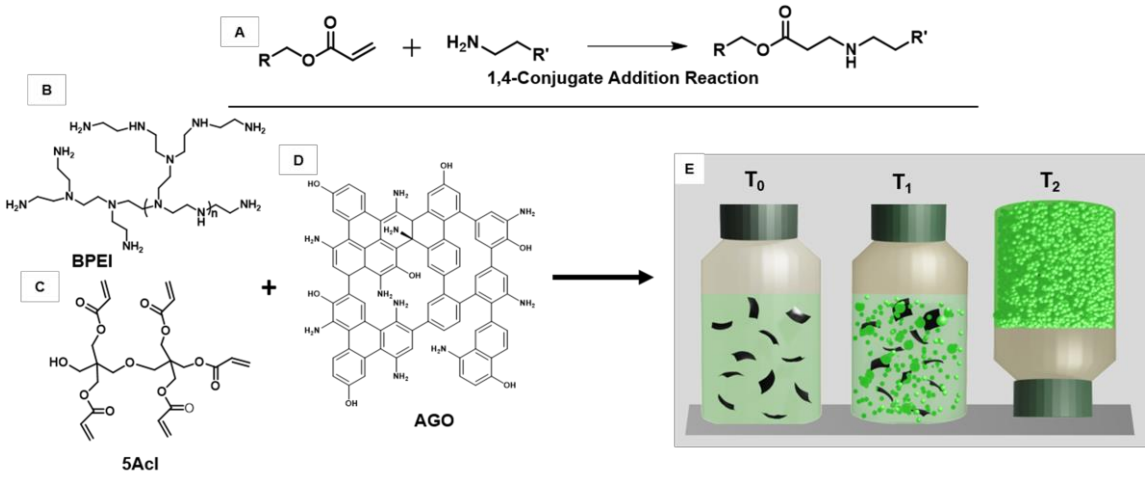

Figure 2.1. A) Schematic representation of the 1,4-conjugate addition reaction between aliphatic acrylate and primary amine groups. B-D) Chemical structures of branched poly(ethyleneimine) (BPEI, B), dipentaerythritol pentaacrylate (5 Acl, C) and schematic representation of amino-graphene oxide (AGO, D). E) Synthesis of reactive polymeric gel from the AGO-doped reaction mixture of 5 Acl and BPEI in methanol.

Thus, the GO sheets were first decorated with primary amine groups (nitrogen 7%). The amino graphene oxide (AGO) was characterized with energy-dispersive X-ray spectroscopy (EDX), Raman spectra, Fourier transform infrared (FTIR), and Field emission scanning electron microscopy (FESEM); (Figure 2.2). The FESEM image in Figure 2.2A reveals the existence of the two-dimensional sheetlike morphology of amino graphene with lateral dimensions extending from 2 to 8 μm^2. The EDX analysis carried out at different AGO sheets yielded an approximate composition of the sheets to be 63:30:7 of carbon, oxygen, and nitrogen atoms, respectively. Figure 2.2B, further compared the Raman spectrum of GO with that of AGO. Both the spectra show prominent D and G bands at 1330 cm^{-1} and 1595 cm^{-1}, respectively. The ratio I_D/I_G was found to be decreased for AGO with respect to GO, suggesting the removal of some of the defects during the process of amine functionalization. The FTIR spectra of GO and amino graphene samples were compared, where both the spectra confirmed the presence of O−H groups and (sp^2) C=C groups, the characteristic peaks are observed at around 3350 cm^{-1} and 1625 cm^{-1}, respectively. However, the appearance of new peaks at 1380 cm^{-1} and 1237 cm^{-1} in the AGO sample, corresponding to the N−H in-plane bending vibration and the C−N stretching, revealed the presence of amine groups in the sheets. The hump at 3230 cm^{-1} can also be assigned to the $-NH_2$ stretching vibration of amino-graphene oxide sheets (Figure 2.2C). The synthesized AGO was found to be chemically reactive with 5 Acl molecules, as shown in Figure 2.2D-F. The reaction mixture

of AGO and 5 Acl was aggregated and precipitated—likely due to mutual chemical reaction between 5 Acl and AGO through a 1,4-conjugate addition reaction. The reaction between AGO and 5 Acl was monitored with FTIR analysis. A significant depletion of IR peak intensity at 1409 cm^{-1} was noticed with respect to IR signature for carbonyl group at 1735 cm^{-1} as shown in Figure 2.2F.

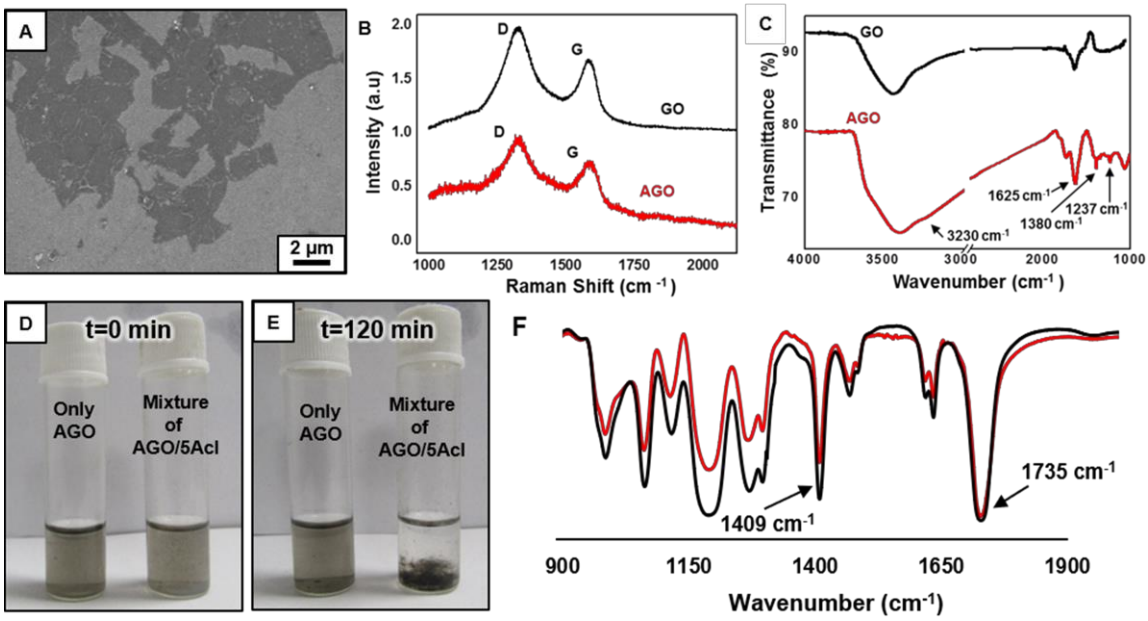

Figure 2.2. A) FESEM image of amino-graphene oxide (AGO), B) Raman spectra of AGO (red) and GO (black). C) FTIR spectra of AGO (red) and graphene oxide (GO) (black), D-E) Digital images are illustrating the visual change in the mixture of AGO/5Acl (right most vial at each panel) and the solution of AGO (left most vial at each panel) with time. The mixture of AGO/5Acl was aggregated after 120 min and it was eventually sediment (E), however the dispersion of AGO remained stable over this period. F) FTIR spectra of both the 5Acl molecules (black) and the aggregates (red) that are formed after mixing of AGO and 5Acl. Both IR spectra were normalized with reference to carbonyl peak intensity. The peaks at 1735 cm^{-1} and 1409 cm^{-1} are corresponded to the signatures of carbonyl stretching and C-H stretching of β carbon of vinyl group respectively.

Next, 1 mL of 5 Acl (132.5 mg/mL) and 0.125 mL of BPEI (50 mg/mL) were mixed in methanol at 20°C. This composition was unable to provide the gel material (Figure 2.3A-D, labelled as SHM_0); however, the addition of AGO (4.25 µg/ mL) resulted in the polymeric gel material within 1 h (Figure 2.3A-D, labelled as SHM_1). This result indicated that the added AGO expedited and controlled the gelation process, likely through the 1,4-conjugate addition reaction between the grafted primary amine groups (from AGO and BPEI) and acrylate groups (from 5 Acl). Additional control experiments were designed to understand the role of grafted amines on AGO sheets on this polymeric gelation process. In cases where pristine GO (300.77 µg/mL) sheets (lacking primary amine groups) were added, a mild yellowish transparent solution (labelled as GO; Figure 2.3A-D) was observed. However, any

further physical changes in the solution were not noticed even after a day. This experiment unambiguously revealed the active participation of grafted amines from AGO in the synthesis of the polymeric gel material. On the addition of AGO (the final concentration of AGO in the solution is 4.25 µg/mL) in the mixture of BPEI/5 Acl in methanol, the colorless mixture slowly transformed into a faint turbid solution (after 20 min) and then converted to a milky solution (after 30 min).

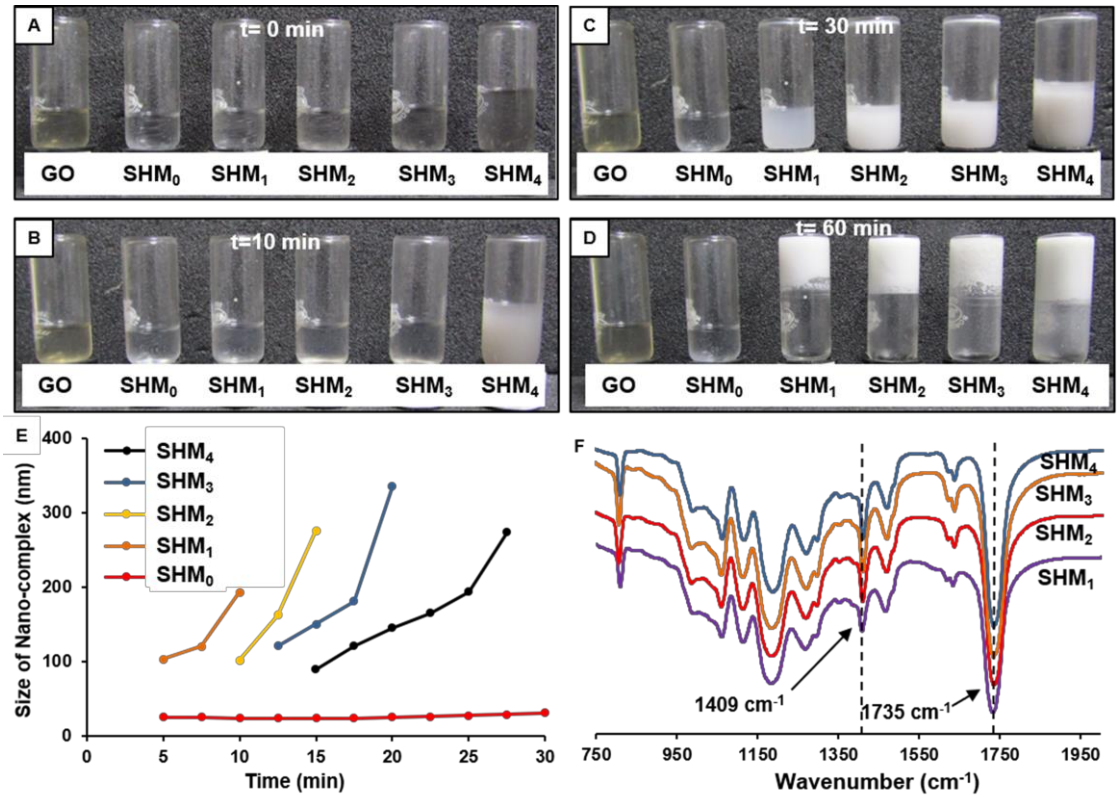

Figure 2.3. A-D) Digital images illustrating the effect of GO and AGO (GO, SHM_0, SHM_1, SHM_2, SHM_3 and SHM_4) addition in mixture of BPEI/5Acl in methanol. All solutions were transparent (A) at beginning, the AGO added solutions (SHM_1, SHM_2, SHM_3 and SHM_4) turned cloudy with time (B,C). After 60 min, all the AGO doped solutions (last four vial from left in image D; SHM_1, SHM_2, SHM_3 and SHM_4) formed gel materials—but mixture of BPEI/5Acl in presence of GO and in absence of AGO remained transparent (two vials from left in image D). E) DLS study illustrating the growth of the nano-complex in AGO-doped mixtures of BPEI/5 Acl. No such growth of nano-complex was noticed in the BPEI/5 Acl mixture in the absence of AGO doping. F) FTIR spectra of AGO doped (SHM_1, SHM_2, SHM_3 and SHM_4) gel materials.

Eventually, after 1 h, a gel material (labelled as SHM_1; Figures 2.3A-D) was formed. However, this appearance of turbidity in the BPEI/5 Acl mixture occurred more rapidly upon increasing the amount of AGO in the reaction mixture. For example, a highly turbid solution was noticed within 10 min after increasing the AGO concentration to 30.77 µg/mL in the reaction mixture of BPEI/5 Acl (SHM_4), under identical conditions. Whereas other mixtures (labelled as SHM_1, SHM_2, SHM_3) having lesser amounts of AGO doping (4.25, 8.16, and

15.09 μg/mL, respectively) appeared as clear solutions (Figure 2.3A), but eventually became turbid over time (Figure 2.3C-D). Furthermore, dynamic light scattering (DLS) study confirmed the existence of polymeric-nano-complexes in the AGO-doped mixtures of BPEI/5 Acl; these nano-complexes grew over time and aggregated to form bigger particles. Both the formation and growth of nano-complexes were delayed when smaller amounts of AGO were used as shown in Figure 2.3E. No growth of nano-complexes was observed in the mixture of BPEI/5 Acl in the absence of AGO doping. Thus, this study revealed that AGO doping not only initiates the gelation process but also controls the rate of gelation processes. The existence of residual reactive functional moieties in the polymeric materials was characterized by FTIR spectral analysis. Interestingly, two characteristic IR peaks (Figure 2.3F) at 1735 cm^{-1} and 1409 cm^{-1} corresponding to the carbonyl stretch and symmetric deformation of the C−H bond for the β carbon of the vinyl groups were observed respectively. These IR signatures revealed the existence of residual acrylate groups in the polymeric materials irrespective of the AGO-doping amount. Furthermore, the post-chemical modification of the material by exploiting these residual acrylate functional groups with strategically selected amine-containing hydrophobic small molecules provided a basis to adopt extreme water fouling properties in the material. The highest AGO-doped polymeric material (SHM_4) displayed extreme liquid water repellency both in air (Figure 2.4A, B) and under oil (Figure 2.4C, D) with advancing contact angle above 160°, once it was post-functionalized with the primary amine-containing hydrophobic small molecule (decylamine). The FTIR spectral analysis confirmed the successful post-chemical modification of the material, the characteristic peak at 1409 cm^{-1}, which denotes that the residual acrylate groups were almost exhausted in the polymeric material on treatment with decylamine (Figure 2.4E). Furthermore, a 5 μL aqueous droplet dropped on this synthesized superhydrophobic material from 7 mm height was observed to bounce twice before its settlement on the surface (Figure 2.4F-K) and the droplet could readily roll off from the surface on tilting the superhydrophobic material at 3° and streams of water bounced away from the surface after hitting the surface of the material (Figure 2.4M). This is consistent with the Cassie−Baxter (CB) state in the superhydrophobic material, and the existence of the metastable trapped air layer in the material is evident from the presence of shiny reflection of light at the water/material interface (Figure 2.4O). As expected, this facile chemical approach also provided an exceptional control on the modulation of mechanical properties in the polymeric material. The polymeric material (SHM_1) with a low content of AGO was found to be tough,

and the compressive stress and strain at yield were measured to be ~347 kPa and 41%, respectively; however, the material (SHM_4) with more AGO sheets was found to be highly elastic (Figure 2.5A).

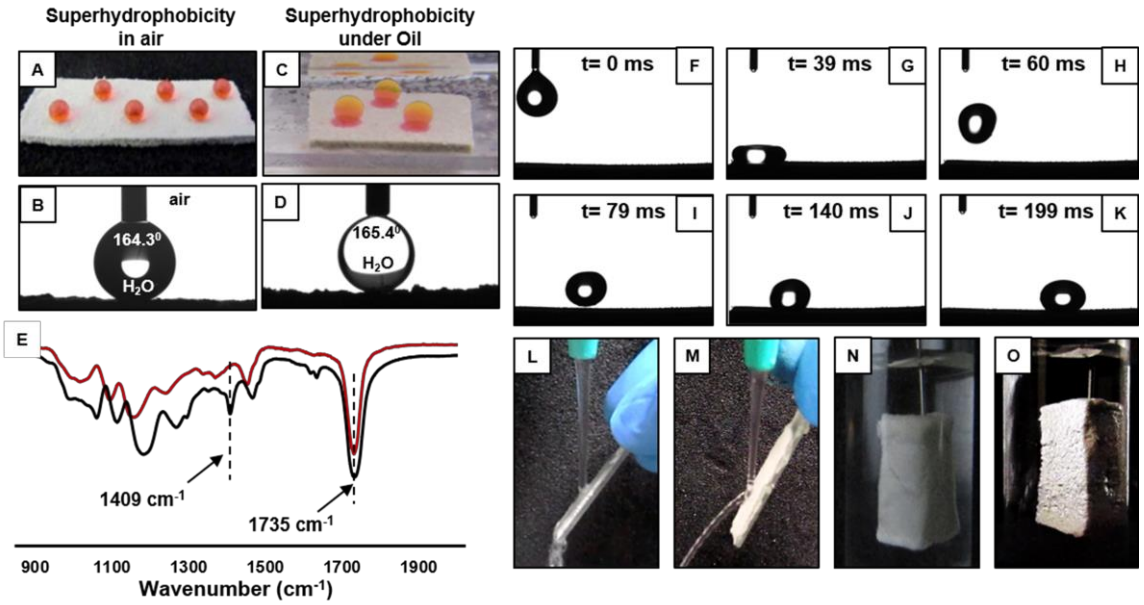

Figure 2.4. A−D) Digital (A, C) and advancing water contact angle (CA) images (B, D) of beaded water droplets on the decylamine-treated polymeric material in air (A, B) and under hexane (model oil, C, D). E) FTIR spectra of the material before (black) and after (red) post-modification with decylamine. F-K) Demonstration of the rolling off of 5 μL water droplet on the 3˚ tilted superhydrophobic surface which was dropped from 0.7 cm height. L-M) Digital images of untreated (L) and decylamine treated (M) dried polymeric materials (SHM_4)—which are placed under stream of water, N-O) Digital images of untreated (N) and decylamine treated (O) dried material under water, untreated material was completely wetted, but decylamine treated material is appeared shiny because of trapped air.

Furthermore, the compressive modulus gradually decreased from 1237.56 ± 129.40 kPa (SHM_1) to 15.57 ± 2.93 kPa (SHM_4) with increasing the content of modified graphene oxide in the polymeric sample (Figure 2.5A). Thus, the polymeric materials became more elastic on increasing the covalent integration of AGO sheets through the 1,4-conjugate addition reaction. Furthermore, the synthesized polymeric material was repetitively deformed 1000 times with a compressive strain of 80%. The material remained nonadhesive superhydrophobic with an advancing water contact angle above 156° and contact angle hysteresis below 10° even after successive deformations of the same polymeric material 750 times. However, the material became highly adhesive superhydrophobic with contact angle hysteresis of 28° after extending this consecutive deformation 1000 times, as shown in Figure 2.5B. Furthermore, the antiwetting property of other polymeric materials (lower AGO-doped) was examined in detail. All other synthesized polymeric materials (SHM_1, SHM_2, SHM_3) were efficient in displaying extreme liquid water repellency (having θ_{Adv}>150° and θ_{Hys}<4°)

after post-chemical functionalization with decylamine, irrespective of the mechanical properties of the materials (Figure 2.6G).

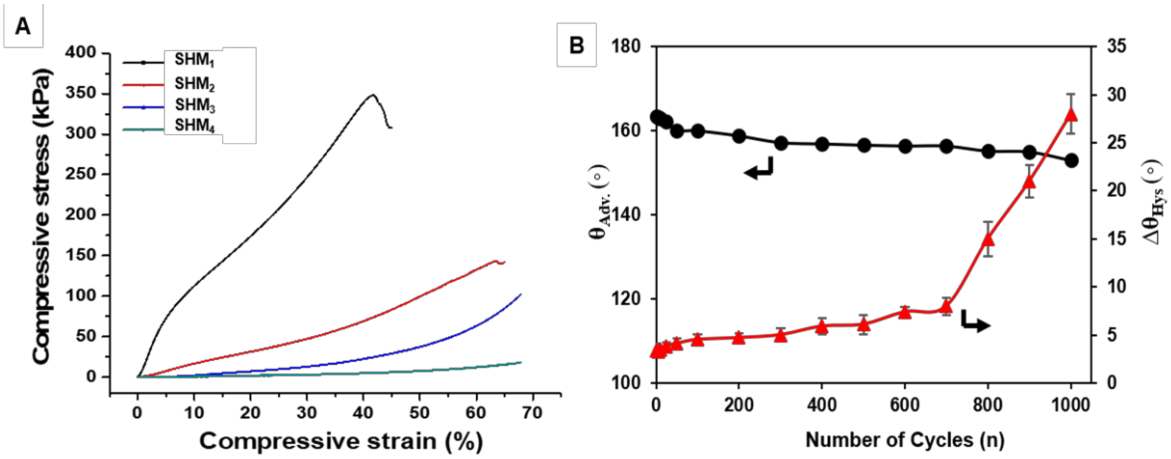

Figure 2.5. A) Compressive stress−strain curve of AGO-embedded polymeric materials (SHM_1, SHM_2, SHM_3 and SHM_4). B) The plot accounting the change in the water-wettability with successive mechanical deformation of the synthesized material (SHM_4) with 80 % compressive strain.

The AGO-doping level in the synthesized polymeric materials has the same impact on controlling the topography of the polymeric material, as confirmed by studying the morphology of these synthesized polymeric materials under a field emission scanning electron microscope. The morphology of the polymeric materials was apparently similar in low magnification irrespective of the AGO-doping level in the materials, as shown in Figure 2.6A, C, E; the monoliths remained highly porous with randomly arranged granular domains. However, the topography in each material was appropriate enough to display the desired antiwetting property. However, in the high magnification, the granular domains in the material were observed to be more diffused and larger in nature upon increasing the AGO-doping amount in the materials (Figure 2.6B, D, F). Doped AGO sheets in the material might be folded around these polymeric granular structures during the gelation process, and any phase-separated domain, populated with AGO sheets, was not observed in the material. Moreover, the increase in the diffused interconnected structure in SHM_4 is most likely because of more complexation of AGO sheets with polymeric granules in the material and these diffused interconnections among the granular structures through flexible AGO sheets are hypothesized to be the key component in achieving the desired physical flexibility in the materials. Therefore, this AGO doped material could provide a basis for developing a highly flexible self-standing superhydrophobic material, which can be molded into arbitrary shapes and sizes (Figure 2.6H-J), including the structure of vessels that are present in guava leaf

(Figure 2.6H). Moreover, the properties of the material allow it to be machined, e.g., to make an array of wells (Figure 2.6J) that could be useful in restricting the motion of aqueous droplets on extremely nonadhesive antifouling surfaces and would eventually facilitate various prospective demonstrations, including developing biosensors for protein detection, tissue engineering, protein crystallization, high-throughput drug sensing, etc.

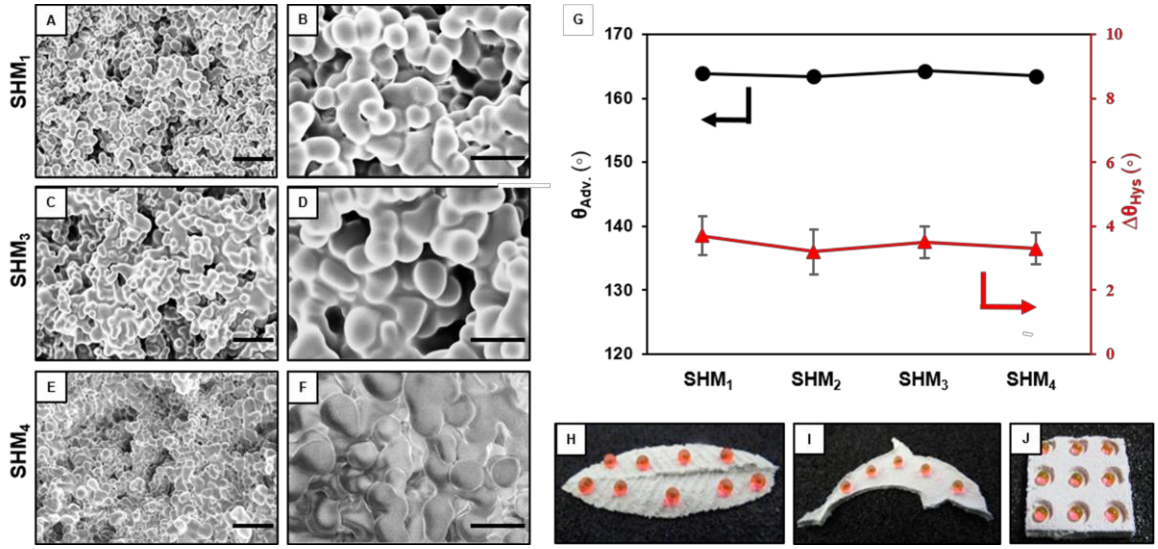

Figure 2.6. A–F) FESEM images of AGO-doped materials (SHM_1, SHM_2, SHM_3 and SHM_4) in low magnification (A, C, E; scale: 10 µm) and in high magnification (B, D, F; scale: 5 µm). G) Advancing water contact angle (θ_{Adv}, black line) and water contact angle hysteresis (θ_{Hys}, red line) on various AGO-doped polymeric materials after decylamine treatment. H-J) Digital images of the superhydrophobic material that was molded in structures of guava leaf (H), dolphin (I), and array of wells (J).

2.3.2. Synthesis of AGO-doped self-healable and abrasion tolerant superhydrophobic coating

Further, such an approach was extended to develop a self-healable and abrasion tolerant superhydrophobic coating. An adequately AGO-incorporated (8.16 µg/mL) mixture of BPEI/5Acl, before its transformation to a semisolid gel material, was extended to prepare a thick (1 mm) and stable polymeric coating (denoted as SHC_3) by spreading the milky solution onto a clean glass substrate (Figure 2.7A). After air-drying, the polymeric coating (SHC_3) was found to be superhydrophilic in the air with a contact angle (CA) of 0° (Figure 2.7C). But, the same polymeric interface was efficient in repelling water droplets extremely with an advancing water contact angle (θ_{adv}) of 162.1° (Figure 2.7D) and contact angle hysteresis (θ_{hys}) of 3.3°—after strategic chemical modification of the residual acrylates groups in the polymeric coating (SHC_3) with decylamine molecules. However, more defective coatings

(Figure 2.7B) with multiple cracks were also noticed on decreasing (from 4.25 μg/mL (SHC_2) to 2.17 μg/mL (SHC_1)) the concentration of AGO in the deposition solution.

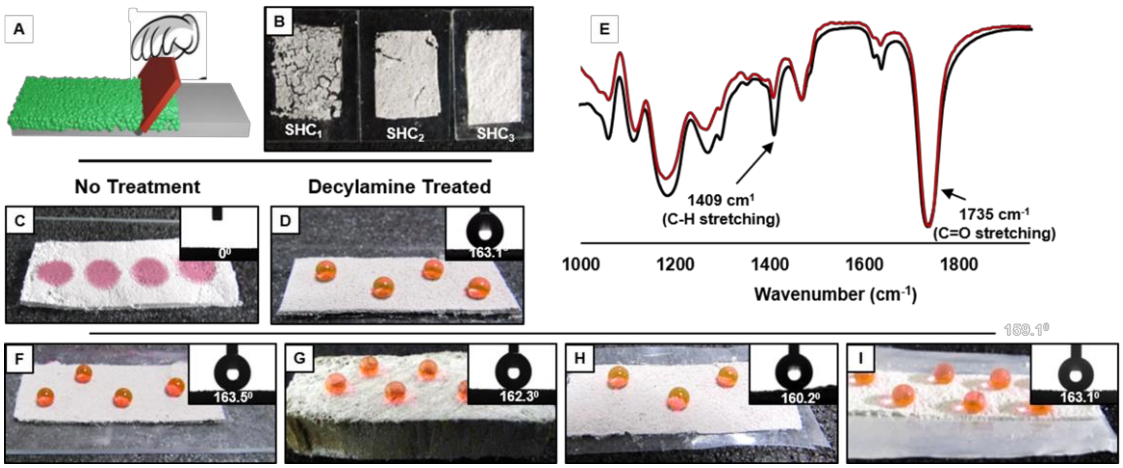

Figure 2.7. A) Schematic illustration of preparation process of the polymeric coating. B) Digital image of polymeric coatings that are incorporated with various amounts of AGO (SHC_1 (2.17 μg/mL), SHC_2 (4.25 μg/mL), and SHC_3 (8.16 μg/mL)). C-D) Digital images and advancing contact angle images (inset) on the stable polymeric coating (SHC_3) before (C) and after (D) decylamine treatment. E) FTIR spectra of the polymeric coating (SHC_3) before (black) and after (red) post-chemical modification with decylamine molecules. F-I) Digital images and contact angle images (inset) of beaded water droplets on a polymeric gel (post-modified with decylamine)-coated glass (F), wood (G), plastic (H), and Al foil (I).

In the absence of AGO, the nearly transparent mixture of BPEI/5Acl was found to be inappropriate to provide such a coating. Similarly, the mixture of BPEI/5Acl in the presence of GO was also unable to provide coatings with desired antiwetting properties. This controlled study supported that the primary amine groups in AGO played a crucial role in the higher AGO doping in the BPEI/5Acl mixture provided a crack- and peel-free coating, most likely due to high mechanical strength of the flexible AGO sheets that were embedded in the polymeric coating. Moreover, this coating solution was also used in coating various rigid (glass and wood) and flexible (filter paper, Al foil and plastic film) substrates. Next, the polymeric coating (SHC_3) was exposed to various and common harsh physical insults that are generally practiced in examining the durability of the embedded antifouling property of the synthesized materials. First, our developed material was treated with abrasive sand paper, where the abrasive surface of the sand paper was rubbed on the polymeric coating with 100 g of an applied load—which resulted in severe physical damage to the polymeric coating, and the top surface of the polymeric coating was physically eroded in the form of some powdery fragments. Nevertheless, the extreme water repellency in the material was found to be intact with θ_{adv}~162.1° and contact angle hysteresis of θ_{hys}~3.9° (Figure 2.8A-C). Moreover, at the end, the abrasive surface of the sand paper—which was covered with these powdery

fragments of the polymeric coating, was also capable of displaying the nonadhesive superhydrophobicity (Figure 2.8D-E).

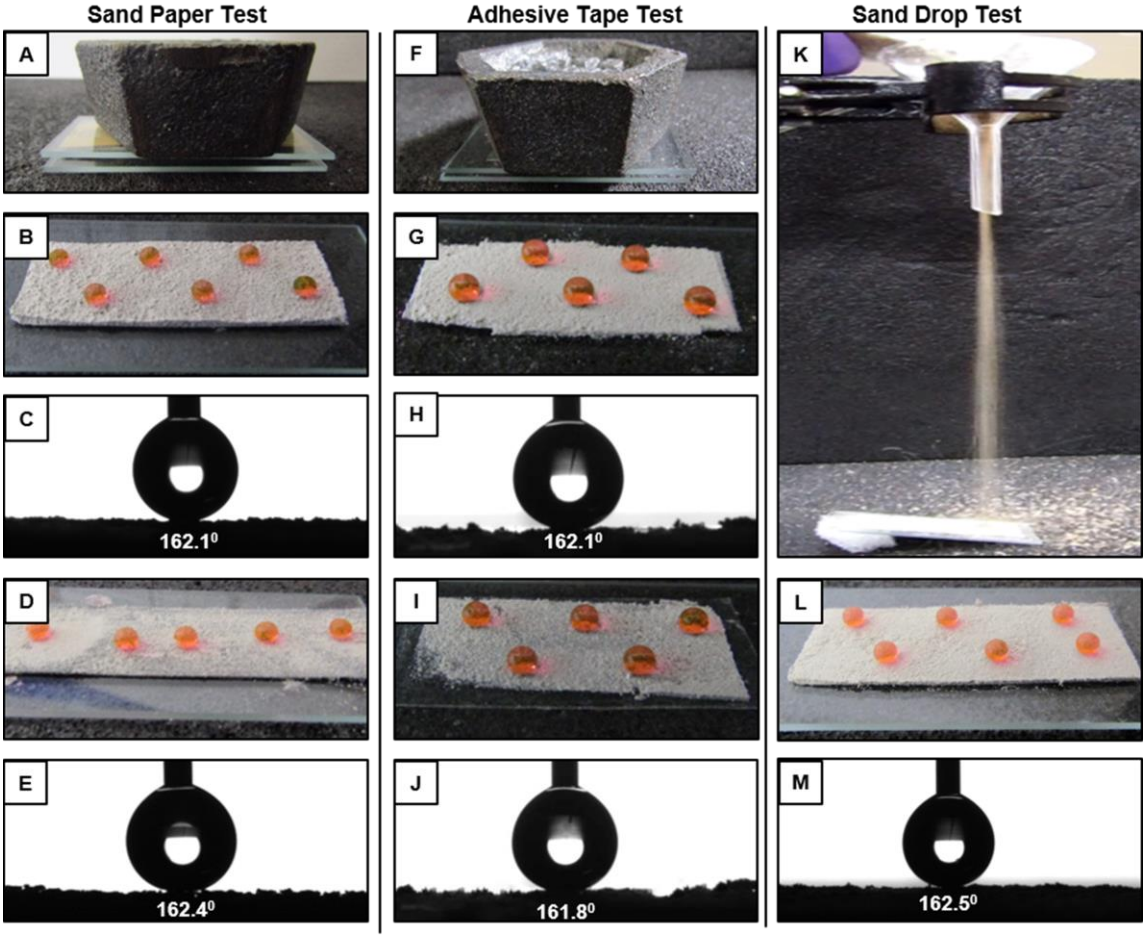

Figure 2.8. A) Digital images of the set up for sand paper test, where abrasive sand paper (grit no. 400) was sandwiched between the polymeric coating and applied load (100 g) and rubbed on the polymeric coating for at least 10 times. B-E) Digital images (B, D) and advancing contact angle images (C, E) of beaded water droplets (red color aids visual inspection) on both the polymeric coating (B, C) and abrasive sand paper (D, E) after performing the abrasive sand paper test. F) Digital images of the set up for adhesive tape test, where adhesive surface of the tape was brought in contact with polymeric coating and a pressure (with 500g load) was applied to achieve uniform and improve contact between the adhesive surface and polymeric coating. G-J) Digital images (G, I) and contact angle images (H, J) of beaded water droplets on both the polymeric coating (G-H) and adhesive tape surface (I-J), after peeling off the adhesive tape from the polymeric coating, during this adhesive tape peeling process, polymeric coating was fractured, and top surface of the coating was transferred to adhesive tape (I). K) Digital images of the set up for sand drop test, where 150 g of sand grains was poured onto the polymeric coating (tilted at 45°) from a height of 20 cm. L-M) Digital images (L) and contact angle images (M) of beaded water droplets on the polymeric coating after performing the sand drop test.

Second, an adhesive tape was placed in contact with the polymeric coating—with a 500 g load. The load was strategically applied to facilitate the interfacial contact between the adhesive surface and the surface of the polymeric coating (Figure 2.8F). At the end, the tape was manually peeled off from the polymeric coating. During this process, the top surface of

the polymeric coating was arbitrarily fractured, and some portions were transferred to the adhesive surface. As a result, the interior of the polymer coating was exposed to the air; however, the polymeric coating was not peeled off or detached from the substrate during this abrasion process. The freshly cleaved and exposed surfaces that were either immobilized onto the adhesive tape or remained on the glass substrate (the leftover portion of the coating) exhibited extreme water repellency with θ_{adv}>160° and θ_{hys}<5° (Figure 2.8G−J). This simple demonstration unambiguously revealed the existence of bulk (including the surface and interior) superhydrophobicity in the synthesized polymeric coating. Third, the polymeric coating (SHC_3) was exposed to a stream of sand that was poured from a 20 cm height, but both the physical integrity and the embedded extreme water repellency of the polymeric coating remained unaltered—and the water droplets were beaded on the polymeric coating with θ_{adv} ~ 162.5° and contact angle hysteresis of θ_{hys}~4.0° (Figure 2.8L, M). Further, these results supported the existence of an inherently stable polymeric coating with robust superhydrophobicity, where additional engineering of the interface between the polymeric coating and the surface of the substrate is not essential. In general, polymer-based soft materials are highly susceptible to deformation after the application of pressure, which may eventually destroy the topography that is essential to adopt superwettability in the materials. However, the attempts to address such important challenges are very few in the literature and most of these demonstrations were associated with the application of external stimuli (e.g., heat treatment) for restoring the essential topography in the physically damaged interfaces. The appropriate optimization of external stimuli for initiating the healing process would be extremely challenging in the diverse practical scenarios. Therefore, the design of polymeric coating—which would be capable of self-healing the extreme water repellency on the physically damaged interfaces—without requiring any external treatments (pH, light, heat or humidity etc.), is highly desirable and important for the practical utility of this bioinspired interface. Here, the AGO-incorporated polymeric coating was observed to be highly efficient in self-healing the superhydrophobicity in the damaged polymeric interface. As a proof of concept demonstration, an external pressure of 188 kPa was applied on the polymeric coating to examine the tolerance of both the physical integrity and embedded antifouling property of the synthesized material. The polymeric coating (SHC_3) was physically deformed at the location of applied pressure (Figure 2.9A), and the anti-fouling property was also significantly affected. The nonadhesive (θ_{hys}~3°) superhydrophobic coating became highly

adhesive (θ_{hys}~50°) due to the perturbation in the topography of the polymeric coating (physically deformed).

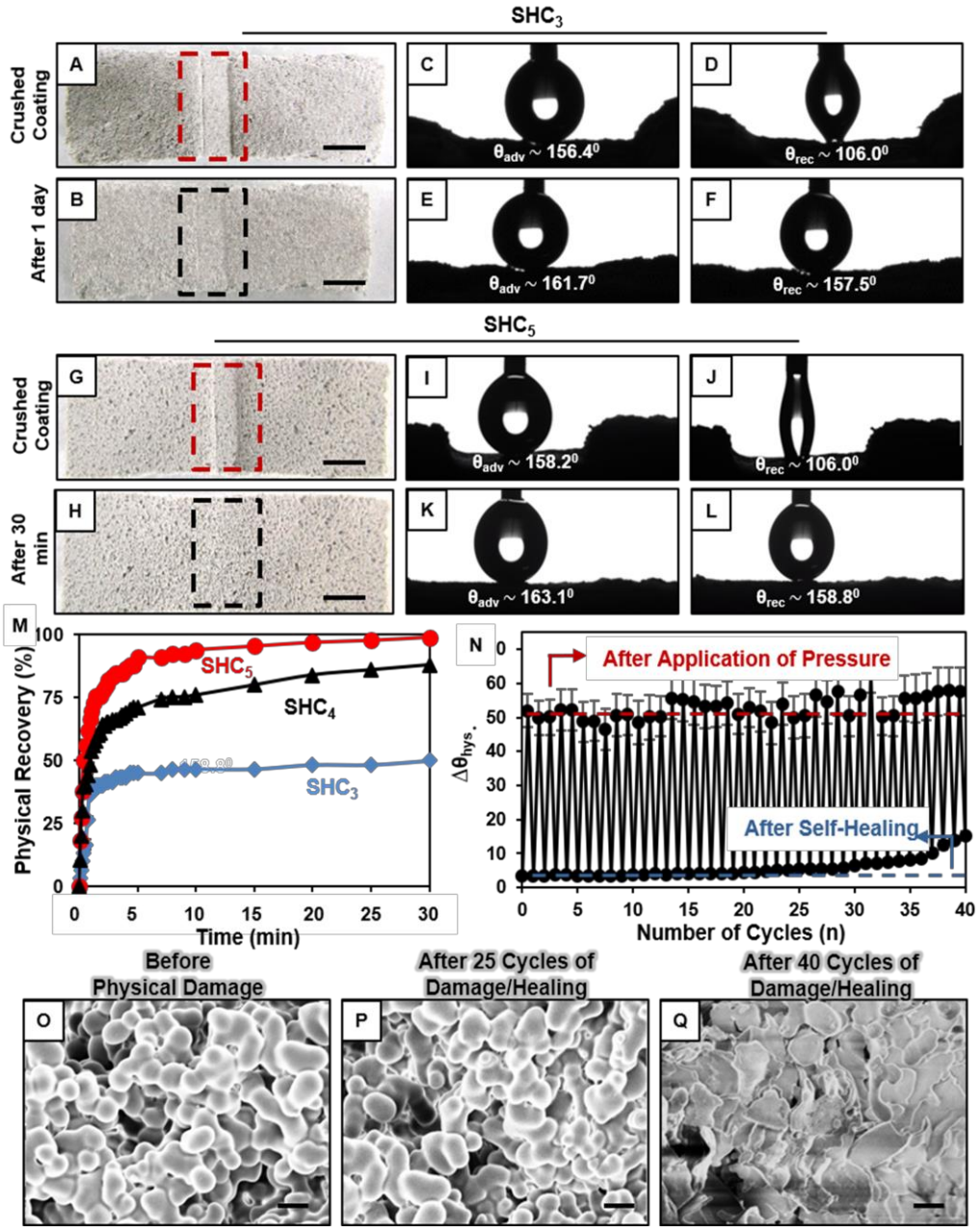

Figure 2.9. A−F) Digital images (A,B; scale bar: 5 mm) and advancing (C,E)/receding (D,F) contact angle images of polymer coating (SHC_3) after incurring the physical damage (A,C,D) and after partial physical recovery of the coating (B,E,F) after 1 day. C−L) Digital images (C,H; scale bar: 5 mm) and advancing (I,K)/receding (J,L) contact angle images of polymer coating (SHC_5) after incurring the physical damage (G,I,J) and after self-healing (H,K,L) of the damage. M) Plot comparing the rate of physical recovery of polymeric coatings (SHC_3, SHC_4, SHC_5) with time, after crushing the polymeric coating with applied pressure (~188 kPa). N) The plot accounting the changes in the advancing contact angle hysteresis of beaded water during repetitive (40 times cycles) physical damage/self-healing process. (SHC_5). O−Q) FESEM images (scale bar: 10 μm) of polymeric coating (SHC_5) before incurring physical damage (O) and after performing damage/healing cycles for 25 times (P) and 40 times (Q).

However, after releasing the applied pressure, the physical shape of the polymeric coating

was gradually being self-healed with time without the requirement of any kind of manual intervention, and after 1 day, the recovery of physical deformation was estimated to be 72% (Figure 2.9A-F). Moreover, the polymeric coating was able to restore the native nonadhesive superhydrophobicity with a θ_{hys} of ~3°, and an example of such self-healing of the bioinspired wettability in the polymeric coating without application of any external stimulus is unprecedented. Interestingly, the process of recovery for both the physical deformation and anti-fouling property in the polymeric coating can be further significantly accelerated by incorporating more AGO sheets in the polymeric coating. The appropriately post-functionalized polymeric coating (SHC_5) having a higher amount (30.77 μg/mL) of AGO was highly efficient in rapid and complete recovery of both the physical deformation and the intrinsic antifouling property. Upon the release of the applied pressure, the physically damaged (Figure 2.9G) material with highly adhesive (θ_{hys}~50°, Figure 2.9I-J) superhydrophobicity (θ_{adv}~158°, Figure 2.9I) was noticed to be proficient in restoring both the native physical shape (Figure 2.9H) and embedded nonadhesive (θ_{hys}~4°, Figure 2.9K-L) superhydrophobicity (θ_{adv}~163°, Figure 2.9K)—without any external interventions. These recoveries of physical deformation and wettability processes were exponential with time. Both the physical damage and the embedded antifouling property were completely self-healed under ambient conditions within 30 min. The rate of healing depended on the amount of loading of AGO in the bio-inspired coating as shown in Figure 2.9M. Next, the same polymeric interface was exposed to repetitive physical damage/self-healing process through the successive application of pressure and followed by the release of the applied pressure. After incurring each instance of physical damage on the polymeric coating, the self-healing of the native antifouling property in the polymeric coating was characterized by estimating the water CA hysteresis (θ_{hys}; which accounts for the extent of adhesive interaction between the beaded water droplet and the polymeric interface). The polymeric coating was capable of restoring the nonadhesive antifouling property 25 times with a θ_{hys} below 5°. The morphologies of the polymeric coating were characterized with FESEM imaging (Figure 2.9O-P) before the incurring of physical damage and after this repetitive (25 times) performance of the damage/ healing processes. In both cases, the topography of the polymeric coatings was found to be indistinguishable with a similar random arrangement of granular domains. Further, on increasing this damage/healing cycle at the same location of the polymer coating, a gradual and continuous increment in contact angle hysteresis was noticed. After extending this damage/ healing cycle 37 times on the same polymeric

interface, the θ_{hys} was measured to be higher than 5°—but still below 10°. Thus, even after 37 cycles of the repetitive self-healing process, the polymeric coating remained efficient in restoring the nonadhesive superhydrophobicity—without demanding any manual interventions as shown in Figure 2.9N. However, incomplete healing of both the physical deformation and wettability was noticed after repeating the damage/healing cycles 40 times, and the polymeric coating was found to be permanently adhesive with a θ_{hys} of 15° (Figure 2.9N). Moreover, the topography of the material was observed to be significantly deformed, where granular domains appeared flattened (Figure 2.9Q) even after 1 week, and only 60% physical deformation was self-healed in the polymeric coating. Generally, the superhydrophobic surfaces with θ_{hys} below 10° and above 10° are considered nonadhesive (lotus leaf) and adhesive (rose petals) superhydrophobic interfaces, respectively. The synthesized polymeric coating displayed both of these bioinspired interfaces. After the application of external pressure (188 kPa) on the polymeric coating, the embedded bioinspired wettability, i.e., nonadhesive superhydrophobicity (lotus leaf), gets compromised, and another bioinspired wettability—which is recognized as adhesive superhydrophobicity (rose petal) was developed with a θ_{adv} of ~159° and $\theta_{hys} > 50°$ as shown in Figure 2.10A, B, likely through attaining a Cassie−Wenzel transitional state. Eventually, this transient switching of two bioinspired wettabilities energetically helps in the collection/immobilization of the aqueous phase at the desired location without any spilling or spreading of the beaded aqueous phase on the polymeric coating as shown in Figure 2.10C. Further, this transient and reversible transition between two bioinspired wettabilities from nonadhesive ($\theta_{hys}<5°$) to adhesive ($\theta_{hys}>50°$) superhydrophobicity, and vice versa, was exploited in immobilizing the water-soluble agents on the polymeric coating—directly from the aqueous phase which might be interesting in various fundamental and applied contexts. As a proof of concept demonstration, a pressure above 188 kPa was applied at three different locations of the polymeric coating for inducing adhesive superhydrophobicity at those selected locations through the physical deformation of the polymeric coating (Figure 2.10D). The polymeric coating was immediately immersed in red-colored aqueous solution of rhodamine dye molecules for 10 s. Then, the polymeric coating was taken out from colored aqueous solution water to open air. The polymeric coating was found with an adhered red aqueous phase only at those three selected locations (Figure 2.10E) —which were physically deformed by the application of appropriate external pressure and no further spilling or spreading of the red aqueous phase was noticed on the polymeric coating. Over time, the red aqueous phase was

air-dried and the physically deformed interfaces on the polymeric coating were completely recovered with the nonadhesive superhydrophobicity (θ_{adv} of ~161° and θ_{hys} ~3°), even though the water-soluble molecules were impregnated in the polymeric coating as shown in Figure 2.10F.

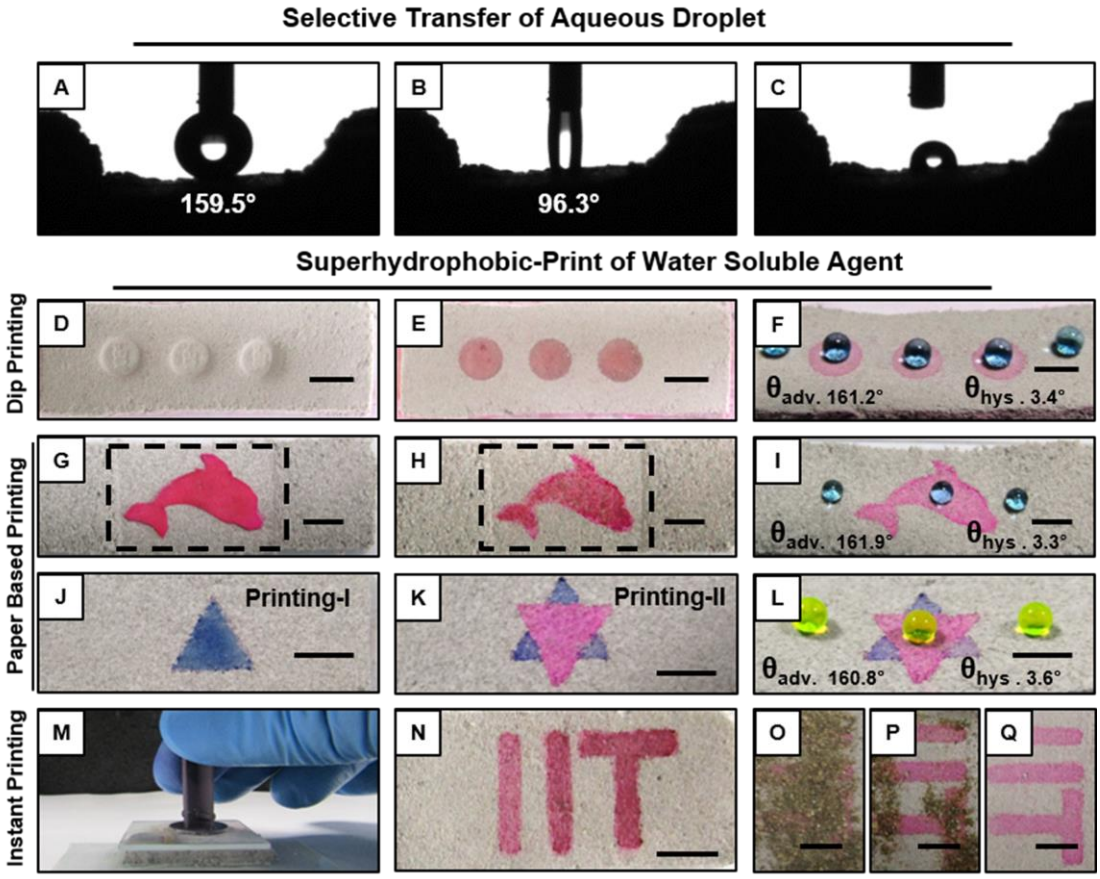

Figure 2.10. A−C) Demonstration of breaking of beaded water droplet (θ_{Adv} ~160°; 1 µL) by adhesive interaction with the physically damaged polymeric coating (SHC_5) during receding of water droplet (B, C). (D−F) Digital images (scale bar: 5 mm) of physically damaged (D, with three circular spots) polymeric coating after selective collection (E) of aqueous solution of rhodamine 6G and after self-healing (F) of the physical damage. (G−I) Digital images (scale bar: 5 mm) of a paper-based contact printing process with a dolphin shaped paper, where the paper was soaked with an aqueous solution of rhodamine dye prior to bringing contact with physically damaged (marked with dotted box) polymeric coating (G). On removal of the paper, the polymeric coating was found with an impregnated aqueous phase (H), and finally a self-healed superhydrophobic print (I, dolphin shape) of rhodamine molecules was observed after air-drying of the aqueous phase. (J−L) Digital images (scale bar: 5 mm) illustrating the two steps (printing I and II, J, K) of contact printing of two different dye molecules (methylene blue and rhodamine 6G) on the physically damaged polymeric coating with triangular shaped paper. M, N) Instant printing of rhodamine dye on a superhydrophobic surface by using a "lab-made" stamp of "IIT" (M) that was inked with an aqueous solution of rhodamine prior to execution.

This superhydrophobic printing of hydrophilic molecules provided a simple basis to protect water sensitive hydrophilic agents from unwanted exposure to the aqueous phase. Next, a facile, paper-based and contact-mediated, impregnation of hydrophilic small molecules on the

polymeric coating was developed, and the polymeric coating was decorated with a superhydrophobic print of water-soluble agents—without exposing the entire polymeric coating to the aqueous phase. First, a paper was cut in the shape of a dolphin and was wetted with an aqueous (red color) solution of rhodamine prior to bringing it into contact with a physically deformed and comparatively flattened interface (denoted with the dotted box in Figure 2.10G) of the polymeric coating. The wet paper was kept on the polymeric surface for a few minutes to ensure the selective transfer of the aqueous phase from the wet paper to the polymeric interface. After gentle removal of the adhered paper from the polymeric coating, a hydrated print in the shape of a dolphin appeared on the surface of the polymeric coating (Figure 2.10H). Then, the polymeric coating was allowed for air-drying, and at the end, both the physical shape and antifouling property (with θ_{adv} of ~162° and θ_{hys} ~ 3°, Figure 2.10I) were self-healed in the material—even after impregnation of hydrophilic small molecules onto the polymeric coating. As compared to the previous process, a tiny amount of aqueous phase was used in this paper-based contact printing approach. Moreover, a complex print—that was composed of multiple (blue (methylene blue) and red (rhodamine) color dyes, Figure 2.10J−L) hydrophilic molecules—was developed through successive and strategic incorporation of dye molecules, one (the print I, Figure 2.10J) after another (print II, Figure 2.10K) following a repetitive physical deformation and healing of polymeric coating as shown in Figure 2.10L. A filter paper with a triangular shape was used for location selective incorporation of two different dye molecules. Then, a direct and instant immobilization of hydrophilic small molecules on the superhydrophobic polymeric coating was achieved through selective immobilization of an aqueous solution of desired small molecules during the induction of the physical deformation on the polymeric coating. The object—which was used for inducing the physical deformation on the polymeric coating—was first inked with an aqueous solution of dye prior to exerting the required pressure on the polymeric coating. A wood-based crude stamp with a shape of IIT (short form of Indian Institute of Technology) was developed at our lab for proof of concept demonstration, where a very small volume (<10 μL) of aqueous solution (red ink) of rhodamine was used to wet the wooden stamp ("IIT") prior to bringing it into contact with a polymer coating and was followed by the application of manual moderate pressure on the material. Instantly, the aqueous solution of rhodamine dye was transferred to the polymeric coating (Figure 2.10N). With time, the aqueous phase evaporated, and both the antifouling property and the physical deformation were self-healed in the polymeric coating and eventually provided a rapid and facile approach

to develop a print of hydrophilic molecules on the extremely water repellent superhydrophobic interfaces (with θ_{adv} of ~161° and θ_{hys} ~ 4°), where a beaded water droplet can instantly roll off on slight tilting (even less than 5°) of the surface. This instant rolling of a beaded water droplet on the nonadhesive superhydrophobic surface actively helped in collecting/removing dust and the dirt particles that were deposited on the superhydrophobic print and eventually provided a facile basis to develop a self-cleaning and waterproof superhydrophobic print of water-soluble agents (Figure 2.10O−Q).

2.4. Conclusion

In conclusion, the current report exploited a simple and robust1,4-conjugate addition reaction between amine and acrylate groups for strategic and covalent integration of modified graphene oxide, which is well-recognized for its impeccable mechanical properties. The optimum incorporation of AGO sheets in the reaction mixture of BPEI/5Acl allowed preparing a covalently cross-linked "amine-reactive" gel which was remained highly flexible and durable polymeric material, which were appropriate to display extreme water repellency both in air and under oil. Furthermore, this semisolid gel material allowed us to mold it in desired shapes, which could be useful in various prospective applications including protein detection, tissue engineering, protein crystallization, high throughput drug sensing, etc. The same reaction mixture (before gelation) was exploited to develop a highly durable and absolutely self-healable superhydrophobic coating without requiring any external intervention (or stimuli). Moreover, the synthesized polymeric coating was inherently capable of a facile and unique reversible switching of two bioinspired wettabilities—that are nonadhesive (lotus leaf) and adhesive (rose petal) superhydrophobicity. This transient and reversible switching between adhesive and non-adhesive bioinspired wettability was strategically exploited in developing rewritable aqueous patterns on the extremely water repellent polymeric coating. Further, this synthesized polymeric coating was capable of impregnating hydrophilic agents directly from the aqueous phase without sacrificing the embedded antifouling property. Such interfaces could be useful for many fundamental and applied interests, including the synthesis of smart drug delivery systems, catalysis, self-assembly of colloids, cell culture chips, robust open microfluidic systems, reusable chemical sensing, etc. Moreover, this facile and scalable synthetic approach for developing a superhydrophobic coating with impeccable tolerant to practically relevant severe settings could be useful in broad contexts and various prospective applications.

2.5. Reference

1. J. Genzer, K and Efimenko, *Science,* 2000, **290**, 2130.
2. K. Liu, X. Yao and L. Jiang, *Chem. Soc. Rev.,* 2010, **39**, 3240.
3. A. Tuteja, W. Choi, M. L. Ma and J. M. Mabry, *Science,* 2007, **318,** 1618.
4. H. Bellanger, T. Darmanin, E. T. de Givenchy and F. Guittard, *Chem. Rev.,* 2014, **114**, 2694.
5. X. Deng, L. Mammen, H. J. Butt and D. Vollmer, *Science,* 2012, **335,** 67.
6. Z. Chu and S. Seeger, *Chem. Soc. Rev.,* 2014, **43**, 2784.
7. L. Feng, S. H. Li, Y. S. Li, H. J. Li, L. J. Zhang, J. Zhai, Y. L. Song, B. Q. Liu, L. Jiang and D. B. Zhu, *Adv. Mater*., 2002, **14**, 1857.
8. X. M. Li, D. Reinhoudt and M. Crego-Calama, *Chem. Soc. Rev*., 2007, **36**, 1350.
9. X. Zhang, F. Shi, J. Niu, Y. G. Jiang and Z. Q. Wang, *J. Mater. Chem.,* 2008, **18**, 621.
10. X. Yao, Y. Song and L. Jiang, *Adv. Mater.,* 2011, **23**, 719.
11. E. Ueda and P. A. Levkin, *Adv. Mater.,* 2013, **25**, 1234.
12. L. Wen, Y. Tian and L. Jiang, *Angew. Chem. Int. Ed.,* 2015, **54,** 3387.
13. A. Gao, Q. Wu, D. Wang, Y. Ha, Z. Chen and P. Yang, *Adv. Mater.,* 2016, **28**, 579.
14. Y. Y. Yan, N. Gao and W. Barthlott, *Adv. Colloid Interface Sci.,* 2011, **169**, 80.
15. X. Feng and L. Jiang, *Adv. Mater.,* 2006, **18**, 3063.
16. T. Verho, C. Bower, P. Andrew, S. Franssila, O. Ikkala and R. H. A. Ras, *Adv. Mater.,* 2011, **23**, 673.
17. L. Ionov and A. Synytska, *Phys. Chem. Chem. Phys.,* 2012, **14**, 10497.
18. U. Manna and D. M. Lynn, *Adv. Mater.,* 2013, **25,** 5104.
19. J. E. Mates, I. S. Bayer, J. M. Palumbo, P. J. Carroll and C. M. Megaridis, *Nat. Commun.,* 2015, **6**, 8874.
20. M. Paven, R. Fuchs, T. Yakabe, D. Vollmer, M. Kappl, A. N. Itakura and H.-J. Butt, *Adv. Funct. Mater.,* 2016, **26,** 4914.
21. W.-K. Lee, W.-B. Jung, S. R. Nagel and T. W. Odom, *Nano Lett.,* 2016, **16**, 3774.
22. X. T. Zhu, X. Zhang, X. Men, J. Yang, K. Wang, X. Xu, X. Zhou and Q. Xue, *J. Mater. Chem.,* 2011, **21**, 15793.
23. Y. Li, L. Li and J. Q. Sun, *Angew. Chem., Int. Ed.,* 2010, **49**, 6129.
24. H. X. Wang, Y. Xue, J. Ding; L. Feng, X. Wang and T. Lin, *Angew. Chem., Int. Ed.,* 2011, **50**, 11433.

25. U. Manna, M. C. D. Carter and D. M. Lynn, *Adv. Mater.,* 2013, **25**, 3085.
26. M. Wu, Y. Li, N. An and J. Sun, *Adv. Funct. Mater.,* 2016, **26,** 6777.
27. T. Lv, Z. Cheng, E. Zhang, H. Kang, Y. Liu and L. Jiang, *Small,* 2017, **13**, 1503402.
28. W. Wang, J. Salazar, H. Vahabi, A. Joshi-Imre, W. E. Voit and A. K. Kota, *Adv. Mater.,* 2017, **29**, 1700295.
29. T. Lv, Z. Cheng, D. Zhang, E. Zhang, Q. Zhao, Y. Liu and L. Jiang, *ACS Nano,* 2016, **10**, 9379.
30. B. D. Hatton and J. Aizenberg, *Nano Lett.,* 2012, **12**, 4551.

Title: Single Multilayer Coating for Achieving Stretchable and Abrasion Tolerant Superhydrophobic and Underwater Superoleophobic Interfaces*

Stretchable and durable superhydrophobic and underwater superoleophobic interfaces are of potential interest for developing various smart materials. In general, nature-inspired water (lotus leaf mimicking superhydrophobicity in air) and oil (fish scale-inspired superoleophobicity underwater) repellent interfaces that are associated with specific physical and chemical parameters, are developed by adopting separate synthesis processes. However, a slight perturbation of the essential topography and chemistry is likely to cause permanent damage to these two distinct nature-inspired artificial wettabilites. In this chapter, the covalent integration of the chemically reactive polymeric nanocomplex and amino graphene oxide through layer-by-layer (LbL) deposition technique provided a single and simple method to fabricate highly stretchable and abrasion tolerant both the fish scale and lotus leaf-inspired interfaces. These interfaces were capable of sustaining: (a) large tensile deformation (100%) for multiple times (500 times), and, (b) severe physical/chemical exposures—including physical erosion of the polymeric coating, prolonged exposure to extremes of pH, salinity, ultraviolet radiation, physical manipulations, and so on. Furthermore, such a durable material was deposited on various substrates, and thus, would be of potential interest for diverse prospective applications in practically relevant harsh conditions.

* **A. Das,** S. Sengupta, J. Deka, A. M. Rather, K. Raidongia U. Manna. *J. Mater. Chem. A,* 2018, **6**, 15993.

3.1 Introduction

A common approach for synthesizing stretchable superhydrophobic and under-water superoleophobic interfaces is fundamentally challenging to achieve. Such interfaces have immense potential for developing various smart applications related to stretchable electronics, gas sensors, flexible microfluidics, functional textiles, wearable devices, oil transportation and so on.[1-7] Generally, the induction of tensile deformations on such special interfaces leads to change in the super liquid wettability.[8,9] Nevertheless, a few designs have provided extreme water repellent (inspired by the lotus leaf) interfaces that remained unaffected, even after incurring tensile deformation.[1-7] Together with tensile deformation, these bio-mimicking interfaces are likely to be exposed to other physical/chemical harsh insults, such as, scratching, stretching, creasing, twisting, exposure to ultraviolet (UV) radiation and complex aqueous media and so on, during packaging, transportation and performance of synthesized materials at the sites of practical applications.[7,10] However, these important durability issues have not been examined for most of the reported stretchable and thin conventional superhydrophobic interfaces.[1-6] The applicability of the reported stretchable materials is less likely possible in practically relevant severe settings. In the previous chapter, we have developed a highly durable superhydrophobic coating by using the doctor blade method. Such coating was capable of sustaining severe physical damage, including the removal of the top surface of the coating. The freshly exposed interiors of the reported coatings have adequate topography and chemistry to display uninterrupted superhydrophobicity.[11,12] However, this doctor blade method introduced in chapter 2 was inappropriate to coat geometrically complex objects and such coatings also failed to sustain tensile deformation. Furthermore, the examples of stretchable fish-scale inspired underwater superoleophobicity that specifically perform underwater, are also rare in the literature due to the poor sustainability of the highly water-compatible coatings (that are mostly synthesized from the polymeric gel, brittle metal oxides and electrostatic multilayers) under the applied tensile strain (TS).[13-17, 18–22] In general, the substrates with a high Young's modulus are selected to avoid large tensile deformation/ distortion of the synthesized special interfaces and thus, a change in the topography of the water-compatible hierarchical interfaces are mostly avoided.[13-17,18–22] Such approaches are absolutely incapable of providing stretchable superoleophobicity underwater. The nature-inspired special interfaces that are efficient not only in sustaining: (1) tensile deformation (often referred to as stretching) but also, (2) various other physical and chemical abrasions would be useful in various fundamental and

applied contexts. A common way to synthesize stretchable nature-inspired wettabilities with high durability would be most appropriate for the practical use of highly prospective, nature-inspired interfaces in the near future. In this chapter, a common and simple chemical approach has been developed for synthesizing: (a) highly stretchable, and (b) durable (capable of withstanding various physical/chemical abrasions) special interfaces that remained proficient in displaying, (c) nature-inspired various bulk wettabilities, including lotus leaf-inspired superhydrophobicity and fish scale mimicking underwater superoleophobicity. In this rational design, the covalent integration of chemically reactive polymeric nano-complexes (CRPNC) and amino-graphene oxide (AGO) was achieved following a substrate independent, simple and covalent deposition process, i.e., a 1,4-conjugate addition mediated layer-by-layer (LbL) coating technique, without using any sophisticated instrumental set up. The synthesized multilayers of CRPNC and AGO were found to be chemically reactive for further chemical manipulations, and displayed durable superhydrophobicity in air and superoleophobicity under water, depending on the selection of chemical post-modulations of the reactive and bulk multilayer coatings. The multilayers with special and bulk bio-mimicking wettability was successively (500 times) exposed to tensile deformations (100% strain) and still remained capable of repelling the beaded liquid droplet (water in air/oil under water) with advancing liquid contact angle above 150º and contact angle hysteresis of below 10º. Furthermore, the synthesized material with a physically damaged interface was also able to show both the liquid wettability during tensile deformations. Moreover, the synthesized material was found to be liquid (oil/water) repellent, even after prolonged exposure to various complex aqueous media (extremes of pH, salinity, and so on) and UV radiation.

3.2 Experimental Section

3.2.1. Materials

D-glucamine (>95%) was procured from TCI (Tokyo Chemical Industry), India. Silicone elastomer kit was procured from Electrochem, India. Sources of other chemicals have already been mentioned in the Chapter 2.

3.2.2. General considerations

All the instrumental details have been provided in the Chapter 2.

3.2.3. Synthesis of amino graphene oxide (AGO)

The detailed synthetic procedure of amino graphene oxide has been discussed in the Chapter 2.

3.2.4. Preparation of PDMS film and multilayer construction

Silicone elastomer and curing agent were mixed in 10:1 ratio and the mixture was poured into a Petri-dish followed by heating at 80°C for 3 hours to get the PDMS film. Fabrication of reactive film by LbL deposition process: The solution of 5Acl (0.252 M) and BPEI (0.105 M) in methanol were prepared in separated glass vials. Then, 5 ml of 5Acl and 1 ml of BPEI were mixed and kept for 10 minutes for initiating the formation of chemically reactive' polymeric nano-complex (CRPNC) in the reaction solution. Another dipping solution—that is AGO, was prepared in ethanol/water (1:1) mixture (4 ml; 25 µL of NH_3 (25%) was added in the dipping solution to prevent any protonation of grafted primary amine on AGO). Then, the freshly prepared CRPNC and AGO were covalently integrated into the multilayers coating on the selected substrates (glass, PDMS, wood, plastic, aluminium and gloves) following Layer-by-Layer (LbL) deposition process. The detailed process was as follows; a) the selected substrates were immersed in the solution of AGO for 30 s, b) substrates were removed and washed with two consecutive methanol bath for 30 s prior to c) place in the solution of CRPNC in methanol for 30 s, and then d) substrates were washed in the manner described in step (b). This whole deposition cycle was repeated iteratively 15 times. After the completion of the first cycle of deposition of AGO and CRPNC, the dipping time of the selected substrate in the respective dipping solutions and washing solutions was reduced to 15 sec. After fabrication, films were washed with methanol for 30 min prior to air dry the samples.

3.2.5. Post chemical-modification with amine-containing small molecules

The chemically reactive multilayers coatings were treated with appropriate chemicals to achieve desire nature-inspired interfaces. The multilayers coating were immersed in octadecylamine solutions (in ethanol, 2.5 mg mL^{-1}) for achieving superhydrophobicity in air, and the same chemically reactive coatings were immersed in D-glucamine solution (in water, 2.5 mg mL^{-1}) for adopting underwater superoleophobicity. After 12 h treatment, the polymeric coatings were washed thoroughly with ethanol/water for one hour to remove unreacted and loosely bound amine-containing small molecules and dried in the open air.

3.2.6. Physical/chemical durability of the anti-wetting property

The multilayers coatings embedded with either superhydrophobicity in air or superoleophobicity underwater were exposed to various practically relevant severe

physical/chemical challenges—including exposures to various physical manipulations (e.g.; bending creasing, twisting etc.), sand paper abrasion test, adhesive tape peeling test, sand drop test, UV irradiation and chemically harsh (extremes of pH, salinity etc.) aqueous media. The details of these durability tests have been accounted in the following sections;

3.2.6.1. Tensile deformation test

The multilayers coated superhydrophobic PDMS film was manually stretched with the different tensile strains. The stretching percentage was calculated by measuring the change in length of the material before and after incurring the tensile deformation using the following formula:

Percentage (%) of stretching = [Final length – Initial length]/ [Initial length] x 100

3.2.6.2. Sand paper abrasion test

First, a piece of sandpaper was attached to a glass slide with double-sided adhesive tape and the abrasive surface was placed on the multilayers coated PDMS films. Then the sand paper was rubbed manually across the coated substrate four times back and forth with an applied load of 200 g. The external load was applied to improve the contact between the abrasive sand paper surface and multilayers coatings. This abrasive test led to physical erosion of the polymeric coating. So, the effect of tensile deformation of such physically damaged interfaces is also investigated. The anti-wetting property was examined with visual inspection and contact angle measurements.

3.2.6.3. Sand drop test

The PDMS films were kept tilted at 45° inclination and then 150 g of sand grains were poured onto the polymeric coated PDMS films from a height of 20 cm using a glass funnel. After this test, the anti-wetting property was examined with visual inspection and contact angle measurements and the impact of further physical deformation was also investigated.

3.2.6.4. Adhesive tape test

First, a fresh adhesive interface of a double-sided adhesive tape was attached on a glass slide and then another adhesive surface was brought in contact with the multilayers coatings with an applied load of 200 g. Then, the adhesive tape was peeled off from the films. Then, the embedded super-wetting property was examined on the adhesive tape treated substrate with and without applied tensile strain (100%).

3.2.6.5. Complex aqueous/UV exposure

The coated PDMS films were immersed in different harsh aqueous media, including artificial sea water (solution of 0.226 g $MgCl_2$, 0.325 g $MgSO_4$, 2.673 g NaCl, and 0.112 g $CaCl_2$ in

100 mL of deionized water), 0.01 M NaOH (pH = 12), 0.1 M HCl (pH = 1), river water (Brahmaputra river, Assam, India), and kept under UV exposure (254 nm and 365 nm) for 10 days. Then, the anti-wetting property was examined with contact angle measurements at a regular time interval.

3.3. Results and Discussions

3.3.1. Synthesis and characterization of multilayers of 'chemically reactive' polymeric nanocomplex/amino-graphene oxide

In the recent past, a few elegant approaches were introduced for synthesizing lotus leaf-inspired thin (nanometer scale) and stretchable interfaces following deposition of various nanomaterials, including silver nanoparticle, polyaniline nanostructure, carbon black, graphene sheets, carbon nanofibers and silica nanoparticles.[1–6] In general, such approaches for depositing 'chemically non-reactive' (refers to an inability to react spontaneously and covalently with other chemicals) nanomaterials only provided the desired hierarchical topography for developing lotus leaf-inspired stretchable superhydrophobicity in air. Moreover, these designs remained inappropriate for developing fish scale-mimicking underwater superoleophobicity. Furthermore, many of these earlier reports were very specific about using certain substrates.[1-4,6] In the chapter 2, the flexible amino graphene oxide (AGO) nanosheets were incorporated following a sol-gel conversion process for developing compressible superhydrophobic monoliths and coating. However, such material remained inefficient for providing stretchable fish scale and lotus leaf-inspired coatings. In this chapter, AGO and CRPNC were appropriately and covalently integrated through successive 1,4-conjugate addition reactions (as shown in Figure 3.1A-C) for developing: (1) highly stretchable, (2) substrate independent, and, (3) both durable lotus leaf and fish scale-inspired wettabilities through LbL deposition process. The synthesized chemically reactive multilayers of CRPNC/AGO (Figure 3.1C, 15 bilayers, where each bilayer is comprised of deposition of CRPNC and AGO) were found to be hydrophobic (98.5°) in air and oleophobic (87.5°) under water as shown in Figure 3.1D-G. The field emission scanning electron microscopy (FESEM) images of these multilayer coatings revealed the presence of an arbitrary association of CRPNC that are covalently integrated with flexible AGO sheets (Figure 3.1H-I) through 1,4-conjugate addition reactions. The hierarchical topography consisted of micro/nano domains required for developing nature-inspired special wettability. Furthermore, the successful incorporation of AGO in the multilayer coating was confirmed

from the Raman spectral analysis, where both the characteristic G and D bands of AGO (Figure 1J, black) appeared.

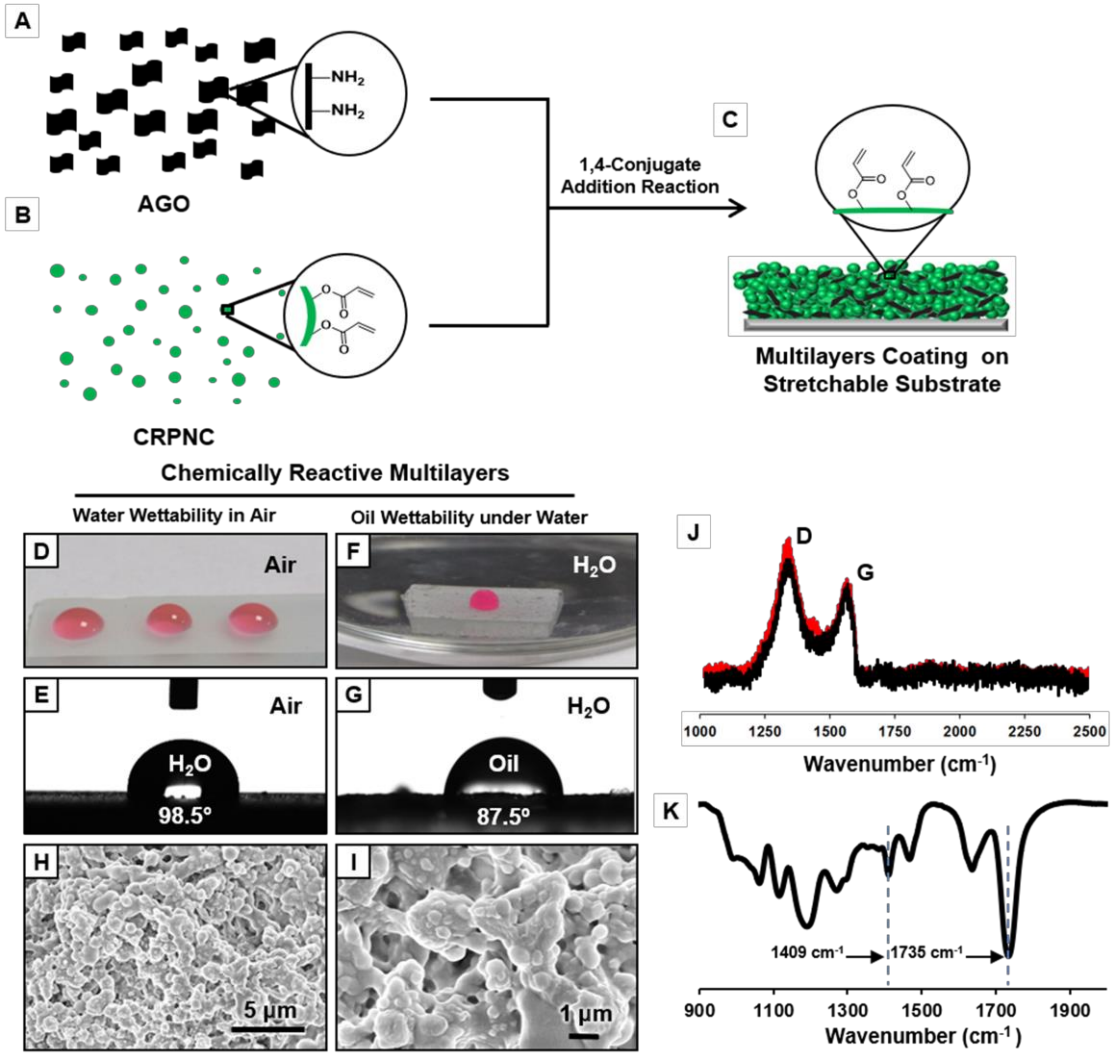

Figure 3.1. A-B) Schematic illustrating the covalent integration of amine grafted graphene oxide (A; AGO) and a chemically reactive polymeric nano-complex (B; CRPNC), prepared by mixing branched polyethylenimine (BPEI) and penta-acrylate in methanol) using a 1,4 conjugate addition reaction. C) Schematic representation of the multilayers of CRPNC/AGO having amine reactive residual acrylate groups all through the polymeric coating, including the surface and interiors. D–G) Digital (D and F) and contact angle (E and G) images of beaded water droplets (in air, D and E) and oil droplets (under water, F and G) on the untreated multilayer coated glass slide. H-I) FESEM images of multilayer coatings under low (H) scale: 5 µm and high (I) scale: 1 µm magnifications. J) Raman spectra of the multilayer coatings before (black) and after (red) exposure of the interiors. K) Fourier-transform infrared (FTIR) spectra of the multilayer coating.

Even after removal of the top surface of the coating following an adhesive tape peeling process, the exposed interior (shown in red), of the synthesized coating also displayed the characteristic Raman spectral signature for AGO as shown in Figure 3.1J. This result

indicated the existence of AGO all through the polymeric coating, including the top interface and the interiors.

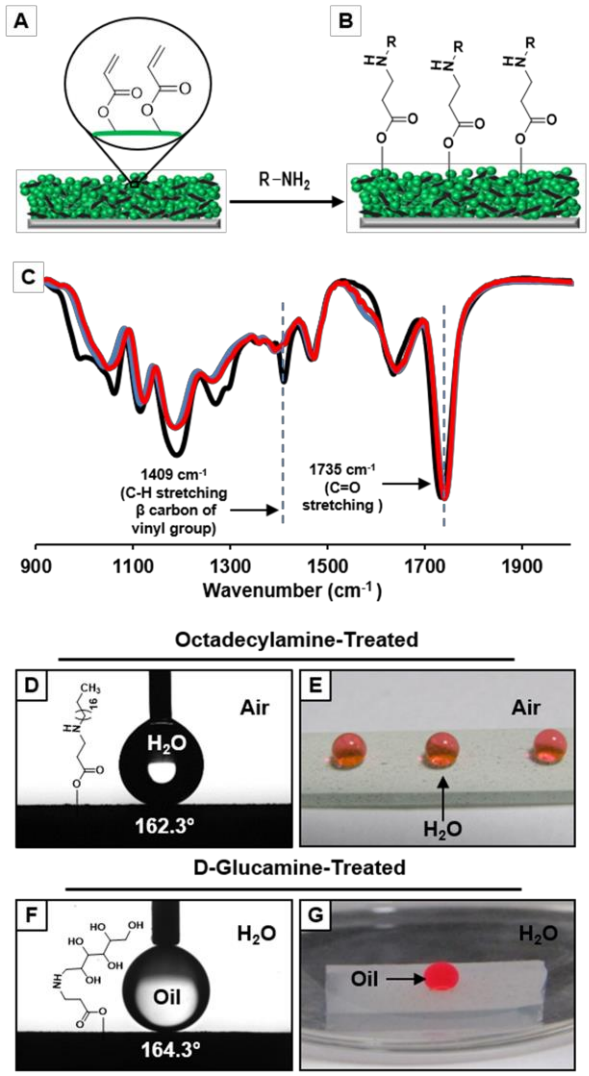

Figure 3.2. A-B) Schematic of post-modifications of the multilayers with primary amine-containing small molecules through 1,4-conjugate addition reaction and this post-modification is all throughout the coating, including the top surface and interiors. C) Fourier-transform infrared (FTIR) spectra of the multilayer coating before (black) and after post-modification with a primary amine containing small molecules, (e.g., ODA (red) and D-glucamine (blue)). D-G) Advancing contact angle (D and F) and digital (E and G) images of beaded water ((D and E), in air) and oil ((F and G), under water) droplets on multilayer coatings which were treated with ODA (D and E) and D-glucamine (F and G) molecules.

The multilayer coating (thickness ~ 2.4 mm) of CRPNC/AGO consisted of residual acrylate groups. Thus, the inherently 'chemically reactive' multilayer coating allowed further post-chemical modifications through a simple 1,4-conjugate addition reaction. The prominent appearance of infrared (IR) peaks at 1409 cm^{-1} and 1735 cm^{-1} unambiguously referred to the characteristic signatures for (a) the symmetric deformation of the C–H bond for the β carbon

of the vinyl groups and (b) the carbonyl stretching. This IR study eventually confirmed the existence of residual acrylate groups in the synthesized material as shown in Figure 3.1K. Next, the multilayer coating was individually exposed to two distinct primary amine-containing small molecules, D-glucamine (hydrophilic) and ODA (hydrophobic) as shown in Figure 3.2A-B, and this resulted in the significant reduction of the IR peak intensity at 1409 cm^{-1} (Figure 3.2C, blue (D-glucamine treated) and red (ODA modified) curves) was noted in comparison to the IR peak at 1735 cm^{-1}. During the 1,4-conjugate addition reaction, the carbonyl groups were retained and the vinyl groups were consumed. Thus, the significant change in IR peak intensity at 1409 cm^{-1} with respect to the IR signature for the carbonyl group (at 1735 cm^{-1}) strongly suggested the covalent integration of the primary amine-containing small molecules in the multi-layered coatings. Thus, the multilayer coating of CRPNC/AGO having residual acrylate group observed to be 'chemically reactive' to primary amine-containing small molecules as shown in Figure 3.2C. The impact of these two distinct chemical modulations in the chemically reactive multi-layered coating through the 1,4-conjugate addition reaction was significant on the liquid (oil/water) wettability.

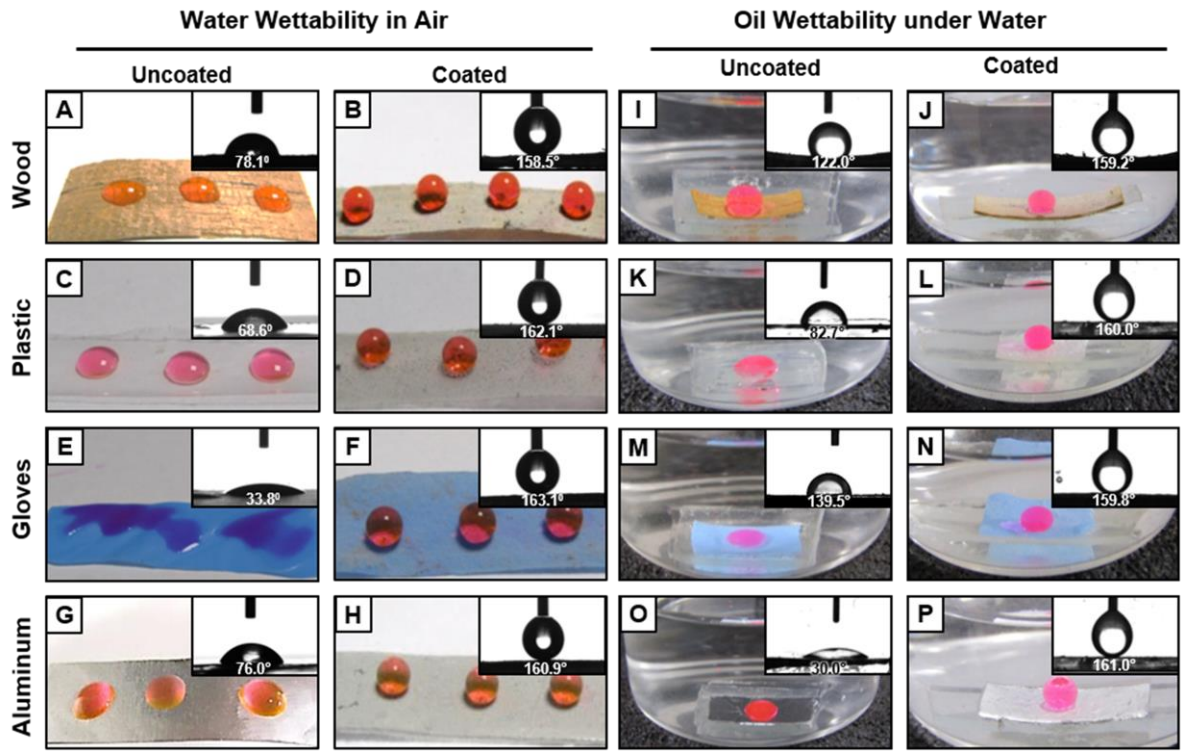

Figure 3.3. A–P) Digital images and contact angle images (inset) of beaded water droplets (in air, A-H) and beaded oil droplets (under water, I-P) on uncoated (A ,C, E, G, I, K, M, O) and multilayers-coated (post-modified with octadecylamine, B, D, F, H and post-modified with D-glucamine, J, L, N, P) substrates—including wood (A-B, I-J), plastic (C-D, K-L), gloves (E-F, M-N) and Al foil (G-H, O-P).

The ODA treated multilayers displayed extreme water repellency with an advancing water

contact angle of ~162° as shown in Figure 3.2D-E. On the other side, the D-glucamine treated multi-layered coating found to be underwater superoleophobicity where the oil droplets beaded with an advancing oil contact angle of ~164º under water as shown in Figure 3.2F-G. Thus, the covalent and simple chemical modulation of a single multilayered coating provided a simple basis for integrating two distinct, nature-inspired special wettabilities: superhydrophobicity in air and underwater superoleophobicity. Furthermore, various flexible and rigid substrates, including wood, plastic, gloves and metal surfaces were coated with the 'chemically' reactive multilayers of CRPNC/AGO. Eventually, provided both superhydrophobicity in air and superoleophobicity under water with the liquids' (oil/ water) advancing contact angle above 150° were achieved on the various substrate depending on the selection of appropriate post-covalent modifications as shown Figure 3.3.

3.3.2. Stretchable nature-inspired wettability

The same multilayers were constructed on a strategically selected, easily deformable substrate, which was polydimethylsiloxane (PDMS) film (thickness: ~0.25 mm). The featureless and smooth interface was inherently stretchable under applied manual tensile strain (TS). The multilayered coating on the PDMS was post-modified with appropriate chemical functionalities (e.g., D-glucamine and ODA molecules) for adopting nature-inspired extreme water (in air) and oil (under water) repellent interfaces. The superhydrophobic multilayered coated PDMS (denoted as SH-PDMS) film that repelled the beaded water droplet with an advancing contact angle of ~162° (Figure 3.4A-B) and contact angle hysteresis of ~3° was exposed to physical deformations. The SH-PDMS films were manually and gradually stretched and the stretched interfaces having 100% TS remained water repellent with advancing water contact angle of ~160° (Figure 3.4C-D) and contact angle hysteresis of ~5°. As expected, no change in water wettability was observed after releasing the applied strain as shown in Figure 3.4E-F. Next, the tensile deformation was successively carried out to examine the impact of repetitive deformation of a multilayer coating on the embedded special wettability. The advancing water contact angle was measured at regular intervals of the consecutive tensile deformation (applied TS = 100%) of the multilayer-coated PDMS as shown in Figure 3.4G. The advancing water contact angle was noticed to be slightly perturbed, however, the non-adhesive superhydrophobicity remained intact with an advancing water contact angle of above 150° and contact angle hysteresis of well below 10°, even after 500 times repetitive tensile deformation of the SH-PDMS. Then, covalently cross-

linked and 'chemically reactive' multilayer-coated PDMS that displayed underwater superoleophobicity (denoted as UWSO-PDMS), after the post-chemical modification with D-glucamine molecules, was gradually exposed to tensile deformation (from 0 to 100% strain). The UWSO-PDMS remained capable of repelling beaded oil droplets under water, with advancing oil contact angle above 160° and contact angle hysteresis below 10° before and after incurring the tensile deformation (with 100% TS), and after releasing the applied TS as shown in Figure 3.4H-M.

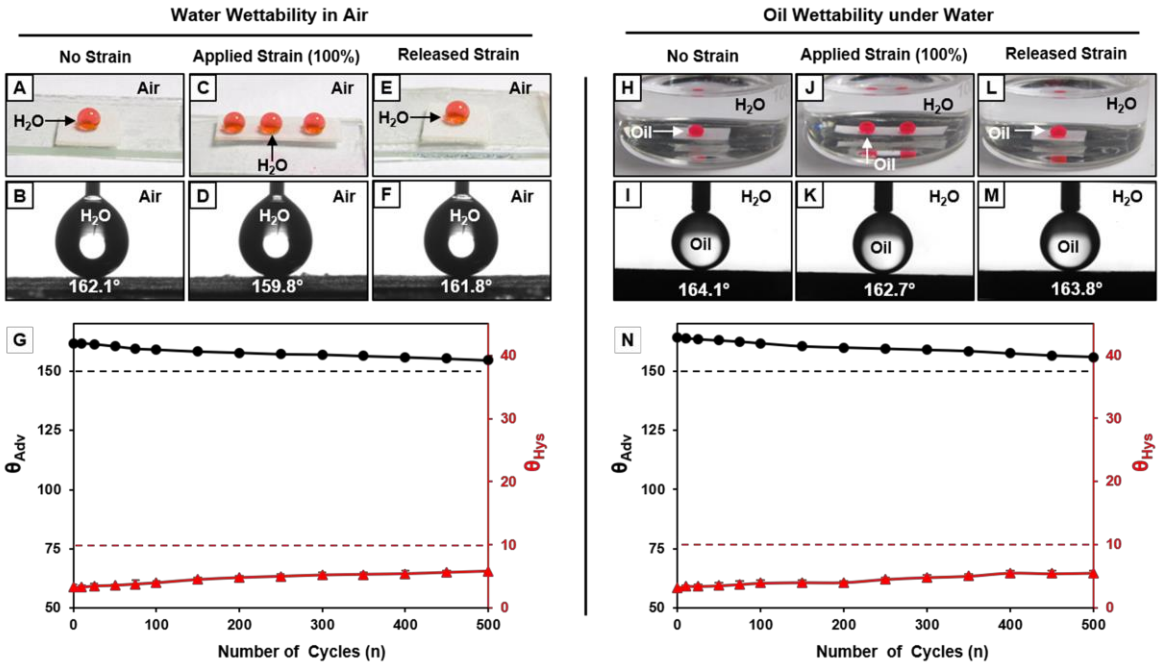

Figure 3.4. A–F) Digital (A, C and E) and contact angle (B, D and F) images of beaded water droplets (in air) before (A and B) and after (C and D) application of external tensile strain (100%) on the multilayer coatings, and after releasing the applied strain (E and F). G) A plot showing the change in advancing contact angle (black) and contact angle hysteresis (red) of beaded water droplet on multilayer coatings (treated with ODA) during the repetitive (500 cycles), tensile (100%) deformation process. H–M) Digital (H, J and L) and contact angle (I, K and M) images of beaded oil droplets (under water) on multilayer coating before (H–I) and after (J and K) tensile deformation (100%), and after releasing (L and M) the applied tensile stress under water. N) The plot showing the change of advancing contact angle (θ_{adv}, black) and contact angle hysteresis (θ_{hys}, red) of beaded oil droplets on multilayer coatings, where the multilayer coating on PDMS film was repetitively (500 times) exposed to 100% tensile deformations.

Furthermore, oil droplets on the physically deformed interfaces under water were noticed to roll off when the interface was tilted by 4°, which strongly suggests the existence of durable fish-scale inspired wettability. Next, the UWSO-PDMS was repetitively exposed to physical deformation with 100% TS and the oil wettability under water was regularly monitored using oil contact angle measurements. However, the multi-layered coating remained non-adhesive superoleophobic underwater with advancing contact angle above 160° and contact angle

hysteresis below 10° as shown in Figure 3.4N. Then, the change in topography in the multilayer coating during the tensile deformation (with 100% TS) was examined and compared with the multilayer coating before applying the strain and after releasing the applied strain as shown in Figure 3.5. The topography of the multilayers that were physically deformed with 100% TS was noticed to be different from the multilayer before incurring any physical deformation. The hierarchical domains cracked arbitrarily and separated (in the range of 2–4 μm) along the direction of the applied TS, however, no peeling of multilayers from underneath the substrate was noticed. Rather, the cracked multilayers exposed the interior of the coating (Figure 3.5C-D), which was still capable of displaying the nature-inspired special liquid wettability (Figure 3.4C, D, J and K). Thus, together with the top interface, the interior of the synthesized material was also capable of displaying nature-inspired wettability. As a consequence, there was no apparent change in the advancing liquid contact angle and contact angle hysteresis on the physically deformed multilayered coating, in comparison to the native interfaces.

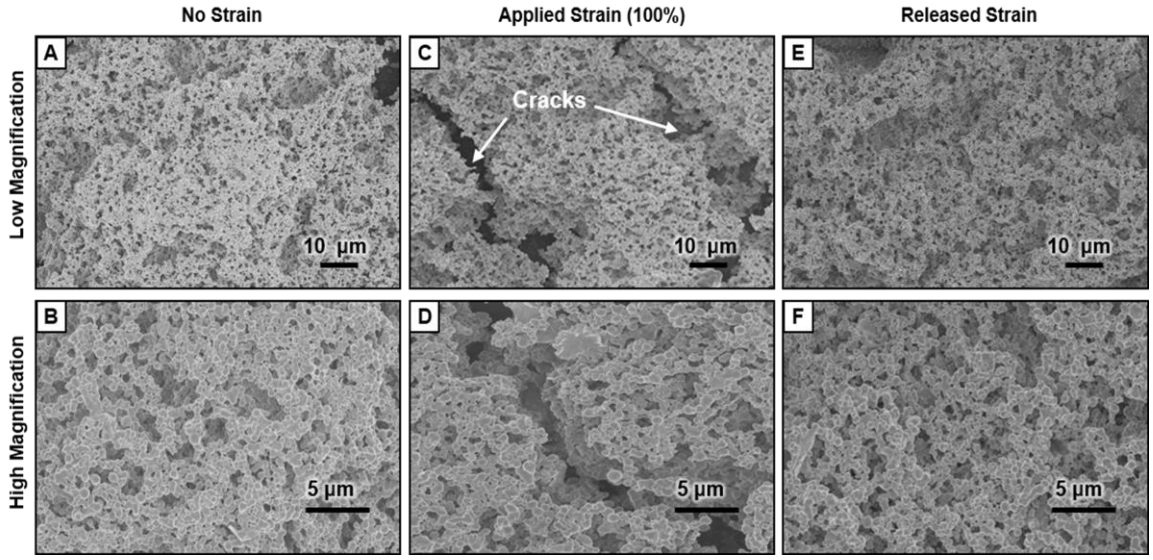

Figure 3.5. A–F) FESEM images of multilayer coatings both in low (scale bar: 10 μm, A, C and E) and high (scale bar: 5 μm, B, D and F) magnifications, before (A and B) and after (C and D) applying 100% TS, and after (E and F) releasing the applied strain.

Nevertheless, the topography of the multilayers became indistinguishable from the native multilayers after releasing the applied pressure as shown in Figure 3.5E-F and this resulted in minimal change in the embedded nature-inspired wettability in the multilayer coating (Figure 3.4E-F and Figure 3.4L-M).

3.3.3. Physical/chemical durability of nature-inspired wettability

In the earlier reports, most of the stretchable lotus leaf-inspired interfaces were extended to study the performance of the special wettability under applied TS, however, the impact of other practically relevant severe settings on the stretchable superhydrophobic coatings were not often examined.[1-6] The durability study of the stretchable material in other relevant harsh settings would be important for various prospective applications in real-world settings.[23] The, currently synthesized multilayers that were capable of displaying superhydrophobicity (in the air) and superoleophobicity (under water), were exposed to various physically/ chemically severe conditions and the embedded super-liquid-wettability was examined in detail.

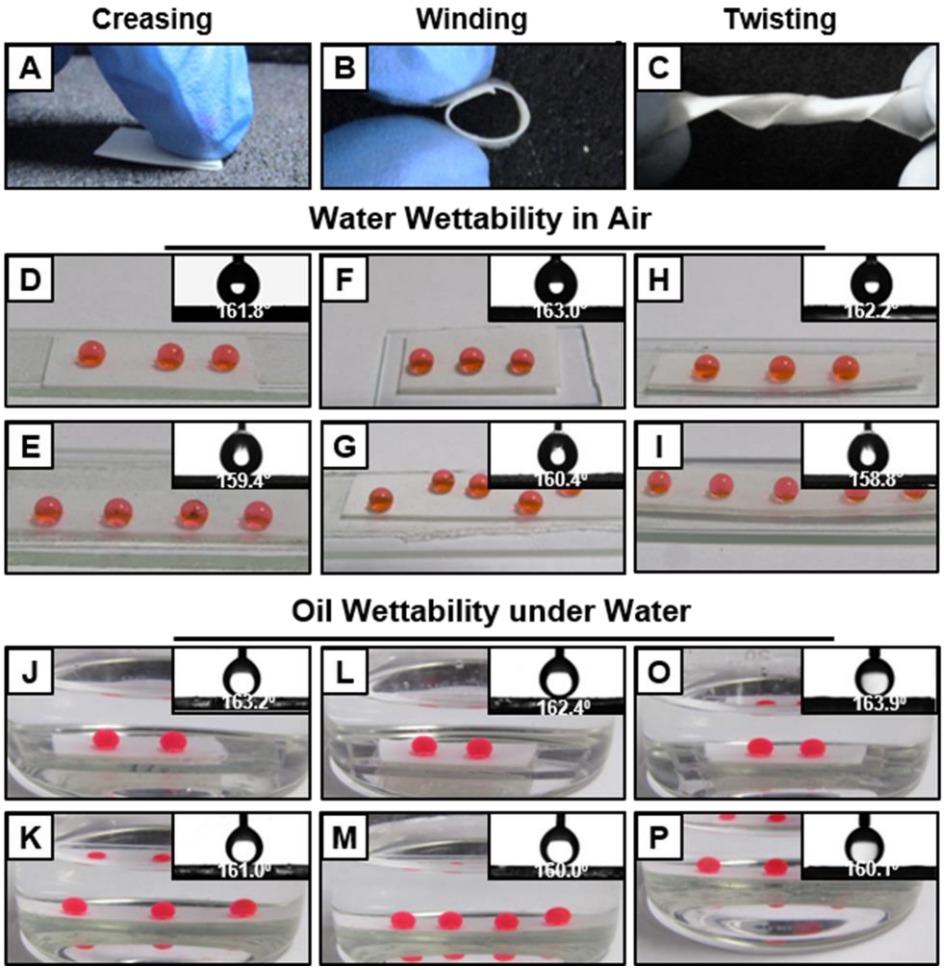

Figure 3.6. A-P) Digital and contact angle (inset) images accounting the effect of various physical manipulations— including creasing (A), winding (B) and twisting (C) on the embedded super-water repellent property (in air) of the multilayers (ODA treated, D-I) and the embedded super-oil repellent property (under water) of the multilayers (D-glucamine treated, J-P) coated PDMS film before (D, F, H, J, L, O) and after (E, G, I, K, M, P) application of 100% tensile strain.

The multilayered coatings that were exposed to various practically relevant challenging settings, were physically deformed further with 100% TS and the water and oil wettability were examined separately. The detailed and extensive examinations on the durability of the

synthesized nature-inspired stretchable materials were rarely demonstrated in the literature in the past. Both SH-PDMS and UWSO-PDMS were separately exposed to various physical manipulations including creasing, winding and twisting for multiple times (10 times), prior to examining the water (in air) and oil (under water) wettability as shown in Figure 3.6. Both of the SH-PDMS and UWSO-PDMS were found to display extreme water and oil repellency respectively, with an advancing liquid (oil/water) contact angle above 150° as shown in Figure 3.6. Furthermore, the multilayered coatings were exposed to more severe and practically relevant challenges including adhesive tape test, sand paper abrasion and so on. The multilayer coatings were exposed to the standard adhesive tape peeling test, with an applied pressure of 10 kPa.[23,49]

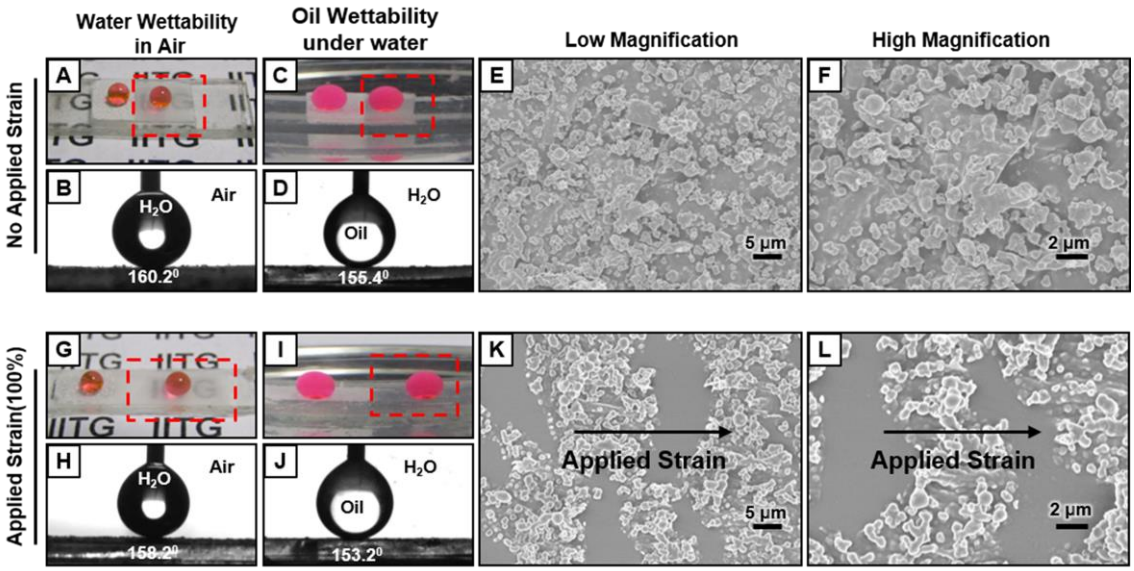

Figure 3.7. A,C) Digital images comparing the water (A, in air, ODA treated) and oil (C, under water, D-glucamine treated) wettability on the multilayer coatings before and after (the dotted red box indicates the physically abraded polymeric coatings) the adhesive tape peeling test. B,D) Contact angle images of beaded water (in air) and oil (under water) on the physically damaged multilayers. E-F) FESEM images of the multilayers in low (E, scale bar: 5 µm) and high (F, scale bar: 2 µm) magnifications after performing the adhesive tape test. G–I) The digital images of beaded water (in air, G) and oil (under water, I) droplets on the physically deformed (100% TS) multilayers with/without exposures to the adhesive tape test, red boxes (G and I) denote the adhesive tape treated area. H-J) The contact angle images of beaded water (in air, H) and oil (under water, J) droplets on adhesive tape treated and physically deformed (with 100% TS) multilayers. K-L) FESEM images of physically deformed multilayer coating that was exposed to the adhesive tape test in low (K, scale bar: 5 µm) and high (L, scale bar: 2 µm) magnifications.

However, no physical change and embedded liquid wettability in the multi-layered coating were noticed. So, the applied pressure was increased more than five-fold (an applied pressure of 56 kPa) so that the top portion of the multilayer eroded away during the standard adhesive tape peeling process. Nevertheless, the embedded anti-water wettability remained unchanged

with advancing water contact angle above 150° and contact angle hysteresis below 10° as shown in Figure 3.7A-B. This simple demonstration unambiguously revealed the presence of bulk super water wettability, where the top interface and the interiors of the polymeric coating associated with appropriate topography and chemistry and conferred nature-inspired super liquid wettability. As expected, the topography of the multilayered coating was significantly perturbed during the severe abrasion process as confirmed from the FESEM imaging (Figure 3.7E-F), in comparison to the native multilayers (Figure 3.5A-B), but the physically damaged multilayer coating still remained capable of displaying extreme water wettability in air (Figure 3.7A-B). Furthermore, this multilayer coating, after the physical erosion, was exposed to 100% TS deformation, and the physically damaged and deformed interface exhibited superhydrophobicity with an advancing water contact angle above 150° and contact angle hysteresis below 10° (Figure 3.7G-H). This result strongly revealed the presence of highly robust and stretchable lotus leaf-inspired wettability in the synthesized multilayer coating. A very similar response was noticed for the UWSO-PDMS, where the physically abraded (after the adhesive tape peeling test, Figure 3.7C-D) UWSO-PDMS that was exposed to TS deformation (100%) and the physically abraded and stretched multilayers (post-modification with D-glucamine) remained under water superoleophobic with an advancing oil contact angle of above 150° and contact angle hysteresis of below 10° as shown in Figure 3.7I-J. The examples of such impeccable and exemplary sustainability/durability of the lotus leaf/fish scale inspired interfaces are rare in the literature. The morphology of the stretched multilayer interface was examined using FESEM imaging, where the multilayers of CRPNC/AGO were found with random cracks and exposed the underneath substrate as shown in Figure 3.7K-L. However, this cracked multilayer coating displayed both uninterrupted superhydrophobicity in air and superoleophobicity under water (Figure 3.7G–J). Another severe physical abrasion was carried out on the multilayer coating following the standard sand paper abrasion test, where the sand paper was rubbed manually (with a speed of 1.4 cm s^{-1}) across the coated substrate with a back and forth motion for four times under an applied pressure of 56 kPa. As expected, this abrasion process damaged the interfaces, however, these damaged interfaces were still capable of repelling the beaded water (in air, Figure 3.8A-B) and oil (under water, Figure 3.8I-J) droplets. Furthermore, such physically damaged interfaces were exposed to tensile (100%) deformations. Nevertheless, the robust multilayer coatings, which were either post-modified with ODA (SH-PDMS) or D-glucamine (UWSO-PDMS), were found to remain superhydrophobic in air (Figure 3.8C-D)

and superoleophobic under water (Figure 3.8K-L). Next, 150 g of sand was dropped on the multilayer coating to examine the impact of this physical challenge on nature-inspired wettability. Both the SH-PDMS and UWSO-PDMS remained superhydrophobic (Figure 3.8E, F, G and H) and underwater superoleophobic (Figure 3.8M, N, O and P) respectively, before (Figure 3.8E, F, M and N) and after (Figure 3.8G, H, O and P) tensile deformations (100%).

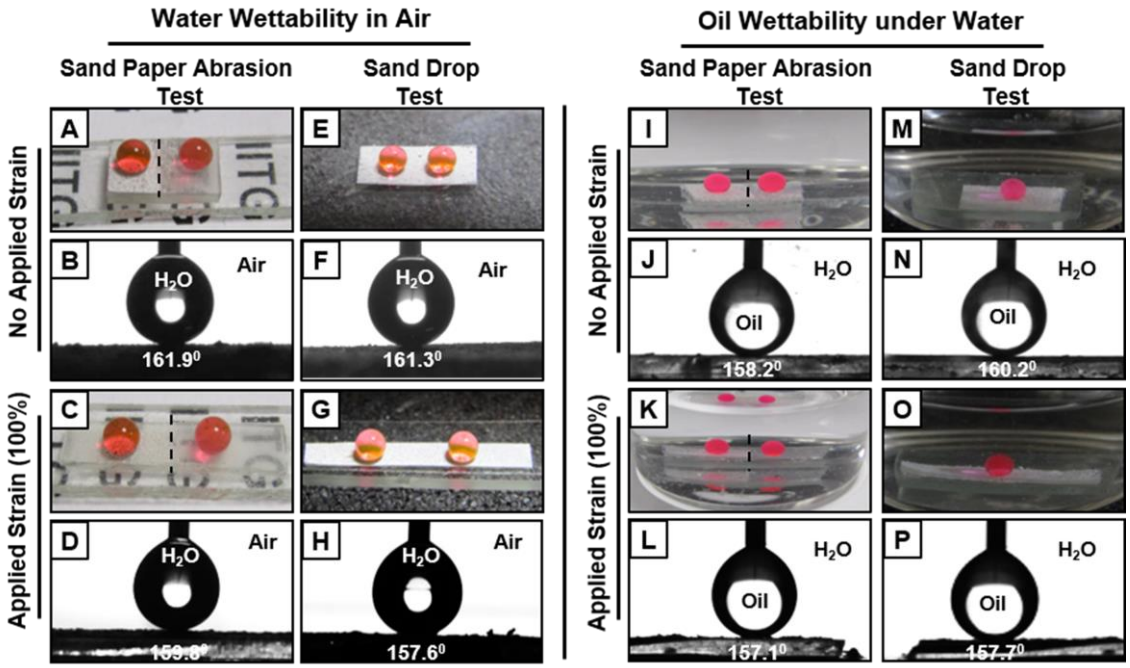

Figure 3.8. A-P) Digital (A,C,E,G,I,K,M,O) and contact angle (B,D,F,H,J,L,N,P) images of beaded water (in air; A-H) and oil (under water; I-P) droplets on the multilayers (post-modified with octadecylamine (A-H) and D-glucamine (I-P) coated PDMS films after performing the abrasive sand paper test (A-B, I-J) and sand drop test (E-F, M-N). Selectively, portion of the coatings were exposed for abrasive sand paper and adhesive tape tests, and the right part of the dotted lines in the digital images (A,C,I,K) are refereeing to the physically abraded area, whereas entire coatings are exposed for sand drop tests. The multilayers coated PDMS films–that are exposed to abrasive sand paper test (A-B, I-J) and sand drop test (E-F, M-N), were further stretched with applied tensile strain of 100% in air (C,D,G,H) and under water (K,L,O,P), and both the water (C,D,G,H) and oil (K,L,O,P) wettability were examined with digital images (C,G,K,O) and measuring contact angles (D,H,L,P) of beaded liquids (water/oil).

Furthermore, these covalently cross-linked (through the 1,4-conjugate addition reaction) multilayer coatings that were individually modified with D-glucamine or ODA were exposed to various complex aqueous phases, (e.g., extremes of pH, salinity, and so on) and UV radiation, which were relevant to the practically relevant diverse scenario. Both the SH-PDMS and SO-PDMS were placed under UV radiation (at 254 nm and at 365 nm simultaneously), river water (Brahmaputra River, Guwahati, India), artificial sea water and extremes of pH (1 and 12) for 10 days (Figure 3.9). Both the SH-PDMS and UWSO-PDMS

continued to display the nature-inspired wettabilities, superhydrophobicity and underwater superoleophobicity with advancing liquid (oil/water) contact angle above 150° and contact angle hysteresis below 10° as shown in Figure 3.9.

In the past, many of the nature-inspired interfaces were developed by associating silane-based chemistry, which was fundamentally labile under UV irradiation.[13-17,24-27]

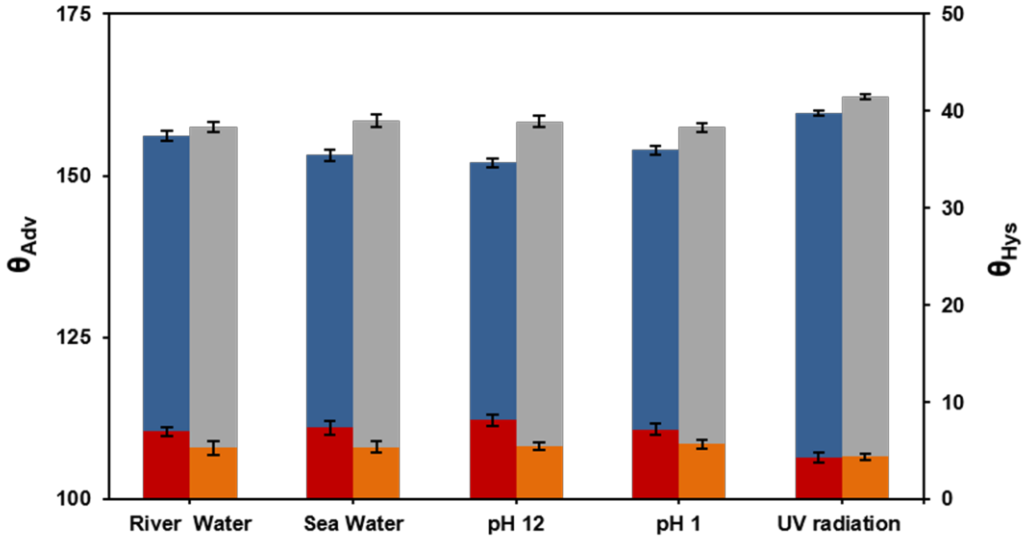

Figure 3.9. Plots accounting the advancing contact angle (blue and grey) and contact angle hysteresis (red and orange) of water (in air, blue and red) and oil (under water, grey and orange) droplet on the superhydrophobic (in air, blue and red) and superoleophobic (under water, grey and orange) after prolong (10 days) exposures to various chemically and radiative severe conditions including river water, artificial seawater, extremes of pH (1 and 12) and UV irradiation (at λ_{max} = 254 and 365 nm).

These SH-PDMS and UWSO-PDMS were continuously exposed to UV radiation (simultaneously at 254 nm and 365 nm) for 10 days, and furthermore, the UV treated multilayered coatings were physically deformed with 100% TS, and both the oil and water wettability of the multilayers were examined in detail. Both the lotus leaf and fish-scale inspired wettability remained preserved without significant change in liquid (oil/water) wettability, in comparison to its native multilayer coating. This high chemical durability of the embedded nature-inspired wettability was strongly attributed to the rational association of robust 1,4-conjugate addition reaction in both: (a) integration of nanomaterials, (i.e., CRPNC and AGO), and appropriate chemical modulation of the covalently crosslinked multilayers of functional nanomaterials. This general coating approach with the ability to adopt various nature-inspired stretchable and durable wettability will contribute immensely towards various prospective applications in practically relevant settings.

3.4. Conclusions

Highly durable and stretchable nature-inspired multilayered coating were introduced through strategic and covalent integration of two distinct nanomaterials: chemically reactive polymeric nanocomplex and primary amine grafted flexible graphene oxide nanosheets. This approach provided a simple and common basis to develop multilayered coatings that were embedded with stretchable and durable superhydrophobicity (in air) and superoleophobicity (under water). Such nature-inspired interfaces were capable of sustaining both large tensile deformation and severe physical damages simultaneously. The featureless, smooth interfaces of stretchable PDMS film was coated with such multilayered coatings—that remained efficient in withstanding various severe physical (e.g., creasing, bending, twisting, physical erosions and so on) and chemical challenges (e.g., extremes of pH, sea water, river water, UV irradiation and so on). The multilayer coatings with and without severe physical damage displayed uninterrupted extreme liquid (oil/water) wettabilities, even after incurring large tensile deformation (with 100% strain). The substrate independent deposition process following simple and covalent layer-by-layer deposition through 1,4-conjugate addition reaction was exploited further in decorating various substrates with such nature-inspired and durable wettability, which has exemplary durability. Such stretchable interfaces that were associated with important and highly durable nature-inspired multiple special wettabilities, would be a potential interest for a wide range of smart and prospective applications in practical settings.

3.5. References

1. S. J. Cho, H. Nam, H. Ryu and G. Lim, *Adv. Funct. Mater.,* 2013, **23**, 5577.
2. J. Zang, S. Ryu, N. Pugno, Q. Wang, Q. Tu, M. J. Buehler and X. Zhao, *Nat. Mater.,* 2013, **12**, 321.
3. F. Liu, F. Sun and Q. Pan, *J. Mater. Chem. A*, 2014, **2**, 11365.
4. J. E. Mates, I. S. Bayer, J. M. Palumbo, J. P. Carroll and M. Megaridis, *Nat. Commun.,* 2015, **6**, 8874.
5. W. K. Lee, W. B. Jung and R. Sidney, *Nano Lett.,* 2016, **16**, 3774.
6. H. Xin, C. Tang, Z. He, H. Shao, K. Xu, J. Mei and W. M. Lau, *Small*, 2017, **13**, 1602353.
7. T. Verho, C. Bower, P. Andrew, S. Franssila, O. Ikkala and R. H. A Ras, *Adv. Mater.,* 2011, **23**, 673.

8. D. Wu, S. Wu, Q. Chen, Y. Zhang, J. Yao, X. Yao, L. Niu, J. Wang, L. Jiang and H. Sun, *Adv. Mater*., 2011, **23**, 545.
9. Y. Wang, Y. Shi, L. Pan, M. Yang, L. Peng, S. Zong, Y. Shi and G. Yu, *Nano Lett.,* 2014, **14**, 4803.
10. L. Ionov and A. Synytska, *Phys. Chem. Chem. Phys.,* 2012, **14**, 10497.
11. A. Das, J. Deka, A. M. Rather, B. K. Bhunia, P. P. Saikia, B. B. Manda, K. Raidongia and U. Manna, ACS Appl. Mater. Interfaces, 2017, **9**, 42354.
12. A. Das, J. Deka, K. Raidongia, and U. Manna, *Chem. Mater.,* 2017, **29**, 8720.
13. Y. Tian, B. Su and L. Jiang, *Adv. Mater.,* 2014, **26**, 6872.
14. L. Wen, Y. Tian and L. Jiang, *Angew. Chem., Int. Ed.,* 2015, **54**, 3387.
15. Z. Chu, Y. Feng and S. Seeger, *Angew. Chem., Int. Ed.,* 2015, **54**, 2328.
16. B. Su, Y. Tian and L. Jiang, *J. Am. Chem. Soc*., 2016, **138**, 1727.
17. M. J. Liu, S. T. Wang, Z. X. Wei, Y. L. Song and L. Jiang, *Adv.Mater.,* 2009, **21**, 665.
18. L. Lin, M. J. Liu, L. Chen, P. P. Chen, J. Ma, D. Han and L. Jiang, *Adv. Mater.,* 2010, **22**, 4826.
19. Z. Xue, S. Wang, L. Lin, L. Chen, M. Liu, L. Feng and L. Jiang, *Adv. Mater.,* 2011, **23**, 4270.
20. L.-P. Xu, J. Peng, Y. Liu, Y. Wen, X. Zhang, L. Jiang and S. Wang, *ACS Nano*, 2013, **7**, 5077.
21. T. Guo, L. Heng, M. Wang, J. Wang and L. Jiang, *Adv. Mater.,* 2016, **28**, 8505.
22. X. Meng, M. Wang, L. Heng and L. Jiang, *Adv. Mater.,* 2018, **30**, 1706634.
23. X. Tian, T. Verho and R. H. A. Ras, *Science,* 2016, **352**, 142.
24. L. Feng, S. H. Li, Y. S. Li, H. J. Li, L. J. Zhang, J. Zhai, Y. L. Song, B. Q. Liu, L. Jian and D. B. Zhu, *Adv. Mater.,* 2002, **14**, 1857.
25. X. M. Li, D. Reinhoudt and M. Crego-Calama, *Chem. Soc. Rev.,* 2007, **36**, 1350.
26. X. Yao, Y. Song and L. Jiang, *Adv. Mater.,* 2011, **23**, 719.
27. E. Ueda and P. A. Levkin, *Adv. Mater*., 2013, **25**, 1234.

Title: Simultaneous Collection of Both Selectively Separated Oil and Water Phases from Oil/Water Mixture

In the recent past, bio-mimicked super liquid-repellent interfaces were recognized as the prospective and energy-efficient solution for remediation of oil contamination, and mostly two-phase oil/water mixtures that were either composed of light oil or heavy oil were demonstrated for gravity-driven and environmentally friendly oil/water separation. In reality, the demonstration of common oil/water separation with a two-phase system under physically/ chemically challenging settings is rare, due to the poor durability of the synthesized bio-mimicked membranes. In this chapter, amine-reactive and covalently cross-linked multilayered coating of CRPNC /AGO has been extended for fabricating two distinct durable and tensile deformation tolerant selective-liquid-permeable membranes. Further, these bio-mimicked membranes were exploited in the gravity-driven selective filtration of oil and aqueous phase from the three-phase oil/water mixture under practically relevant diverse and severely challenging settings, in an unprecedented manner. A prototype was developed through the strategic association of both fish scale and lotus leaf-inspired stretchable membranes, for simultaneous and active filtration of both heavy/light oils and aqueous phases from their respective mixtures. Both the separated oil and aqueous phases were collected in two individual containers. The light/heavy oil phases selectively passed through the stretchable superhydrophobic membrane and the aqueous phase filtrated through the underwater superoleophobic membrane. The developed prototype remained highly efficient in repetitive (at least 25 times) separation and collection of both oil and water phases simultaneously, irrespective of density, surface tension, and viscosity of the oil phase and chemical complexity in the aqueous phase.

* **A. Das**, D. Parbat, A. Shome, U. Manna. *ACS Sustainable Chem. Eng*., 2019, **7**, 11350.

4.1. Introduction

In the past, frequent oil spillage accidents and a large amount of industrial oily waste water discharge imposed a great threat for both marine ecology and environments around the globe. Therefore, the development of an energy-efficient and environmental friendly oil-water separation process is an important research topic. In the past, various oil-water separation techniques, including centrifugation, burning, air flotation, oil skimmers and marine microorganisms' treatment were introduced to remove the oil spillages.[1,2] However, low oil-water separation efficiency and high operation costs limit the applications of these techniques in a practical setting. Recently, lotus leaf-inspired superhydrophobicity and fish-scale inspired underwater superoleophobicity have been introduced as an early basis for energy and environmentally friendly remediation of oil spills.[3–7] In the case of lotus-leaf inspired superhydrophobic interface, the hierarchical topography topped with inert low surface energy coatings allowed the metastable air phase to be trapped and such interfaces have an inherently strong affinity toward oil/oily phases. Meanwhile, highly water-compatible fish-scale inspired interfaces that confined an aqueous phase displayed super oil repellency underwater.[8] In the past, these two distinct bio-mimicked wettabilities were rationally associated with developing membranes for gravity-driven oil/water separations from mostly two-phase oil/water mixtures. In 2004, a seminal report from Jiang and co-workers[4] demonstrated the rational integration of lotus leaf-inspired superhydrophobicity with metal mesh for gravity-driven removal of oil spills from the contaminated aqueous phase, where the separated aqueous phase was accumulated on top of the metal mesh. Later, another membrane, decorated with a fish scale inspired underwater superoleophobicity, was independently and successfully exploited for gravity-driven selective filtration of an aqueous phase from an oil/water mixture, and the other oil/oily phase piled up on top of the membrane.[9,10] Both of these approaches are highly efficient in gravity-driven active filtration/collection of a single liquid (either oil or water) phase from the respective two-phase oil/water mixtures; however, the other liquid phase accumulates on top of the nature-inspired selective liquid repellent membrane.[4–10] This accumulated liquid phase on the top of the biomimicked individual membrane in such previously reported filtration based separation set-ups is likely to block the immediate filtration of the selective liquids—on further addition of any oil/water mixture again. Thus, the removal of that accumulated liquid phase from the top of the liquid-repellent membrane is essential prior to perform any further filtration based oil/water separation. Such obvious interruption in the oil/water separation process is likely to

impose a severe inconvenience/challenge for its practical utility. Moreover, in the reality, the polluted aqueous phase consists of both light and heavy oil/oily contaminants. Thus, the separation of oil/oily contaminants from three-phase oil/water mixtures —that consists of heavy oil, light oil, and aqueous phases under practically relevant severe settings, is more relevant to the existing practical challenge of remediation of oil spillage under diverse scenarios. In general, the demonstration of oil/water separation—even with two-phase mixtures under harsh and challenging settings, is rare in the literature as the durability of the reported bio-mimicked membranes is a major concern.[11,12] To combat the durability issues, some important designs, including external stimuli assisted self-healing and self-repairable approaches are introduced.[13−17] Such designs are fundamentally interesting and important; however, the external stimuli dependent restoration of bio-mimicked wettability in the practically relevant diverse settings are less appropriate for real-world applications.[13−17] In the recent past, the concept of bulk bio-mimicked wettability that consisted of essential topography and appropriate chemistry—three-dimensionally in the reported materials found to be a highly promising approach for addressing the existing durability issues,[18−20] and such designs are inherently capable of sustaining various abrasive exposures and continued to display uninterrupted bio-mimicked wettability even after removal of the top interface, without the aid of any external intervention.[18−21] Such coatings with bulk liquid wettability were mostly developed on the geometrically simple planar substrates.[18−21] The report on semipermeable membranes that would be embedded with such bulk bio-mimicked wettability is yet to be introduced in the literature. Such a material would be appropriate for (1) sustaining various abrasive exposures and (2) separating oil/water mixture successfully, under various severe settings. In the chapter 3, a common and facile synthetic procedure was adopted for developing two distinct and stretchable bio-mimicked coatings on the planar substrate. In this chapter, the multilayer coatings of chemically reactive polymeric nanocomplex (CRPNC) and amino graphene oxide (AGO) nano-sheets have been extended on a selected fibrous substrate following the same deposition process that was introduced in chapter 3. The rational post-chemical modifications of the covalently cross-linked and chemically reactive multilayers of CRPNC/AGO with primary amine-containing selected small molecules (i.e.; octadecylamine and glucamine) provided stretchable and durable superhydrophobic membrane (referred to as SHM) and underwater superoleophobic membrane (denoted as UWSOM) as shown in Figure 4.1. The synthesized membranes that were embedded with two distinct durable bio-mimicked liquids wettability were extended for

demonstrating the instant separation and collection of oil/water mixtures under challenging scenarios. The extreme liquid (oil/water) repellent and selective-liquid-permeable membranes (SHM and UWSOM) continued to separate oil/water mixture—even after incurring various severe physical/chemical challenges— including large tensile deformation (150%), creasing, winding, twisting, sand paper abrasion, sand drop test, adhesive tape peeling test, knife scratch test and prolonged (25 days) exposure to extremely acidic pH, basic pH, artificial seawater, river water, and UV radiation. A lab-made prototype was developed using such durable nature-inspired stretchable membranes (SHM and UWSOM), which was capable of selective separation/collection (above 98%) of oil/oily phase and aqueous phase—from three phases (light oil, heavy oil, and aqueous phase) oil/water mixture under practically relevant severe settings.

4.2. Experimental Section

4.2.1. Materials

Dichloroethane, chloroform were procured from Merck Specialties Private Limited, India. Silicon oil was purchased from Fisher scientific. Polyurethane based fibrous substrate, polypropylene tube, soybean oil, vegetable oil and kerosene oil were brought from a local shop in Guwahati city (Assam, India). Motor oil (Castrol Active 20W-40) was purchased from Castrol India Ltd. at IIT Guwahati, Assam. Sources of other chemicals have already been mentioned in the Chapter 2.

4.2.2. General considerations

All the details related to the used instruments have been provided in the Chapter 2.

4.2.3. Synthesis of amino graphene oxide (AGO)

The detailed synthetic procedure of amino graphene oxide has been discussed in the Chapter 2.

4.2.4. Fabrication of reactive multilayers on the fibrous substrate and post chemical functionalization of the multilayers

The ‘reactive’ multilayer of CRPNC/AGO was prepared and further post-modified with a primary amine-containing small molecule (i.e., octadecylamine for superhydrophobicity and D-glucamine for the underwater superoleophobic property) following the same protocol that is discussed in the Chapter 3. However, insists of using a PDMS substrate, the multilayer coating was deposited on a fibrous substrate (PU) and the layer-by-layer deposition cycle was repeated for 10 times instead of 15 times.

4.2.5. Investigation of physical/chemical durability

A variety of physical and chemical durability tests were performed using SHM and UWSOM materials. The detailed procedures for each experiment are described in the following sections;

4.2.5.1. Physical manipulations and deformations

The multilayers coated fibrous substrates (both SHM and UWSOM) were subject to various practically relevant physical manipulations—including creasing, twisting and wending for multiple times (10 times). Thereafter, the respective liquid wettability was examined following the standard process. Furthermore, these extreme liquid-repellent membranes (SHM and UWSOM) were exposed to manual physical deformation where the tensile strain was gradually increased up to 150 %. The impact of this large tensile deformation on the embedded liquid wettability was examined with dynamic contact angle measurements and visual inspections.

4.2.5.2. Sand paper abrasion test

In this particular abrasion test, an abrasive sand paper (with 400-grit) was manually rubbed across the extreme liquid-repellent membranes for 20 cycles—with an applied pressure of 110 kPa and sliding speed ~4 cm/s. After this sand paper test, the liquid (oil/water) wettability was examined with visual inspection and contact angle measurements.

4.2.5.3. Sand drop test

Both SHM and UWSOM that are attached on a glass slide, were tilted at 45°, and then 150 g of sand grains were dropped from a distance of 20 cm on both the nature-inspired membranes. The embedded superhydrophobicity (in air) and superoleophobicity (under water) were examined with visual inspection and contact angle measurements, before and after performing this physical abrasion test.

4.2.5.4. Adhesive tape test

Firstly, freshly exposed adhesive surfaces were exposed to the SHM and UWSOM with an applied pressure of 110 kPa. This applied load facilitated better contact between the adhesive surface and the surface of the biomimicked membranes. Then, the adhesive tape was manually peeled off from the respective coatings multilayers. This test was repeated for ten times, prior to examining the liquid wettability on the adhesive tape treated interfaces.

4.2.5.5. Exposure to complex aqueous environments and UV radiation

Both SHM and UWSOM substrate were submerged in different chemically harsh aqueous phases—including simulated seawater (solution of 0.226 g $MgCl_2$, 0.325 g $MgSO_4$, 2.673 g

NaCl, and 0.112 g $CaCl_2$ in 100 mL of deionized water), acidic (pH = 1) and alkaline (pH = 12) solutions, river water (Brahmaputra river, Assam, India) for 25 days. Such super liquid-repellent membranes are also kept under UV radiation (254 nm and 365 nm) for 25 days at ambient temperature. Then, the liquid wettability was examined on the treated interfaces with contact angle measurements of beaded liquids droplets.

4.2.5.6. Gravity-driven simultaneous separation of oil-water mixture

For proof of concept demonstration of simultaneous separation and followed by the collection of two distinct liquid (oil/water) phases from their respective mixtures, a prototype was developed by strategic use of the synthesized SHM and UWSOM. Two ends opening of a polypropylene tube was blocked with these two distinct liquids repellent membranes, and a surface hole was made at the middle of the tube for transferring the oil/water mixture—using a glass funnel. A variety of oil/water mixtures that were formulated artificially by mixing both heavier (DCM, chloroform) and lighter (kerosene, motor oil, vegetable oil, silicon oil) oils, were tested with this prototype, where simultaneously and selectively oil phase was passed through the SHM and the only aqueous phase was filtrated through the UWSOM, and these two separated liquid phases were individually collected in two separate containers.

4.3. Results and Discussion

4.3.1. Synthesis of stretchable biomimicked membranes

In the chapter 3, highly stretchable superhydrophobic and underwater superoleophobic multilayer coating have been introduced through a covalent LbL deposition process of chemically reactive nanocomplex (CRPNC) and amino graphene oxide (AGO) followed by appropriate chemical modification. In this chapter, the previous process was further extended for synthesizing both stretchable and durable superhydrophobic membrane (SHM) and underwater superoleophobic membrane (UWSOM) for oil-water separation as shown in Figure 4.1. Both CRPNC and AGO were consecutively deposited on the strategically selected stretchable fibrous substrate (Figure 4.2A-D). The size of the CRPNC was noticed to be increased rapidly (from 60 to 465 nm) with increasing the deposition cycle as confirmed with the dynamic light scattering study (Figure 4.2E). Compare to the earlier design,[22,23] the desired liquid repellent properties were optimized in the fibrous substrate with significantly lesser deposition steps. After repeating the deposition cycles of CRPNC and AGO for 10 times, the morphology of the fibrous substrate was examined with FESEM study, and it was compared with native featureless fibers of the selected substrate (Figure 4.2F). Random

granular domains on each of the fibers of the selected substrate were observed under FESEM (Figure 4.2G) after the deposition of multilayers of CRPNC/AGO.

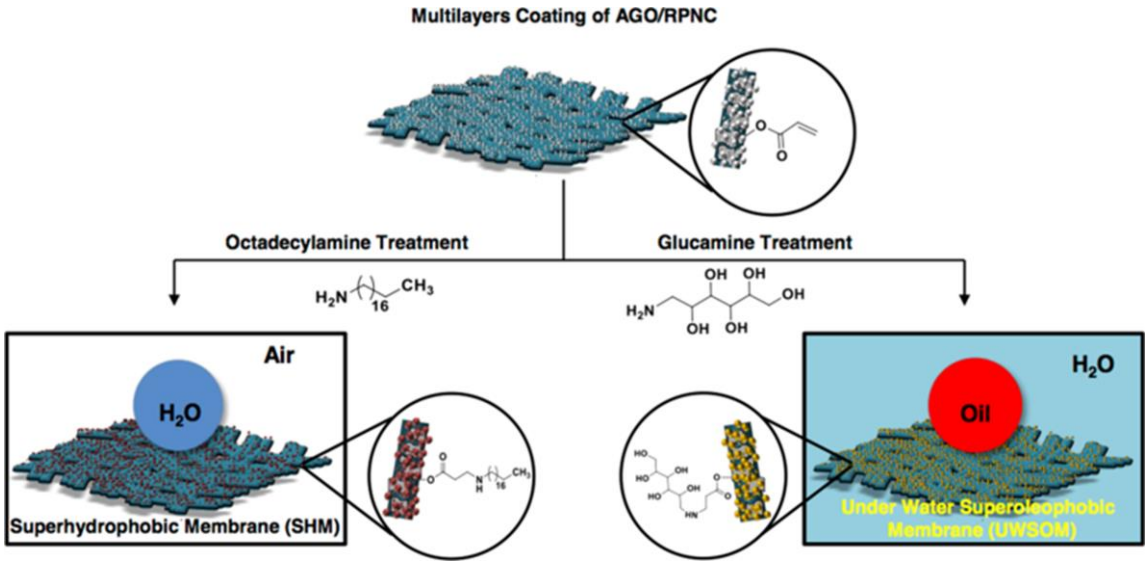

Figure 4.1. Residual acrylate groups in the multilayer coating allowed post-modification of the multilayer coatings with octadecylamine and glucamine. These octadecylamine and glucamine treatments provided both the superhydrophobic (SHM) and underwater superoleophobic membranes (UWSOM), respectively.

Further, this multilayer coating was examined with standard FTIR spectral analysis,[21–25] where the appearance of characteristic IR signatures at 1410 cm^{-1} and 1735 cm^{-1} that are corresponding to (i) the C–H stretching of the β-carbon of the vinyl group and (ii) carbonyl stretching, respectively, confirmed the existence of residual acrylate groups. Furthermore, these residual acrylate groups of readily reacted with primary amine-containing two distinct small molecules i.e., octadecylamine (hydrophobic small molecule) and glucamine (hydrophilic small molecule). After the postmodifications with these selected small molecules, a significant change in IR peak intensity was noted at 1410 cm^{-1}. The change in IR peak intensity at 1410 cm^{-1} was normalized with respect to the IR peak intensity for carbonyl group at 1735 cm^{-1} as the carbonyl groups remained unperturbed during the 1,4-conjugate addition reaction between the amine-containing small molecules and the residual acrylate groups of the multilayers (Figure 4.2L). Thus, the simple demonstration revealed the ability of the residual acrylate functional group in modulating the essential chemistry of the hierarchically featured multilayers coatings. Eventually, such design allowed to associate distinct liquid wettability to the selected fibrous substrate. The octadecylamine treated membrane repelled water in air with a contact angle of ~157° (Figure 4.2H, I), whereas the same multilayer-coated membrane became underwater superoleophobic with an advancing contact angle of ~161°, after post-treatment with glucamine as shown in (Figure 4.2J, K).

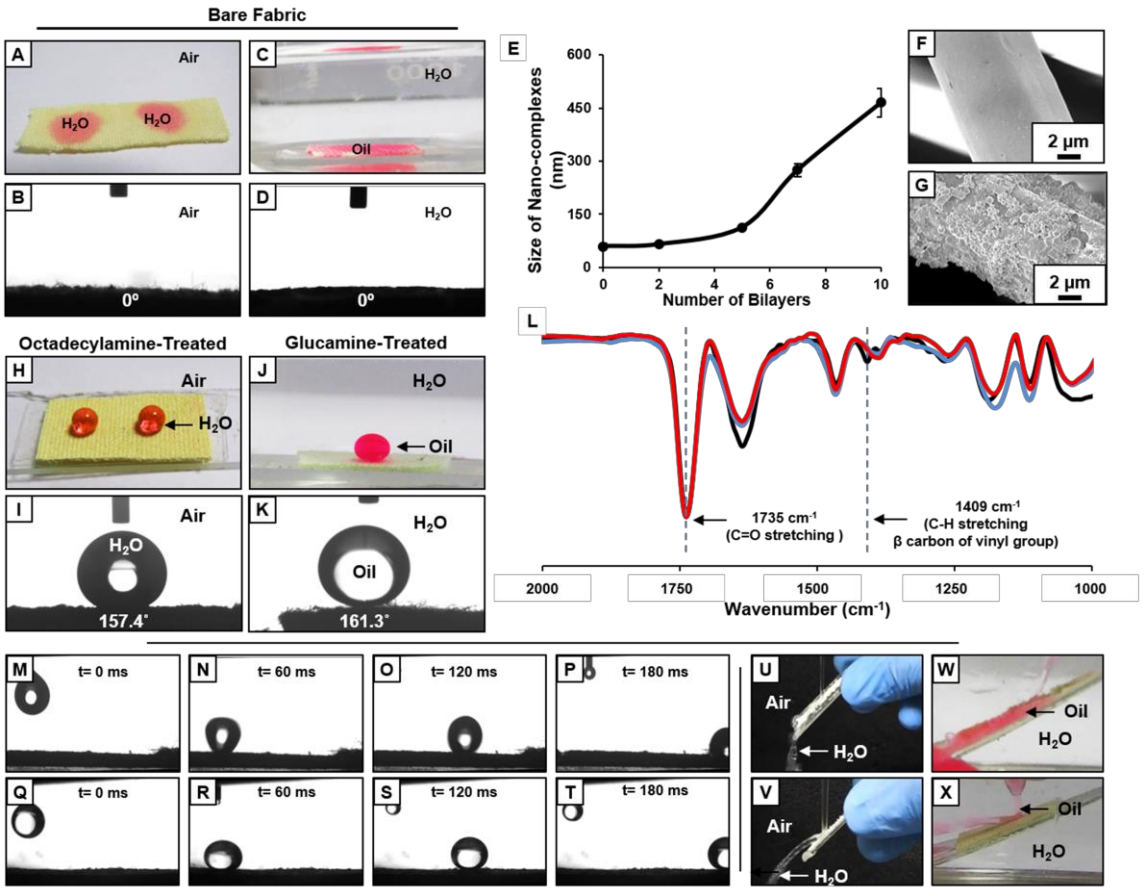

Figure 4.2. A-D) Digital image (A, C) and contact angle image (B, D) of beaded water (in air) and oil (under water) droplets on the bare fibrous substrate. E) DLS study illustrating the growth of nano-complexes in the BPEI/5 Acl mixture with increasing the number of bilayers deposition cycles. F, G) FESEM images of the fibrous substrate before (F) and after (G) deposition of the multilayer (10 bilayers) coating. H–K) Digital image (H, J) and contact angle image (I, K) of beaded water (in air) and oil (under water) droplets on the multilayers coated fibrous substrate, after post-treatment with octadecylamine (H–I) and glucamine (J–K), respectively. L) FTIR spectra of the multilayer coating before (black) and after post-treatment with octadecylamine (red) and glucamine (blue) molecules. M-T) Demonstration of the rolling of beaded water (M-P; 5µL) and oil (DCE: model oil; Q-T; 5µL) on the tilted SHM (5˚) in air and UWSOM (4˚) under water. U-X) Digital images illustrating the wetting (U, W) and bouncing (V, X) of streams of DI water (in air, U-V) and DCE (model oil, under water, W-X) on the bare fibrous substrate (U-W), on the superhydrophobic membrane (V), and on the superoleophobic membrane (X).

The embedded liquid wettability was highly nonadhesive as the beaded liquids (oil/water) droplets are readily rolled off on the slightly tilted interfaces (5° for SHM and 4° for UWSOM) as shown in Figure 4.2M-T. Moreover, both streams of water (in the air) and oil (under water) bounced away from the nature-inspired SHM and UWSOM respectively, as shown in Figure 4.2V, X which suggested the existence of durable nature-inspired wettability. The bio-mimicked interfaces were tilted with the large angles for improving visual inspection of these bouncing phenomena of water and oil on SHM (in the air) and

UWSOM (underwater), respectively. As expected, the streams of both oil and water failed to bounce on a bare fibrous substrate as shown in Figure 4.2U, W.

4.3.2. Investigation of the physical/chemical durability of biomimicked wettability

These extreme and selective liquid-repellent membranes were exposed to physically more severe challenging settings like tensile deformation which is generally known to perturb the extreme liquid wettability. The synthesized biomimicked interfaces remained capable of incurring more tensile strain (total 150%), without compromising the embedded nature-inspired extreme liquid (oil/water) wettabilities. Superhydrophobicity (in air) and superoleophobicity under water. Both the aqueous (in air) and the oil (under water) droplets beaded on the octadecylamine (SHM) and glucamine (UWSOM) treated multilayer coating with liquid contact angle above 150° as shown in Figure 4.3A−D, I.

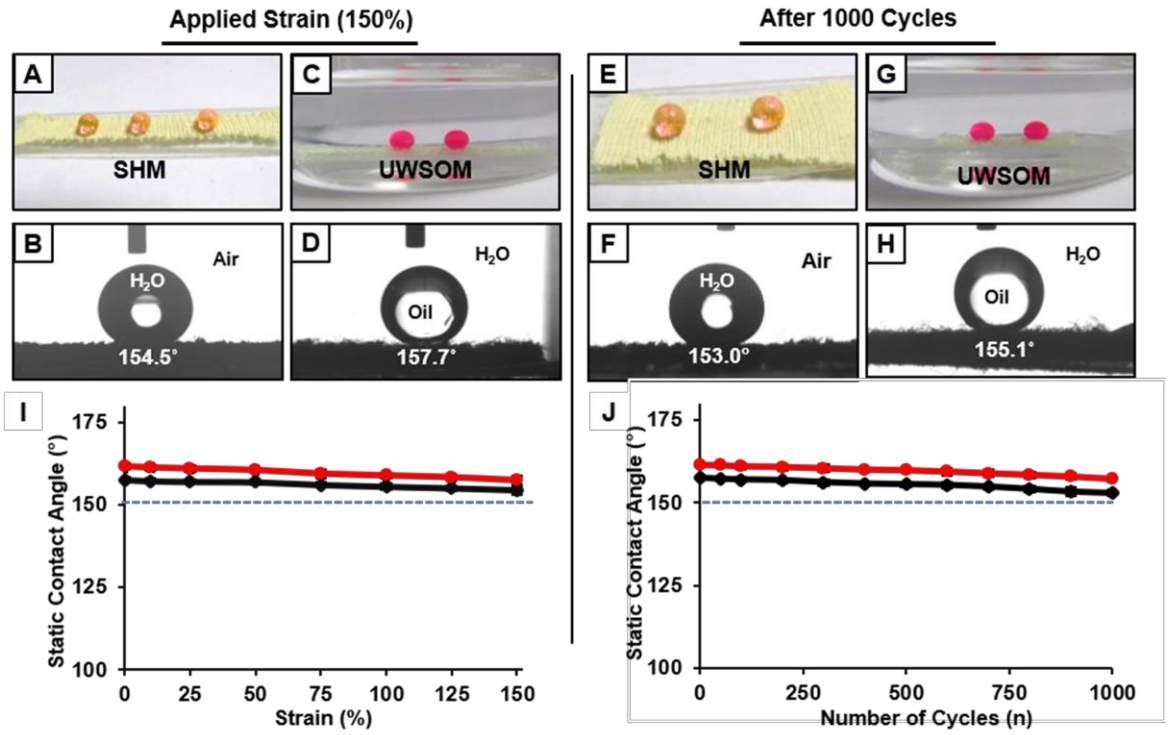

Figure 4.3. A−D) Digital image (A, C) and contact angle image (B, D) of beaded water (A, B; in air) and oil (C, D; under water) droplets on the stretched (with 150% tensile stain) SHM (A, B) and UWSOM (C, D). E-H) Digital (E, G) and contact angle (F, H) images of beaded water (in air; E, F) and oil (under water; G, H) droplet on SHM and UWSOM that are repetitively (1000 times) deformed with 150% tensile strain. I) Plot accounting for the change in static contact angle of beaded water (black line indicating water wettability in air) and oil (red line denoting oil wettability under water) droplets on the SHM (black) and UWSOM (red) during gradual increment of the tensile strain from 0% to 150%. J) In the plot, black and red lines illustrating the changes in water (in air) and oil (under water) wettability during successive (1000 times) tensile deformations of SHM and UWSOM, respectively.

Furthermore, these super liquid wettabilities remained unperturbed even after exposing these

nature-inspired extremely liquid-repellent membranes (SHM and UWSOM) to large (150%) tensile deformation for 1000 times as shown in Figure 4.3E−H, J.

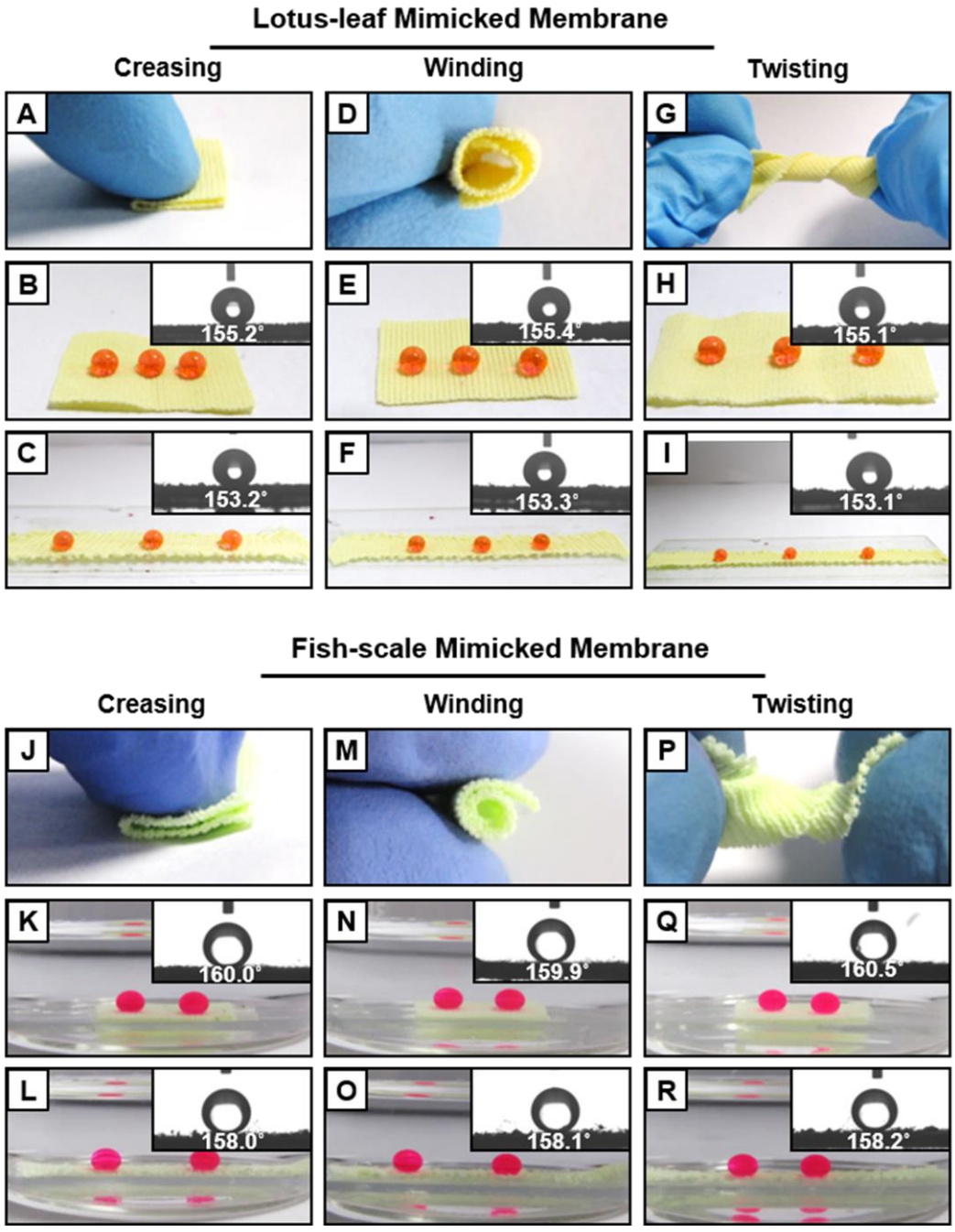

Figure 4.4. A,D,G) Digital images of SHM that is manually creased (A), winded (D) and twisted (G). B,C,E,F,H,I) Digital image and contact angle (inset) images of the beaded water droplet on the SHM after incurring creasing (B), winding (E) and twisting (H), and this water wettability was further examined after application (C,F,I) of 150% tensile strain. J,M,P) Digital images of UWSOM that is manually creased (J), winded (M) and twisted (P). K,L,N,O,Q,R) Digital image and contact angle (inset) images of the beaded water droplet on the UWSOM after incurring creasing (K), winding (N) and twisting (Q), and this water wettability was further examined after application (L,O,R) of 150% tensile strain.

Thus, the current single chemical approach provided highly stretchable two distinct super

liquid-repellent membranes (SHM and UWSOM), such demonstrations are rare in the literature.[21–26] Then, both the SHM and UWSOM were exposed to various common and practically relevant physical manipulations, including creasing, winding, and twisting each for ten times (Figure 4.4A, D, G, J, M, P); however, both oil (under water) and water (in air) repellency remained unaffected with the liquid contact angles above 150° (Figure 4.4B-I, K-R). Further, these nature-inspired wettabilities of the SHM and UWSOM were examined after performing various other severe physical abrasive tests (Figure 4.5) following standard reported protocols.[11] First, both SHM and UWSOM were immobilized on the double-sided adhesive surface and then brought in contact with an abrasive sand paper, Both the biomimicked membranes were rubbed manually with back and forth motion (with an average speed of ~4 cm/s, this speed can be manually tailored) for 20 times under applied pressure of 110 kPa and this applied pressure is significantly higher compared to the pressure (below 15 kPa) imposed in the commonly reported demonstrations.[11] During this severe physical abrasion process, the top portion of the coating was affected, however, both nonadhesive super liquid wettabilities of the membranes (SHM and UWSOM) remained unaltered with liquid contact angle above 150° as shown in Figure 4.5A, B, M, and N. Moreover, the nonadhesive superhydrophobicity and underwater superoleophobicity remained unaltered even after performing the adhesive tape peeling test on the synthesized stretchable membranes (SHM and UWSOM) as shown in Figure 4.5E, F, Q, and R. A freshly exposed adhesive tape was brought in contact with SHM and UWSOM with an applied pressure of 110 kPa for 1 min for improving contact between the adhesive surface and bio-mimicked membranes, and the synthesized SHM and UWSOM faced a severe abrasive challenge during the process of peeling the bio-mimicked membranes from the adhesive surface. Further, a knife scratch test was performed on the synthesized SHM and UWSOM, where the top surface of the biomimicked coatings were exposed to manual and random physical scratches, however that embedded liquid repellency remained unaffected as shown in Figure 4.5I, J, U and V. All the SHM and UWSOM that were exposed to severe physical abrasive tests, were further exposed to large (150%) tensile strain, and the physically deformed membranes (SHM and UWSOM) displayed extreme liquid repellency as shown in Figure 4.5C, D, G, H, K, L, O, P, S, T, W, and X. Such impeccable durability of the synthesized biomimicked membranes is rare in the literature. The exemplary tolerance of the biomimicked wettability in the synthesized SHM and UWSOM under various severe physical abrasive settings is likely due to bulk (both top interface and interior) optimization of essential chemistry and topography in

the polymeric multilayers coatings through 1,4 conjugate addition reaction between amine and acrylate groups.

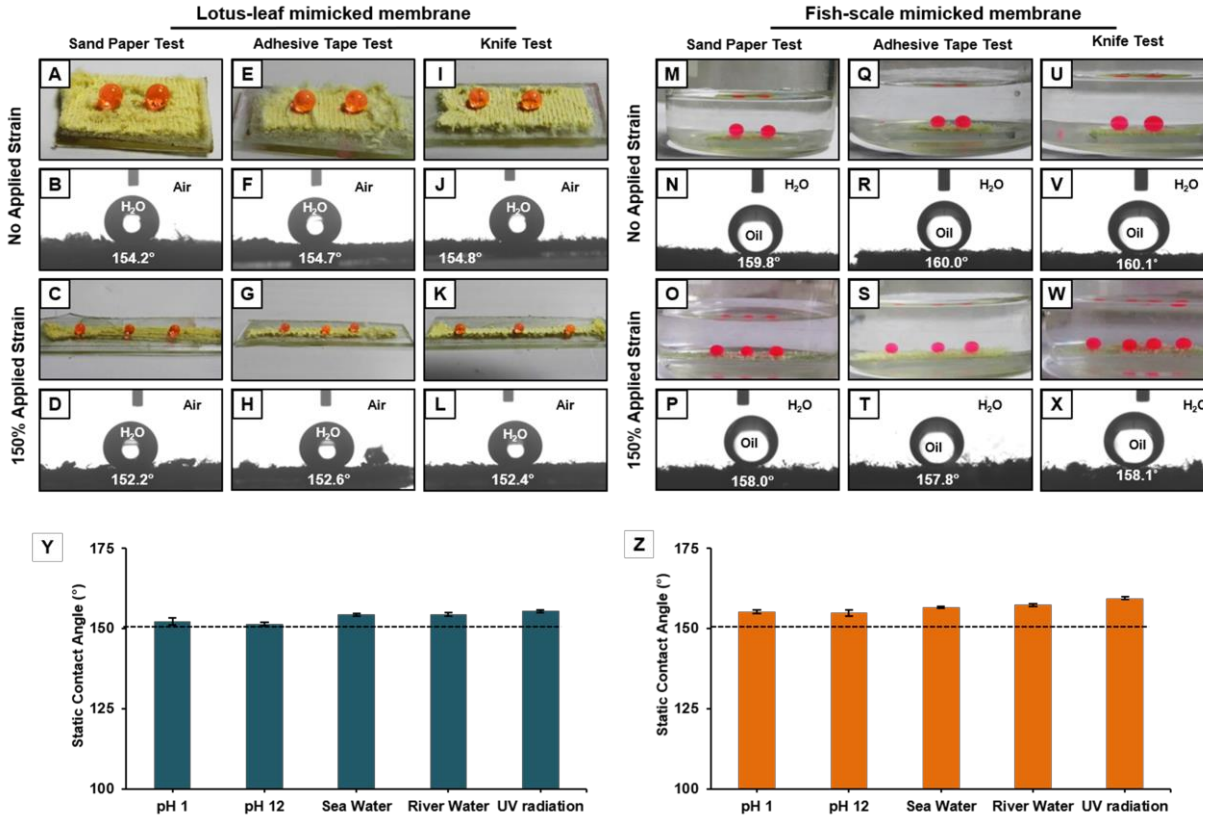

Figure 4.5. A−L) Digital image (A, E, I) and contact angle (B, F, J) images of the beaded water droplet on the SHM in air, after performing sand paper abrasion test (A, B), adhesive tape peeling test (E, F), knife test (I, J). Further, the water wettability examined after exposing these treated SHM to 150% tensile deformations (C, D, G, H, K, L). M−X) Digital image (M, Q, U) and contact angle (N, R, V) images of the beaded oil droplet on the UWSOM, after performing sand paper abrasion test (M−N), adhesive tape peeling test (Q−R), and knife test (U−V). Further, the oil wettability examined after exposing these UWSOM to 150% tensile deformations (O, P, S, T, W, X). Y, Z) Plots accounting the embedded water (in air, Y) and oil (under water, Z) wettabilities on the SHM (Y) and UWSOM (Z) after exposures to various chemically and radiative severe conditions including extremes of pH (1 and 12), river water, artificial seawater, and UV irradiation (at λ_{max} = 254 and 365 nm) for prolonged duration (25 days).

Eventually, both the top interface and interior of the coating remained inherently capable of displaying super liquid wettability. Thus, the exposed interior of the coating after performing the severe physical abrasions tests remained efficient in displaying extreme liquid repellency. Next, the chemical durability of the embedded liquid (oil/water) wettabilities of SHM and UWSOM was investigated in detail, where both of these membranes were continuously exposed to various chemically harsh aqueous phases including highly acidic (pH 1)/alkaline (pH 12) water, artificial seawater, and river water (Brahmaputra river water, Assam, India) for 25 days. However, both SHM and UWSOM continued to display the embedded nonadhesive superhydrophobicity (in air) and superoleophobicity (under water), respectively,

with liquid contact angles above 150° as shown in Figure 4.5Y, Z. At the end, both SHM and UWSOM were exposed to another practically relevant challenge that is prolonged UV radiation where both the membranes were placed under UV radiation at two different maximum wavelengths (i.e.; 254 and 365 nm) simultaneously for 25 days. However, both the membranes remained efficient to display nonadhesive superhydrophobicity/underwater superoleophobicity, with liquid contact angle above 150° (Figure 4.5Y, Z).

4.3.3. Parallel collection of oil and aqueous phases from oil/water mixtures

The highly durable and stretchable synthesized membranes (SHM and UWSOM) that displayed uninterrupted extreme water (in air) and oil (under water) repellency even after exposures to severe physical and chemical challenges were explored in developing a prototype for proof of concept demonstration of simultaneous separation followed by the collection of two distinct separated liquid phases (oil and water) in individual containers. So, a polypropylene tube (diameter 3 cm, length 4.3 cm) with one surface hole (1.5 mm) at the middle of the tube was selected for preparing the above-mentioned prototype, where either ends opening of the tube were tied with SHM and UWSOM as depicted in Figure 4.6A.

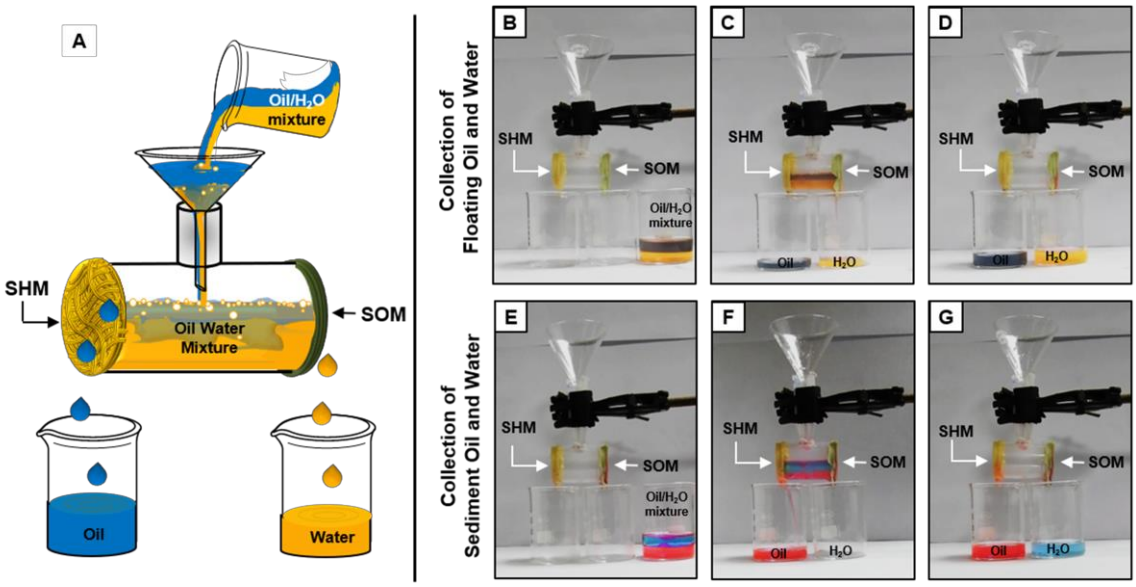

Figure 4.6. A) Schematic illustrating the selective and simultaneous collection of both oil and aqueous phases from its mixture using lab-made prototype, where the superhydrophobic membrane (SHM) and underwater superoleophobic membrane (SOM) selectively allowed to pass separated oil and aqueous phase, respectively. B−D) Digital images illustrating the collection of light oil (kerosene) and water from its mixtures. E−G) Digital images describing the collection of heavy oil (dichloroethane, DCE) and water.

The surface hole was used for pouring different oil/water mixtures. Then, oil/water mixtures consisting of 10 mL aqueous phase (colored with added dye for improved visualization) and 10 mL of kerosene (model light oil) were transferred into the prototype using a glass funnel

as shown in Figure 4.6B-C, the aqueous phase was selectively passed through the UWSOM which was attached at the right end of the prototype and the oil-free aqueous phase was collected in a container that was placed under the prototype. Simultaneously, kerosene also selectively passed through the SHM that was attached at the other end of the prototype, and the selectively filtrated oil phase was collected in another container right under the prototype as shown in Figure 4.6B-C. Thus, two different liquid phases were separated from the oil/water mixture and collected in individual containers. No accumulation of any liquid phase was noted on the top of the used membranes at the end as shown in Figure 4.6D, and such success was attributed to the rational and combinatorial function of two distinct nature-inspired interfaces. Further, this prototype was explored for separating/ collecting heavy oil (dichloromethane (DCE), model heavy oil) and aqueous phase simultaneously from the respective oil/water mixture as shown in Figure 4.6E−G. The efficiency of the separated water/oil phase is calculated following the given equation;

$$S = (V_s/V_c) \text{ X } 100$$

Where S = separation efficiency of the liquids and V_c and V_s represented the volume of the corresponding liquid before and after selective filtration, respectively. The lab-made prototype was also found to be highly efficient (above 98%) in separating and collecting various other oil/ aqueous mixtures irrespective of (a) density, (b) surface tension, and (c) viscosity of the used oil phases (vegetable oil, silicone oil, motor oil, dichloromethane, and chloroform) as shown in Figures 4.7A. After the oil/water separation, the underwater superoleophobic membranes continued to repel oily phases extremely, and thus, the synthesized biomimicked membranes remained appropriate and efficient for long-term use in oil/water separation. Further, various oil/water mixtures contaminated with highly acidic (pH 1) and alkaline (pH 12) aqueous phase, artificial seawater, and river water, were successfully separated using this same prototype as shown in Figure 4.7B. Furthermore, the membranes (SHM and UWSOM) that were exposed to the prolonged (25 days) UV irradiation (simultaneously at λ_{max} = 254 and 365 nm) and successively (1000 times) stretched with 150% TS, were also found to be efficient in isolating/ collecting oil and aqueous phases simultaneously. The current prototype allowed selective and simultaneous filtration of both oil and aqueous phases, without accumulating any single phase on top of the used membranes. After performing the simultaneous separation and collection of the respective liquid phase from the oil/water mixture, the membrane was air-dried before repeating this oil/water separation process with the same SHM and UWSOM. The oil/water separation

process was repeated successfully for a minimum of 25 times, without the aid of any external interventions as shown in Figure 4.7C.

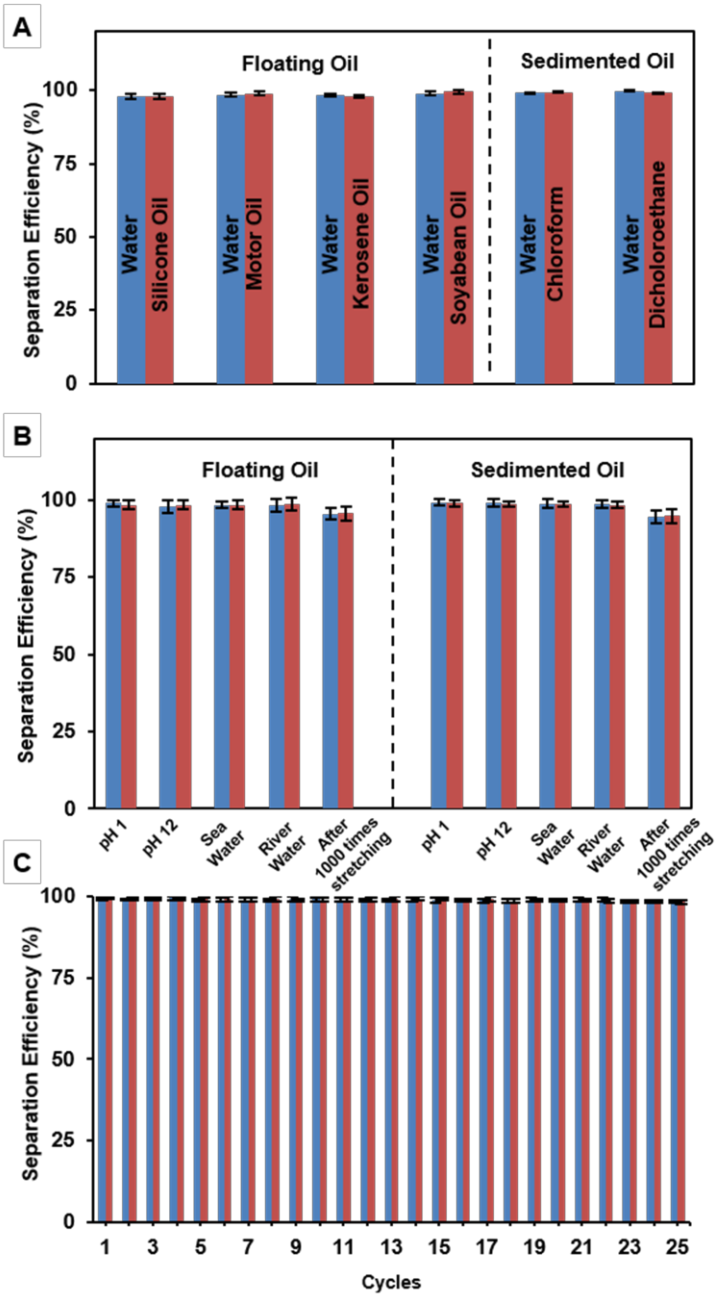

Figure 4.7. A) Plot accounting for separation efficiency of simultaneous oil (orange) and aqueous (blue) phase separation efficiency from various oil/water mixtures, irrespective of the viscosity, surface tension, and density of used oils. (B) Plot illustrating the successful separation, followed by collection of two distinct liquid phases (oil (orange) and water (blue)) from respective oil/water mixtures where the aqueous phase was varied from highly acidic, alkaline, artificial seawater to river water, and the effect of large (150%) physical deformation on its separation performance is also examined. (C) Bar graph representing the ability of repetitive (minimum 25 times) oil (orange) and aqueous (blue) phase separation using the same lab-made prototype.

The successive wetting and drying of biomimicked membranes with a respective liquid phase

have no noticeable impact on the oil/water separation performance. Moreover, the uninterrupted oil/water separation in various harsh settings attributed to the existence of (a) covalent optimization of essential chemistry and (b) robust covalent cross-linkages in the multilayers through the same 1,4-conjugate addition reaction.

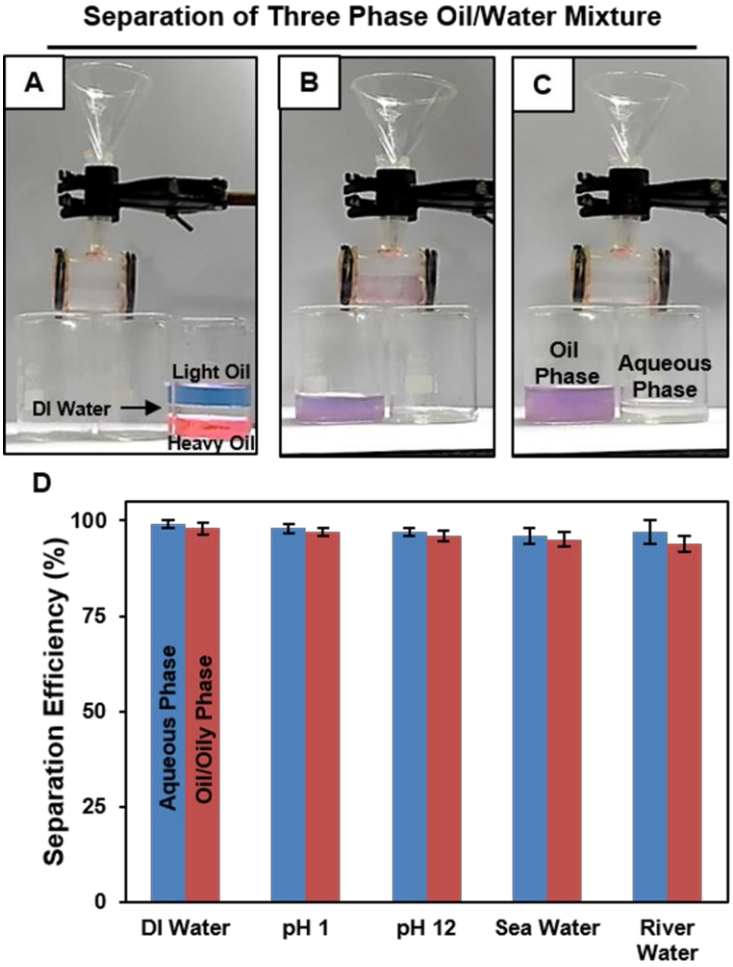

Figure 4.8. A−C) Digital images illustrating the separation of three phase (light oil/water/heavy oil) oil/water mixtures using the prototype made out of stretchable membranes (SHM and UWSOM) that are embedded with two distinct biomimicked liquid wettabilities. C) Both the heavy (DCE, red color) and light (kerosene, blue color) oils selectively passed through the SHM, and the colorless aqueous phase was filtrated through the UWSOM and collected in two separate containers. D) Graph accounting for the separation efficiency of both aqueous phase (blue) and oil phase (orange) under various severe settings, where the DI water was replaced with various chemically complex aqueous phases where the same lab-made prototype.

Most of the designs of biomimicked interfaces are optimized by associating delicate chemistries (i.e., metal−thiol bond and metal−ion interaction, UV sensitive silane chemistry, etc.) and such designs are inappropriate for application in diverse challenging settings.[27−36] As a consequence, the demonstration of oil/water separation performance with the reported materials under severe scenarios are rare in the literature.[37−39] Meanwhile, the current

approach allowed utilization of these nature-inspired interfaces in the remediation of oil spillages under various severe practically relevant scenarios.

4.3.4. Separation of oil and water from three phases oil/water mixture

The demonstration of parallel collection of oil and aqueous phase from the respective oil/water mixtures, and the performance of stretchable biomimicked membranes (SHM and UWSOM) in oil/water separation under practically relevant severe settings, inspired us to extend this approach for separation of the oil and aqueous phase from three-phase (light oil, aqueous phase, and heavy oil) oil/water mixtures. The oil/ water mixture that consisted of three phases kerosene (top layer, blue), DI water (middle layer, colorless), and DCE (a bottom layer, the added red color aids visual inspection) was poured into the lab-made prototype. Instantly both the heavy and light oil phases selectively passed through the SHM, whereas the aqueous phase was collected in a separate beaker after selective filtration through the UWSOM as shown in Figure 4.8A−C. The collected aqueous phase was found to be completely colorless (Figure 4.8C), which strongly suggested that the separated aqueous phase is free from both heavy and light oils. The collection efficiency of the separated oils and DI water were estimated to be above 98% as shown in Figure 4.8D. Moreover, this separation performance remained unaffected, even after replacing the DI water with practically relevant and more complex aqueous phases (e.g.; highly acidic, strongly basic, artificial seawater, river water) as shown in Figure 4.8D. Such unprecedented demonstration is highly relevant for the remediation of water pollution in practical and diverse settings.

4.4. Conclusion

In conclusion, this chapter introduced a facile and single chemical approach for the synthesis of durable and stretchable superhydrophobic (in air) and superoleophobic (under water) membranes—for the first time. These synthesized membranes were strategically exploited in a combinatorial act of two distinct nature-inspired (lotus leaf and fish-scale) wettabilities — superhydrophobicity and superoleophobicity—for parallel and selective separation of various oil/water mixtures repetitively—irrespective of surface tension, density, and viscosity of the used oil phase and chemical complexity in the aqueous phase. This current approach does not demand any external intervention to collect separated liquid phases from the respective oil/water mixture. Such an energy-efficient and unprecedented approach was further successfully extended for the separation of oil and aqueous phases from three-phase oil/water mixtures. The oil/water separation performance remained unperturbed even after associating

practically relevant severe and complex aqueous phases (i.e.; extremes of pH, artificial seawater, river water).

4.5. References

1. M. Ge, C. Cao, J. Huang, X. Zhang, Y. Tang, X. Zhou, K. Zhang, Z. Chen and Y. Lai. *Nanoscale Horiz.,* 2018, **3**, 235.
2. R. K. Gupta, G. J. Dunderdale, M. W. England and A. Hozumi. *J. Mater. Chem. A,* 2017, **5**, 16025.
3. Z. Chu, Y. Feng and S. Seeger, *Angew. Chem., Int. Ed.,* 2015, **54**, 2328.
4. L. Feng, Z. Y. Zhang, Z. H. Mai, Y. M. Ma, B. Q. Liu, L. Jiang and D. B. Zhu, *Angew. Chem., Int. Ed.* 2004, **43**, 2012.
5. H. Che, M. Huo, L. Peng, T. Fang, N. Liu, L. Feng, Y. Wei and J. Yuan, *Angew. Chem., Int. Ed.,* 2015, **54**, 8934.
6. A. M. Rather and U. Manna, *J. Mater. Chem. A,* 2017, **5**, 15208.
7. C. H. Peterson, S. D. Rice, J. W. Short, D. Esler, J. L. Bodkin, B. E. Ballachey and D. B. Irons, *Science*, 2003, **302**, 2082.
8. M. J. Liu, S. T. Wang, Z. X. Wei, Y. L. Song and L. Jiang, *Adv. Mater.,* 2009, **21**, 665.
9. Z. Xue, S. Wang, L. Lin, L. Chen, M. Liu, L. Feng and L. Jiang, *Adv. Mater.,* 2011, **23**, 4270.
10. X. Gao, L. P. Xu, Z. Xue, L. Feng, J. Peng, Y. Wen, S. Wang and X. Zhang, *Adv. Mater.* 2014, **26**, 1771.
11. T. Verho, C. Bower, P. Andrew, S. Franssila, O. Ikkala and R. H. A. Ras, *Adv. Mater.*, 2011, **23**, 673.
12. X. Tian, T. Verho and R. H. A. Ras, *Science*, 2016, **352**, 142.
13. X. Zhu, Z. Zhang, X. Men, J. Yang, K. Wang, X. Xu, X. Zhou and Q. Xue, *J. Mater. Chem.,* 2011, **21**, 15793.
14. H. X. Wang, Y. Xue, J. Ding, L. Feng, X. Wang and T. Lin, *Angew. Chem., Int. Ed.,* 2011, **50**, 11433.
15. M. Wu, Y. Li, N. An and J. Sun, *Adv. Funct. Mater.,* 2016**, 26,** 6777.
16. W. Wang, J. Salazar, H. Vahabi, A. J. Imre, W. E. Voit and A. K. Kota, *Adv. Mater.,* 2017, **29**, 1700295.
17. T. Lv, Z. Cheng, D. Zhang, E. Zhang, Q. Zhao, Y. Liu and L. Jiang, *ACS Nano,* 2016, **10**, 9379.

18. P. A. Levkin, F. Svec and J. M. Frechet, *Adv. Funct. Mater.,* 2009, **19**, 1993.
19. X. T. Zhu, Z. Z. Zhang, G. N. Ren, J. Yang, K. Wang, X. H. Xu, X. H. Men and X. Y. Zhou, *J. Mater. Chem.,* 2012, **22**, 20146.
20. S. T. Yohe, J. D. Freedman, E. J. Falde, Y. L. Colson and M. W. Grinstaff, *Adv. Funct. Mater.*, 2013, **23**, 3628.
21. A. M. Rather and U. Manna, *Chem. Mater.,* 2016, **28**, 8689.
22. D. Parbat and U. Manna, *Chem. Sci.,* 2017, **8**, 6092.
23. S. L. Bechler and D. M. Lynn, *Biomacromolecules,* 2012, **13**, 1523.
24. A. M. Rather, S. Mahato, K. Maji, N. Gogoi and U. Manna, *Nanoscale,* 2017, **9**, 16154.
25. A. Das, S. Sengupta, J. Deka and A. M.. Rather, *J. Mater. Chem. A,* 2018, **6**, 15993.
26. J. Ford, R. Marder and S. Yang, *Chem. Mater.,* 2009, **21**, 476.
27. C. Tan, P. Cai, L. Xu, N. Yang, Z. Xi and Q. Li, *Appl. Surf. Sci.,* 2015, **349**, 516.
28. Z. Cheng, H. Lai, Y. Du, K. Fu, R. Hou, N. Zhang and K. Sun, *ACS Appl. Mater. Interfaces,* 2013, **5**, 11363.
29. Z. Cheng, H. Liu, H. Lai, Y. Du, K. Fu, C. Li, J. Yu, N. Zhang and K. Sun, *ACS Appl. Mater. Interfaces,* 2015, **7**, 20410.
30. L. Feng, S. H. Li, Y. S. Li, H. J. Li, L. J. Zhang, J. Zhai, Y. L. Song, B. Q. Liu, L. Jiang and D. B. Zhu, *Adv. Mater.,* 2002, **14,** 1857.
31. X. Yao, Y. Song and L. Jiang, *Adv. Mater.,* 2011, **23**, 719.
32. L. Wen, Y. Tian and L. Jiang, *Angew. Chem. Int. Ed.,* 2015, **54,** 3387.
33. Z. Chu, Y. Feng and S. Seeger, *Angew. Chem. Int. Ed.,* 2015, **54**, 2328.
34. B. Su, Y. Tian and L. Jiang, *J. Am. Chem. Soc.,* 2016, **138**, 1727.
35. K. Uosaki, M. E. Quayum, S. Nihonyanagi and T. Kondo, *Langmuir* ,2004, **20**, 1207.
36. G. Kwak, M. Lee and K. Yong, *Langmuir*, 2010, **26**, 9964.
37. J. Li, C. Xu, C. Guo, H. Tian, F. Zha and L. Guo, *J. Mater. Chem. A,* 2018, **6**, 223.
38. Y. Long, Y. Shen, H. Tian, Y. Yang, H. Feng and J. Li, *J. Membr. Sci.,* 2018, **565**, 85.
39. J. Li, Z. Zhao, D. Li, H. Tian, F. Zha, H. Feng and L. Guo, *Nanoscale,* 2017, **9**, 13610.

Title: Magnetically Active Confined Superhydrophobicity for Emulsions Separation at Challenging Conditions*

Regular off-shore bulk crude oil spill accidents and uncontrolled discharge of emulsified industrial waste-water are growing concerns as oil contamination in open water reservoirs poses a severe global threat to the aqua eco-system. In the past, bio-inspired superhydrophobic sponges and membranes were successfully used for selective absorption and filtration based 'bulk'-oil separation from oil/water mixtures. However, the superhydrophobicity embedded on these macro-scale objects (sponge and mesh) is fundamentally inappropriate for remediating tiny oil-in-water emulsion droplets as the bulk aqueous phase prevents the access of submicron oil droplets to the selective superoleophilic interfaces. In addition to this, the coating of various chemicals—including asphaltenes, resins, and naphthenic acids around the crude oil droplets pose a severe challenge to oil/water separation; unlike other emulsions that are made out of refined oils. Thus, the design of a single high throughput approach for separation of both water-in-oil and oil-in-water emulsions in practically relevant harsh and challenging settings is extremely important for the efficient remediation of oil/oily pollutants. In the chapter 5, an adequate optimization of both hierarchical topography and low surface energy chemistry in a confined space (in the order of μm dimensions) of GO nanosheets was extended for achieving magnetically active and 2D 'confined-super-water repellence'. A chemically reactive polymeric nanocomplex was covalently deposited on the GO-nanosheets through a facile 1,4-conjugate addition reaction for adopting a chemically reactive and hierarchically featured polymeric interface. Simultaneously, the deposition of iron oxide nanoparticles on the 2D nanosheets rendered the entire material magnetically active. The post-covalent modification of these chemically/magnetically active and hierarchically featured GO-nanosheets with octadecylamine (ODA) yielded magnetically active and 2D 'confined-superhydrophobicity'. Further, this synthesized material was extended for addressing highly relevant and severe global challenges of 'oil-in-water' and 'water-in-oil' emulsion separation by either selective collection (with an efficiency of above 1000 wt%) of tiny oil droplets from bulk water or forming magnetically active 'Pickering-type' aqueous droplets, respectively, under various practically relevant harsh conditions, including extremes of pH, salinity, surfactant contamination, etc.

* **A. Das**, K Maji, S Naskar, U. Manna. *Chem. Sci.,* 2020, **11**, 6556.

5.1. Introduction

In the past, various porous and bulk substrates including polyurethane sponge, fibrous cotton and melamine formaldehyde sponge, were endowed with superhydrophobicity for achieving a very high oil absorption capacity.[1-6] In general, such materials, with a very high absorption capacity, were appropriate for removing the floating and sediment bulk oil phase from aqueous media.[7-11] However, such bulk superhydrophobic substrate remained inefficient for emulsion separation. The most important requirement for emulsion separation is easy accessibility of oil droplets to the selective oil-absorbent interface in the emulsion solution. In reality, superhydrophobic bulk materials have (i) less available surface area to interact with emulsified oil droplets. Moreover, it is always challenging to (ii) keep a large and bulk superhydrophobic material submerged underwater, as highly porous and spongy superhydrophobic materials loaded with a large amount of trapped air prefer to float on the air/water interface.[3-6] Eventually, the low accessibility of emulsified oil droplets to the bulk superhydrophobic interface is likely to pose a severe challenge in separating different practically relevant and viscous oils (e.g. crude oil, vegetable oil, motor oil, etc.) from their respective emulsion solutions. Recently, some superhydrophobic sponges were used for early demonstrations of oil/water separation in emulsions that were prepared mostly using organic solvents and oils having the least viscosity (i.e., toluene, hexane, chloroform, gasoline, etc.).[1-3] However, such spongy materials would be inappropriate for collecting tiny water droplets from water-in-oil emulsions. In this chapter, a different approach has been introduced for (a) achieving easy accessibility of the oil absorbent interface to the dispersed oil-droplets in oil-in-water emulsions and (b) forming magnetically active 'Pickering type' aqueous droplets to remove the aqueous phase from water-in-oil emulsions. Eventually, emulsified liquid phases were efficiently collected from both oil-in-water and water-in-oil emulsions using superhydrophobic GO nano-sheets at practically relevant diverse and severe conditions—including the presence of surfactants, extremes of pH, salinity, etc. In the recent past, the confinement of bio-mimicked wettability on micro-meter scale objects emerged as a promising avenue for various smart applications—including miniaturized chemical reactions, detection of different analytes, confined catalytic activity, contamination-free tiny liquid droplet transport, etc. which are otherwise impossible to achieve with the same liquid wettability embedded on macro-scale objects.[12–22] In the past, superhydrophobicity was achieved on microparticles by associating a low surface energy coating through weak chemical bonding/interactions—including metal–thiol bonding, hydrogen bonding, ionic

interactions, etc. These weak interactions and bondings are less likely to be sustained in practically relevant, diverse and harsh scenarios (i.e., extremes of pH, salinity, etc.). Therefore, the previously reported superhydrophobic microparticles remained mostly inappropriate for utilising under practically relevant harsh conditions, including extremes of pH, salinity, surfactant contamination, etc.[12–18] Further, the confinement of biomimicked wettability on a flexible and 2D object through facile and robust chemistry could provide a simple basis for developing functional materials for prospective applications in 'real-world' scenarios. In this chapter, the rational use of a 1,4-conjugate addition reaction provided a simple and single avenue for co-optimization of both the essential topography and appropriate chemistry on flexible 2D nanosheets. Moreover, the residual chemical reactivity of the confined space allowed to associate a wide range of other chemical functionalities through the facile 1,4-conjugate addition reaction under ambient conditions. Further, the association of iron-oxide nanoparticles and appropriate post-modification of the reactive nanocomplex coated GO-nanosheets resulted in achieving magnetically active 'confined-superhydrophobicity' that was capable of performing both in air and under oil. More importantly, in the past, the submicron particles that displayed either contrasting water wettability or extreme water wettability were extended for proof of concept demonstration of oil-in-water emulsion separation.[13,14,17,19,20] However, the existing challenges of (a) poor oil absorption capacity (below 400 wt%), (b) inability to separate different (cationic, anionic and neutral) surfactant-stabilized emulsions (oil-in-water and water-in-oil) and (c) limited performance in harsh settings are some of the major practical concerns that need to be solved immediately for separating complex forms of various oil/water emulsions in 'real-world' scenarios.[13,14,17,19,20] The synthesized 2D confined-superhydrophobicity was successfully extended for addressing all the above mentioned practically relevant challenges, where the synthesized material not only allowed to soak tiny crude-oil droplets, selectively, from the aqueous phase with a high absorption capacity (above 1000 wt%) but also formed magnetically active 'Pickering-type' droplets for both coalescing and capturing emulsified sub-micron aqueous droplets from water-in-oil emulsions. Moreover, the currently synthesized materials remained highly efficient in (i) separating oil-in-water emulsions stabilized with different types of surfactants (cationic, anionic and neutral), irrespective of both (ii) the size distribution of emulsified oil droplets and (iii) nature of the used oils (i.e. crude and refined oils). Furthermore, (iv) such effective oil/water separation performance remained unaltered even at various practically relevant harsh conditions.

5.2. Experimental Section

5.2.1. Materials

Iron(II) chloride tetrahydrate was purchased from Alfa Aesar, India. A nickel neodymium magnet was purchased from a local shop in Guwahati city (Assam, India). Crude oil was obtained from Indian Oil Corporation Limited, Guwahati. Sources of other chemicals have already been mentioned in the previous chapters.

5.2.2. General considerations

The magnetic properties of synthesized materials were investigated by using a vibrating sample magnetometer (Make: Lakeshore, Model: 7410 series). XRD spectra were recorded using an Xray diffractometer (Make: Rigaku, Model: Micromax-007HF). All-optical microscopy images were recorded using a Confocal Laser Scanning Microscope (CLSM) (Make: Zeiss, Model: LSM 510Meta). XPS spectra were obtained using an X-ray Photoelectron Spectrometer (Make: Thermo Fisher Scientific Pvt. Ltd., UK, Model: ESCALAB Xi+). Other instrumental details have been provided in the Chapter 2.

5.2.3. Synthesis of graphene oxide (GO)

The detailed synthetic procedure of graphene oxide (GO) have been discussed in Chapter 2.

5.2.4. Synthesis of magnetically active amino-graphene oxide (MAGO)

At the beginning, 200 mg of graphene oxide (GO) powder was added to 200 ml of 50% nitric acid. Then, the solution of GO was kept for 24 h at room temperature with continuous agitation for preparing nitro-graphene oxide (NGO). Later, the reaction mixture was thoroughly washed with water and acetone followed by drying under vacuum. Thereafter, freshly prepared NGO (80 mg) was dispersed in 30 ml of water by sonication. Then, 160 mg iron(II) chloride tetrahydrate was added to the solution with continuous agitation for 30 minutes at room temperature. Next, 1 ml of hydrazine hydrate was added to the reaction solution followed by the addition of 1 ml of ammonia solution (25%) to make the solution alkaline with constant stirring. The solution was kept under continuous agitation for 4 h, and then, the temperature was gradually increased to 70°C. The solution was allowed to attain room temperature and the magnetically active amino-GO (MAGO) sheets were collected by the application of a nickel-coated neodymium magnet. The separated MAGO sheets were thoroughly washed with water and acetone several times and finally dried under vacuum.

5.2.5. Synthesis of chemically reactive and magnetically active graphene oxide (CRMAGO)

At first, solutions of BPEI (0.105 M with respect to the polymer repeat unit) and 5 Acl (0.084 M) were prepared separately in methanol. Then, 125 mg MAGO was dispersed in (15 ml) of the 5 Acl solution by sonication followed by the addition of 1 ml of ammoniacal (25 mL of NH_3) BPEI solution. Then the reaction mixture was kept for 1 h under continuous agitation for both the formation and in situ deposition of a chemically reactive polymeric complex on MAGO. At the end, a chemically reactive and magnetically active graphene oxide (CRMAGO) was collected using a neodymium magnet, and the synthesized material was thoroughly washed with THF 5 times and finally dried in a vacuum.

5.2.6. Synthesis of magnetically active 2D superhydrophobic graphene oxide (MASHGO)

The residual acrylate groups in the as-synthesized CRMAGO were further reacted with octadecylamine (ODA) through the 1,4-conjugate addition reaction to achieve a magnetically active and superhydrophobic graphene oxide (MASHGO). At first, a solution of octadecylamine (10 mM) was prepared in an ethanol medium. Then, dried CRMAGO was immersed in the solution for 8 h at room temperature. After the post-chemical modification, the material was thoroughly washed with ethanol several times. After vacuum-drying, the embedded superhydrophobicity was characterized through visual inspection and contact angle measurements.

5.2.7. Separation of the bulk floating oil phase from the aqueous phase

Synthesized MASHGO powder (50 mg) was placed on and around the floating oil phase (1 ml). Immediately, the floating oil phase on the water phase was selectively absorbed by the MASHGO powder. Next, a neodymium magnet which was wrapped with cotton fabric was used to re-collect the MASHGO. During this process, both the floating crude oil and MASHGO were separated and collected from the aqueous phase. The used MASHGO was washed with ethanol and dried in a vacuum for successive use.

5.2.8. Separation of the oil-in-water emulsion

A 10 ml of Nile red-dyed oil was added to the 500 ml of deionized (DI) water and kept under continuous sonication for 1 h. Similarly, other emulsions were prepared using different complex aqueous phases, including extremes of pH (pH 1, and pH 12), river water and artificial seawater, without changing the composition of the oil in the respective emulsions. For preparing surfactant stabilized emulsions, the same composition of oil and aqueous phases was maintained, where three types of surfactants: (i) sodium dodecyl sulphate (SDS, a negatively charged surfactant; 1 mM), (ii) cetyl trimethyl ammonium bromide (CTAB, a

positively charged surfactant; 1 mM) and (iii) Triton-X solution (a neutral surfactant; 1 mM) were added into the aqueous phase. The prepared emulsions were characterized using fluorescence microscopy and dynamic light scattering study. Then, the synthesized MASHGO (25 mg) was added to a highly turbid oil-in-water emulsion (5 ml), and the mixture was manually and vigorously agitated for a few minutes. At the end, the magnet was applied to separate the oil-absorbed MASHGO sheets, which eventually provided an optically transparent aqueous phase. The successful separation of oil droplets from the aqueous phase was characterized through visual inspection, fluorescence microscopy and dynamic light scattering study.

5.2.9. Separation of the water-in-oil emulsion

First, 10 ml of the fluorescein dyed aqueous phase was added to 500 ml of oil and kept under continuous sonication for 1 h. Eventually, a highly turbid solution of the water-in-oil emulsion was formed. Similarly, the emulsions were prepared in different aqueous environments which included extremes of pH (pH 1, pH 12), river water and artificial seawater with the same composition as the emulsion. For the surfactant stabilized emulsion, aqueous phases were individually contaminated with three types of surfactants—including SDS (1 mM), CTAB (1 mM) and Triton-X solution (1 mM) prior to preparing water-in-oil emulsions. All emulsions were characterized by visual inspection, fluorescence microscopy and dynamic light scattering study. Thereafter, the same MASHGO (50 mg) was added to the 10 ml water-in-oil emulsion, followed by manual agitation for a minute. MASHGO helped in capturing water droplets from the oil phase by forming a magnetically active 'Pickering-type' aqueous droplet. This droplet was separated by the application of an external magnet and eventually, a water-free oil phase was obtained.

5.3. Results and Discussion:

5.3.1. Synthesis and characterization of chemically reactive and magnetically active graphene oxide

In the past, two dimensional (2D) graphene oxide nanosheets have been routinely utilized to optimize the essential hierarchical topography on macro-scale objects for adopting superhydrophobicity.[23-27] In contrast to the earlier conventional approaches, here, amino graphene oxide (AGO) nanosheets were strategically decorated with magnetically active Fe_3O_4 nanoparticles and a chemically reactive porous polymeric coating. In the current design, superhydrophobicity was embedded on the graphene oxide nanosheets having a large

surface area and high flexibility for efficient emulsified droplet separation.

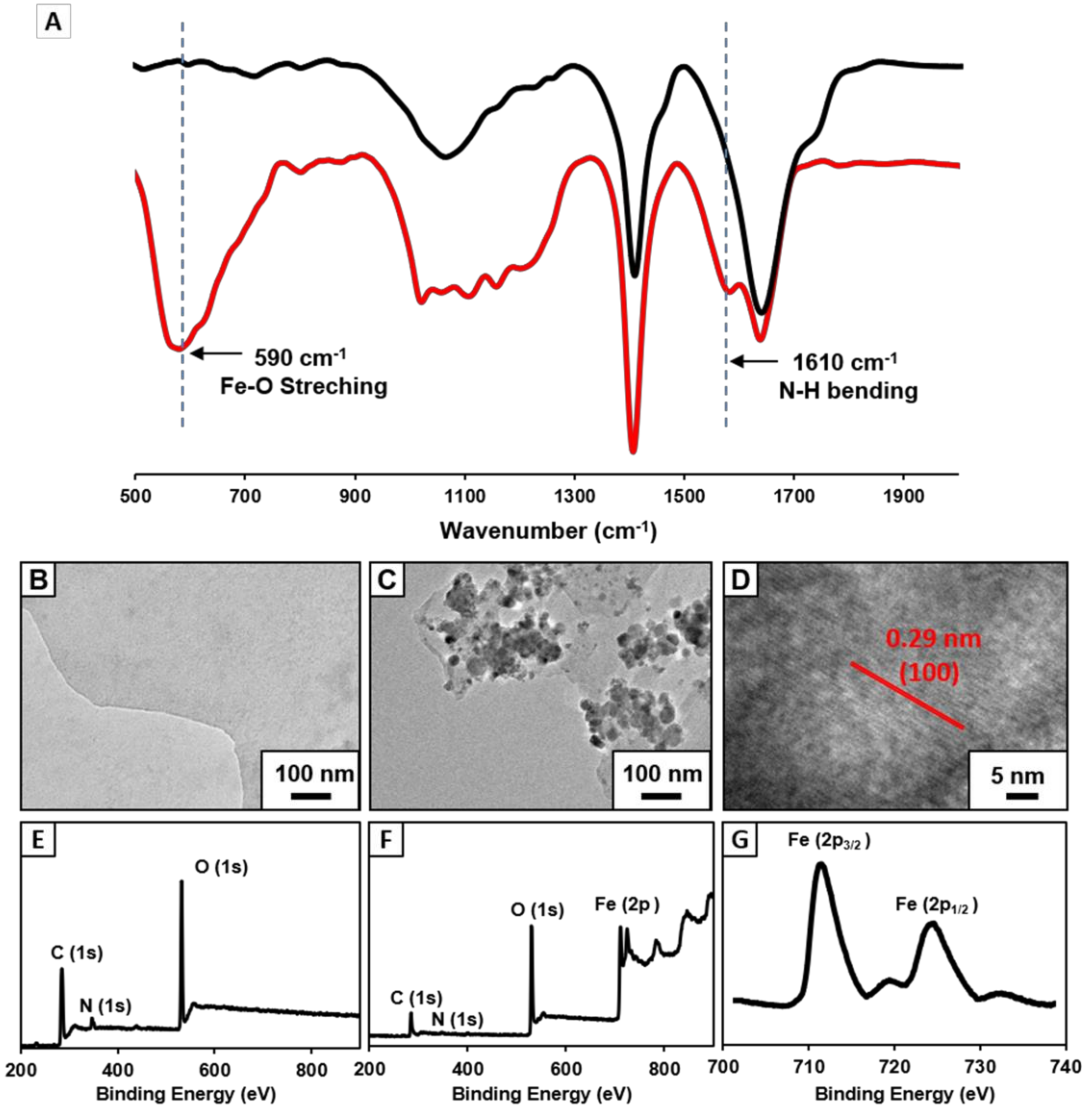

Figure 5.1. A) FTIR spectra of nitro-graphene oxide (NGO (black)) and magnetically active graphene oxide (MAGO (red)). B-C) TEM images of NGO (B) and MAGO (C). D) HRTEM images confirms the deposition of Fe_3O_4 nanoparticles on MAGO. E-G) XPS spectra of NGO (E) and MAGO (F-G).

The large surface area of AGO facilitated the interaction between the superhydrophobic interface and emulsion droplets, and the flexibility of AGO allowed better arrangement around the water droplets in the oil phase of the water-in-oil emulsion. Eventually, rapid and efficient oil-in-water and water-in-oil emulsion separation were achieved. Firstly, magnetically active amino-graphene oxide (MAGO) was synthesized by depositing Fe_3O_4 nanoparticles on nitro-graphene oxide nanosheets. The successful deposition of Fe_3O_4 nanoparticles was confirmed by FTIR spectral analysis, transmission electron microscopy

(TEM), powder Xray diffractometer (XRD) spectra and X-ray photoelectron spectroscopy (XPS) characterization as shown in Figure 5.1. The FTIR spectra of MAGO revealed the existence of a strong broad peak at 590 cm^{-1} correspondings to the Fe–O bond which clearly indicated the successful oxidation of the Fe^{2+} ions to Fe_3O_4 (Figure 5.1A). During the course of this chemical reaction, the nitro-graphene oxide was reduced to amino graphene oxide (AGO) as evident from the appearance of an IR peak at 1610 cm^{-1} corresponding to the N–H bending of primary amine (Figure 5.1A). In the MAGO, Fe_3O_4 is likely to interact with the hydroxyl and amine group of the amino graphene oxide through co-ordination/hydrogen bonds. Additionally, the TEM images of MAGO clearly confirmed the deposition of Fe_3O_4 nanoparticles (Figure 5.1B-C) with a lattice spacing of 0.29 nm which corresponds to the (100) plane of the deposited Fe_3O_4 nanoparticles on the AGO nanosheets as characterized with high-resolution transmission electron microscopy (HRTEM) imaging (Figure 5.1D). The successful deposition of Fe_3O_4 nanoparticles on MAGO was also reconfirmed by XPS analysis as shown in Figure 5.1E-G, where the appearance of binding energy peaks at 726.0 eV and 711.7 eV for Fe $2p_{1/2}$ and Fe $2p_{3/2}$, unambiguously revalidated the successful deposition of Fe_3O_4 nanoparticles on MAGO (Figure 5.1E-G).[30] Further, the X-ray diffraction (XRD) data further confirmed the crystalline nature of the Fe_3O_4 in MAGO where seven distinct diffraction peaks were observed at 30.2º, 35.7º, 37.1º, 43.4º, 53.6º, 57.2º, 62.8°, which can be ascribed to the lattice spacing of (220), (311), (222), (400), (422), (511), and (440) of Fe_3O_4, respectively. Based on these characterizations, it is clear that Fe_3O_4 decorated magnetically active reduce graphene oxide (MAGO) was successfully synthesized. Energy-dispersive X-ray spectroscopic (EDX) analysis also confirmed the existence of Fe element (61.5 wt%) in the MAGO. Thereafter, a chemically reactive polymeric complex,[28,29] synthesized by mixing of BPEI and 5Acl under ambient conditions, was covalently integrated into MAGO. The amine groups of MAGO readily reacted with the residual acrylate groups of the polymeric complex under ambient conditions through the 1,4-conjugate addition reaction, and eventually yielded chemically reactive and magnetically active hierarchically featured GO nanosheets (CRMAGO) as shown in Figure 5.2A-B. The surface topography, residual chemical reactivity and magnetic properties of the synthesized CRMAGO were thoroughly characterized as shown in Figure 5.2D-E, F, K-M. The comparison of field emission scanning electron microscopy (FESEM) images of CRMAGO confirmed the successful immobilization of the polymeric complex as shown in Figure 5.2D-E. The random aggregation of the granular polymeric complex contributed to the construction of hierarchical

topography which is essential for exhibiting extreme water repellence. Further, the existence of residual chemical reactivity in the CRMAGO was investigated following the standard and widely accepted FTIR spectral analysis.

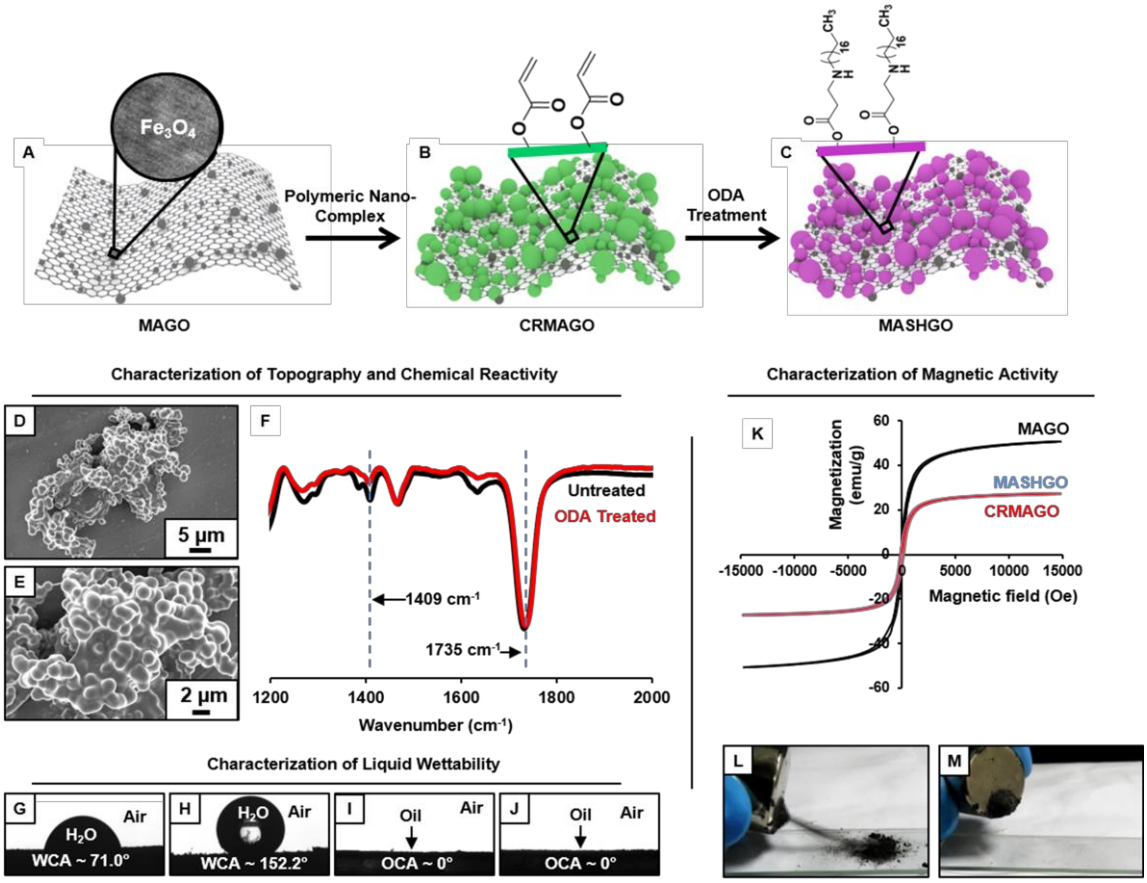

Figure 5.2. A-C) Schematic representating the Fe_3O_4 deposited magnetically active graphene oxide (MAGO, A), chemically reactive, magnetically active and hierarchically featured graphene oxide (CRMAGO, B), and further post modification with octadecylamine (ODA) provided magnetically active and confined superhydrophobicity (MASHGO, C). D–E) FESEM images of magnetically active superhydrophobic graphene oxide (MASHGO) in low (D) and high magnifications (E). F) FTIR spectra of the chemically reactive and magnetically active graphene oxide (CRMAGO) before (black) and after (red) ODA treatment. In the FTIR spectra, the IR peak at 1735 cm^{-1} and 1409 cm^{-1} corresponds to C=O stretching and C–H deformation of the β-carbon of the vinyl group respectively. G–J) Static contact angle images of beaded water (G and H) and oil (I and J) droplets on CRMAGO (G and I) and MASHGO (H and J). K) Magnetization curves of MAGO (black), CRMAGO (red) and MASHGO (blue) at room temperature. L-M) Digital images illustrating the collection of MASHGO using a neodymium magnet (0.5 T).

In the FTIR spectra (Figure 5.2F), the appearance of IR peaks at 1409 cm^{-1} and 1735 cm^{-1} for the C–H deformation of the β-carbon of the vinyl groups and carbonyl stretching, respectively, validated the presence of residual acrylate groups—which were capable of reacting with alkylamines under ambient conditions.

5.3.2. Achievement of confined superhydrophobicity by post covalent modification of CRMAGO

The successful post-chemical modification of the CRMAGO with octadecylamine (ODA) resulted in the depletion of IR peak intensity at 1409 cm^{-1} with respect to the IR peak at 1735 cm^{-1} (served as the internal reference). During the 1,4-conjugate addition reaction between amine and acrylate groups, only the vinyl moiety of the acrylate groups were consumed—and the carbonyl moiety of the acrylate groups remained unaffected (Figure 5.2F). The post covalent modification of the CRMAGO with ODA altered the water wettability resulting in a transition from hydrophilicity (with a water contact angle of ~71°) to superhydrophobicity with a water contact angle of ~152°; however, the extreme oil affinity (with an oil contact angle of 0°) of the material remained intact as shown in Figure 5.2G-J. Next, the embedded magnetic properties in the synthesized materials were thoroughly characterized using a vibrating sample magnetometer (VSM). The MAGO displayed a paramagnetic behaviour with an S-shape magnetic hysteresis curve and a magnetic saturation value (Ms) of 50.7 emu g^{-1} as shown in Figure 5.2K. As expected, a change in the magnetic properties was clearly noted after depositing the chemically reactive hierarchical polymeric coating on MAGO. Nevertheless, the CRMAGO still remained highly paramagnetic with a magnetic saturation value of 27.3 emu g^{-1} as shown in Figure 5.2K. After the post-covalent modification of CRMAGO with ODA, the magnetic properties remained unaltered as noted in Figure 5.2K (blue line). Thus, magnetically active and superhydrophobic graphene oxide (MASHGO) was successfully synthesized. Furthermore, a lab used a magnet (nickel coated neodymium magnet 0.5 T) when brought in close proximity to the material, immediately attracted the entire superhydrophobic GO powder as shown in Figure 5.2L-M. This MASHGO was further extended for addressing challenges related to comprehensive remediation of both oil-in-water and water-in-oil emulsion solutions, irrespective of the size distribution of emulsified droplets, under various practically relevant harsh conditions, including extremes of pH, salinity, surfactant contamination, etc.

5.3.3. Oil-in-water/water-in-oil emulsion separation in challenging settings

As a proof of concept demonstration, firstly, the synthesized MASHGO was placed at the crude oil/water interface where it selectively absorbed the floating oil phase from the aqueous phase as shown in Figure 5.3A-C. The oil absorbed MASHGO was collected from the

air/water interface using a neodymium magnet that was wrapped in the cotton fabric as shown in Figure 5.3D-E.

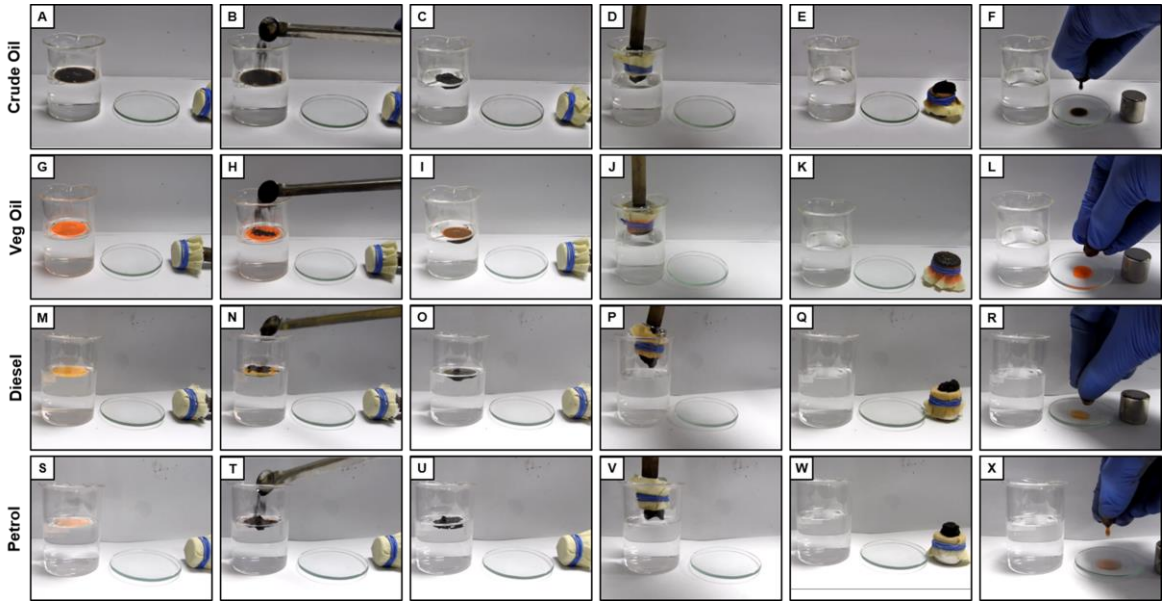

Figure 5.3. A-X) Digital images demonstrating the separation and collection of different floating oils (crude oil (A-F), veg oil (G-L) and diesel (M-R), petrol (S-X)) from water/air interface by using MASHGO and external magnet, where floating oil phases (A, G, M, S) were exposed to MASHGO (B, H, N, T), and immediately respective oil phases were absorbed by MASHGO (C, I, O, U). D-F, J-L, P-R, V-X) The oil-absorbed MASHGO was collected using fabric wrapped external magnet.

The oil absorption capacity of the MASHGO was measured to be above 1000 wt% which was significantly higher than that of the reported superhydrophobic/Janus particles.[13,14,17,19,20] Further, the wrapped cotton fabric on the magnet was removed and manually squeezed to recollect the absorbed oil phase as shown in Figure 5.3F. The same procedure was followed to remove other floating oils (veg. oil, diesel and petrol) from the aqueous phase as shown in Figure 5.3G-X. MASHGO remained efficient to separate various oil phases. The same MASHGO could be reused for oil/water separation after ethanol-washing followed by air-drying. The selective oil-absorption capacity remained mostly unaffected even after 50 times of successive use for oil/water separation (Figure 5.4A) and the extreme water repellence also remained unaltered. Further, this selective oil absorption performance remained unaffected, irrespective of the nature of oil/oily phases (i.e. petrol, diesel and veg oil; Figure 5.4B) used for preparing the respective oil/water mixtures. Moreover, it was found that the oil absorption ability of both the MAGO and CRMAGO was found to be significantly low as compared to that of MASHGO as shown in Figure 5.4B. Moreover, the performance of the MASHGO remained indistinguishable even in practically relevant challenging settings, including extremes of pH, seawater and river water (Figure 5.4C). Next, the MASHGO was rationally

applied to separate both the oil-in-water and water-in-oil emulsions by either selective absorption of the oil phase or forming in situ magnetically active 'Pickering-type' aqueous droplets, respectively.

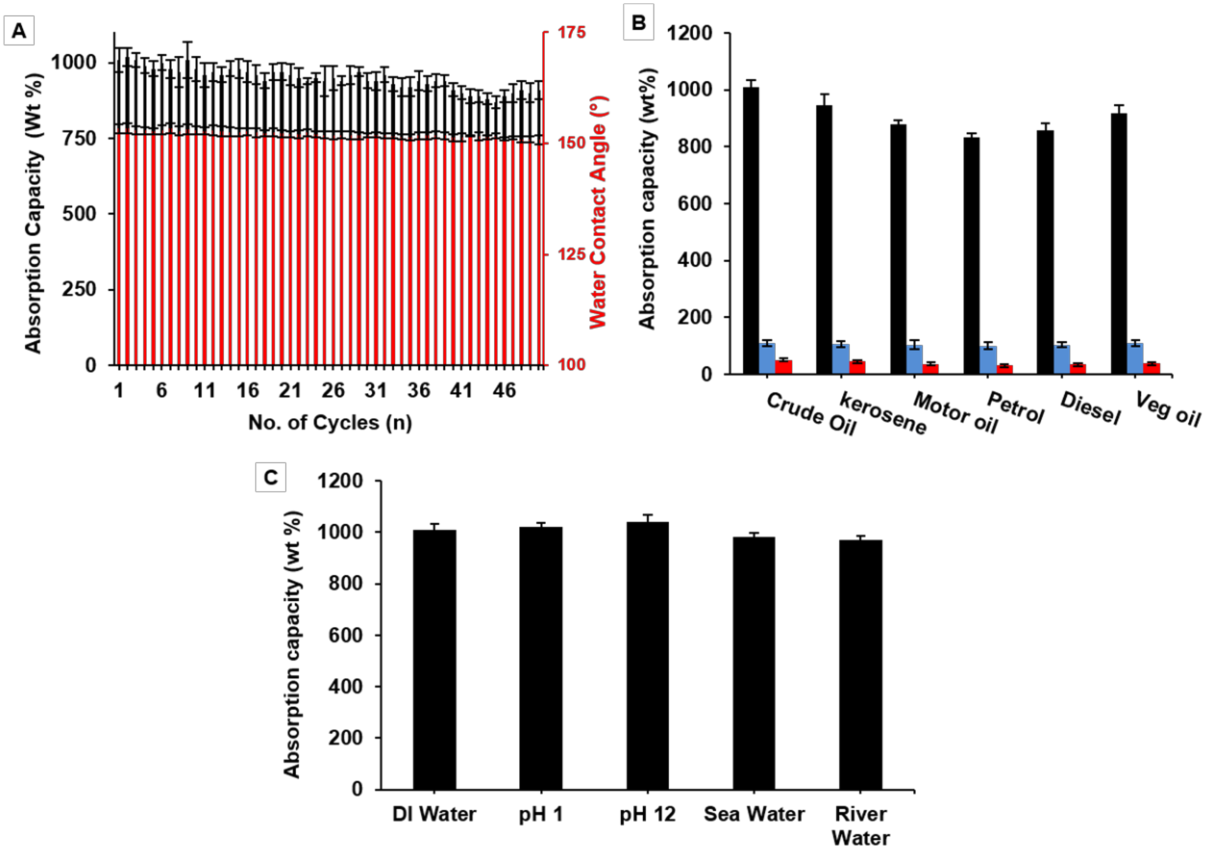

Figure 5.4. Bar graphs accounting crude oil absorption capacity (black) and water wettability (red) of MASHGO after the repetitive (up to 50 cycles) uses. B) The plot comparing the oil-absorption capacity (wt.%) for various oils by MAGO (red), CRMAGO (blue), MASHGO (black). C) The plot accounts the crude oil-absorption capacity (wt.%) in presence of different and complex aqueous phases, including DI water, highly acidic, alkaline, artificial seawater to river water.

At first, a solution of the crude oil-in-water emulsion (2% v/v) was prepared, where water-immiscible Nile red dye added crude oil aided both visual inspection and fluorescence microscopy characterization. Both the formation of emulsified oil droplets (with an average size of 1 mm) in the bulk aqueous phase and the removal of the same oil droplets after treatment with MASHGO were characterized through visual inspection, fluorescence microscopy imaging and dynamic light scattering (DLS) study (Figure 5.5). Two separate vials of the same crude-oil-in-water emulsion solution in the presence (right-side vial) and absence (left-side vial) of added MASHGO were agitated vigorously for 2.5 minutes, where the agitation paved the way towards easy access of emulsified oil droplets to MASHGO. With time, the fluorescence dye added emulsified oil droplets which caused scattering of

light, was selectively absorbed on MASHGO and the transmittance of the highly opaque and brown-colored emulsion solution significantly improved.

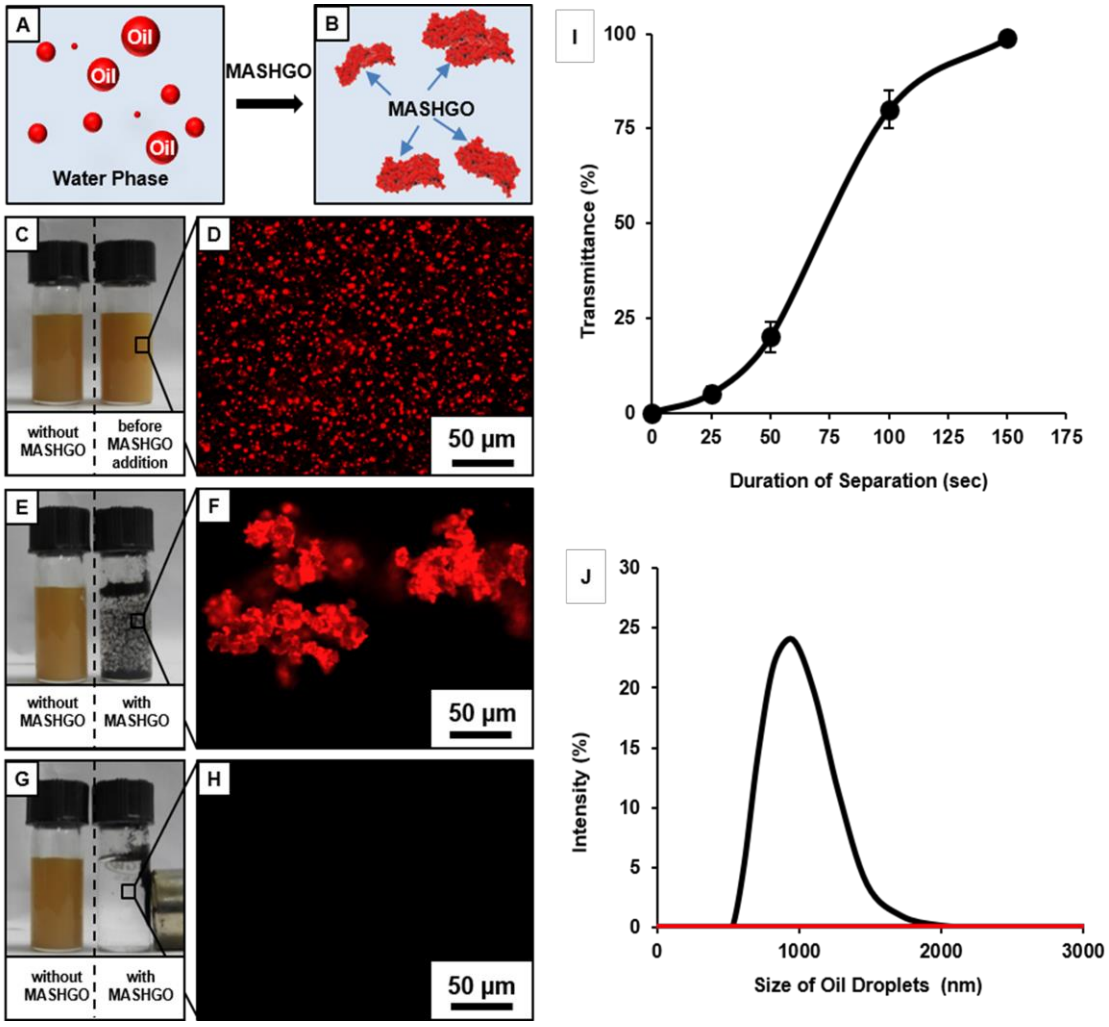

Figure 5.5. A-B) Illustrations of the selective absorption of tiny crude oil droplets by magnetically-active superhydrophobic graphene oxide (MASHGO) from the water phase. C–H) Digital images (C, E and G) and fluorescence microscopy images (D, F and H) demonstrating crude oil-in-water emulsion separation ability of MASHGO, where the crude oil was labelled with Nile red. (C, E and G) Two separate vials of crude oil-in water emulsions with (right-side vial) and without (left-side vial) MASHGO were agitated for 150 seconds (C and E) before the application of a nickel coated neodymium magnet (G). I) A plot showing the change in transmittance (%) of the crude oil-in-water emulsion solution in the presence of MASHGO, where transmittance was recorded after the application of the external magnet. J) DLS study on the crude oil-in-water emulsion before (black) and after (red) performing oil/water separation by MASHGO.

After 2.5 minutes, the opaque, brown-colored emulsion became colorless and completely optically transparent (Figure 5.5G-I), where an external magnet was applied to separate MASHGO from the emulsion solution prior to measuring the transmittance. At the end, an oil-free aqueous phase was obtained on the application of the external magnet (nickel coated neodymium magnet, 0.5 T) as confirmed with visual inspection (Figure 5.5G) fluorescence microscopy imaging (Figure 5.5H), dynamic light scattering (DLS) study (Figure 5.5J). The

selective soaking of crude-oil by the aggregated MASHGO was confirmed via fluorescence imaging in Figure 5.5F, whereas, such a drastic change was not observed for the emulsion solution in the absence of MASHGO (Figure 5.5E). The 2D confined-superhydrophobicity played a crucial role in the successful and rapid separation of oil/water from oil-in-water emulsions. Moreover, the oil/water separation performance by the MASHGO remained intact even on increasing the percentage of crude oil in the respective oil-in-water emulsion. Again, this emulsified crude oil separation ability by the MASHGO remained unaltered in different harsh aqueous environments including high pH, low pH, seawater, and river water (Brahmaputra, Guwahati, Assam, India). Further, various natural and synthetic oils, which produce oil-water emulsions with different size distributions of oil droplets were also successfully separated using MASHGO as confirmed by visual inspection, DLS study and fluorescence microscopy imaging (Figure 5.6). The synthesized material remained efficient for the repetitive separation of the oil-in-water emulsion, at least 50 times. In general, the separation of the surfactant stabilized oil-in-water emulsion is a severe challenge, due to the existence of a protective layer of surfactant around the oil/oily droplets. In this current study, the same MASHGO was also extended for separating different surfactant stabilized oil-in-water emulsions. The synthesized MASHGO displayed an unparallel ability for separating oil/water in different types of surfactant stabilized oil-in-water emulsions (2% v/v). The respective emulsions were prepared in the presence of a positively charged surfactant (CTAB, a concentration of 1 mM), negatively charged surfactant (SDS, a concentration of 1 mM) and non-ionic surfactant (Triton-X, a concentration of 1 mM) as shown in Figure 5.7. Visual inspection, fluorescence imaging and DLS study unambiguously confirmed the successful removal of crude oil droplets from their respective surfactant stabilized emulsions as shown in Figure 5.7. Thus, the confined superhydrophobicity on GO nanosheets played an important role in the comprehensive remediation of oil spillages in practically relevant challenging settings. The application of the same MASHGO powder allowed the successful separation of micron/submicron-sized water droplets from various bulk oil phases as schematically demonstrated in Figure 5.8A-B. For the proof of concept demonstration, a water-in-oil emulsion (2% v/v) was prepared by mixing the fluorescein dyed aqueous phase in kerosene followed by continuous sonication for 1 hour. Fluorescence microscopy and DLS study of the emulsion confirmed the formation of micron/submicron-sized water droplets in kerosene and these aqueous droplets remained homogeneously suspended in the oil phase for several hours (Figure 5.8C-D).

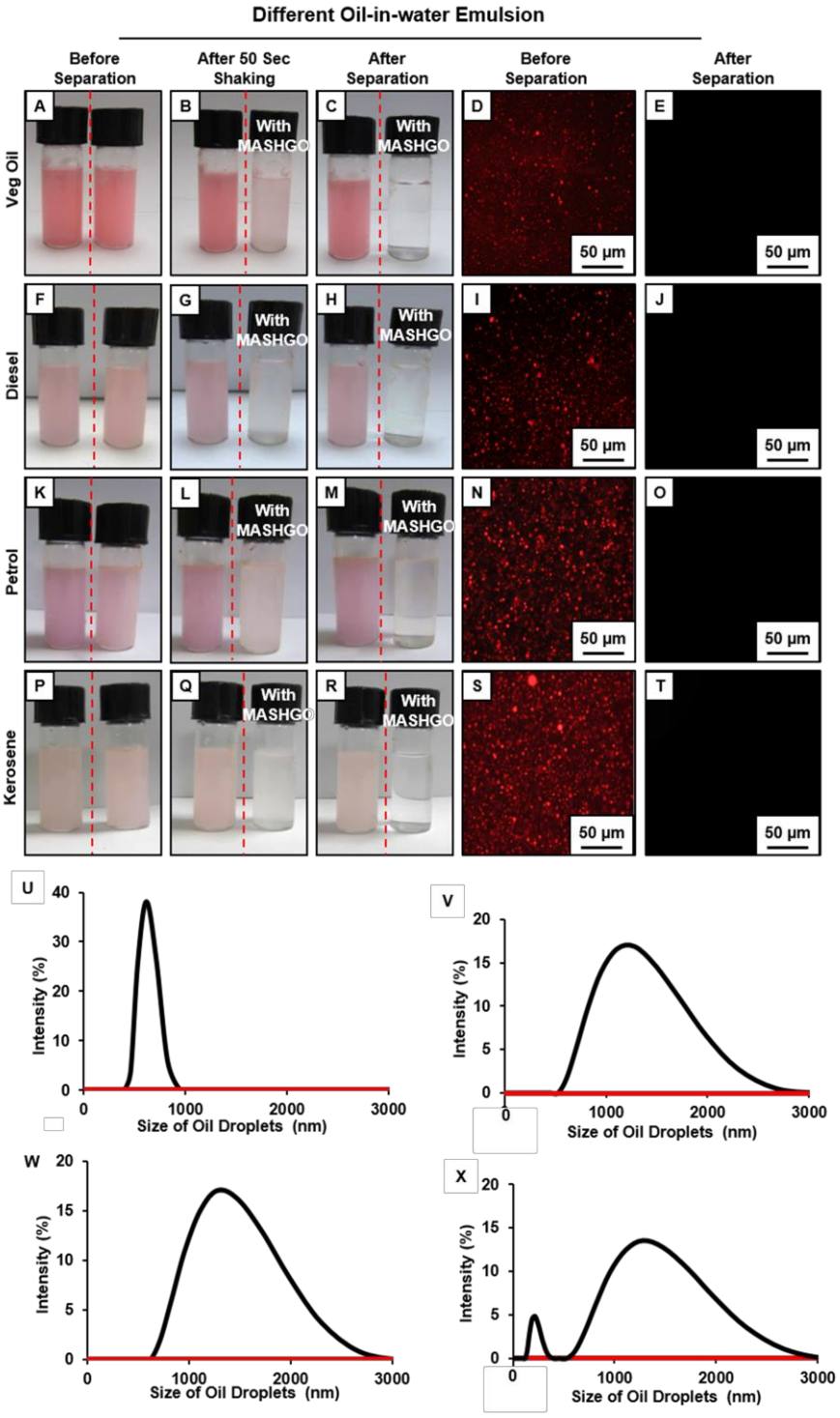

Figure 5.6. A-X) Digital images (A-C, F-H, K-M, P-R), fluorescence microscope images (D-E, I-J, N-O, S-T) and DLS plots (U,V,W,X) accounting successful separation of oil-in-water emulsions that were prepared using various oils (veg oil: A-E, U; diesel: F-J, V; petrol: K-O, W; kerosene: P-T, X), through selective absorption of respective oil droplets by MASHGO. The left-sided and right-sided vials of the dotted red lines denoted crude oil-in-water emulsion without and with MASHGO, respectively. D-E, I-J, N-O, S-T) Fluorescence microscope images of various oil-in-water emulsion before separation (D,I,N,S) and after separation (E,J,O,T) by MASHGO. U,V,W,X) DLS plots of various oil-in-water emulsions before (black) and after (red) oil/water separation by MASHGO.

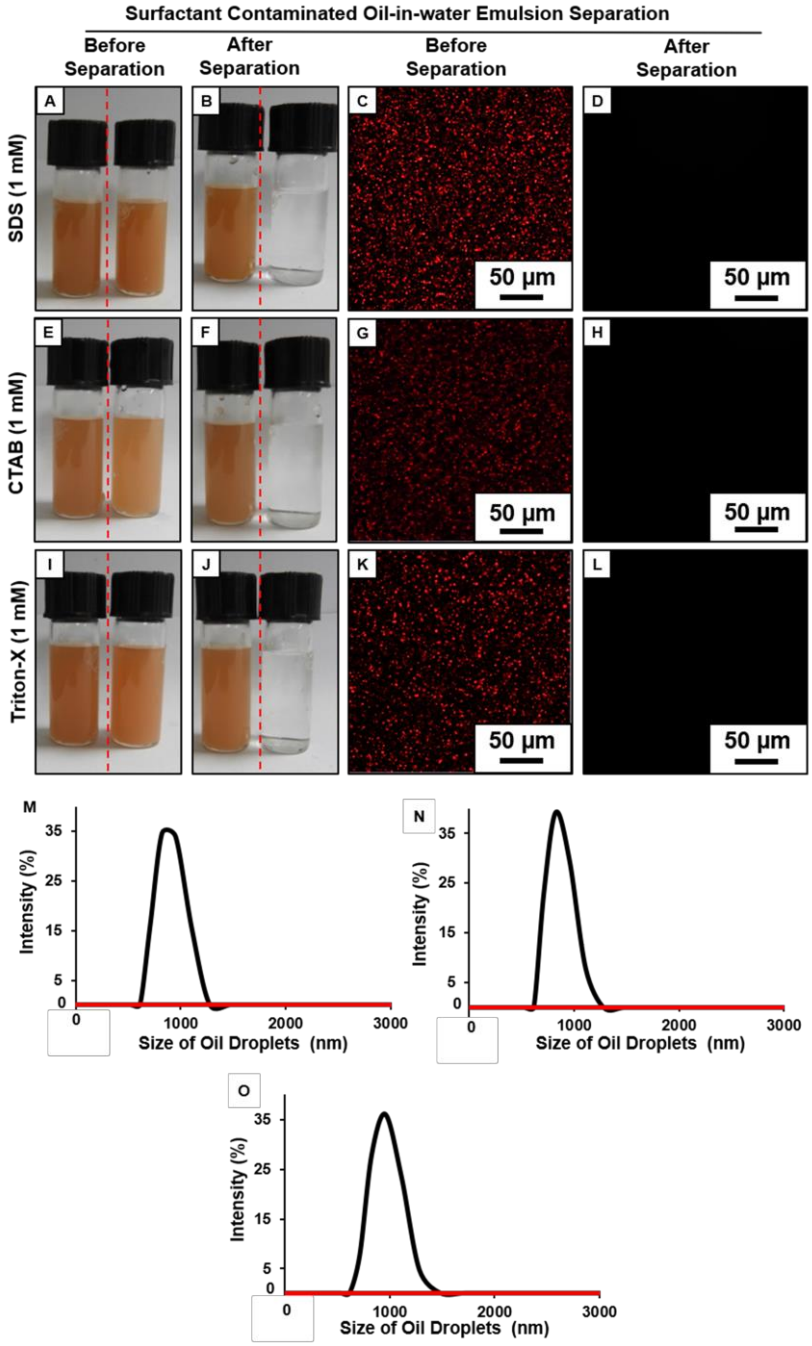

Figure 5.7. (A and B), (E and F) and (I and J)) Digital images of the crude oil-in-water emulsion before (A, E and I), and after (B, F and J) oil/water separation by MASHGO in the presence of anionic (SDS, A-B), cationic (CTAB, E-F) and neutral (Triton-X, I-J) surfactants. The left-side and right-side vials with the dotted red lines denote crude oil-in-water emulsions without and with MASHGO, respectively. (C and D), (G and H) and (K and L)) Fluorescence microscope images of the crude oil-in-water emulsion before (C, G and K) and after (D, H and L) oil/water separation by MASHGO in the presence of different surfactants. M, N and O) DLS plots of the crude oil-in-water emulsion before (black) and after (red) oil/water separation by MASHGO in the presence of SDS (M), CTAB (N), Triton-X (O).

However, the agitated water-in-oil emulsion in the presence of MASHGO formed magnetically active 'Pickering type' droplets, where the MASHGO sheets facilitated the coalescence of submicron water droplets in the oil phase as shown in Figure 5.8E, F. Further,

the fluorescence microscopy images revalidated the formation of the 'Pickering- type' emulsion where the non-fluorescent and black MASHGO sheets were wrapped around the large and fluorescent aqueous droplets as shown in Figure 5.8F.

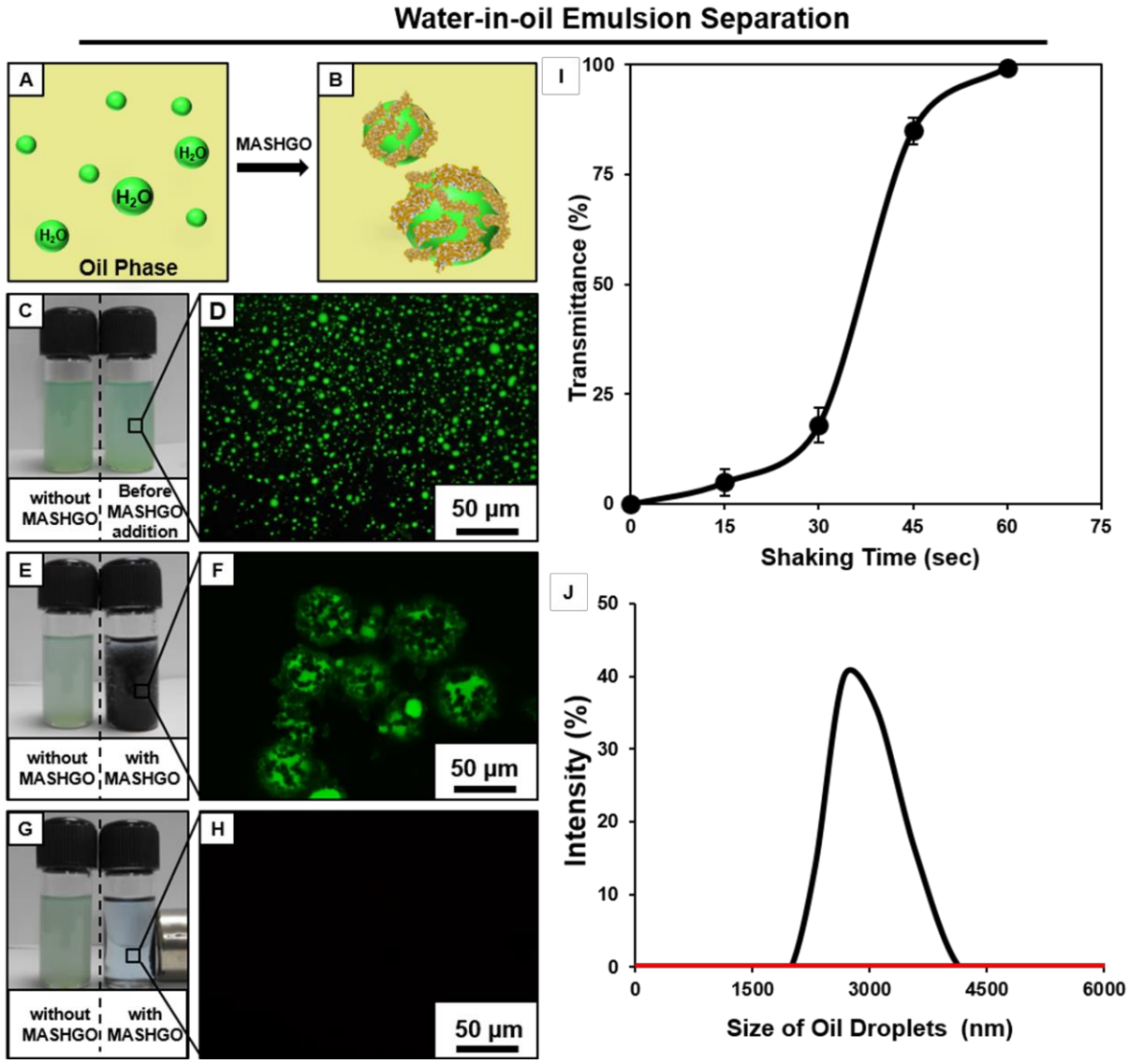

Figure 5.8. A and B) Schematic illustrating the formation of magnetically active 'Pickering type' droplets in the water-in-oil emulsion in the presence of MASHGO. C–H) Digital images (C, E and G) and fluorescence microscopy images (D, F and H) representing the water-in-kerosene oil emulsion before addition of MASHGO (C and D), after addition of MASHGO (E and F) and after the application of the external magnet (G and H). E and G) Digital images of two separate vials of the same water-in-kerosene oil emulsion solutions in the presence (right-side vial) or absence (left side vial) of added MASHGO. I) A plot showing the change in transmittance (%) of the water-in-oil emulsion solution in the presence of MASHGO during the course of oil/water separation, where the transmittance is recorded after application of the external magnet. J) DLS study on the water-in-oil emulsion before (black) and after (red) performing oil/water separation by MASHGO

The inherent tendency of the synthesized MASHGO towards extreme water repellence in the oil phase provided the basis of forming a 'Pickering-type' droplet as similar to the dry liquid marbles in air. Further, the hydrophobic particles have an energetic preference to settle at the

water-oil interface of the water-in-oil emulsion and form the Pickering emulsion.[31]

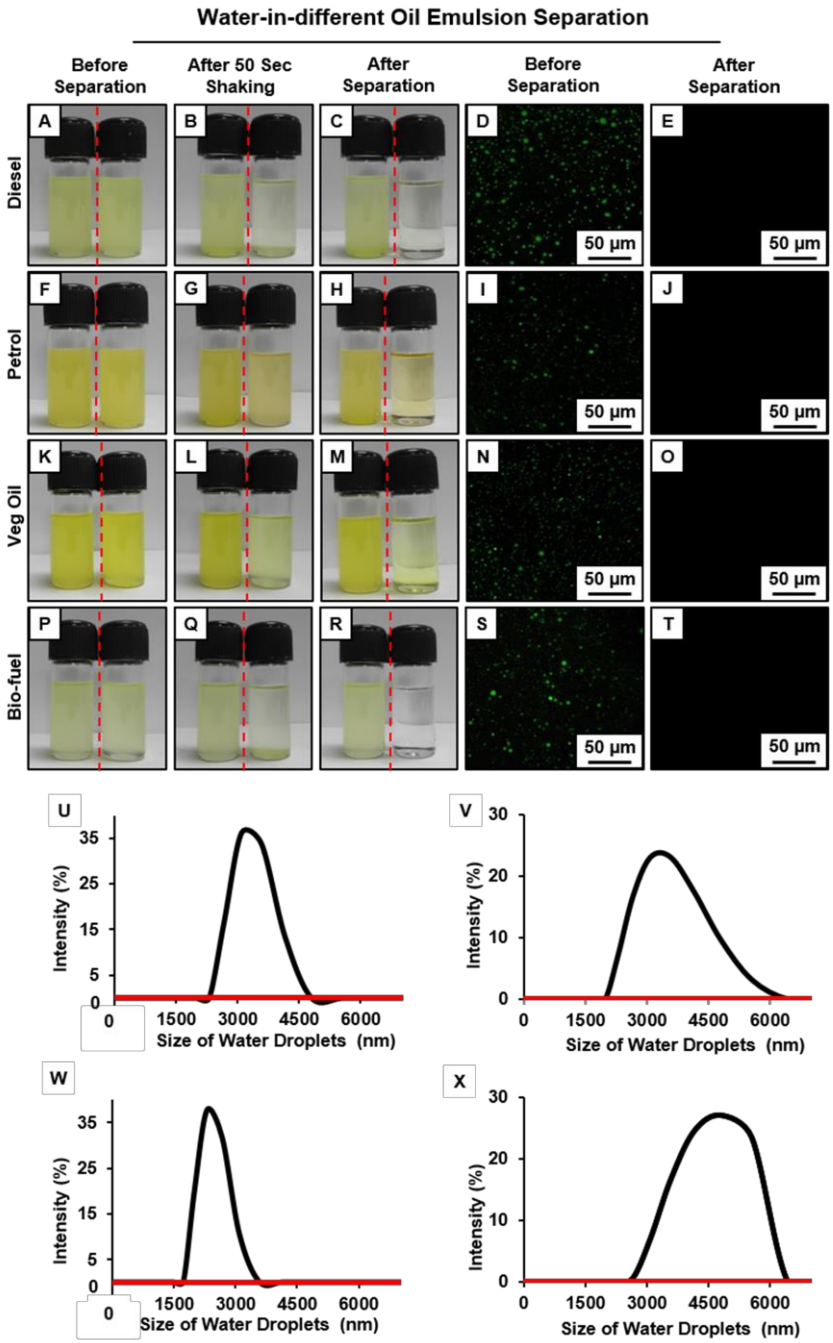

Figure 5.9. A-C, F-H, K-M, P-R) Digital images of water-in-oil emulsions that were prepared using various oils (Diesel; A-C, petrol; F-H, Veg oil; K-M, bio-fuel; P-R), before (A, F, K, P), during (after 50 sec; B, G, L, Q) and after (C, H, M, R) oil/water separation by MASHGO. The left-sided and right-sided vials of the dotted red lines denoted water-in-oil emulsion without and with MASHGO, respectively. D-E, I-J, N-O, S-T) Fluorescence microscope images of various water-in-oil emulsions ((Diesel; D-E, petrol; I-J, Veg oil; N-O, bio-fuel; S-T)) before (D, I, N, S) and after oil/water separation (E, J, O, T) by MASHGO. U, V, W, X) DLS plots of various water-in-oil emulsion before (black) and after (red) separation by MASHGO (Diesel; U, petrol; V, Veg oil; W, bio-fuel; X).

Further, the MASHGO wrapped water droplets were easily removed from kerosene by the

application of an external magnet as shown in Figure 5.8G. Eventually, a completely clean oil phase with 100% transmittance was recovered (Figure 5.8I).

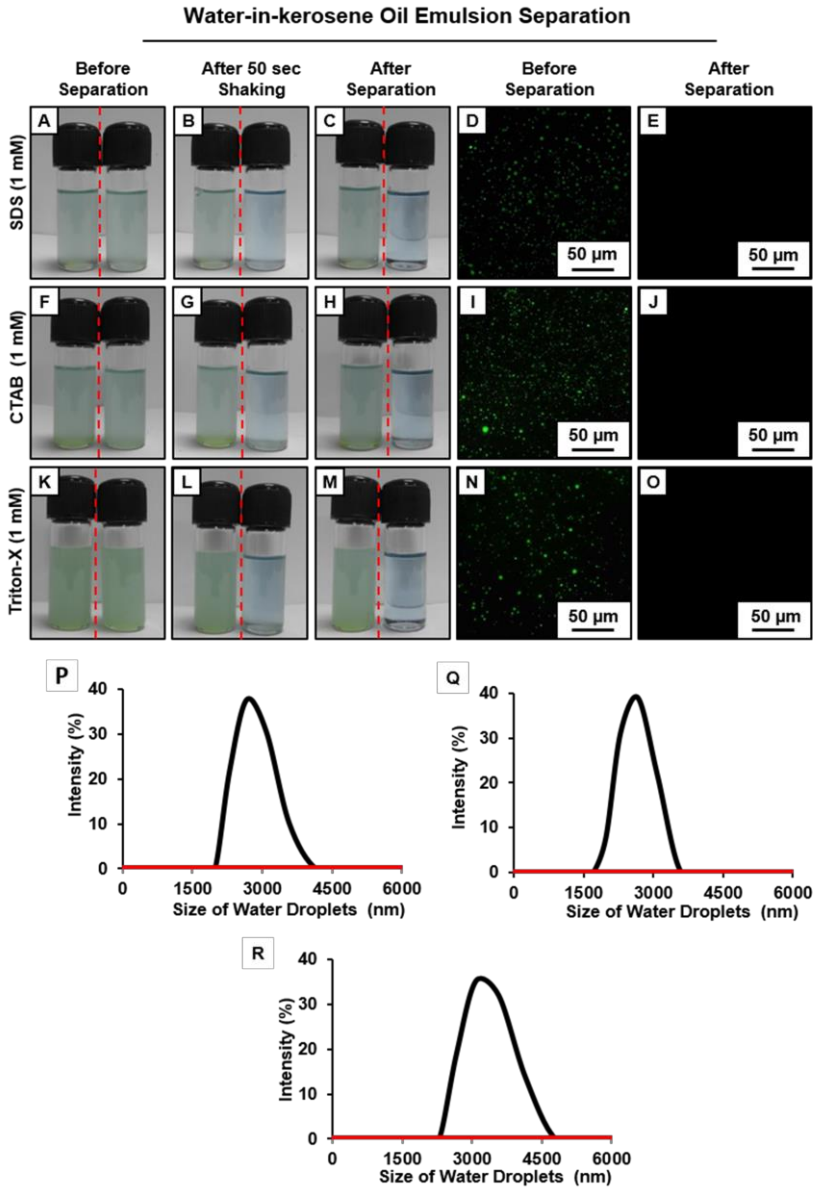

Figure 5.10. A-C, F-H, K-M) Digital images of water-in-kerosene oil emulsion before (A, F, K), during (after 50 sec, B, G, L) and after (C, H, M) oil/water separation by MASHGO in presence of different surfactants (SDS; A-C, CTAB; F-H, Triton-X; K-M). The left-sided and right-sided vials of the dotted red lines denoted water-in-kerosene oil emulsion without and with MASHGO. D-E, I-J, N-O) Fluorescence microscope images of water-in-kerosene oil emulsion before (D, I, N) and after (E, J, O) oil/water separation by MASHGO in presence of different surfactants (SDS; D-E, CTAB; I-J, Triton-X; N-O). P, Q, R) DLS plots of water-in-kerosene oil emulsion before (black) and after (red) oil/water separation by MASHGO in presence of different surfactant (SDS; P, CTAB; Q, Triton-X; R).

Moreover, visual inspection (Figure 5.8G), fluorescence microscopy imaging (Figure 5.8H) and the DLS study (Figure 5.8J) revalidated this successful removal of aqueous contaminants from the oil phase by the MASHGO. This oil/water separation performance remained

unperturbed even on increasing the amount of aqueous phase in the respective water-in-oil emulsion. Moreover, the performance of oil/water separation from the water-in-oil emulsion by MASHGO remained unaltered for different types of oil phases (e.g. veg oil, petrol, diesel, and bio-fuel) (Figure 5.9). Even more, the surfactants (SDS, DTAB, Triton-X) stabilized water-in-oil emulsions were tested with MASHGO. Interestingly, the contaminated aqueous phase was successfully separated as shown in Figure 5.10.

5.4. Conclusions

In this chapter, a chemically reactive, magnetically active and hierarchically featured coating was introduced on individual GO nano-sheets following a simple and robust chemical approach for achieving two dimensional (2D) magnetically active confined superhydrophobicity. The synthesized MASHGO remained highly capable of separating oil/water from both oil-in-water and water-in-oil emulsions, irrespective of the nature of the oil used for preparing emulsions and even in the presence of practically relevant chemically complex scenarios. Moreover, this current approach was efficient for the rapid separation of submicron-oil droplets stabilized with different surfactants. Further, the oil/water separation performance remained unaltered irrespective of the size distributions of micron/sub-micron liquid droplets in the respective emulsions either by selective absorption of oil droplets (in the aqueous phase) or formation of magnetically active 'Pickering-type' aqueous droplets in the oil phase. Therefore, confined superhydrophobicity on 2D nano-sheets can be envisioned as a promising and facile approach for high throughput cleaning of oil spills, fuel purification, etc. Further, this chemically and magnetically active design of GO nano-sheets could be useful in developing various functional materials by adopting appropriate post-covalent modification through the 1,4-conjugate addition reaction.

5.5. References

1. J. Wang, F. Han, B. Liang and G. Geng, *J. Ind. Eng. Chem.,* 2017, **54,** 174.
2. T. Yu, F. Halouane, D. Mathias, A. Barras, Z. Wang, A. Lv, S. Lu, W. Xu, D. Meziane, N. Tiercelin, S. Szunerits and R. Boukherroub, *Chem. Eng. J.,* 2020, **384**, 123339.
3. J. Wang and Y. Zheng, *Sep. Purif. Technol.,* 2017, **181**, 183.
4. Z. Lei, Y. Deng and C. Wang, *J. Mater. Chem. A*, 2018, **6**, 3258.

5. H. Zhu, D. Chen, W. An, N. Li, Q. Xu, H. Li, J. He and J. Lu, *Small*, 2015, **11**, 5222.
6. C. Ruan, K. Ai, X. Li and L. Lu, *Angew. Chem., Int. Ed.,* 2014, **53**, 5556.
7. J. Gu, H. Fan, C. Li, J. Caro and H. Meng, *Angew. Chem., Int. Ed.,* 2019, **58**, 5297.
8. S. Yuan, J. Zhu, Y. Li, Y. Zhao, J. Li, P. V. Puyveldea and B. V. Bruggen, *J. Mater. Chem. A*, 2019, **7**, 2723.
9. X. Dong, S. Gao, J. Huang, S. Li, T. Zhu, Y. Cheng, Y. Zhao, Z. Chen and Y. Lai, *J. Mater. Chem. A*, 2019, **7**, 2122.
10. R. Qu, Y. Liu, W. Zhang, X. Li, L. Feng and L. Jiang, *Chem. Sci*., 2019, **10**, 4089.
11. L. Kang, J. Li, J. Zeng, W. Gao, J. Xu, Z. Cheng, K. Chen and B. Wang, *J. Mater. Chem. A,* 2019, **7**, 16447.
12. Y. Zhao, J. Fang, H. Wang, X. Wang and T. Lin, *Adv. Mater*., 2010, **22**, 707.
13. L. Zhang, J. Wu, Y. Wang, Y. Long, N. Zhao and J. Xu, *J. Am. Chem. Soc.,* 2012, **134**, 9879.
14. L. P. Xu, X. Wu, J. Meng, J. Peng, Y. Wen, X. Zhanga and S. Wang, *Chem. Commun.,* 2013, **49**, 8752.
15. Y. E. Miao, H. K. Lee, W. S. Chew, I. Y. Phang, T. Liu and X. Y. Ling, *Chem. Commun.,* 2014, **50**, 592.
16. H. K. Lee, Y. H. Lee, I. Y. Phang, J. Wei, Y. E. Miao, T. Liu and X. Y. Ling, *Angew. Chem.,* 2014, **126**, 5154.
17. C. Duan, T. Zhu, J. Guo, Z. Wang, X. Liu, H. Wang, X. Xu, Y. Jin, N. Zhao and J. Xu, *ACS Appl. Mater. Interfaces,* 2015, **7,** 10475.
18. S. Huang, Y. Zhang, J. Shi and W. Huang, *ACS Sustainable Chem. Eng.,* 2016, **4**, 676.
19. Y. Song, J. Zhou, J. B. Fan, W. Zhai, J. Meng and S. Wang, *Adv. Funct. Mater.,* 2018, **28**, 1802493.
20. H.-J. Chen, T. Hang, C. Yang, G. Liu, D. Lin, J. Wu, S. Pan, B. Yang, J. Tao and X. Xie, *Nanoscale,* 2018, **10**, 1978.
21. M. Tenjimbayashi, S. Samitsu and M. Naito, *Adv. Funct. Mater.,* 2019, **29**, 1900688.
22. X. Zhuo and S. Troels, *Angew. Chem., Int. Ed.,* 2019, **58**, 11952.
23. H. B. Jiang, Y. L. Zhang, D. D. Han, H. Xia, J. Feng, Q. D. Chen, Z. R. Hong and H. B. Sun, *Adv. Funct. Mater.,* 2014, **24**, 4595.
24. L. Xu, G. Xiao, C. Chen, R. Li, Y. Mai, G. Sun and D. Yan, *J. Mater. Chem. A*, 2015, **3**, 7498.

25. J. N. Wang, Y. L. Zhang, Y. Liu, W. Zheng, L. P. Lee and H. B. Sun, *Nanoscale,* 2015, **7**, 7101.
26. K. Jayaramulu, K. Kumara, R. Datta, C. Rçsler, M. Petr, M. Otyepka, R. Zboril and R. A. Fischer, *Angew. Chem., Int. Ed.,* 2016, **55**, 1178.
27. J. Gu, H. Fan, C. Li, J. Caro and H. Meng, *Angew. Chem., Int. Ed.,* 2019, **58**, 5297.
28. D. Parbata and U. Manna, *Chem. Sci.,* 2017, **8,** 6092.
29. A. M. Rather, N. Jana, P. Hazarika and U. Manna, *J. Mater. Chem. A*, 2017, **5**, 23339.
30. W. Wang, B. Tang, B. Ju, Z. Gao, J. Xiu and S. Zhang, *J. Mater. Chem. A,* 2017, **5**, 958.
31. B. P. Binks and R. Murakami*, Nat. Mater*., 2006, **5**, 865.

Title: Common Avenue for Different Superhydrophobic Interfaces That Embedded with Tailored and Stable Oil Wettability in Air

Abstract

Lotus-leaf-inspired superhydrophobic interface extremely repels aqueous phase—but inherently displays super-oil-affinity in air. On the other side, the superamphiphobic interface repels both aqueous phase and oil/oily phase extremely with contact angle above 150°. The fundamental criteria for optimizing such distinct super liquid wettabilities are different, and distinct synthetic approaches were adopted to achieve these two different types of liquid-repellent interfaces for different prospective and relevant applications. In the previous chapters, the covalent integration of the chemically reactive polymeric nanocomplex and amino graphene oxide through sol-gel and layer-by-layer deposition techniques have been extended to develop both the fish scale and lotus leaf-inspired interfaces, but those interfaces were failed to show in air, oil repellency. In this Chapter 6, a rapid and scalable spray deposition of a reaction mixture of a strategically selected two small molecules that readily reacted through 1,4-conjugate addition reaction process, has been introduced for tailoring different oil-wettability in air, without perturbing superhydrophobicity. An appropriate dilution of a reaction mixture provided a facile basis for customizing oil wettability—starting from superoleophilicity to superoleophobicity keeping intact the super water repellence. The synthesized superhydrophobic and superamphiphobic interfaces remained efficient for sustaining exposures of various practically relevant physical manipulations & abrasions and chemically complex aqueous phases. Furthermore, both the superhydrophobic and superamphiphobic interface was successfully extended for comparing oil/water separation, anti-fouling and self-cleaning performances. Such a simple and common synthetic approach fo preparing extremely water repellent interfaces having differences in oil-wettability in air would be useful for practically relevant outdoor applications.

6.1. Introduction

The Lotus-leaf-inspired interfaces that simultaneously displays extreme repellence towards aqueous phase and super affinity for oil/oily phase are widely recognized as a superhydrophobic interface,[1-10] whereas the interfaces that extremely repel both water and oil phase with contact angle above 150° are formally defined as superamphiphobic interface.[11-20] While a hierarchically featured interface with low surface energy atop provided contrasting and extreme wettability for aqueous phase,[1] the superamphiphobic interfaces demand a more specific structural features apart from regular co-optimization of hierarchical topography and low surface energy.[11] Thus, the design of a superamphiphobic interface is more challenging, and generally, distinct strategies were adopted to synthesize superhydrophobic/superoleophilic and superamphiphobic interfaces.[1-20] In the past, mostly, different polymers and metal oxides were used to achieve essential topography, and further co-optimization of essential low surface energy conferred desired super-liquid repellent interfaces.[1-12] The separate association of superoleophilicity or superoleophobicity with superhydrophobicity is important for diverse and relevant applications.[1-20] For example, superhydrophobic interface that embedded with super-oil affinity allowed selective filtration-based oil/water separation,[21-22] whereas, self-cleaning and antifouling performance of superamphiphobic interfaces remained superior over lotus-leaf inspired superhydrophobic interface.[11-20] Nevertheless, a common synthetic approach for selective and controlled integration of the desired oil-wettability with the extremely water-repellent interface is unprecedented. In this Chapter 6, strategically selected two small molecules— (3-aminopropyl)trimethoxysilane (APTMS) and 3,3,4,4,5,5,6,6,7,7,8,8,9,9,10,10,11,11,12,12,12- heneicosafluorododecyl acrylate (HFDDA) (Figure 6.1A) that readily reacted in toluene through 1,4 conjugate addition reaction (Figure 6.1B) at ambient conditions, provided a simple and rapid basis for controlled tailoring of desired oil wettability without altering the embedded superhydrophobicity. A simple dilution of the reaction mixture of selected two small molecules, prior to spray deposition, allowed a single step co-optimization of essential topography and chemistry for achieving three distinct liquid-repelling coatings, where oil wettability varied from superoleophilicity to superoleophobicity—without perturbing the superhydrophobicity. The optically transparent and extremely water repellent coatings that embedded with tailored oil-wettability in air, continued to display unaltered extreme liquid repellence even at practically relevant various and severe challenging settings, including exposures to physical manipulations, abrasions,

chemically complex liquids, high temperature, UV-radiation etc. Furthermore, such interfaces were extended to compare oil/water separation, self-cleaning and antifouling performances.

6.2. Experimental

6.2.1. Materials:

(3-Aminopropyl)trimethoxysilane (APTMS), 3,3,4,4,5,5,6,6,7,7,8,8,9,9,10,10,11,11,12,12,12- Heneicosafluorododecyl acrylate (HFDDA), sodium dodecyl sulphate (SDS), Hexadecyltrimethylammonium bromide (CTAB), triton x-114, Methylene blue, Nile red, Polyethylene glycol, Diiodomethane were obtained from Sigma Aldrich (Bangalore India). Sources of other chemicals have already been mentioned in the previous chapters.

6.2.2. General Considerations:

Transmittance spectra were recorded using the Perkin-Elmer Lambda 750 (UV/Vis/NIR Spectrometer). Other instrumental details have been provided in the previous chapters.

6.2.3. Fabrication of Superhydrophobic fabric:

Firstly, the reaction mixture was prepared by mixing of 200 µl of (3-Aminopropyl)trimethoxysilane and 660 mg of 3,3,4,4,5,5,6,6,7,7,8,8,9,9,10,10,11,11,12,12,12-Heneicosafluorododecyl acrylate (molar ratio of 1:1) in 10 ml toluene. Then the reaction mixture was continuously agitated for 20 minutes. Next, the reaction mixture was spray deposited on the polyurethane fabric (10 cm x 10 cm) and kept for drying in the hot oven to obtain superamphiphobicity. Besides, the reaction mixture was diluted 2 times (denoted as dilution-I) and 4 times (referred as dilution-II) prior to its spray deposition provided superhydrophobicity/oleophobicity and superhydrophobicity/superoleophilicity respectively. The respective liquid wettability was examined through visual inspection and contact angle measurements.

6.2.4. Physical and chemical durability:

Various physical and chemical durability tests were conducted on the synthesized superamphiphobic and superhydrophobic/superoleophilic coatings. The details of each experimental procedure are explained in the following sections.

6.2.4.1. Physical deformations tests:

Both the freshly prepared superamphiphobic and superhydrophobic/superoleophilic interfaces were subjected to various physical manipulations—including creasing, twisting and, finger

wiping, tissue paper wiping for multiple times. Thereafter, the respective liquid wettability was examined following the standard process.

6.2.4.2. Knife Scratch Test:

In this test, superamphiphobic and superhydrophobic/superoleophilic coatings were randomly scratched with a sharp metal knife for several times. After that, the anti-wetting property of both the fabric was characterized using contact angle instruments.

6.2.4.3. Adhesive tape peeling test:

An freshly exposed adhesive tape was separately placed on both the superamphiphobic and the superhydrophobic/superoleophilic coatings (3 cm x 1 cm) with an applied external pressure of 25 kPa for 1 minute. Then, the adhesive tape was manually peeled off from the coatings. The water and dodecane wettability was examined on the treated interface using contact angle measurements.

6.2.4.4. Sand Paper Abrasion Test:

In sand paper abrasion test, a 400-grit abrasive sand paper (3 cm x 1 cm) was manually rubbed with back and forth motion across both the superamphiphobic and superhydrophobic/superoleophilic interface (5 cm x 1.5 cm) for 250 cm abrasion distance— with an applied pressure of 25 kPa and an average speed of ~12 cm/s. After this test, the liquid wettability was examined with visual inspection and contact angle measurements.

6.2.4.5. Exposure to a different aqueous environment and UV radiation:

The superamphiphobic and superhydrophobic/superoleophilic coatings were separately exposed to different and complex aqueous environments— including distilled water, highly acidic (pH 1) & alkaline (pH 12) media, artificial seawater (solution of 0.226 g $MgCl_2$, 0.325 g $MgSO_4$, 2.673 g NaCl, and 0.112 g $CaCl_2$ in 100 mL of deionized water), river water (Brahmaputra river, Assam, India), surfactants contaminated aqueous phase (SDS, 2 mM; CTAB, 2 mM; Triton-X, 2 mM) for 10 days. They were also exposed to UV irradiation (254 nm and 365 nm) and high (80°C) temperature for 10 days. The water and dodecane wettability was separately investigated by monitoring the contact angle of beaded liquid droplets.

6.2.5. Gravity-driven oil/water separation:

A lab-made prototype was developed by using one end opened-glass tube which was covered with a fibrous substrate that embedded with either superamphiphobic or superhydrophobic/superoleophilic coating. A side-hole was also made at another end of the glass tube for pouring the oil-water mixture. The three-phase oil/water mixture that consisted

of heavy model oil (DCE, pink-coloured bottom layer), aqueous layer (blue coloured-middle layer) and petrol (yellow-coloured top layer) was poured in the lab-made prototype where superamphiphobic fabric restricted the passage of both the aqueous and oil phase. But, in the case of superhydrophobic interface, only the oil phase was selectively passed through it and collected in a separate beaker.

6.3. Results and discussion:

6.3.1. Synthesis and characterization of three distinct liquid-repellent interfaces

In the past, 1,4-conjugate addition reaction between amine and acrylate remained an elegant avenue for synthesizing functional polymeric coatings.[23-27] In the previous chapters, this chemical approach has been successfully extended for controlled optimization of both 1) the water wettability in-air and 2) the oil-wettability under water through strategic selection of post covalent modification of a chemically reactive multi-layered coating of polymeric nano-complexes and AGO. In the earlier synthetic approach, one bioinspired (lotus leaf) liquid (water) wettability was achieved in the expense of another bio-inspired (fish-scale) liquid (oil) wettability. In contrast to the previous methods, in this chapter, two selected small molecules—APTMS and HFDDA have been mixed with a molar ratio of 1:1 to allow spontaneous 1,4-conjugate addition reaction between amine and acrylate groups at ambient condition. In this design, HFDDA is expected to provide appropriate low surface energy and APTMS that are recognized for facile polymerization[28-29] (as evident from the infra-red (IR) spectral signature for Si-O-Si bridge[30] at 1028 cm^{-1} (Figure 6.1D)) likely to allow a uniform coating. Thereafter, a standard and widely accepted Fourier transform infrared attenuated total reflectance spectra (FTIR-ATR) spectra were recorded at a regular time interval, to monitor the progress of chemical reaction between selected small molecules (HFDDA and APTMS) through 1,4-conjugate addition reaction.

The characteristic IR signatures for a) C-H deformation of β-carbon of vinyl group and b) stretching of carbonyl moiety at 1410 cm^{-1} and 1730 cm^{-1}, respectively, confirmed the existence of acrylate groups in the reaction mixture of APTMS and HFDDA at t=0 min as similar to the solution of HFDDA (Figure 6.1A).

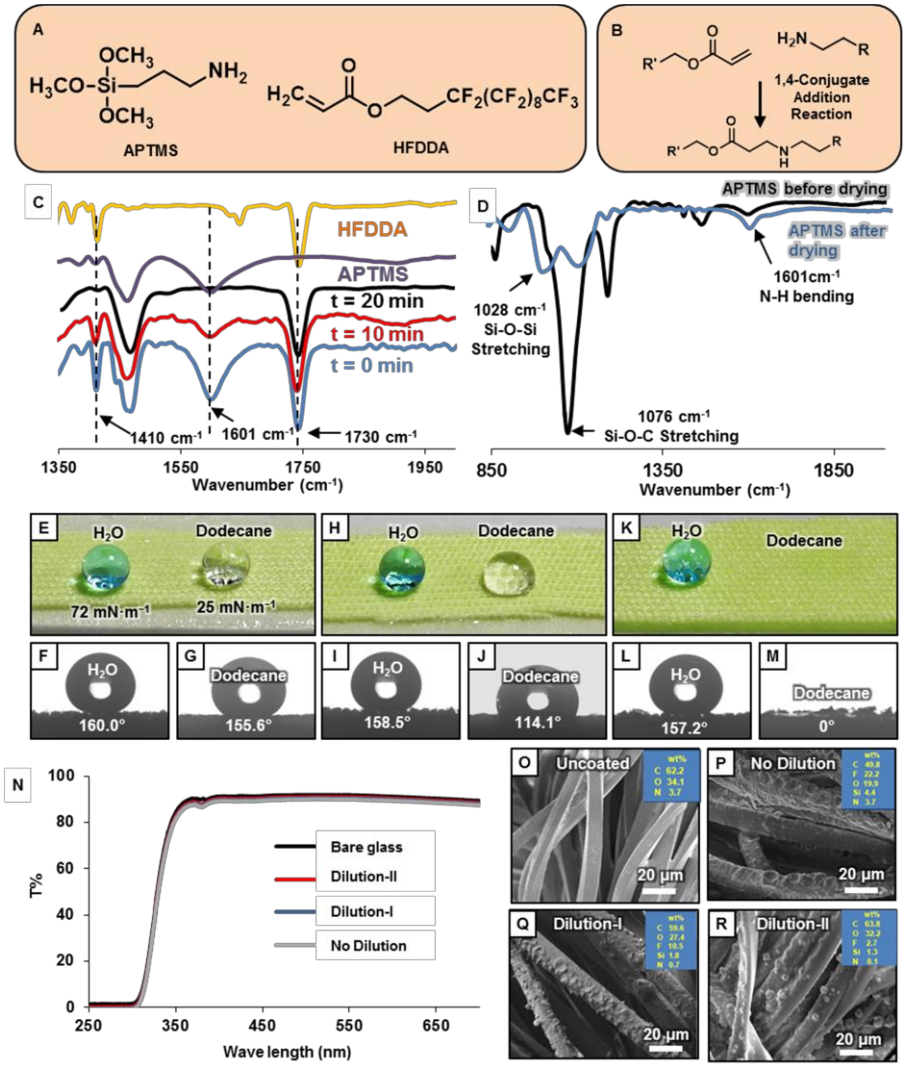

Figure 6.1. A-B) Chemical structures of (3-Aminopropyl)trimethoxysilane (APTMS) and 3,3,4,4,5,5,6,6,7,7,8,8,9,9,10,10,11,11,12,12,12-Heneicosafluorododecyl acrylate (HFDDA). B) Depiction of the 1,4-conjugate addition reaction between primary amine of APTMS and acrylate groups of HFDDA. C) The Fourier-transform infrared attenuated total reflectance (FTIR-ATR) spectra accounting the 1,4 conjugate addition reaction in the reaction mixture (1:1) of HFDDA (yellow) and APTMS (violet) in toluene, where FTIR-ART spectra were recorded at regular time intervals, including 0 min (blue), 10 min (red) and 20 min (black). In the FTIR-ATR spectra, the IR peaks at 1730 cm^{-1}, 1601 cm^{-1} and 1410 cm^{-1} characterized the signatures for C=O stretching, primary N–H bending and C–H deformation of the β-carbon of the vinyl group, respectively. D) FTIR-ATR spectra of the solution (black) and coating (blue) of (3-aminopropyl)trimethoxysilane. The appearance of IR peak at 1028 cm^{-1} for Si-O-Si linkage revealed the polymerization during the drying process of the spray deposited solution of (3-aminopropyl)trimethoxysilane. E–M) Digital images (E, H and K) and contact angle images (F, G, I, J, L and M) of beaded water (F, I and L) and beaded dodecane (G, J and M) droplets on the three distinct water repellent interfaces where the reaction solutions of the selected small molecules were spray deposited on the selected fibrous substrate without dilution (E–G) and with dilution-I (H–J) & dilution-II (K–M). N) Optical transmittance spectra of uncoated (black) and coated (red, blue and grey) glass slides, where the coating was achieved by depositing the reaction mixture without dilution (grey) and with dilutions--including dilution-I (blue) & dilution-II (red). O–R) FESEM images and EDX data (inset) of bare fabric (O) and small molecule derived coated fabric (P–R), where the coatings were achieved on the selected fibrous substrate by spray deposition of the reaction solution without dilution (p) and with dilution-I (Q) & dilution-II (R).

During the course of 1,4-conjugate addition reaction between acrylate and amine groups, only

vinyl moiety of acrylate group was compromised and carbonyl moiety remained unperturbed at the end of the reaction. As a result, with the progression of the reaction between the selected reactants (APTMS and HFDDA), the IR peak intensity at 1410 cm^{-1} was gradually reduced, and a significant depletion of the IR peak intensity was noted at t=20 min as shown in Figure 6.1A. Parallelly, the IR signature at 1601 cm^{-1} for N-H bending for primary amine moiety of APTMS was completely disappeared in the reaction mixture at t=20 min. Thereafter, the reaction mixture was spray deposited on a selected fibrous substrate that readily soaks both oil and water in air. After air-drying of the deposited reaction mixture, the coated fibrous substrate displayed super repellence to liquids having both high (water: 72 $mN.m^{-1}$) and low (Dodecane (a liner hydrocarbon): 25 $mN.m^{-1}$) surface tensions. The droplets of water and dodecane (DD) beaded with CA of 160° and 155° (Figure 6.1E-G) respectively, and the beaded droplets rolled away on tilting the interface below 10° (Figure 6.2A-F). Further, the facile and rapid deposition of the superamphiphobic coating was adopted. The submerged and shiny interface (Figure 6.2M-N) of the synthesized superamphiphobic coating in both the water and the DD revealed the appropriate entrapment of external third phase—air, which provided heterogeneous and extreme water and oil wettability.[1,11] Thereafter, the reaction mixture was diluted 2 times of its initial concentration, keeping the composition (molar ratio of 1:1) of the selected reactants unaltered, and this specific dilution has been denoted as 'Dilution-I' in the rest of the text. The spray deposition of this diluted reaction solution yielded a superhydrophobic—but oleophobic interface (Figure 6.1H), where the water droplet beaded with CA of ~158° and the droplet of DD wet on the same interface with CA of ~114° as shown in Figure 6.1I-J. On increasing the dilution of the reaction mixture to 4 times (which is referred as Dilution-II), the same spray deposition process provided a lotus-leaf inspired superhydrophobic interface, where water was extremely repelled with CA of ~ 157°—but the droplet of DD was immediately spread with CA of 0° as shown in Figure 6.1K-M. Thus, the same reaction mixture of small molecules with identical composition provided three different types of water repellent coatings, depending on the appropriate dilution of the same reaction mixture, prior to spray deposition.

Further, the liquid wettability of small molecules derived all three types of extremely water repellent coatings having differences in their oil-wettability (i.e. superoleophilicity and oleophobicity and superoleophobicity), were examined using other various liquids including alcohol (EtOH), toluene, (1,2-dichloroethane (DCE)), diiodomethane (CH_2I_2), PEG and glycerol as accounted in Figure 6.3. This interface failed to display extreme repellence for

liquids having surface tension below 23 $mN.m^{-1}$ (Figure 6.3). Furthermore, the small molecules derived all three types of coatings embedded with distinct combination of both oil- and water-wettability, remained highly optically transparent (99 %), very similar to bare glass as shown in Figure 6.1N.

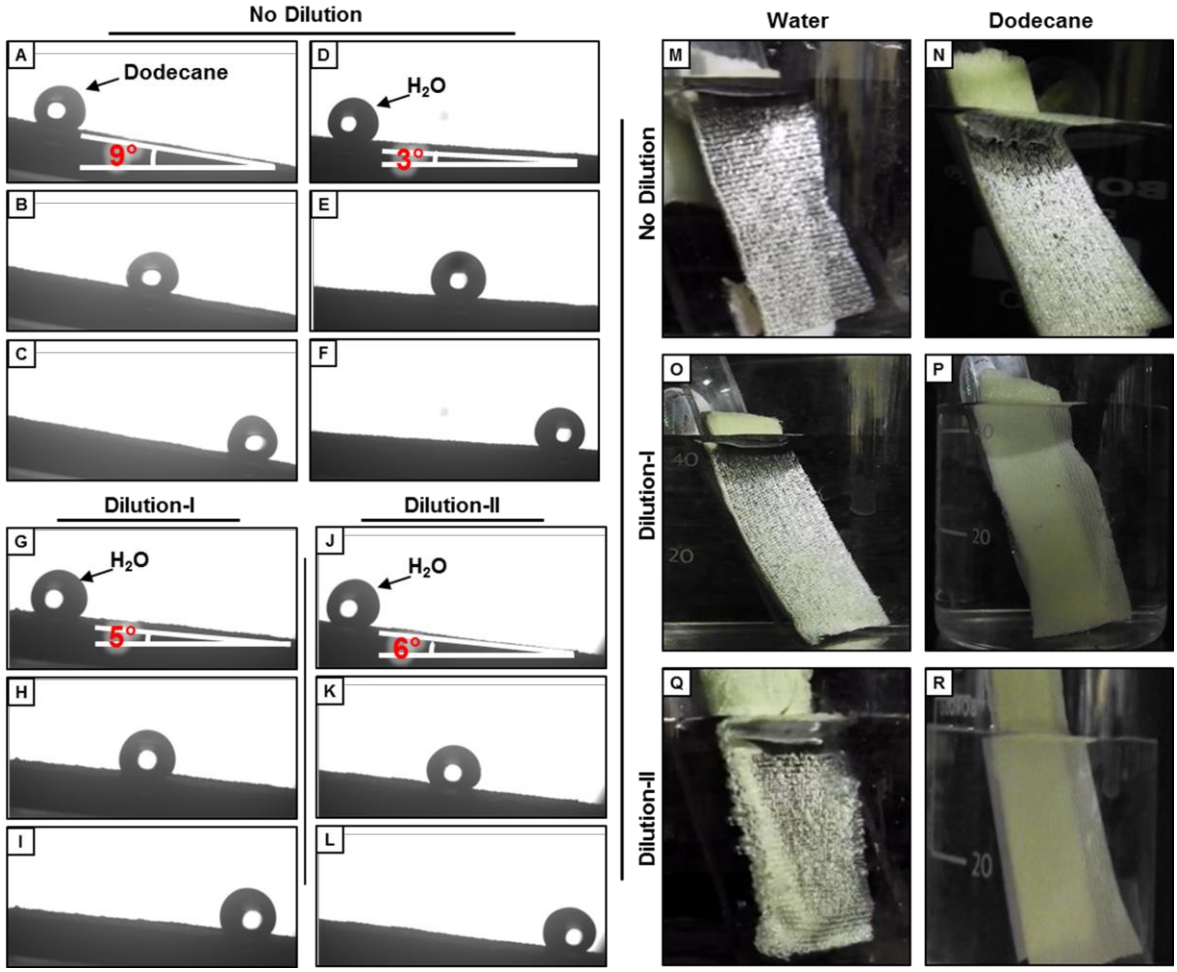

Figure 6.2. A-L) Demonstration of the rolling of beaded dodecane droplet (10 µL; A-C) and water droplet (10 µL; D-L) on the tilted three distinct coating that are embedded with superhydrophobicity/superoleophobicity (A-F), superhydrophobicity/oleophobicity (G-I) and superhydrophicity/superoleophilicity(J-L)). The reaction solution without dilution (A-F), with dilution-I (G-I) and with dilution-II (J-L) were deposited on the selected fibrous substrate to achieve these different coatings. M-R) Digital images of superhydrophobic/superoleophobic (denoted as superamphiphobic) (M-N), superhydrophobic/oleophobic (O-P) and superhydrophic/superoleophilic (Q-R) interface under water (M,O,Q) and under dodecane (N,P,R). The superamphiphobic interface appeared shiny in both the water and the dodecane because of entrapped air layer which conferred extreme water and oil repellence (M-N). The superhydrophobic/oleophobic (O-P) and superhydrophic/superoleophilic (Q-R) interfaces became shinny only under water whereas they are completely wetted on submerging in dodecane.

The past studies validated the difference in the requirement of topography towards super water/oil wettabilities. While, the lotus-leaf inspired superhydrophobic interfaces require a hierarchical topography with the arbitrary arrangement of nano/micro-domains,[31] the springtails-inspired superoleophobic interfaces mostly demand more specific and re-entrant

texture.[11,16]

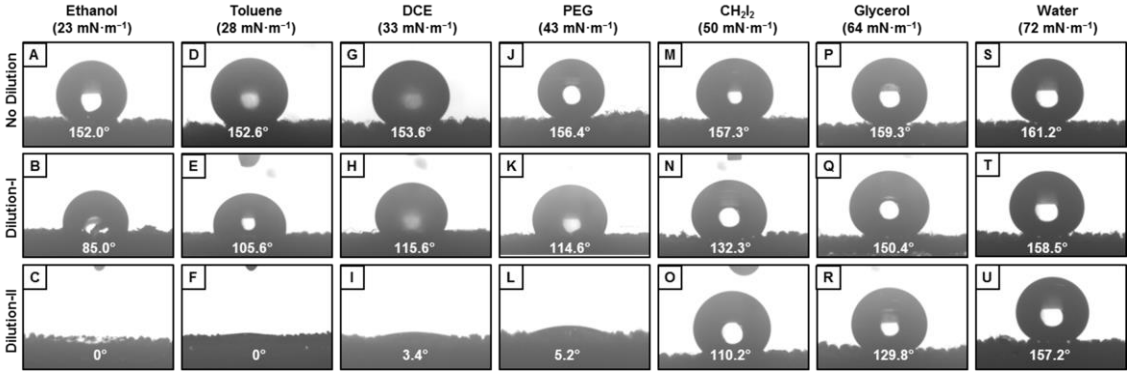

Figure 6.3. A-U) Static contact angle images of beaded droplets of various liquids including ethanol (AC), toluene (D-F), 1,2-dichloroethane (G-I), polyethylene glycol (J-L), diiodomethane (M-O), glycerol (PR) and water (S-U) on the three distinct coatings that were associated with (superamphiphobicity (A,D,G,J,M,P,S), superhydrophobicity/oleophobicity (B,E,H,K,N,Q,T) and superhydrophicity/superoleophilicity (C,F,I,L,O,R,U,)). The reaction solution without dilution (A,D,G,J,M,P,S), with dilution-I (B,E,H,K,N,Q,T) and with dilution-II (C,F,I,L,O,R,U,) were spray deposited on the selected fibrous substrate to achieve three distinct coatings.

In this chapter, the small molecules derived all three different coatings that embedded with different liquid wettability displayed completely distinct and essential topography as shown in Figure 6.1 P-R. on the other side, the EDX analysis revealed that all three distinct coatings were embedded with key elements (F and Si) that belong to used reactants (HFDDA and APTMS) in the reaction mixture, irrespective of the dilution of the deposition solution (Figure 6.1O-R). However, the change in the density of HFDDA is expected with the dilutions of the reaction mixture. The percentage of fluorine in the coated fibrous substrates decreased with the dilution of the reaction mixture as confirmed with elemental analysis (Figure 6.1O-R). Thus, both the change in the topography and the fluorine chemistry (HFDDA) played a crucial role for tailoring oil wettability—while the superhydrophobicity remained unaltered.

6.3.2. Physical/chemical Durability of Synthesized Superamniphobic and Superhydrophobic Interfaces

The durability of both lotus-leaf-inspired superhydrophobic and superamphiphobic interfaces was investigated in details. Their performances were compared at practically relevant different and difficult circumstances, including exposures of various physical manipulations, physical abrasions, UV-light, high temperature, extremes of pH, sea water etc. Firstly, both the superhydrophobic and superamphiphobic interfaces were separately exposed to creasing, twisting, tissue paper wiping and finger wiping for multiple times, prior to examining the

liquid wettability with droplets of water and dodecane. The treated interfaces repelled both the beaded droplets of water and dodecane with contact angle above 155° as shown in Figure 6.4A-G. Similar to the superamphiphobic interface, the synthesized superhydrophobic coating also displayed uninterrupted super water repellence.

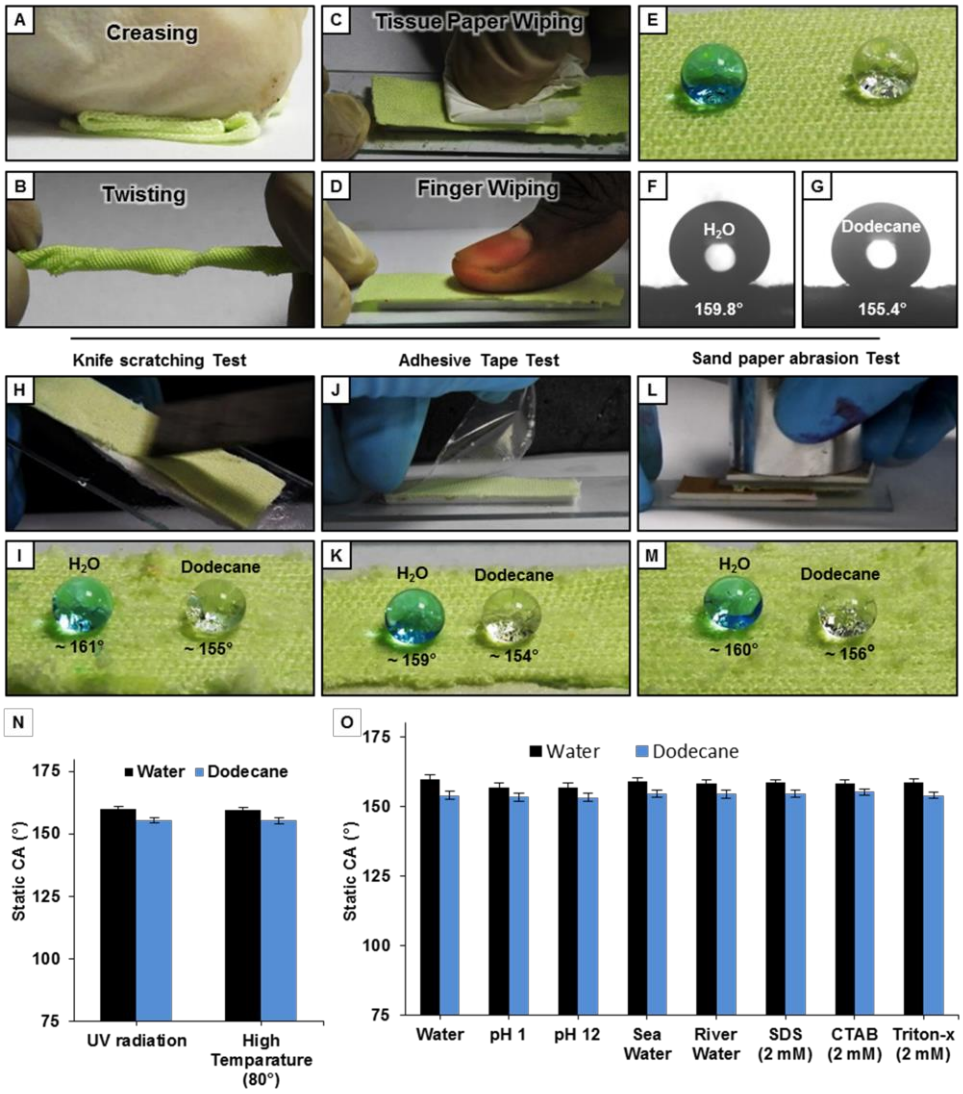

Figure 6.4. A–D) Digital images depicting the processes of various physical manipulations, including creasing (A), twisting (B), tissue paper-wiping (C) and fingerwiping (D) on the synthesized superamphiphobic coating. E–G) Digital image (E) and contact angle images (F and G) of the beaded water (F) and dodecane (G) droplets on the superamphiphobic fabric after incurring creasing, twisting, finger wiping, and tissue paper wiping tests. H, J and L) Digital images of the experimental setup of knife scratching test (H), adhesive tape test (J), and sandpaper abrasion test (L) on the superamphiphobic coating. I, K and M) Digital images of beaded water and dodecane droplets on a superamphiphobic interface after performing the knife scratching test (I), adhesive tape test (K), and sandpaper abrasion test (M). N and O) Plots accounting the impact of practically relevant various harsh exposures on the superamphiphobic fabric (no dilution) including UV irradiation (at λmax = 254 and 365 nm) and high (80 °C) temperature, DI water, highly acidic (pH 1) & alkaline (pH 12) media, artificial-sea water, river water (Brahmaputra, Guwahati and Assam), and surfactant contaminated aqueous phase (SDS, CTAB, Triton-X; 2 mM), for 10 days.

Thereafter, more challenging and different physical abrasive exposures were incurred on

both the superhydrophobic and superamphiphobic coatings.

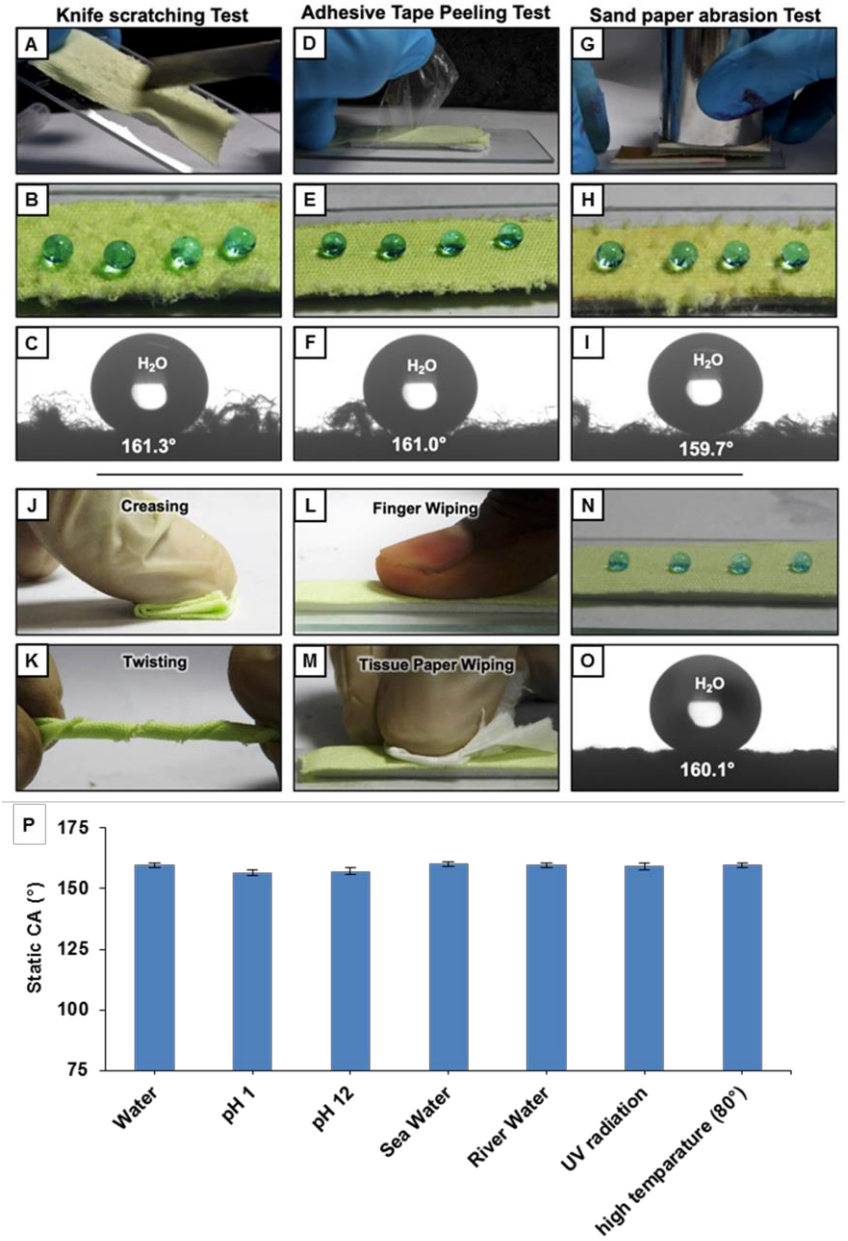

Figure 6.5. A,D,G) Digital image representing the experimental setup for knife scratching test (A), adhesive tape test (D), sand paper abrasion test (G) . B-I) Digital image (B,E,H) and static contact angle (C,F,I) images of beaded water droplet on superhydrophobic interface (that prepared following dilution-II of the reaction miture, prior to spray deposition) after performing the knife scratching test (B-C), adhesive tape test (E-F), sand paper abrasion test (H-I). J-M) Digital images of the same superhydrophobic interface that is manually creased (J), twisted (K), whipped by finger (L) and whipped by tissue paper (M) . N-O) Digital image (N) and water contact angle Images (O) of the beaded water droplet on the superhydrophobic interface after incurring creasing, twisting, finger wiping, tissue paper wiping. P) Plots accounting the impact of practically relevant diverse and harsh exposures on the superhydrophobic coating (that achieved following dilution-II of the reaction mixture before spray deposition) including DI water, highly acidic (pH 1) & alkaline (pH 12) media, artificial-sea water, river water (Brahmaputra, Guwahati, Assam), surfactants contaminated aqueous phase (SDS, CTAB, Triton-X; 2mM), UV irradiation (at λmax = 254 and 365 nm) and high (80°C) temperature for 10 days.

Firstly, physical scratches were introduced on the freshly prepared liquid-repellent interfaces,

using a sharp knife as shown in Figure 6.4H. The physically damaged interfaces displayed extreme oil and water repellence with CA above 150° (Figure 6.4I). Next, a freshly exposed adhesive tape was separately applied on both the superhydrophobic and superamphiphobic interfaces with an external load of 25 KPa that facilitated the uniform contact between the liquid-repellent interface and the adhesive surface. The embedded and extreme liquid-wettability remained unperturbed, even after the adhesive tape peeling test (Figure 6.4J-K). Furthermore, an abrasive sand paper was rubbed on the small molecules derived superamphiphobic interfaces with a distance of 250 cm, however, the droplets of water and dodecane beaded on the sand paper treated superamphiphobic interface with CA above 150° (Figure 6.4L-M). A very similar durability was observed for the synthesized superhydrophobic interface as well (Figure 6.5A-O). Next, small molecules derived and physical-abrasion tolerant both superhydrophobic and superamphiphobic interfaces were exposed to UV light (254 nm and 365 nm) and relatively high (80°C) temperature for 10 days. However, both the superhydrophobic and superamphiphobic interfaces remained capable of sustaining such treatments without perturbing their embedded super oil/water wettability as shown in Figure 6.4N and Figure 6.5P. Furthermore, both the water-repelling interfaces that embedded with either superoleophilicity or superoleophobicity were exposed to various and complex aqueous phases, including DI water, highly acidic (pH 1) & alkaline (pH 12) media, artificial-sea-water, river water (Brahmaputra, Guwahati, Assam) and surfactants contaminated aqueous phase for 10 days. Even after such prolonged and harsh treatments, the small molecules derived both superhydrophobic (Figure 6.5P) and superamphiphobic (Figure 6.4O) coatings continued to perform with unaltered super-liquid (oil/water) repellence, where the contact angle of beaded droplets of water and dodecane remained above 150°. Thus, the strategic use of 1,4-conjugate addition reaction between selected small molecules and followed by simple spray-deposition process yielded highly tolerant and different water-repellent interfaces that were embedded with tailored oil-wettability in air. High tolerance on the embedded extreme liquid repellence in the synthesized superhydrophobic and superamphiphobic coatings would be appropriate for achieving an uninterrupted performance at practically relevant diverse outdoor scenarios.

6.3.3. Application of Synthesized Superamniphobic and Superhydrophobic Interfaces

The abilities of both the synthesized superhydrophobic and superamphiphobic interfaces were extended to compare its ability for some important and relevant applications—including

oil/water separation, self-cleaning and anti-fouling of different liquids.

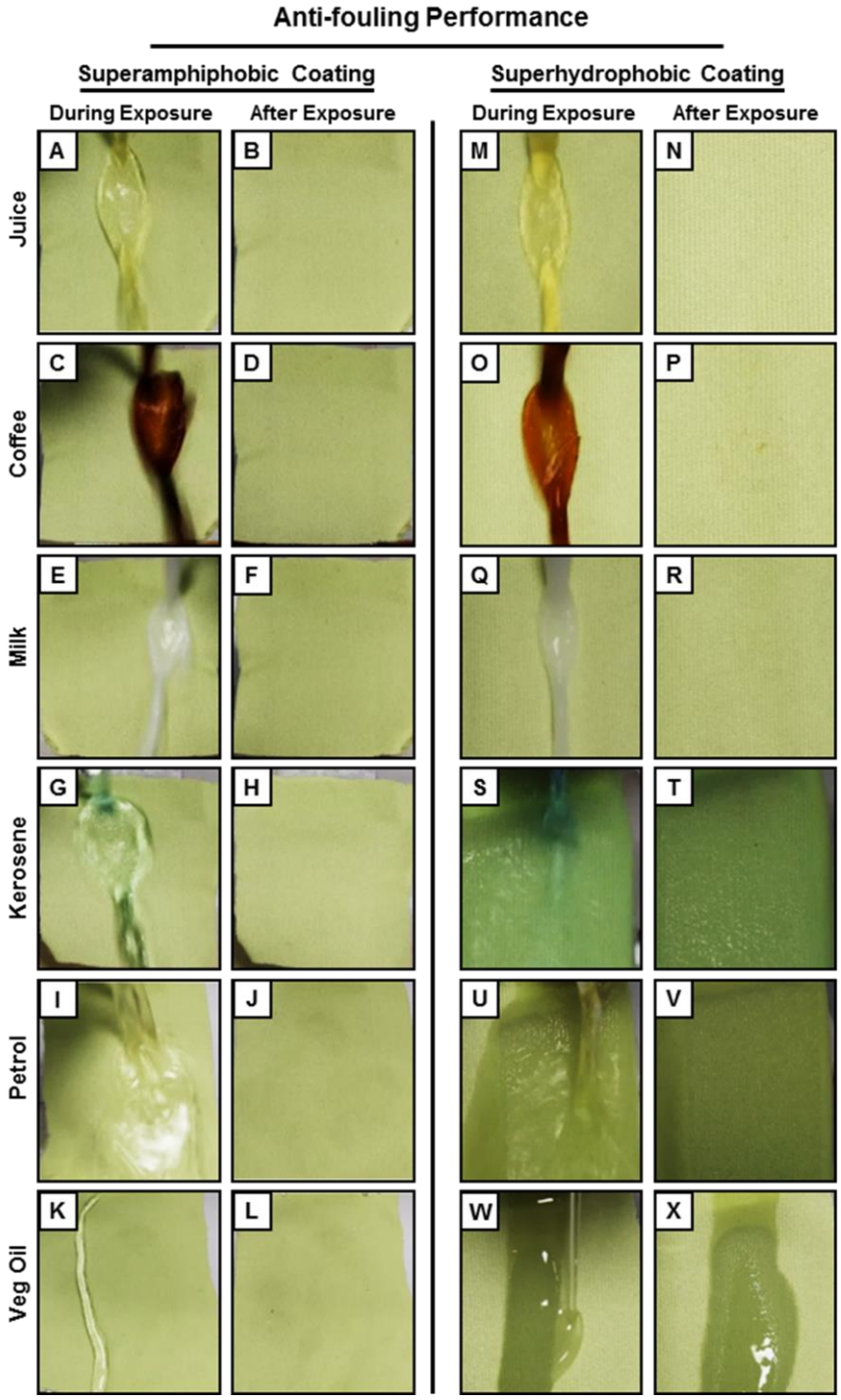

Figure 6.6. (A–L) Digital images depicting the successful antifouling performance of superamphiphobic coating, where the stream of various aqueous phases including cold (4 °C) juice (A and B), hot (60 °C) coffee (C and D), cow's milk (E and F) and commonly used oil/oily phases including kerosene (G and H), petrol (I and J), and veg oil (K and L), were poured on the synthesized coating. (M–X) Digital images depicting both the success (M–R) and failure (S–X) in antifouling performance of superhydrophobic coating (prepared following dilution-II) with various aqueous phases including a stream of cold (4 °C) juice (M and N), hot (60 °C) coffee (O and P), cow's milk (Q and R) and with various oil/oily phases including kerosene (S and T), petrol (U and V), and veg oil (W and X).

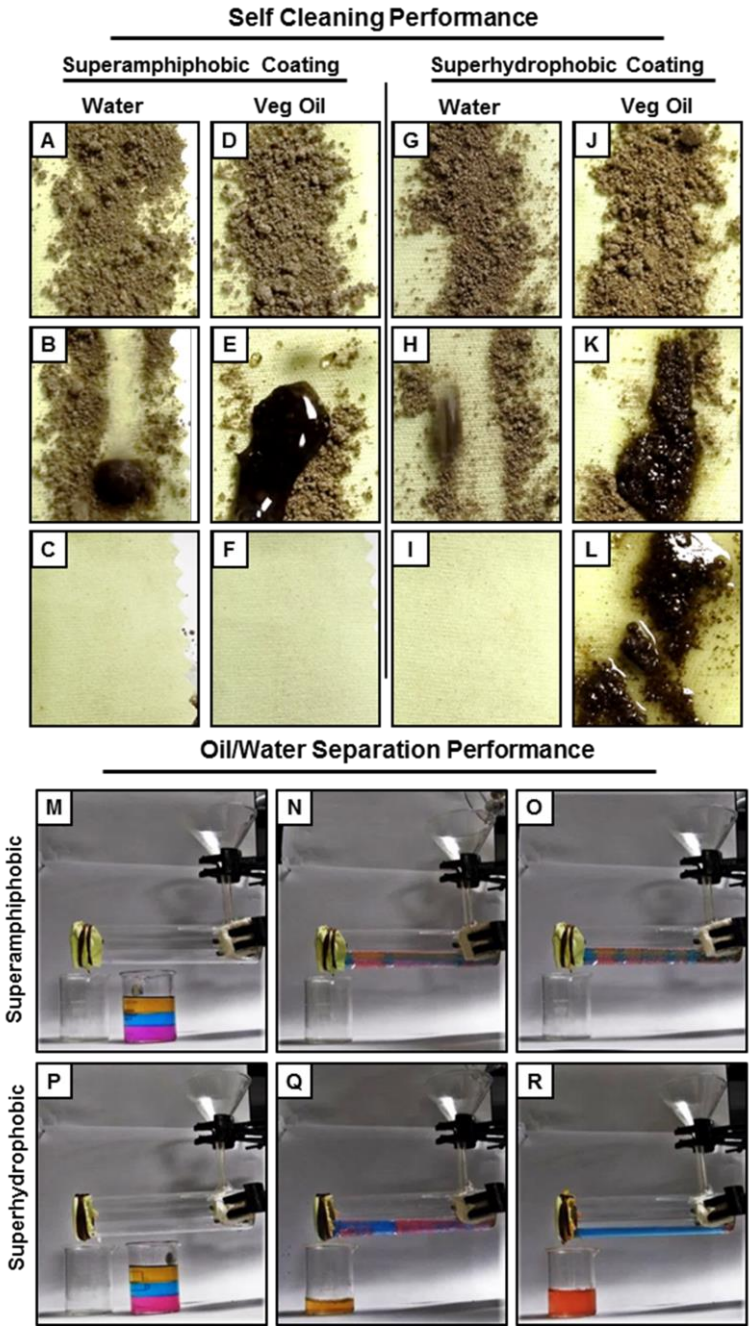

Figure 6.7. A–F) Illustrating the self-cleaning of deposited dust and dirt on the superamphiphobic fabric under the exposures of water (A–C) and veg oil (D–F). G–L) Digital images illustrating the success in the selfcleaning performance of the superhydrophobic fabric with water (G–I) and the failure in the self-cleaning performance of the superhydrophobic fabric with vegetable oil (denoted as veg oil; J–L). M–O) Digital images depicting the failure in the selective separation of oil from a three-phase (light oil/water/heavy oil) oil–water mixture using a superamphiphobic coating, where superamphiphobicity prevented the passage of both oil and aqueous phases. P–R) Digital images illustrating the successful separation of three phases (light oil/water/heavy oil) oil– water mixtures using a superhydrophobic coating, where extreme water repellency prevented the passage of the aqueous phase—but the embedded super-oil-affinity allowed the selective passage of the oil phase under a gravitation force.

The superamphiphobic interface that extremely repelled various oil/oily and aqueous phases is highly useful for preventing fouling caused by spillages of commercially available various

and relevant aqueous and oily phases, including juice, coffee, milk, kerosene, petrol and vegetable oil as demonstrated in Figure 6.6A-L. In comparison to superamphiphobic coating, the superhydrophobic interface that associated with superoleophobicity remained only effective to prevent aqueous-fouling (Figure 6.6M-R), but the same interface failed to prevent fouling that caused by oil/oily spillages as shown in Figure 6.6S-X —likely due to the existence of embedded super-oil-affinity in the lotus-leaf inspired superhydrophobic coatings (Figure 6.1K-M). Next, the self-cleaning ability of both the interfaces was compared under the streams of both water and oil. The synthesized superamphiphobic coating displayed the ability for self-cleaning the deposited dust and dirt under the exposures of both water and oil phases, and at the end, a dry and clean interface was recovered as shown in Figure 6.7A-F. In comparison, the superhydrophobic interface lost the self-cleaning ability under the exposure of oil-stream (Figure 6.7J-L), though it remained efficient to self-clean the deposited dust and dirt under aqueous exposure as shown in Figure 6.7G-I. In the past, lotus-leaf inspired extremely water repellent interfaces that embedded with superoleophilicity have been explored for gravity-driven oil/water separation.[21-22] The small molecules derived superhydrophobic coating remained efficient for selective filtration of oil phase from oil/water mixture as demonstrated in Figure 6.7P-R.

A three-phase oil/water mixture that consists of heavy model oil (DCE, pink coloured bottom layer), aqueous layer (blue coloured-middle layer) and petrol (yellow-coloured top layer) was poured in the lab-made prototype, where the synthesized superhydrophobic fibrous interface was used as a selective oil-filtrating membrane. As expected, the extreme water repellence restricted the passage of the aqueous phase but the embedded super oil-affinity allowed the oil/oily phase to selectively pass through the synthesized superhydrophobic membrane as shown in Figure 6.7P-R. In the contrary, the synthesized superamphiphobic interface that extremely repelled both oil and aqueous phase prevented the passage of both the phases. Eventually, the superamphiphobic interface became inappropriate for environmentally friendly and gravity-driven oil/water separation as shown in Figure 6.7M-O. Thus, both the superhydrophobic and the superamphiphobic interfaces associated with contrasting oil wettability have superior performance over one another, depending on their strategic and relevant uses.

6.4. Conclusion

In conclusion, here, a facile and common synthetic approach has been introduced for achieving different water repellent coatings that are embedded with distinct oil-wettability in air. A 1,4-conjugate addition reaction between rationally selected small molecules at ambient conditions, followed by spray deposition allowed to co-optimize essential topography and chemistry for achieving optically transparent, durable and different oil-wettability (in air) starting from superoleophilicity to superoleophobicity, keeping the embedded superhydrophobicity unperturbed. The synthesized superhydrophobic and superamphiphobic interfaces remained capable of sustaining a diverse range of practically relevant challenging exposures. Further, such interfaces were extended for comparing their performances towards various important and relevant applications. Such an elegant synthetic strategy would be useful in developing various functional interfaces.

References

1. X. M. Li, D. Reinhoudt and M. Crego-Calama, *Chem. Soc. Rev*., 2007, **36**, 1350-1368.
2. X. Yao, Y. Song and L. Jiang, *Adv. Mater*., 2011, **23**, 719.
3. B. Su, Y. Tian and L. Jiang, *J. Am. Chem. Soc.,* 2016, **138**, 1727.
4. Q. Li and Z. Guo, *J. Mater. Chem. A*, 2018, **6**, 13549.
5. Y. Si, Z. Dong and L. Jiang, *ACS Cent. Sci*., 2018, **4**, 1102.
6. A. I. Neto, P. A. Levkin and J. F. Mano, *Mater. Horiz.,* 2018, **5**, 379.
7. M. Ge, C. Cao, J. Huang, X. Zhang, Y. Tang, X. Zhou, K. Zhang, Z. Chen and Y. Lai, *Nanoscale Horiz*., 2018, **3**, 235.
8. T. Xu, L.-P. Xu, X. Zhang and S. Wang, *Chem. Soc. Rev*., 2019, **48**, 3153..
9. Z. Wang, L. Scheres, H. Xia and H. Zuilhof, *Adv. Funct. Mater.,* 2020, **30**, 1908098.
10. D. Wang, Q. Sun, M. J. Hokkanen, C. Zhang, F. -Y. Lin, Q. Liu, S. -P. Zhu, T. Zhou, Q. Chang, B. He, Q. Zhou, L. Chen ,Z. Wang ,R. H. A. Ras and X. Deng, *Nature,* 2020, **582**, 55.
11. A. Tuteja, W. Choi, M. Ma, J. M. Mabry, S. A. Mazzella, G. C. Rutledge, G. H. McKinley and R. E. Cohen, *Science*, 2007, **318**, 1618.

12. X. Deng, L. Mammen, H.-J. Butt and D. Vollmer, *Science*, 2012, **335**, 67.
13. K. Liu, M. Cao, A. Fujishima and L. Jiang, *Chem. Rev.,* 2014, **114**, 10044.
14. S. Wang, K. Liu, X. Yao and L. Jiang, *Chem. Rev*., 2015, **115**, 8230.
15. L. Wen, Y. Tian and L. Jiang, *Angew. Chem. Int. Ed*., 2015, **54**, 3387 .
16. J. Yong, F. Chen, Q. Yang, J. Huo and X. Hou, *Chem. Soc. Rev.,* 2017, **46**, 4168.
17. J. Ai and Z. Guo, *Chem. Commun*., 2019, **55**, 10820.
18. Y. Sun and Z. Guo, *Nanoscale Horiz*., 2019, **4**, 52.
19. C. Yan, P. Jiang, X. Jia and X. Wang, *Nanoscale*, 2020, **12**, 2924.
20. W. S. Y. Wong, T. P. Corrales, A. Naga, P. Baumli, A. Kaltbeitzel, M. Kappl, P. Papadopoulos, D. Vollmer and H. -J. Butt, *ACS Nano*, 2020, **14**, 3836.
21. L. Feng, Z. Zhang, Z. Mai, Y. Ma, B. Liu, L. Jiang and D. Zhu, *Angew. Chem*., 2004, **116**, 2046 .
22. Z. Chu, Y. Feng and S. Seeger, *Angew. Chem. Int. Ed*., 2015, **54**, 2328 .
23. R. A. Farrer, C. N. LaFratta, L. Li, J. Praino, M. J. Naughton, B. E. A. Saleh, M. C. Teich and J. T. Fourkas, *J. Am. Chem. Soc*., 2006, **128**, 1796.
24. J. Ford, S. R. Marder and S. Yang. *Chem. Mater.,* 2009, **21**, 476.
25. S. L. Bechler and D. M. Lynn, *Biomacromolecules*, 2012, **13**, 1523.
26. D. Parbat, S. Gaffar, A. M. Rather, A. Gupta and U. Manna, *Chem. Sci*., 2017**,8**, 6542.
27. A. Das, S. Sengupta, J. Deka, A. M. Rather, K. Raidongia and U. Manna, *J. Mater. Chem., A*, 2018, **6**, 15993.
28. J. B. Brzoska, I. B. Azouz and F. Rondelez, *Langmuir*, 1994, **10**, 4367.
29. W. -M. Munief, F. Heib, F. Hempel, X. Lu, M. Schwartz, V. Pachauri, R. Hempelmann, M. Schmitt and S. Ingebrandt, *Langmuir*, 2018, **34**, 10217.
30. A. N. Lazarev, Vibrational Spectra and Structure of Silicates; Consultants Bureau: *New York*, 1972.
31. A. M. Rather, A. Shome, S. Kumar, B. K. Bhunia, B. B. Mandal, H. K. Srivastava and U. Manna, *J. Mater. Chem. A*, 2018, **6**, 17019.

Conclusion and Future Plan

This chapter includes a general summary of the current thesis work and the future work plan related to this thesis works in various possible directions. Generally, the conventional bio-mimicked anti-wettabilities that were associated with delicate/weak chemical interaction remained susceptible to permanent damage under severe physical and chemical insults which limited its practical applications. However, there are a few designs that have provided durable lotus leaf-inspired and fish-scale inspired interfaces, but those reported materials were prepared by adopting tedious/complex methods. Even sometimes harmful chemicals that have an adverse effect on human health and the environment were associated. In my thesis works, I intend to fabricate durable and extreme anti-wetting interfaces (superhydrophobic and underwater superoleophobic) through a simple fabrication procedure that can sustain severe physical abrasions, large tensile/compressive strain and harsh chemical environment. Therefore, a facile and catalyst-free 1,4-conjugate addition reaction between the amine and acrylate groups was adopted where covalently integration of amino graphene oxide (AGO) and chemically reactive nanocomplex (CRNC) provided physically deformable and abrasion tolerant lotus leaf-inspired superhydrophobic interfaces. Furthermore, the control incorporation of amino graphene oxide provides an opportunity to tailor the mechanical property of the prepared material. This synthetic approach was further exploited to develop durable, self-healable and substrate independent superhydrophobic coating where the physically damaged interface was able to self-heal the anti-wetting property without any external intervention. Next, I have developed stretchable and abrasion tolerant lotus leaf-inspired superhydrophobic and fish-scale inspired underwater superoleophobic interfaces through the layer-by-layer deposition of AGO and CRNC followed by appropriate post covalent modifications (octadecylamine for superhydrophobic interface and D-glucamine for underwater superoleophobic interface). The synthesized bio-inspired interfaces remained efficient to tolerate large and repetitive tensile deformations (with 100% strain)—even after incurring severe various physical (e.g., creasing, bending, twisting, physical erosions and so on) and chemical challenges (e.g., extremes of pH, seawater, river water, UV irradiation and so on). This approach was further extended to develop durable and stretchable both superhydrophobic and underwater superoleophobic membranes by constructing the multilayer coating on a stretchable fibrous substrate. Moreover, the embedded liquid wettabilities of both the bio-mimicked membrane remained unaltered after incurring various physical abrasions and prolong harsh chemical exposure. These fibrous bio-mimicked

membranes were further explored for energy-efficient, selective and simultaneous separation of various oil/water mixtures irrespective of surface tension, density, and viscosity of the used oil phase. Moreover, both the oil and water separation efficiency remained unaltered even presence of practically relevant severe and complex aqueous phases (i.e.; extremes of pH, artificial seawater, river water) in the oil-water mixture. Next, a chemically reactive and magnetically active two dimensional (2D) graphene nano-sheet was introduced which was able to show confined-superhydrophobicity after post-modification with long-chain alkyl amine. This synthesized material was highly capable of separating oil/water from both oil-in-water and water-in-oil emulsions. The emulsion separation performance remained intact in various practically relevant and complex conditions (pH 1, pH 12, seawater, river water and surfactant contaminated). After that, I have introduced a distinct and unique approach to associate different oil-wettability with superhydrophobicity. A reaction mixture of small molecules and its strategic dilution prior to allowed to achieve three different superhydrophobicity that separately associated with superoleophilicity, oleophobicity and superoleophobicity.

Thus, considering the importance of research work in this thesis, it is clearly understood that this thesis work can be further extended in various advanced research directions in near future. Graphene oxide and its reduced form are well recognized for various important properties including electrical and thermal conductivity. In this thesis work, amine-functionalized reduced graphene oxide was strategically associated to develop highly durable, stretchable and self-healable bio-inspired interfaces (lotus-leaf and fish-scale inspired). Such interfaces have great potential to develop various water repellent advanced materials including stretchable motion sensors, underwater vibration sensors, supercapacitors, piezoelectric pressure sensors and other flexible electronics. Additionally, owing to the high surface area and presence of different functional groups on graphene oxide sheets, the current approach can be rationally associated with drugs, proteins, enzymes and other biomolecules for developing various other functional materials. Moreover, the superhydrophobic environment of our synthesised material could be very useful to enhance the efficiency of various heterogeneous catalysts for selective chemical reactions. Furthermore, the durable underwater superoleophobic interface can be useful for anti-platelet adhesion, oil droplets transportation and so on. Thus, the graphene oxide-based current approach for developing durable bio-inspired anti-wetting interfaces has immense potential in developing different functional smart materials in the near future.

List of Publications

1. **A. Das,** J. Deka, K. Raidongia and U. Manna, *Chem. Mater.,* 2017*,* **29***, 8720***.**
2. **A. Das,** J. Deka, A. M. Rather, B. K. Bhunia, P. Pratim Saikia, B. B. Mandal, K. Raidongia and U. Manna. *ACS Appl. Mater. Interfaces,* 2017, **9***,* 42354.
3. **A. Das,** S. Sengupta, J. Deka, A. M. Rather, K. Raidongia and U. Manna. *J. Mater. Chem. A,* 2018, **6**, 15993.
4. **A. Das**, D. Parbat, A. Shome and U. Manna. *ACS Sustainable Chem. Eng*., 2019, **7**, 11350.
5. **A. Das**, K Maji, S Naskar and U. Manna. *Chem. Sci.,* 2020, **11**, 6556.
6. **A. Das**, U. Manna. *Nanoscale*, 2020, **12**, 24349.

Other Publications

1. U. Baruah, **A. Das** and U Manna, *ACS Appl. Mater. Interfaces,* 2019, **11**, 28571.
2. S. Das, **A. Das**, D. Parbat and U. Manna, *ACS Appl. Mater. Interfaces,* 2019*,* **11***,* 34316.
3. K. Maji, **A. Das**, M. Hirtz and U. Manna, *ACS Appl. Mater. Interfaces,* 2020*,* **12**, 14531.
4. D. Parbat, **A. Das**, K. Maji and U Manna, *J. Mater. Chem. A,* 2020, **8**, 97.
5. A. Shome, A. Das, N. Rawat, A. M. Rather and U. Manna, *J. Mater. Chem. A,* 2020, **8**, 15148.
6. K. Maji, **A Das**, M. Dhar, U. Manna. *J. Mater. Chem. A*, 2020, **8**, 25040.
7. **A. Das,** A .Shome and U. Manna. *J. Mater. Chem. A*, 2021,**9,** 824.
8. M. Dhar, **A. Das**, A. Shome, A. Borbora, and U. Manna. *Mater. Horiz.,* 2021, Accepted Manuscript, DOI: 10.1039/D1MH00857A.

Conferences/Seminars Attended

- Presented poster entitled “Self-Cleanable and Self-Healable superhydrophobic print of water-soluble agent” in **‘Chemconvene’ (2017)** organized by Department of Chemistry, IIT Guwahati.

- Presented Model based on "Stretchable and Porous Superhydrophobic Fibrous Substrate for Oil Spill Cleanup" in '**Research Conclave' (2018)** organized by Students' Academic Board (SAB), IIT Guwahati.
- Presented poster entitled "Self-Healable Superhydrophobic Print of Water Soluble Agents—A Contradictory Concept" in **'Research Conclave' (2018)** organized by Students' Academic Board (SAB), IIT Guwahati.
- Presented poster entitled "Stretchable and Durable Fish Scale and Lotus Leaf-Inspired Multilayers" in the International Conference - **'Frontiers in Chemical Sciences (FICS 2018)** organized by Department of Chemistry, IIT Guwahati.
- Presented poster entitled "Self-Healable and durable Superhydrophobic interface" in '**SPSI, MACRO', 2018** organized by IISER Pune and CSIR-NCL Pune.
- Presented poster entitled "Simultaneous collection of both oil and water phases from oily wastewater using bio-mimicked membranes" in **International Conference on Advanced Nanomaterials and Nanotechnology (ICANN-2019)** conducted by Centre for Nanotechnology, Indian Institute of Technology Guwahati.